Predicting the survival of coral reefs

A biophysical modelling approach

Gijs G. Hendrickx

TU Delft Deltares

Cover: Wave breaking over a coral reef [Image from *The Earth Chronicles of Life*[1]].

[1]The death of corals will lead to an increase in waves in the ocean. (2018, March 7). Retrieved on April 2, 2020 from https://earth-chronicles.com/science/the-death-of-corals-will-lead-to-an-increase-in-waves-in-the-ocean.html

Predicting the survival of coral reefs

A biophysical modelling approach

by

Gijs G. Hendrickx

in partial fulfilment of the requirements of the degree of

Master of Science
in Hydraulic Engineering

at Delft University of Technology
to be defended publicly Thursday, April 16, 2020 at 15h00

Student number: 4296532

Thesis committee

Prof.dr. Peter M. J. Herman, Chair	TU Delft / Deltares
Dr.ir. Jasper T. Dijkstra	Deltares
Prof.dr. Julie D. Pietrzak	TU Delft
Dr.ir. Arjen P. Luijendijk	TU Delft / Deltares

Delft University of Technology
Faculty of Civil Engineering
Department of Hydraulic Engineering
Section of Environmental Fluid Mechanics

An electronic version of this thesis is available at
http://repository.tudelft.nl/

Abstract

KEY POINTS

- A biophysical model framework (BMF) for corals is developed in which four environmental factors are included: (1) light; (2) hydrodynamics; (3) temperature; and (4) acidity.
- The full feedback loop between corals and their environment forms the core of this model framework, where the morphological development is new and closes the feedback loop.
- The developed BMF predicts the coral response to environmental input via (mainly) process-based relations within the accuracy of climate projections.
- The BMF supports both the deep reef refugia hypothesis (DRRH) and the turbid reef refugia hypothesis (TRRH).
- The BMF contributes to the development of protection and recovery programs and is not site-specific.
- The BMF is developed for long-term predictions—in the order of decades to centuries—but runs on daily averages and is therefore applicable for assessing the response of corals on shorter time-scales; such as months to years.

The increasing pressure on Earth's ecosystems due to climate change becomes more and more evident. This is especially visible at coral reefs. Therefore, a proper understanding of the biophysical mechanisms controlling these ecosystems is required to accurately predict their survival. Such an understanding is also required to develop efficient recovery and protection programs vital to the maintenance of these ecosystems. This leads to the goal of contributing to the survival of corals by developing a biophysical model framework (BMF); a model in which biology and physics meet.

Biodiversity, beauty and corresponding tourist value are not the only reasons to save these ecosystems. There are three more: (1) the protective function of coastal areas; (2) the production of renewable resources; and (3) the fixation of nutrients, carbon and other chemicals. Beside the human benefits of the existence of corals, also a large part of the marine animal kingdom depend on corals and coral reefs. Coral reefs are estimated to host more than 25% of all marine life, while occupying less than one per cent of the ocean floor. This leads to the analogy of coral reefs being aquatic tropical rain forests.

The research on marine ecosystems is relatively young and the phenomenon of coral bleaching is yet to be fully understood. Therefore, there is no comprehensive framework in which the complex interactions between corals and their environment are combined. In this study, a BMF is developed

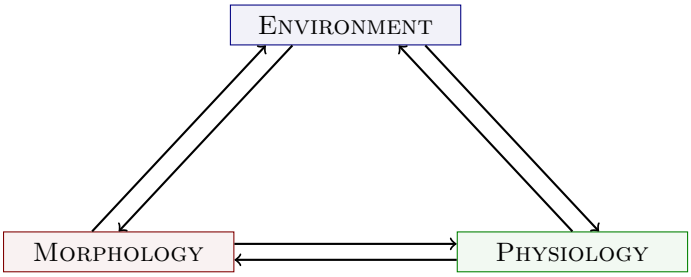

Figure 1: Main items of the feedback loop between corals and their environment. The three main items of the feedback loop are presented in the coloured boxes; and the arrows indicate the interaction between them.

in which four environmental factors are included in a feedback loop with the coral's biology: (1) light; (2) hydrodynamics; (3) temperature; and (4) acidity.

Literature from multiple disciplines is combined to find the interdependencies between corals and their environment. These relations include coral growth, coral bleaching, storm damage, and coral recovery. All these processes are validated if there is sufficient data on the topic. The BMF shows good agreement with the available data.

For the connection with the hydrodynamics, a coupling is made between the biological model developed here and Delft3D Flexible Mesh; a hydrodynamic model. In this coupling, the feedback loop as presented in Figure 1 forms the core. The main focus of liteature lies on two aspects: (1) the effect of the coral structure on the environment, such as the hydrodynamics; or (2) the biological response of the coral to the environment, such as coral bleaching due to thermal stresses. Due to this limited focus only fragments of this feedback loop are covered but never the full cycle. This study closes the feedback loop by including the morphological development of corals.

Because of the inclusion of the morphological development, the developed biophysical model framework (BMF) is a big leap forward in understanding the world of coral reefs, as it is the first construction of a BMF (1) that closes this feedback loop; and (2) including four environmental factors that are leading in the coral development. Nevertheless, more environmental factors play a role in the coral dynamics. Therefore, the framework is constructed such that these can be added relatively easily. Examples of such factors are nutrient concentration and sediment load.

The results of the BMF show compliance with two hypotheses on refugia in the face of climate change: (1) the deep reef refugia hypothesis (DRRH); and (2) the turbid reef refugia hypothesis (TRRH). The first—DRRH—states that damage due to bleaching and storms is reduced for deeper reefs, and so these reefs may form refugia for shallower reefs. The latter—TRRH—states that increased turbidity of the water reduces the damage due to bleaching. The agreement between the BMF and the DRRH is presented in Figure 2, where the model results comply with the hypothesis.

Furthermore, the BMF creates the ability to assess recovery and protection programs; e.g. the susceptibility of coral bleaching can be reduced by diminishing the light-intensity. This is in line with the DRRH and the TRRH. Either via increasing the turbidity, increasing the depth, or a combination of both. Moreover, the BMF encompasses the determination of the bleaching susceptibility of corals based on the temperature history of the specific location; even if there are no corals living at the moment. Hereby, the suitability of certain locations can be assessed to function as refugia. The agreements with the DRRH and the TRRH show the potential of the BMF to aid in the development of protection and recovery programs.

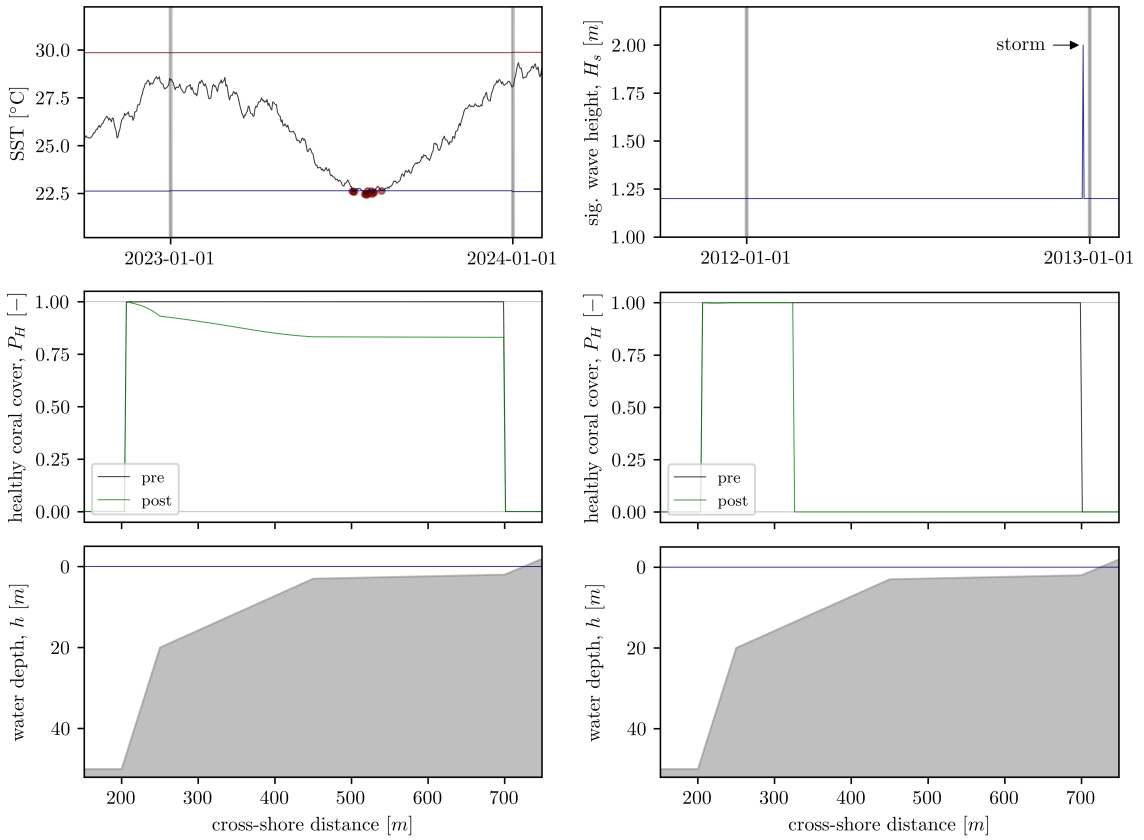

(a) Bleaching. **(b)** Dislodgement.

Figure 2: Spatially varying bleaching and dislodgement responses in correspondence with the deep reef refugia hypothesis. The gray bars in the top plots indicate the moments of pre- and post-stress presented in the lower plots. Bleaching and dislodgement are represented by a reduction in the healthy coral cover, P_H. The bathymetry is presented in the bottom plots. **(a)** The upper plot presents the snapshot of the sea surface temperature (SST) time-series considered, where the lower and upper limits of the thermal range are represented by the blue and red lines, respectively. **(b)** The upper plot presents the hydrodynamic loading given as the significant wave height (H_s), where the storm event is marked.

Finally, an extensive sensitivity study is performed, which gives insight in the key factors determining the coral development. Outcomes of this study indicate that correctly determining the tipping point—for both the occurrence of bleaching and dislodgement—is essential in predicting the long-term development of coral reefs in combination with the recovery of the reef after such an event. In terms of the dislodgement, the coral morphology plays a major role. Contrary to its importance little is known about the coral morphology and its development over time. Therefore, this study presents a set of recommendations that enable the most progress in understanding the coral development. The morphological development is key and grouping the corals by—among others—morphology shows the largest potential for improving the BMF as (1) the damage due to storms is better incorporated in the BMF; and (2) the wide spreading in biological traits of corals can be reduced because different types of corals are partly the reason behind this spreading.

Foreword

In front of you is my thesis that concludes my years as a student at Delft University of Technology. In succession of my bachelor in Civil Engineering, I have been focussing on water in the master Hydraulic Engineering. During my master, my interest in water grew as it is such a fascinating element. I have attended the many facets of water: coasts, rivers, hydrology, renewable energy, estuaria, density currents, etc. No problem can be solved with just one of these facets and knowledge of many helps in finding the best solution. In this final work of my master, I have added an extra topic to this list: marine ecology.

In fact, this study consists for a large portion of an ecological research. The reason for this cross-over is the potential of the combination: ecological hydraulic engineering. Topics as *Building with Nature* and *Nature-based solutions* are gaining more and more momentum, and for good reasons. One of them is the connectivity between ecology and engineering.

The connectivity of ecology and engineering became evident to me after watching a mini-documentary by Chris Agnos: *"How Wolves Change Rivers"*. The fascinating aspect shown is the strong connection between the living and the non-living; so-called biophysics—the study where biology and physics meet. This documentary highlights the effect of wolves on rivers. At first, an unusual connection. However, it makes sense when one follows the logic; I recommend you to watch the mini-documentary of less than five minutes.[2]

The discovery of this connection all started by asking a very important question: *Why?* Why did the rivers change after the reintroduction of wolves? In the face of nature-based solutions, one extra question must be asked: *What if?* What if wolves are reintroduced around other rivers, will this also stabilise those river banks?

Such connections are not rare phenomena. Everyone can find such connections everywhere. All you have to do is look outside and ask the question: *Why?* Become the little child of earlier days, when you kept on asking why things are as they are; up to the moment your parents started answering: *Because I say so!* I have been that little child throughout my study and at the same time the adult trying to give the answers. Although, I have never seeked refuge in the *Because I say so!*-option.

To be able to answer the *What if?*-question, a thorough understanding of the system is necessary; i.e. the *Why?*-question. At the moment, the broad implementation of nature-based solutions is halted by limited knowledge. The complexity of natural processes is not yet fully understood and so

[2]The mini-documentary can be found on the website of Sustainable Human: https://earthmaven.io/sustainablehuman/new-stories/how-wolves-change-rivers-FNwiZckBfEaRPI1PBbJ3mA (retrieved April 7, 2020). The duration is 4:17.

implementation is not without risks. Reducing the uncertainty is the most effective way to promote the philosophy.

It is therefore that I wanted—and still want—to contribute to the acquisition of knowledge on this multidisciplinary topic. In my belief, a topic with great potential. And so, I did. This thesis is a contribution to the knowledge on the complex world of corals and coral reefs. Not quite a low entry level into ecology, due to the complexity of the coral: an animal living in collaboration with marine plankton.

In this study, I have focused mainly on the *Why?*-question: *Why* are corals disappearing under certain environmental conditions, and are they thriving under others? This question is at the basis of my thesis, titled *"Predicting the survival of coral reefs"*.

If you want to make predictions, you have to ask a lot of other *Why?*-questions as well; *Why* are coral reefs degrading? *Why* do corals bleach due to global warming? *Why* should we care about corals dying? This study gives answers to many of those *Why?*-questions. The result is a robust but flexible biophysical model framework. Now we can start asking the next question: *What if?*

Gijs G. Hendrickx
Rotterdam, April 2020

Acknowledgements

This work could not have been realised without the support of others. First of all, the thesis committee for the insightful feedback and for thinking along with me. Peter Herman for your critical reviews on the biological formulations and provision of suggestions on substitutions. Jasper Dijkstra as my daily supervisor for your support in the approach of the study and your critical read-through. Julie Pietrzak for letting me zoom out again and rethink what the purpose of my study was—and is. Arjen Luijendijk for your provision of valuable insights in modelling approaches over large ranges of time-scales, such as with coral growth.

Second, the contacts at United States Geological Survey (USGS): Curt Storlazzi and Lauren Toth. You both provided useful comments on the approach and the model. Also your network helped in the acquisition of data, which is sparse in the field of coral development.

Third, beside the facilities Deltares provided, Bob Smits deserves special mentioning. I am grateful for the many moments you helped in the set up of the hydrodynamic model and the coupling with Python. Also the other graduate students based at Deltares, you have been a great support. I enjoyed the many conversations during the lunch and coffee breaks. Especially the ones in which the topics did not align with the thesis subjects.

Fourth, the many researchers around the world who have been more than willing to provide data, explanations, discussions and other interesting papers on the topic: Fuad Al-Horani, Andrew Baird, Michael Colella, Simon Donner, Christian Evenhuis, Peter Edmunds, Emily Howells, Jaap Kaandorp, Joshua Madin, Rob Ruzicka and Shay Viehman. You all showed great interest in the study. It is your acknowledgement of the benefit and potential of my study, that motivated me to continue; it showed me the relevance of my study. Also special thanks goes to the National Oceanic and Atmospheric Administration (NOAA) for their freely available data sets.

Last but not least, my parents. You both supported me in your own way. Dad, I owe you for the many evening and weekend hours you spent on reading the drafts and provide them with lots of comments. Mom, thank you for your concern on my mental well-being. You made sure that I slept enough and did not forget to take breaks.

Thank you all!

Contents

Appendix

List of Figures

List of Tables

List of Symbols

Latin symbols

a_c	axial distance between corals	$[m]$
a_f	wave-orbital motion	$[m]$
a_p	absorptivity of the coral	$[-]$
A_S	suitable substratum for coral colonisation	$[m^2 m^{-2}]$
B_c	coral biomass	$[m^2]$
b_c	diameter of the base of the coral	$[m]$
C_b	non-vegetated bottom Chèzy coefficient	$[m^{1/2} s^{-1}]$
C_d	drag coefficient	$[-]$
C_f	friction coefficient	$[-]$
C_m	inertia coefficient	$[-]$
C_{sp}	species constant	$[-]$
C_s	Smagorinsky coefficient	$[-]$
C_v	vegetation-based Chèzy coefficient	$[m^{1/2} s^{-1}]$
$\langle d_c \rangle$	representative coral diameter	$[m]$
D	diffusion coefficient	$[m^2 s^{-1}]$
d_c	diameter of the plate of the coral	$[m]$
d_c	larval diameter	$[m]$
E_a	activation energy	$[J\ mol^{-1}]$
f_w	wave-energy dissipation factor	$[-]$
$\dot{G}$	calcification rate	$[kg\ s^{-1} m^{-2}]$
g	gravitational acceleration ($g = 9.81\ ms^{-2}$)	
g_C	calcification constant	$[kg\ s^{-1} m^{-2}]$
h	water depth	$[m]$
h_c	coral height	$[m]$
H_s	significant wave height	$[m]$
$\langle I_z \rangle$	biomass-averaged light-intensity, or representative light-intensity	$[mol$ photons $m^{-2} s^{-1}]$
I_0	incoming solar radiation	$[mol$ photons $m^{-2} s^{-1}]$
I_k	saturation light-intensity	$[mol$ photons $m^{-2} s^{-1}]$
$I_k^{\max}$	maximum steady-state saturation intensity	$[mol$ photons $m^{-2} s^{-1}]$
I_k^S	quasi-steady saturation light-intensity	$[mol$ photons $m^{-2} s^{-1}]$
I_z	light-intensity at depth z	$[mol$ photons $m^{-2} s^{-1}]$
K	carrying capacity	$[m^2 m^{-2}]$
k	thermal conductivity	$[J m^{-1} s^{-1} K^{-1}]$
K_0	thermal species constant	$[-]$
K_0^*	solubility constant of carbon dioxide	$[mol\ kg^{-1} atm^{-1}]$
K_1^*	first stoichiometric equilibrium constant of carbonic acid	$[-]$
K_2^*	second stoichiometric equilibrium constant of carbonic acid	$[-]$
K_a'	stoichiometric solubility product	$[mol^2 kg^{-2}]$
K_d	light-attenuation coefficient of photosynthetically active radiation	$[m^{-1}]$
k_s	roughness length	$[m]$
$\mathbf{L}_c$	vector morphological dimensions ($\mathbf{L}_c = [d_c\ h_c\ b_c\ t_c\ a_c]$)	$[m]$
L	base height receiving light	$[m]$
L_d	drag length-scale	$[m]$
L_s	shear length-scale	$[m]$
N_c	stems density	$[\text{stems}\ m^{-2}]$
N_l	number of released coral larvae due to mass spawning	[larvae]
$\mathbf{P}$	vector population state of coral ($\mathbf{P} = [P_H\ P_R\ P_P\ P_B]$)	$[m^2 m^{-2}]$
Pr	Prandtl-number ($\text{Pr} = \nu/\alpha$)	
p	water pressure	$[Nm^{-2}]$
$P(I)$	photosynthetic light dependency	$[-]$
$P(I,T,u)$	photosynthesis (proxy) as function of light, temperature and flow ($P(I,T,u) = P(I) \cdot P(T) \cdot P(u)$)	$[-]$
$P(T)$	photosynthetic thermal dependency	$[-]$
$P(u)$	photosynthetic flow dependency	$[-]$
$P_{\max}$	maximum photosynthetic rate (proxy)	$[-]$
$P_{\max}^{\max}$	maximum steady-state maximum photosynthetic rate (proxy)	$[-]$
$P_{\max}^S$	quasi-steady maximum photosynthetic rate (proxy)	$[-]$
P_B	bleached coral cover	$[m^2 m^{-2}]$
P_D	dead coral cover	$[m^2 m^{-2}]$
$P_G^{\max}$	maximum gross photosynthesis	$[mol\ O_2\ m^{-2} s^{-1}]$

P_H	healthy coral cover	$[m^2 m^{-2}]$
P_N	net photosynthesis	$[mol\ O_2\ m^{-2} s^{-1}]$
P_P	pale coral cover	$[m^2 m^{-2}]$
P_R	recovering coral cover	$[m^2 m^{-2}]$
p_s	probability of settlement of coral larvae	$[-]$
P_T	total living coral cover	$[m^2 m^{-2}]$
$P_u^{\min}$	minimum flow-induced photosynthetic efficiency	$[-]$
$\overline{R}$	gas constant ($\overline{R} = 8.31446261815324\ JK^{-1}mol^{-1}$)	
R	dark respiration	$[mol\ O_2\ m^{-2} s^{-1}]$
r_δ^+	wall-coordinate of the velocity boundary layer	$[-]$
r_B	bleaching rate	$[s^{-1}]$
r_f	form ratio; height-to-diameter ratio of coral morphology	$[-]$
r_G	growth rate	$[s^{-1}]$
r_M	mortality rate	$[s^{-1}]$
r_p	plate ratio; base-to-width and thickness-to-height ratio of coral morphology	$[-]$
r_R	recovery rate	$[s^{-1}]$
r_s	spacing ratio; diameter-to-axial distance ratio of coral morphology	$[-]$
Re	Reynolds-number ($\mathrm{Re} = (ud)/\nu$)	
S	salinity	$[PSU]$
$s_{c,l}$	lateral distance between two consecutive corals	$[m]$
$s_{c,s}$	streamwise distance between two consecutive corals	$[m]$
s_c	spacing between corals	$[m]$
s_d	dislodgement surviving fraction	$[-]$
S_P	potential coral recruitment contribution to the healthy coral cover	$[m^2 m^{-2}]$
S_V	potential coral recruitment contribution to the coral volume	$[m^3]$
Sc	Schmidt-number ($\mathrm{Sc} = \nu/D$)	
ΔT	thermal range of corals	$[K]$
ΔT_c	increase in coral temperature relative to the ambient temperature	$[K]$
T_c	coral temperature	$[K]$
t_c	thickness of the plate of the coral	$[m]$
T_{hi}	upper limit of the thermal range of corals	$[K]$
T_{lo}	lower limit of the thermal range of corals	$[K]$
T_{opt}	optimal temperature for calcification	$[K]$
T_p	peak wave period	$[s]$
T_w	water temperature	$[K]$
u_*	shear velocity	$[ms^{-1}]$
u_b	bulk flow velocity	$[ms^{-1}]$
u_{cm}	wave-current in-canopy flow velocity	$[ms^{-1}]$
u_{cr}	critical flow velocity	$[ms^{-1}]$
u_c	constricted in-canopy flow velocity	$[ms^{-1}]$
u_f	above-canopy flow velocity	$[ms^{-1}]$
u_m	wave-current flow velocity	$[ms^{-1}]$
u_p	porous in-canopy flow velocity	$[ms^{-1}]$
u_w	wave-orbital velocity	$[ms^{-1}]$
V_c	coral volume	$[m^3]$

Greek symbols

α	thermal diffusivity	$[m^2 s^{-1}]$
α_c	unidirectional limit of wave-attenuation coefficient	$[-]$
α_i	inertial limit of wave-attenuation coefficient	$[-]$
α_w	wave-attenuation coefficient	$[-]$
β_I	steady-state exponent of saturation intensity	$[-]$
β_P	steady-state exponent of maximum photosynthetic rate (proxy)	$[-]$
$\gamma(\Omega_a)$	aragonite dependency	$[-]$
δ	thickness velocity boundary layer	$[m]$
δ_c	thickness diffusion boundary layer	$[m]$
δ_t	thickness thermal boundary layer	$[m]$
ζ	optical depth	
θ_I	spreading of light	$[^\circ$ or $rad]$
ι	acclimation exponent	$[s^{-1}]$
κ	von Kármán constant ($\kappa = 0.41$)	
κ_a	measure of the half-rate of the aragonite dependency	$[-]$
λ_f	frontal λ-parameter; frontal area over coral's footprint	$[-]$
λ_p	planar λ-parameter; planar area over coral's footprint	$[-]$
ν	kinematic viscosity of water	$[m^2 s^{-1}]$
ρ	density of water	$[kg\ m^{-3}]$
ρ_c	density of coral skeleton	$[kg\ m^{-3}]$
σ_t	tensile strength of substratum	$[Nm^{-2}]$
Φ	vegetation density	$[\text{stems}\ m^{-1}]$
ϕ	angle between wave-induced and current-induced flow velocities	$[^\circ$ or $rad]$
χ_f	overall proportionality constant of the form ratio	$[-]$
$\chi_{p,u}$	flow proportionality constant of the plate ratio	$[-]$
χ_p	overall proportionality constant of the plate ratio	$[-]$
$\chi_{s,I}$	light proportionality constant of the spacing ratio	$[-]$
$\chi_{s,u}$	flow proportionality constant of the spacing ratio	$[-]$
χ_s	overall proportionality constant of the spacing ratio	$[-]$
ω	wave frequency	$[s^{-1}]$
Ω_0	aragonite solubility state	$[-]$
Ω_a	aragonite saturation state	$[-]$

Chapter 1

Introduction

Corals are animals; colonial, sessile polyps. That means that corals consists of multiple polyps living in a colony—a so-called coral colony—and they are attached to a surface. The coral forms a hard skeleton of calcium carbonate ($CaCO_3$)—often called aragonite—to protect itself. Constructing this skeleton costs a lot of energy and so the coral is engaged in a mutual collaboration with photosynthetic organisms; so-called zooxanthellae. This collaboration is called a symbiosis as both parties benefit from it. Figure 1.1 shows an assemblage of different coral species to illustrate the high diversity and the complexity.

Figure 1.1: Photograph of different coral species. Credit: Nichole Price, Bigelow Laboratory for Ocean Sciences.

1.1 Problem statement

The increasing pressure on Earth's ecosystems due to climate change becomes more and more evident [e.g. Scheffer et al., 2001; Walther et al., 2002]. These pressures are especially visible at coral reefs [Hoegh-Guldberg et al., 2007; Hughes et al., 2003, 2019]. Worldwide, there is a massive reduction in coral cover due to the effects of climate change [e.g. Hoegh-Guldberg, 1999].

Because of climate change, coral reefs are more susceptible to bleaching, which may result in the death of corals [e.g. Hoegh-Guldberg, 1999; Riegl and Purkis, 2009]. The main driver of the bleaching of corals is the temperature [e.g. Lesser, 2011], but it is influenced by multiple environmental factors. The four aspects of climate change that have the most pronounced impact on the well-being and the growth of corals are:

Sea-level rise Due to sea-level rise (SLR), the depth at which the coral colonies are situated is affected. This water depth influences the light-intensity for photosynthesis, which enhances the calcification rate of corals. The hydrodynamics are also influenced by SLR; the water depth affects the flow velocity and the breaking of waves.

Global warming The health of corals is substantially influenced by global warming [e.g. Hoegh-Guldberg et al., 2007]. Corals survive in a species-dependent thermal range and a long-term stay outside this range will result in coral bleaching, which may lead to death. Global warming is highly correlated with the increased concentrations of atmospheric carbon dioxide (CO_2) and other greenhouse gasses.

Storm intensity and frequency The intensity and frequency of extreme weather events will increase due to climate change. Such events increase the hydrodynamic loads on coral reefs, which can result in increased dislodgement and breakage of coral colonies. When the damage due to frequent storms outweighs the capability of recovery, the reef will not survive.

Ocean acidification Increased CO_2 concentrations in the atmosphere are directly related to their concentrations in the water, which affects the *p*H of water. This negatively influences the calcification of corals and thereby their growth. The increase of CO_2 concentrations in the oceans is known as ocean acidification (OA) in the literature on climate change.

The combinations of the four aspects are important because they can positively as well as negatively influence the health of coral reefs; e.g. higher temperatures in combination with increased light-intensity result in more coral bleaching compared to the individual stressors [e.g. Jokiel and Coles, 1977].

The importance of coral reefs is not only based on ecology, but on human lives as well. Nowadays, around 90% of the people live in coastal regions [Lincke and Hinkel, 2018] and SLR can result in the displacement of hundreds of millions of people [Hinkel et al., 2014; Nicholls et al., 2011]. This number does not include the effects of the reduction in coral cover as coastal protection, and so can rise when the degradation of coral reefs is taken into account. Globally, millions of people are protected by coral reefs due to wave dissipation [Harris et al., 2018]. This significant reduction in wave forcing on the shoreline is of major importance, as the damage to reef-protected areas would double when these coral reefs are no longer present [Beck et al., 2018].

Furthermore, the daily life of many people depends on coral reefs. The three most important service contributions of coral reefs beside the protection of the shoreline are (1) the provision of renewable resources such as fisheries; (2) the fixation of nutrients and other chemicals such as CO_2; and (3) the opportunities for tourism and leisure [Moberg and Folke, 1999; Principe et al., 2012].

1.2 Research objective

The goal of this research is to contribute to the survival of corals. To achieve this goal, a biophysical model framework (BMF) is developed. Here, biological and physical processes are brought together. In a BMF the interactions and dependencies between the two are assessed as well, which are otherwise enforced or assumed constant; i.e. a biophysical model includes the feedback loop between organisms and the environment. Two concrete contributions can be realised with such a BMF:

1. This BMF enables the opportunity to test protection and recovery programs in advance. The BMF serves as a tool for the development of these programs for coral reefs. It gives more insight in the complex world of corals and coral reefs.
2. This BMF enables selecting the most promising research objectives on coral development. The key aspects on the well-being and survival of corals are found by performing sensitivity analyses with this BMF. As time is running out fast for corals if the status quo is maintained, these analyses form a guideline on the allocation of the limited resources and time towards the low-hanging fruits in the undiscovered world of coral reef biophysics.

This study entails the development of the biophysical model framework (BMF) in an attempt to answer the following research question:

How can the biophysical interactions between corals and the environment be modelled?

Multiple disciplines are brought together to define the biophysical interactions between corals and their environment. These descriptions are largely based on literature. The study focusses on (1) the implementation of the many relations found in literature; (2) filling the missing links between different processes; and (3) the translation from concepts and relations into a model framework. From this main question, four sub-questions arise that guide in answering this research question:

1. What are the biological characteristics of corals?
2. What are the components of the feedback loop between the coral and its environment?
3. What are the biophysical interactions between corals and their environment?
4. What are the main biophysical interactions determining the coral development?

1.3 Scope of the research

This research does not cover all aspects of the complex interactions between corals and their environment because (1) not all aspects are fully understood nor have reached consensus among the academics; (2) there is no existing biophysical model framework (BMF) to continue on and so only the main aspects are included in this study due to time-limitations; and (3) simplifications are used to improve model efficiency, i.e. reduce computational time. The scope of this study is listed below:

1. The BMF comprises four environmental factors: (1) light; (2) temperature; (3) hydrodynamics; and (4) acidity. The latter is included by using the aragonite saturation state, which is a proxy of the effects of the full oceanic carbon system. This system describes the intertwined relations between the atmospheric carbon dioxide (CO_2) concentration and the acidity of the ocean waters. The BMF requires the need of an iterative pH model to include the full oceanic carbon system. This substantially increases the computational time and also adds to the amount of input parameters needed.

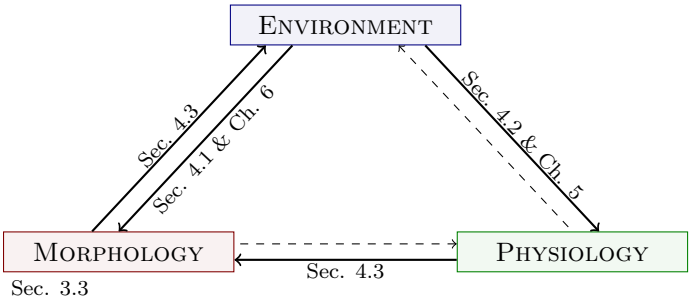

Figure 1.2: Main items of the feedback loop between corals and their environment. Solid arrows are interactions included in this study; dashed arrows are not included in this study. The chapters and sections in which the content is elucidated are added to the arrows and the subject of the coral morphology.

2. The growth of corals is based on the energy surplus produced due to photosynthesis, which is called light-enhanced calcification (LEC). It assumes that the magnitude of the calcification rate is linearly related to the magnitude of the photosynthetic rate and that the energy supply originating from photosynthesis is key for the coral's development. More details on the LEC are given in Section 2.3.
3. The determination of the in-canopy flow is based on linear wave theory, which is applicable for small wave heights compared to the water depth and the wave length. Even though this criterion is not always met, it gives a good first estimation of the attenuation of waves and flow inside the canopy.

1.4 Contribution of the research

The goal of this study is to contribute to the survival of corals (*see* Sec. 1.2) by developing a biophysical model framework (BMF) about corals. The coupling between biological and physical processes on coral reefs makes this study unique. The complex feedback loop between corals and their environment forms the core of this study (*see* Fig. 1.2).

This feedback loop between the corals and their environment consists of three main subjects: (1) environment; (2) physiology; and (3) morphology (*see* Fig. 1.2). The physiology describes the biological processes such as photosynthesis and calcification, and the morphology describes the structure of the coral colony and its development. The connections from the morphology to the environment and from the environment to the physiology are relatively well-established fields of research. The connection from the environment to the morphology has recently been studied. Contrary to this research, it only focusses on the damage due to storms instead of taking normal conditions into account.

To close the feedback loop between corals and their environment, the coral morphology plays a crucial role. The coral morphology mainly determines the coral (micro-)environment, which in turn affects the physiology. Nevertheless, limited research has been performed on this aspect of the feedback loop. The incorporation of this aspect in the coral dynamics is new, but essential.

The aim is to develop a robust biophysical model framework (BMF), which is (mainly) process-based to enables broad usage. This framework forms the basis to which more aspects of coral development can be added, as the study of corals is relatively young. The BMF has to be both robust and flexible. Only then a BMF has the potential to (1) be used independent of the location; (2) make predictions

within the accuracy of the input data; and (3) give insight in the complex interactions defining the feedback loop between the coral and its environment.

To demonstrate the potential of the developed BMF, the similarities between the results of the BMF and two hypotheses on the coral survival in the face of climate change are assessed: (1) the deep reef refugia hypothesis (DRRH); and (2) the turbid reef refugia hypothesis (TRRH). In short: the DRRH states that deep reefs may serve as refugia for shallow reefs under climate change; and the TRRH states that turbid reefs can serve as refugia in the face of climate change. Section 2.5 goes more into depth on these hypotheses and discusses the reasoning behind them.

1.5 Thesis outline

This report follows the standard structure: (1) introduction; (2) methods; (3) results; (4) discussion; (5) conclusions and recommendations. The part on the methods is most extensive in this study as it encompasses the description of the biophysical model framework (BMF). After the introduction, first the biophysical framework is described in Chapter 2. Here, the biophysical mechanisms are introduced and qualitatively discussed. Next, the model framework is presented (Ch. 3), which forms the basis of this study. The methods conclude with the descriptions of the biophysical relations and their implementation in the BMF (Chs. 4 to 6). The biophysical relations are largely based on literature, which is translated into the model framework. Certain simplifications are inevitable and an attempt is made to reduce the amount of parameters as much as reasonably possible.

The first two aforementioned sub-questions (*see* Sec. 1.2) are covered in the first two chapters: Chapters 2 and 3, respectively. Chapters 4 to 6 are dedicated to answering the third sub-question. The translation from the formulations as given in Chapters 4 to 6 into the model framework is provided in Appendix A, which contains the numerical schemes applied.

The presentation of the results is twofold because of the limited availability of data. Verification and validation of the BMF is performed where possible (Ch. 7). However, as the research on marine ecosystems is still relatively young, there is no data available on all. Therefore, an extensive sensitivity analysis is included to answer the last sub-question (Ch. 8)—also for the verified and validated modules of the framework. This sensitivity analysis gives insight in the low-hanging fruit with large opportunity for further research.

The report concludes with a discussion of the results and the BMF itself in Chapter 9. This discussion forms the basis of Chapter 10 in which conclusions and recommendations are drawn. The presented structure is summarised in Figure 1.3.

Finally, after the bibliography, a glossary is included due to the multidisciplinary character of this research. The disciplines of biology and physics have a leading role, but also certain aspects of chemistry are included.

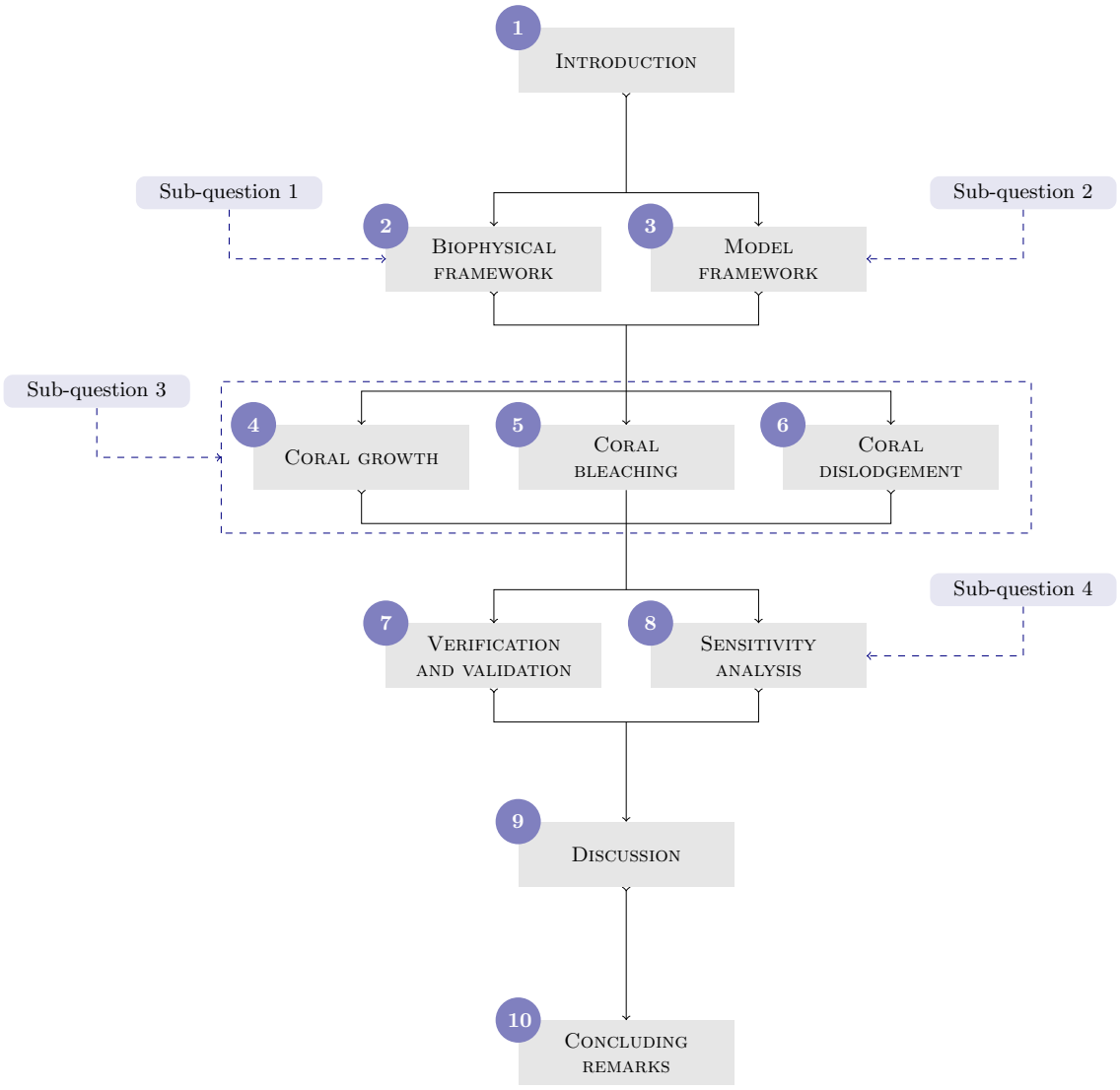

Figure 1.3: Thesis outline. This report follows the standard structure in which the part on the methods is extended due to the description of the biophysical model framework.

Chapter 2

Biophysical framework

The interactions between corals and their environment are very complex due to (1) the coral's dependency on many environmental factors; and (2) the coral's symbiosis with zooxanthellae, which are photosynthetic organisms. The two are related as the dependency of corals on their symbionts—i.e. zooxanthellae—results in the inclusion of more environmental dependencies.

Furthermore, corals can die due to environmental stressors following two pathways: (1) coral bleaching; and (2) coral dislodgement. The first is based on biochemical processes, and the latter is due to mechanical stresses. As the principle of coral dislodgement is straightforward, it is not further elaborated on here. However, the principle behind coral bleaching is not as plain since there is no full consensus on the leading mechanisms.

This chapter starts with an introduction into coral reefs and corals in which the basics and some essential terms are introduced (Secs. 2.1 and 2.2, resp.). The first focusses on the large scale—i.e. reef scale—and the latter zooms in on the coral animal and its symbiosis with the zooxanthellae. In continuation of this symbiosis, two essential biochemical mechanisms are further highlighted: (1) light-enhanced calcification (LEC) in Section 2.3; and (2) coral bleaching in Section 2.4. Finally, in line with the biophysics of corals and coral reefs, two hypotheses are introduced in Section 2.5: the deep reef refugia hypothesis (DRRH) and the turbid reef refugia hypothesis (TRRH). Both are getting more attention in the face of climate change and are assessed in this study as well.

2.1 Introduction into coral reefs

This study focusses on coral reefs and their interaction with the environment, which is limited to the interactions with hermatypic coral. This type of corals construct the hard, calcareous substrates that form the rigid structure of the coral reef. Other coral species—that do not contribute to the framework of the reef—are not included. Hereby, the definition of a coral reef as given by Done [2011a] is used:

> A tract of corals growing on a massive, wave-resistant structure and associated sediments, substantially built by skeletons of successive generations of corals and other calcareous reef-biota.

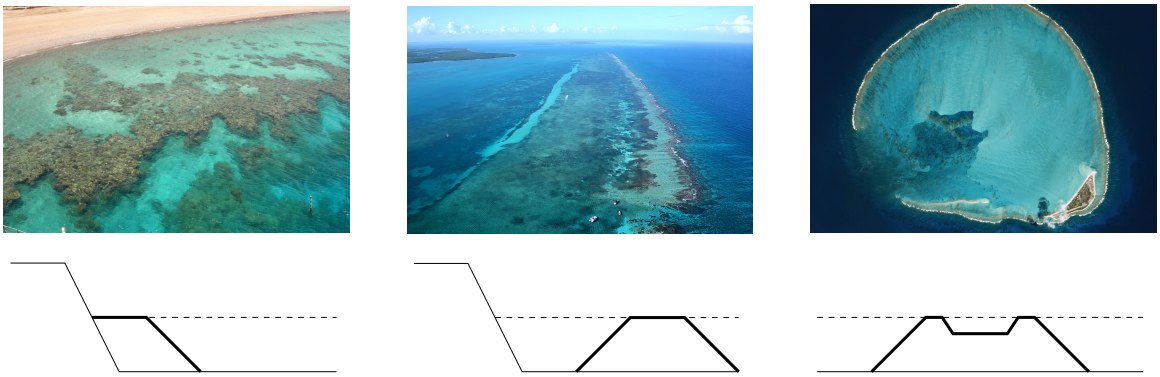

(a) Fringing reef.
Photo credit: Mark A. Wilson.

(b) Barrier reef.
Photo credit: Lars Ruecker.

(c) Atoll.
Photo credit: USGS.

Figure 2.1: Schematisations of three types of coral reefs. The most distinct types of reefs are presented: **(a)** fringing reef; **(b)** barrier reef; and **(c)** atoll. Thin, black lines represent bed level; thin, dashed lines represent water level; and thick, black lines represent the coral reef formation.

Coral reefs come in different formations, where many classifications have been made in which the development of the coral reef plays a central role [Darwin, 1842; Fairbridge, 1950; Hopley, 1982; Maxwell, 1968]. The most concise classification consists of three reef types:

Fringing reef A fringing reef is defined as a reef that grows very close to the shore and is generally attached to the shore. There are cases where a small submerged back reef is present (*see* Fig. 2.1a). [Smithers, 2011]

Barrier reef A barrier reef—also known as ribbon reef—is separated from the shoreline by a lagoon and looks like a (submerged) offshore breakwater (*see* Fig. 2.1b). [Andréfouët and Cabioch, 2011]

Atoll An atoll is a ring-shaped reef of which the outer edges are commonly near mean sea level and protect the inner platform against hydrodynamic loads (*see* Fig. 2.1c). [Woodroffe and Biribo, 2011]

The general geomorphic reef zonation includes four parts of the coral reef: (1) reef slope; (2) reef front; (3) reef flat; and (4) reef lagoon [Blanchon, 2011]. These four zones are visualised in Figure 2.2. Note that in the case of a fringing reef, there is no clear lagoon behind the reef flat; in case of a barrier reef, there is a land mass at the other side of the lagoon; and in case of an atoll, the lagoon in enclosed by reef flats at both sides.

Furthermore, the reef front is the zone with the highest hydrodynamic loads, where almost all of the wave breaking occurs due to the steep slope [Cabioch, 2011; Hearn, 1999; Lugo-Fernández and Roberts, 2011]. The wave-energy is further attenuated by the reef flat [Ferrario et al., 2014; von Arx, 1948].

Even though the corals in the Atlantic ocean are often said not to be real corals—because they are commonly attached to other structures [Bosboom and Stive, 2015]—they are seen as real corals in this study. This terminology is based on the evolution of the reef, and it is not based on its physical character.

Coral reefs are often classified as complex and rich ecosystems in which there is close interaction between the living and non-living [Stoddart, 1969]. Coral colonies are a perfect example of this

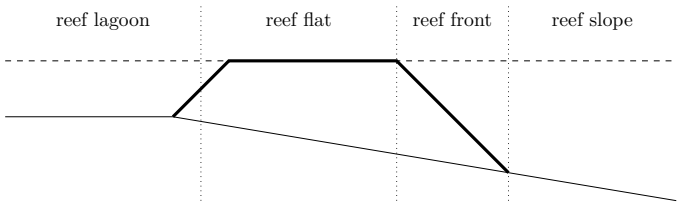

Figure 2.2: Schematisation of the general geomorphic zonation. Thin, black lines represent bed level; thin, dashed lines represent water level; thick, black lines represent the coral reef; and dotted lines represent the zonation.

behaviour, where the hermatypic corals construct the structure of the coral reef via calcification. These hard, limestone structures provide habitats for marine life. This complex interaction results in the most diverse marine habitats, but is also susceptible to changes and thus is a fragile and endangered ecosystem [Spalding et al., 2001]. Coral reefs are more than once named the tropical rain forests of the marine world, due to their ecological complexity and diversity [Brown et al., 2002], and their high biological productivity [Hatcher, 1988].

Furthermore, coral reefs are very efficient in dissipating wave energy and thereby function as natural (submerged) breakwaters [von Arx, 1948]. Already a narrow reef flat has substantial impact on the waves; the first 150 metres reduce 50% of the incoming wave energy. This can build up to 97% for longer flats, where on average 84% of the wave height is attenuated [Ferrario et al., 2014].

2.2 Introduction into corals

The coral animal itself is a colonial, sessile polyp; the coral consists of multiple polyps living in a colony—a coral colony—and is attached to a surface [Veron, 2011]. A coral creates the calcareous skeleton to be resistant against the wave forces [Veron, 2011]. Even though corals are hunting animals, most of their energy supply originates from the symbiosis with zooxanthellae [Anthony and Fabricius, 2000]. These photosynthetic organisms produce photosynthate—of which 95% is transferred to the coral host [Done, 2011b]—and get protection of the coral skeleton in return [Jokiel, 2011b; Nakamura et al., 2005].

This symbiosis between the coral and the zooxanthellae results in complex interactions between the coral-zooxanthellae symbiont and their environment. The best known environmental dependencies are (1) light [e.g. Anthony and Hoegh-Guldberg, 2003a; Graus and Macintyre, 1976; Kaniewska et al., 2011]; (2) temperature [e.g. Al-Horani, 2005; Evenhuis et al., 2015; Jokiel and Coles, 1977]; (3) flow [e.g. Finelli et al., 2006; Jimenez et al., 2011; Hearn et al., 2001]; (4) acidity [e.g. Buddemeier et al., 2008; Jokiel, 2011b]; (5) nutrient availability [e.g. Atkinson and Bilger, 1992; Holcomb et al., 2012; Langdon and Atkinson, 2005]; and (6) sediment concentration [e.g. Erftemeijer et al., 2012; Storlazzi et al., 2015].

To add to the complexity, many of these environmental factors are intertwined—linearly as well as non-linearly. For example, the acidity of the water relates to the oceanic carbon chemistry, which is influenced by the temperature, amongst others [Mucci, 1983]; and the nutrient availability is highly dependent on the flow conditions as advective transport is substantially faster than diffusive transport.

Furthermore, the biochemical processes related to the calcification and the acidity are complex and not fully understood [Allemand et al., 2004; Goreau, 1959; Jokiel, 2011a,b; McConnaughey and

Whelan, 1997; Schneider and Erez, 2006a]. Therefore, the influence of the acidity is commonly based on the relation between the aragonite saturation state and the calcification rate, which is a more established method [e.g. de Putron et al., 2011; Marubini et al., 2001; Ries et al., 2010].

2.3 Light-enhanced calcification

The enhancement of the calcification rate in light is an established principle [e.g. Goreau, 1959; Moya et al., 2006] and is called light-enhanced calcification (LEC). This enhancement is related to the photosynthetic rate of the zooxanthellae housed in the coral skeleton [e.g. Anthony and Hoegh-Guldberg, 2003b; Al-Horani, 2005; Jokiel, 2011b; Nakamura et al., 2005]. Thereby, an increased photosynthetic production results in an increased calcification rate and the two commonly show comparable dependencies on environmental factors [e.g. Dennison and Barnes, 1988; Mass et al., 2007; Moya et al., 2006; Strahl et al., 2019].

As the light-enhanced calcification (LEC) is substantially larger than the dark calcification rate [e.g. Al-Horani et al., 2007; Moya et al., 2006; Strahl et al., 2015, 2019], the LEC is considered dominant and the leading mechanism. Therefore, the calcification rate is a function of the photosynthetic rate and so of all the environmental factors affecting the photosynthesis.

2.4 Coral bleaching

Coral bleaching is the process in which the symbiosis between the coral host and their symbiotic zooxanthellae is broken down due to environmental stress [Carilli et al., 2012]. The exact mechanism of coral bleaching is still under debate. This study follows the Oxidative Theory of Coral Bleaching, which states that coral bleaching is caused by the expel of zooxanthellae due to overproduction of oxygen, and thereby reactive oxygen species (ROS) [Lesser, 1997; Nielsen et al., 2018]. The production of ROS during photosynthesis is common [Baird et al., 2009a; Rehman et al., 2016]. At normal photosynthetic rates, the organism produces enough defences to counteract the toxicity and to keep it below critical levels [Lesser, 2006]. When the coral cannot produce enough defences against the ROS, it expels the zooxanthellae [Baird et al., 2009a] which are the producers of the toxic. Thereby, the coral host reduces the concentration of ROS.

However, by expelling the zooxanthellae, the symbiosis is disrupted and the coral will die when these disruptive environmental conditions will prolong [Nielsen et al., 2018]. The expulsion of the zooxanthellae results in the removal of the coral's essential energy suppliers [Anthony, 2000; Done, 2011b] and results in an energy deficit.

Furthermore, the occurrence of bleaching is fully related to the thermal conditions, but other stressors can reduce the resistance of the coral-zooxanthellae to bleaching [Carilli et al., 2012]; other stresses reduce the 'immune system' of the symbiont and so it becomes more susceptible to bleaching. Such stresses are light-intensity, nutrient run-off, sedimentation, overfishing and ocean acidification (OA) [Jokiel and Coles, 1977; Carilli et al., 2010; Wooldridge, 2009; Anthony et al., 2007, 2008]. As these stresses interact with the temperature, they modify the bleaching threshold and/or severity.

2.5 Reef refugia hypotheses

The deep reef refugia hypothesis (DRRH) is gaining increasing support [Lesser et al., 2009; Bongaerts et al., 2010, and references therein] and was first pioneered by Glynn [1996]. According the DRRH, deep reefs form an essential refugia for shallow reefs in the face of climate change [Glynn, 1996;

Hughes and Tanner, 2000; Lesser et al., 2009]. Deep reefs are defined as being at great depth, but remain light dependent [Bongaerts et al., 2010]. This is often characterised as the depth-range of 30 metres up to the euphotic depth. Until 30 metres water depth, a reef is defined as shallow. Deep reefs are also called mesophotic reefs due to the reduced light-intensity.

This reduced light-intensity is suggested to be one of the major reasons that deep reefs can form refugia for the shallow reefs, as thermal stresses leading to bleaching are exacerbated by light [Jokiel and Coles, 1977]. As light is attenuated down the water column, bleaching severity is higher in shallow reefs [Vermeij and Bak, 2002; Wilkinson and Souter, 2008]. This finding has also led to the hypothesis that increasing the turbidity protects the corals against severe bleaching [Cacciapaglia and van Woesik, 2015, 2016; Perry et al., 2012; Santodomingo et al., 2016; Van Woesik et al., 2012]; i.e. the turbid reef refugia hypothesis (TRRH).

Beside the reduced thermal stresses—and so reduced damage due to bleaching—deep reefs are also less damaged by tropical storms due to reduced flow velocity at depth [Bongaerts et al., 2010; Lesser et al., 2009]. However, indirect storm damage—e.g. debris avalanches and sedimentation—can result in substantial damage to the deep coral reef [Bak et al., 2005; Dollar, 1982].

The deep reefs can contribute to the recovery of shallow reefs as recruitment source after bleaching and storm events [Hughes and Tanner, 2000; Lesser et al., 2009]. However, their effective contribution is questioned due to the connectivity between deep and shallow reefs and the suitability of deep reef coral species to colonise shallow reefs [Bongaerts et al., 2010].

Furthermore, deep reefs are not totally free of stresses. The cool upwelling waters that are present at certain deep reefs reduce the heat stress [Bak et al., 2005; Lesser et al., 2009], but can also result in cold water bleaching. Moreover, deep reefs are more susceptible to drowning as a result of sea-level rise (SLR) [Cooper et al., 2008]. This susceptibility increases in combination with other threats associated with climate change, such as global warming and ocean acidification (OA), whereas these processes reduce the calcification rate [Bongaerts et al., 2010].

Moreover the turbid reef refugia hypothesis (TRRH), beside the protective function of the turbidity—reducing the light-intensity—there are also downsides to the increased turbidity. The main disadvantage is the possible smothering of corals due to the increased sediment concentrations [Dubé et al., 2017; Smith and Hughes, 1999; Wilkinson and Souter, 2008]. Furthermore, the hydrodynamic loading remains the same on a turbid, shallow reef and so there is no reduced damage due to storms.

On the other hand, high sediment concentrations may enhance the survival of corals by providing more other food resources by which the coral relies less on the photosynthetic energy supply [Anthony and Fabricius, 2000; Anthony et al., 2007]. When corals are less dependent on their zooxanthellae, expulsion of them due to thermal stresses becomes less decisive. Thereby, corals may thrive in turbid waters [Cacciapaglia and van Woesik, 2016; Perry et al., 2012; Santodomingo et al., 2016], which is in contradiction with previous thoughts [Kleypas and Eakin, 2007, and references therein].

All in all, the interesting findings underlying the deep reef refugia hypothesis (DRRH) are twofold (1) bleaching severity reduces with increasing attenuation of light; and (2) storm damage reduces with increasing depth. The first also underlies the turbid reef refugia hypothesis (TRRH). The increasing attenuation of light is a combination of the turbidity of the water and the depth. This results in the possible protection of corals due to a high turbidity [Van Woesik et al., 2012]. The other aspects of the DRRH and the TRRH are not part of the processes included in the biophysical model framework (BMF) developed in this study.

Chapter 3

Model framework

The aim of this chapter is to provide the model framework of the biophysical model framework (BMF) of which the biophysics are discussed in more detail in Chapters 4 to 6. It starts with an overview and the main steps taken in Section 3.1 after which the time-scales are elaborated on in Section 3.2. The latter is of importance due to the difference in time-scales of the environmental conditions in combination with the slow growth of corals. Finally, the morphological representation of the corals is presented in Section 3.3.

3.1 Model design

The structure of the biophysical model framework (BMF) consists of three phases: (1) the environment; (2) the physiology; and (3) the morphology. These phases are further subdivided in various processes, as visualised in Figure 3.1.

The main interactions between the phases and processes are:

- The temperature at the coral is a function of all environmental factors except the acidity. It is this "feeling" temperature that is used for further calculations.
- The photosynthesis is given as function of the light, thermal and flow conditions describing the photosynthetic efficiency based on these environmental factors. Based on these forcings, the photosynthesis is positive (i.e. growth) or negative (i.e. decay). The sign of the photosynthetic response determines if the coral bleaches. Furthermore, the photosynthetic rate determines the calcification rate.
- The rate of change of the coral morphology is determined by the calcification rate, and the environmental stressors determine the optimal morphology. The latter determines to what morphology the coral is changing, if its present morphology differs from the optimal.
- The changes in coral morphology mainly result in changes in the hydrodynamics; as the hydrodynamics friction changes. Thereby, the flow over and through the canopy is affected, which gives rise to differences in the physiological responses.
- The effects of storms is given by the dislodgement of corals, which results in the reduction of coral cover. This reduction is represented by (1) setting the total coral cover to zero; and (2) setting all morphological dimensions to zero This represents the absence of corals.

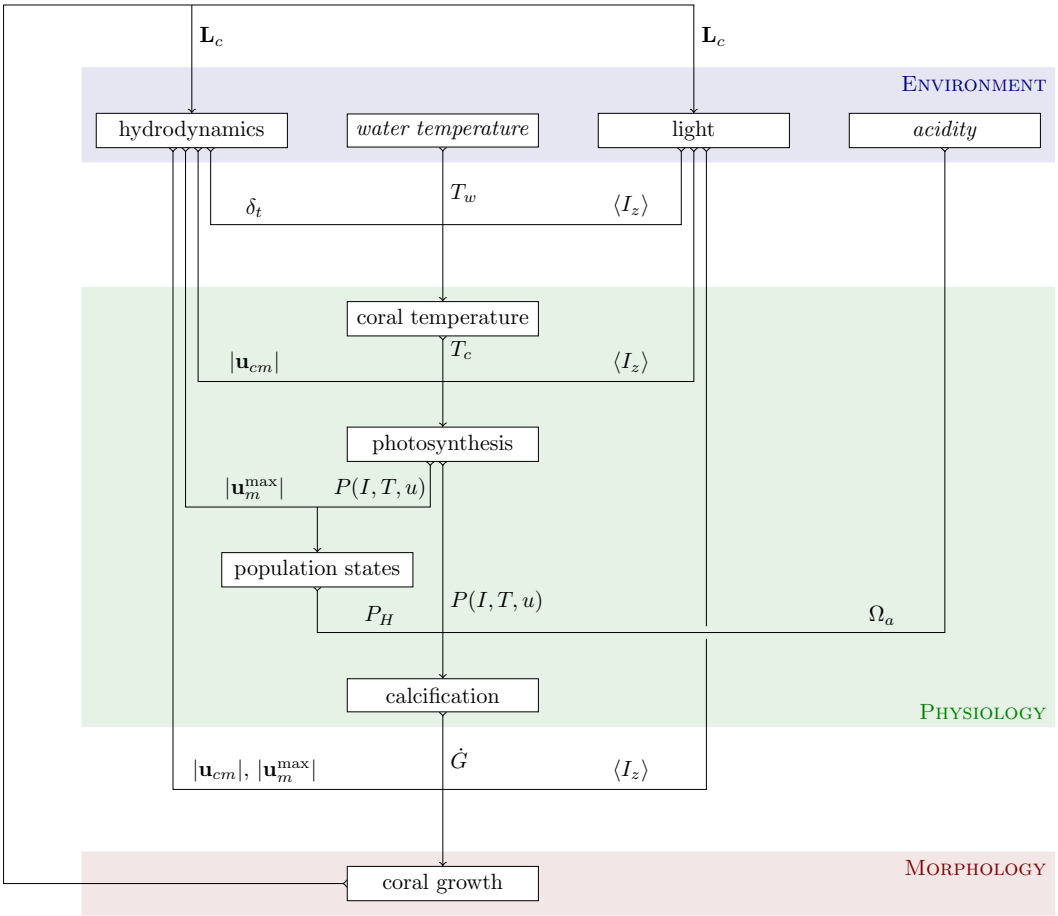

Figure 3.1: Design of the biophysical model framework. The blue-shaded section indicates the environment of corals; the green-shaded section indicates the physiology of corals; and the red-shaded section indicates the morphology of corals. $\mathbf{L}_c$ is the vector containing the morphological dimensions, $\mathbf{L}_c = [h_c\ d_c\ t_c\ b_c\ a_c]$; δ_t the thickness of the thermal boundary layer; T_w the temperature of the water; $\langle I_z \rangle$ the representative light-intensity; $|\mathbf{u}_{cm}|$ the magnitude of the mean wave-current in-canopy flow; T_c the coral temperature; $P(I,T,u)$ the photosynthetic rate (proxy); P_H the healthy coral cover; Ω_a the aragonite saturation state; $\dot{G}$ the calcification rate; and $|\mathbf{u}_m^{\max}|$ the magnitude of the maximum wave-current bulk flow.

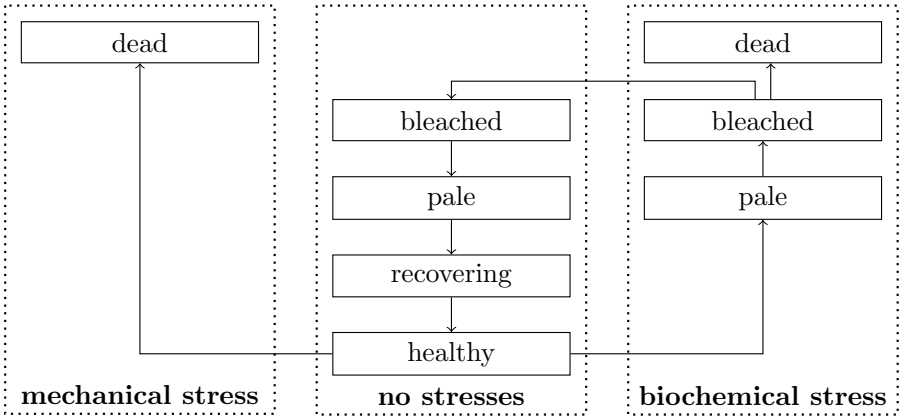

Figure 3.2: Pathways of loss and decay of corals due to environmental stresses. The mechanical stresses indicate the pathway due to coral dislodgement, i.e. due to storm events; the biochemical stresses indicate the pathway due to coral bleaching, i.e. due to bleaching events. The population states are further specified in Chapter 5 [modified from Evenhuis et al., 2015].

The main part of the model design as presented in Figure 3.1 is discussed in Chapter 4, which is on the coral growth. The decay of the corals is divided over two chapters due to the different mechanisms: Chapter 5 is on the coral bleaching and the biochemical processes associated with it; and Chapter 6 is on the coral dislodgement and the corresponding mechanical processes. In Chapters 4 to 6, the biophysical processes are described; and in Appendix A the numerical representations of the leading formulations and their solutions are presented.

The dynamics concerning the health of corals—i.e. population states (*see* Ch. 5)—are presented in Figure 3.2. In Chapter 4, all corals are considered to be in a healthy state and contribute to the growth. Chapter 5 takes the bleaching of corals into account as well as the recovery after a bleaching event, and thus focusses on the right hand side of Figure 3.2. In Chapter 6, the effects of storms are included due which the whole coral colony can be removed resulting in either healthy coral cover, or no coral cover. Thereby focussing on the left hand side of Figure 3.2.

3.2 Time-scales

The processes included in the determination of the coral growth are taking place at a wide range of time-scales. The hydrodynamics are in the shortest time-scales in which wind-waves and swell are in the order of seconds, while tides are in the order of hours up to days [Bosboom and Stive, 2015; Holthuijsen, 2007]. The physiological processes are based on daily fluctuations [Evenhuis et al., 2015] and the photo-acclimatisation is in the order of days to weeks [Anthony and Hoegh-Guldberg, 2003a]. The time-scale associated with thermal-acclimatisation is years to decades [Donner, 2011; McClanahan, 2017] and so is the growth of corals [e.g Lough et al., 2016; Marubini et al., 2001], where the latter even extends to centuries. An overview of all the time-scales is given in Figure 3.3 in which the temporal spreading is clearly visible.

This wide spreading of time-scales gives rise to the use of various update-intervals to reduce the computational time, as schematised in Figure 3.4. The frequency of coupling between the tides and waves—wind-waves and swell waves—depends on the tidal range. A large tidal range, results in significant changes in water level, hence water depth. This parameter is of importance for the development of waves when they move through the water; e.g. depth-induced wave-breaking.

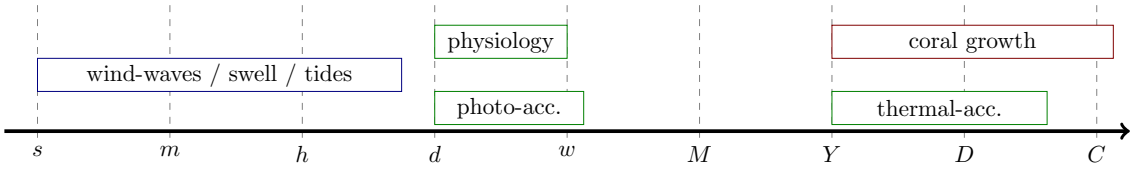

Figure 3.3: Time-scales associated with modelling coral growth. s: seconds; m: minutes; h: hours; d: days; w: weeks; M: months; Y: years; D: decades; and C: centuries.

The physiological processes—e.g. the photosynthesis and the population dynamics—are based on daily averages, but can be updated afterwards as they do not influence the light-conditions, nor the hydrodynamics. The parameters associated with the thermal-acclimatisation are updated annually, because these are based on annual statistics. To prevent the use of an extra time-related loop in the biophysical model framework (BMF)—which would only add to the BMF's complexity—all aspects of the physiology and the morphology are updated annually.

Nevertheless, the distinction between the two update-intervals is still given in Figure 3.4, whereas upgrading the BMF could give rise to the need of such an extra loop to save computational time. Furthermore, the mention of the third loop in Figure 3.4 highlights the difference in time-scales that is present (*see* Fig. 3.3).

The problem of far-reaching time-scales is also profound in morphodynamics [e.g. Luijendijk et al., 2017, 2019; Ranasinghe et al., 2011]; the study on the development of the bed due to hydrodynamic loading. Due to this comparison, methods developed in this field are used as a starting point for the long-term modelling of coral development. The options are fourfold [Li et al., 2018]: (1) input reduction; (2) model reduction; (3) acceleration factor; and (4) time-scale compression. The first two—input reduction and model reduction—act on the scale of the hydrodynamics [de Vriend et al., 1993], but in the case of coral growth modelling also on the coral physiology. The total acceleration of the simulation due to the four options is given by the product of them all [Li et al., 2018], and so all options can be combined to result in a model as efficient as possible.

The four aforementioned approaches form the basis in reducing the computational time of the model and are described below in which their application for efficient modelling of coral development is presented as well.

Input reduction The reduction of the input focuses on reducing the wave climate to a representative set of wave cases [Benedet et al., 2016; Walstra et al., 2013]. The time-series of wave data—including significant wave height, peak wave period, and wave direction—are compiled to certain representative quantities that result in comparable results [Walstra et al., 2013]. There are three methods used in morphodynamics that possibly suite the purpose for coral growth [Benedet et al., 2016]: (1) Fixed Bins Method (FBM); (2) Energy Flux Method (EFM); and (3) Energy Flux with Extreme Wave Conditions Method (EFEM). Other methods are fit to sediment transport, which is not of interest in this case.

Model reduction The method of model reduction implies to simplify the model by (1) reducing the amount of processes, scales and/or dimensions; and/or (2) simplifying the processes included [Li et al., 2018]. The aim of the following chapters—Chapters 4 to 6—is to develop simplified, but representative formulations for the biophysical processes. Based on the sensitivity analysis (Ch. 8), a further reduction of the processes is evaluated.

Acceleration factor Since recently, it is common practice to use a morphological acceleration factor for the modelling of morphodynamics [Lesser et al., 2004; Roelvink, 2006]. This morpho-

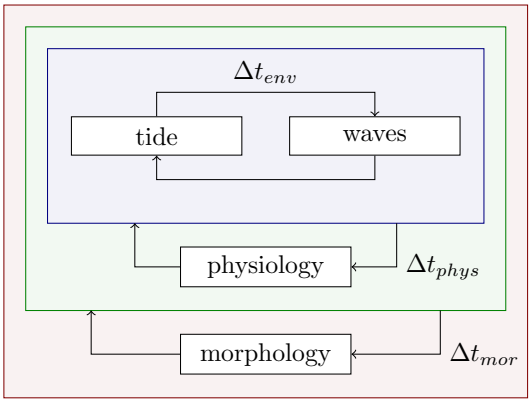

Figure 3.4: Schematisation of the coupling between different parts of the coral growth model. Both the tide and the waves (includes wind-waves and swell) are computed using the hydrodynamic model, which couples these models online with a frequency as given by Δt_{env}; Δt_{phys} is the time-interval between every online coupling between the hydrodynamic model and the physiological processes; and Δt_{mor} is the time-interval at which the morphology is coupled to the rest of the model.

logical acceleration factor simply magnifies the morphological change such that the simulation time represents a longer morphological development time [Lesser et al., 2004].

The morphological acceleration factor results in realistic morphological developments if the key assumption is met: there is (approximately) a linear relation between the hydrodynamics and the morphodynamics [Li et al., 2018]. When the morphological acceleration factor is chosen too large, it results in numerical instabilities and an unrealistic evolution of the bed [Ranasinghe et al., 2011].

This philosophy behind the morphological acceleration factor is appropriate to accelerate the coral development as well, introducing a coral growth acceleration factor.

Time-scale compression The time-scale compression approach states that the time-series on the environmental conditions are compressed by a given factor [Li et al., 2018]. In this way, it is analogous to the morphological acceleration factor, but acts on the forcing-site of the story instead of the responsive-site. Thereby, both approaches can be combined with substantial reductions in computational time [Li et al., 2018; Luijendijk et al., 2019].

When the time-scale compression approach is used, all time-series are compressed except the tidal forcing [Luijendijk et al., 2019]. The compression of the tidal signal will increase the tidal velocities; hence an unrealistic representation of reality. In the case of modelling coral development, this would result in the compression of multiple time-series: (1) incoming solar radiation; (2) sea surface temperature (SST); (3) wave forcing; and (4) aragonite fluctuations.

In this study, the input reduction is implemented to near its maximum: the wave climate is represented by an annual representative wave climate. Storms are added to this time-series based on their return period to account for the possible dislodgement of corals due to severe storms. Therefore, the coral growth acceleration factor and the time-scale compression approach are not applied in this study. Nevertheless, the options are mentioned as they are relevant for more detailed studies in which the hydrodynamics cannot be represented by annual means; e.g. when there are significant differences in wave climate between seasons. As this study focusses on the proof of concept of the model, the computational time is substantially reduced by using one representative wave climate for the 'normal' conditions and release storms on the reef based on their return period.

(a) *Acropora cervicornis.*
Credit: Albert Kok.

(b) *Goniastrea favulus.*
Credit: Larry Basch.

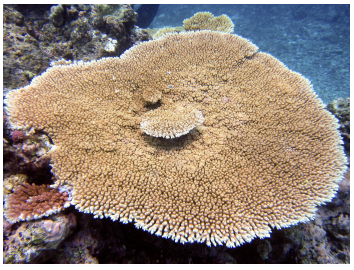

(c) *Acropora hyacinthus.*
Credit: Ryan McMinds.

Figure 3.5: Photographs of various coral morphologies. (a) Branching coral; **(b)** massive coral; and **(c)** plating coral.

3.3 Morphological representation

Corals appear in various morphologies of which a few are presented in Figure 3.5. Beside the wide variety in possibilities, coral morphologies are also complex structures (*see* Fig. 3.5). Being able to model the morphology of the coral and its interactions within the feedback loop (*see* Fig. 1.2) requires the simplification of these complex structures.

Therefore, corals are represented as two-layered cylinders in an equally staggered formation (*see* Fig. 3.6). This is a rather simple representation for such a complex structure. Nevertheless, multiple shapes of corals can be well represented with this schematisation and corals are often even represented by ordinary cylinders for model purposes [e.g. Chindapol et al., 2013; Kaandorp et al., 2003; Lowe et al., 2005a,b]. The commonly used cylinder is extended to a two-layer cylinder in this study as a more detailed representation of the morphology is desired for the computations on coral dislodgement (*see* Sec. 6.1) in which the width of the base of the coral plays a major role [Madin and Connolly, 2006]. This does not result in all morphologies to become tabular corals, which would be a bad representation of the possibilities. However, it allows the recreation of more possible morphologies of which the tabular shape is one. Moreover, the effects of the coral on its environment can be well determined according this representation (*see* Sec. 4.1).

These two-layered cylinders are fully described by five parameters: (1) the width of the plate, d_c; (2) the height of the coral, h_c; (3) the width of the base of the coral, b_c; (4) the thickness of the plate of the coral, t_c; and (5) the axial distance between coral branches, a_c (*see* Fig. 3.6). Based on these parameters, the effects of corals on the flow can be determined via a rigid vegetation model [Lowe et al., 2005a; Baptist, 2005; Zeller et al., 2015]. For the coral, the staggered arrangement is most valuable, since it is most space-efficient. This representation does not fully align with the radial growth of corals [e.g. Muko et al., 2000; Kaandorp and Sloot, 2001; Hoogenboom et al., 2008] but this does not impose significant changes on the effects of corals on their surroundings [Lowe et al., 2005a; Asher and Shavit, 2019].

The morphological development in this study is based on phenotypic plasticity; i.e. the coral morphology changes during its lifetime due to the environmental conditions [Todd, 2008], which is possible due to coral growth. The main environmental factors that play a role in the coral morphology are light and hydrodynamics [e.g. Jaubert, 1977; Chappell, 1980; Lesser et al., 1994; Kruszyński et al., 2007]. Next to these two factors, sedimentation is also believed to influence the morphology of corals [Chappell, 1980; Hoogenboom et al., 2008, and references therein]. However, this last contributor is not taken into account in this study.

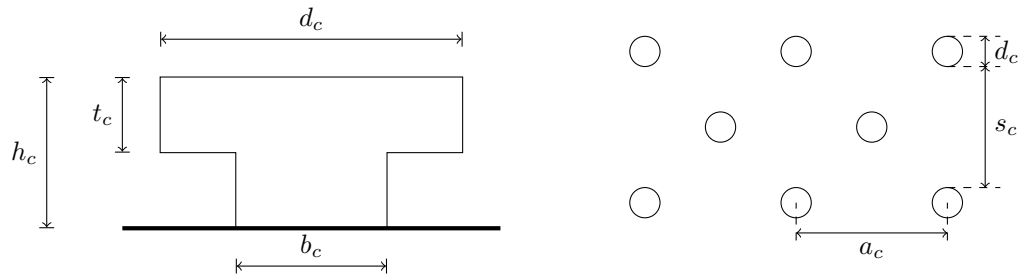

(a) Front view. **(b)** Plan view.

Figure 3.6: Schematisation of the characteristics of the coral morphology. h_c is the height of the coral colony; d_c the width of the plate; t_c the thickness of the plate; b_c the width of the base; s_c the spacing between corals; and a_c the axial distance between corals.

The morphology of the coral as function of the light and flow conditions is described by three morphological ratios: (1) the form ratio, $r_f = h_c/d_c$; (2) the plate ratio, $r_p = b_c/d_c$; and (3) the spacing ratio, $r_s = d_c/a_c$. Because the base-to-width ratio and the thickness-to-height ratio are related, and there are no descriptions on the thickness of the plate, the plate ratio encompasses both. Thus the three ratios are defined as:

$$r_f = \frac{h_c}{d_c} \qquad (3.1a) \qquad r_p = \frac{b_c}{d_c} = \frac{t_c}{h_c} \qquad (3.1b) \qquad r_s = \frac{d_c}{a_c} \qquad (3.1c)$$

Thereby, the design of the coral canopy is fully described by these three ratios in combination with the volume of the two-layered cylinder; i.e. the coral volume.

There are four limitations imposed on the morphology: one in horizontal extension; one in vertical extension; and two mathematically.

1. The horizontal limit is due to geometrical constraints, which is defined as the width at which a coral touches the closest other coral. This limits the spacing ratio:

$$r_s \leq \frac{1}{\sqrt{2}}$$

2. In the vertical direction, the upper limit is given by the water depth. Corals are marine animals and so need to be in the water. Even though corals can survive subaerial exposure due to the tide [Cabioch, 2011; Solihuddin et al., 2015; Woodroffe and Webster, 2014], this is not taken into account as it affects their morphology [Chappell, 1980] and so further complicates matters. This results in a vertical upper limit of the coral height described by the water depth during lowest spring tide:

$$h_c \leq h - z_{\text{LST}}$$

where h is the water depth relative to mean sea level; z_{LST} the water level at lowest spring tide; and z is directed downwards with $z = 0$ at mean sea level.

3. The first mathematical limitation is on the plate ratio, which has a maximum of one. It is physically not sound for the thickness of the plate to exceed the height of the coral. Nevertheless, it is physically possible for the width of the base to exceed the width of the plate. This would indicate a tapering or hemispherical shape. Because this results in extra geometrical constraints and adds complexity, also the base-to-diameter ratio is defined to have a maximum

value of one. Moreover, the plate ratio must be split in two otherwise. Thus:

$$r_p \leq 1$$

4. Finally, all ratios are larger than zero, as negative values are physically nonsense. A ratio equal to zero suggests that there are no corals.

$$r_f \geq 0 \qquad r_p \geq 0 \qquad r_s \geq 0$$

Chapter 4

Coral growth

The growth of corals is based on all four environmental factors, but only the light-intensity and hydrodynamics are inside the feedback loop. Note that the light-intensity through the water column is not influenced by the corals, but the energy from the light the corals receive is influenced by their growth rate and form. The same holds for the hydrodynamics; the oceanic forcing is not influenced as much by the corals, but the in-canopy flow through the coral canopy is largely affected by the corals as well as the above-canopy flow via the bottom friction due to corals.

The growth of corals can be categorised in two aspects of growth:

1. growth rate, which is the amount of skeleton that accumulates under the considered environmental conditions that is in line with the calcification of corals; and
2. growth form, which is the shape of the coral skeleton as function of the environmental conditions, i.e. the coral morphology.

The growth rate—or calcification rate—is based on the coral physiology, which is the biochemical response of organisms to their environment. The change in the morphology of corals depends on the optimal morphology due to the environment, but on the growth rate as well; the calcification rate determines the rate of morphological change. The focus of this chapter is on the biochemical processes that drive the calcification and the morphological development resulting from it. Thus, the mechanisms that result in the loss of coral cover are not part of this chapter but are discussed in Chapters 5 and 6 on coral bleaching and dislodgement, respectively.

This chapter starts with the descriptions of the coral environment in Section 4.1 in which the environmental factors are translated to representative values for corals. Next, the two aspects of growth are treated separately: Section 4.2 covers the coral physiology in which the effects of all four environmental factors on the growth rate are discussed; and Section 4.3 presents the dynamics associated with the coral morphology due to the environmental conditions.

Due to the fact that all is related and part of an infinite feedback loop, references are made throughout this chapter to sections later on as well as explanations given at the start of this chapter. Due to the interrelated nature of the processes, this is inevitable. Therefore, this chapter ends with a summary (Sec. 4.4) to get a clear understanding of the physics associated with coral growth, without one having to reread the whole chapter. Nevertheless, rereading this chapter results in the best understanding of the full feedback loop, as all pieces fall in place.

4.1 Coral environment

The growth of corals based on the environmental conditions—as discussed in the following sections—results in morphological changes. These changes occur at various length-scales due to the fractal nature of corals [Brown et al., 2002]. These various length-scales are limited to the characteristic ratios as discussed in Section 3.3. The combination of growth and—possibly—changing morphologies impact the coral macro- and micro-environment.

Due to this feedback, the environmental conditions as perceived by the coral may differ from the ambient water. The water column over a coral reef is considered well-mixed due to (1) a relatively small depth [e.g. Ackleson, 2003]; and (2) a lot of mixing due to the turbulent energy generated by the roughness of the reef [e.g. Böhm et al., 2013; Reidenbach et al., 2006b]. Therefore, the effects due to the acidity of the water are considered homogeneous and so are not part of the elaboration in this section. The other three environmental factors, however, need modifications, which are presented in this section.

First, the light-intensity as representative for the coral photosynthesis is determined in Section 4.1.1 after which the flow structure due to the coral canopy is discussed in Section 4.1.2. Finally, the thermal conditions are presented as here both the light and flow conditions are of importance (Sec. 4.1.3).

4.1.1 Light availability

The availability of light for photosynthesis depends on the combination of two factors: (1) the light-intensity at depth; and (2) the biomass. Therefore, first the attenuation of light through the water column is discussed followed by the description of the biomass of the coral colony. Finally, the two aspects are combined to retrieve a representative light-intensity.

Light attenuation

The light-intensity is attenuated through the water column and thus decreases with depth. This attenuation of light is described by the Beer-Lambert law, which shows an exponential decay with depth:

$$\frac{I_z}{I_0} = e^{-\zeta} \tag{4.1}$$

where I_z is the light-intensity at depth; I_0 the light-intensity at the surface water; and ζ the optical depth, which is defined by:

$$\zeta = \int K_d(z)\ \mathrm{d}z \tag{4.2}$$

where K_d is the light-attenuation coefficient (LAC) of photosynthetically active radiation (PAR); and z is directed downwards with $z = 0$ at mean sea level.

The LAC is a measure of the turbidity of the water, and is a function of salinity, suspended particulate matter (SPM), coloured dissolved organic matter (CDOM), among others [Freitas et al., 2019; Kratzer et al., 2003]. As salinity, SPM, CDOM, etc. can vary over depth—and in general do—also the LAC varies over depth; hence the integral notation in Equation (4.2). However, the LAC is often taken constant to simplify matters, which reduces Equation (4.2) to the product of the LAC and depth.

This assumption does not give rise to significant errors as the variable LAC over depth results in limited effects on the PAR-profile; this is clearly illustrated in the study of Pavlov et al. [Fig. 7, 2015]. The large variations in salinity, SPM, and CDOM over depth found in this study resulted in

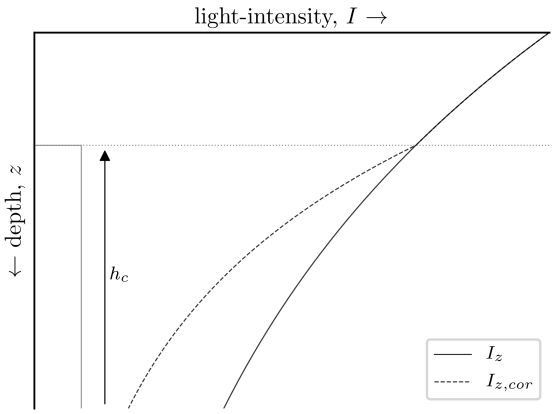

Figure 4.1: Visualisation of the attenuation of light through the water column with and without corals. I_z is the attenuation of light due to the water; $I_{z,cor}$ the attenuation of light due to the water and the coral canopy.

limited deviations in the PAR-profile compared to a constant LAC. Moreover, such large variability is not expected over a coral reef due to the aforementioned well-mixed water column.

Furthermore, the presence of the coral further attenuates the light, which is part of the shading effect [Stambler and Dubinsky, 2005; Muko et al., 2000; Hoogenboom et al., 2008]. Full incorporation of this effect requires the further attenuation of light inside the coral canopy [Kaniewska et al., 2011]. The shading effect could be incorporated by adding a coral-related LAC, which is added to the water-related LAC. This modification is visualised in Figure 4.1.

Moreover, the seabed in shallow waters reflects the light, which is again attenuated as it propagates upwards in the water column [Ackleson, 2003]. Thereby, the effect of the increased attenuation of light due to the corals is (partly) contradicted by the reflection of light by the reef. Due to a lack of data on the quantitative changes on the LAC, these processes are not taken into account.

Coral biomass

The photosynthetic and calcification rates are given per biomass, as only the biomass contributes to the photosynthetic processes. In corals, all the biomass is at the surface and the rest consists of the dead coral skeleton [e.g. Allemand et al., 2004; Jokiel, 2011b]. Therefore, the biomass of corals can be represented as the coral surface that receives light, which is key for photosynthesis.

Due to the possible wider top of the coral colony, the light of the lower section is (partly) blocked (*see* Fig. 4.2). A total blockage of the light to the lower sections would be true for (1) solely vertically directed light; and (2) a low base-to-diameter ratio. Therefore, the spreading of the light in the water column has to be taken into account. This results in the following formulation for the biomass of the coral:

$$B_c = \frac{1}{4}\pi d_c^2 + \pi d_c t_c + \pi b_c L \tag{4.3}$$

in which

$$L = h_c\,(1 - r_p)\left(1 - \frac{1}{2r_f \tan\left[\frac{1}{2}\theta_I(z)\right]}\right) \tag{4.4}$$

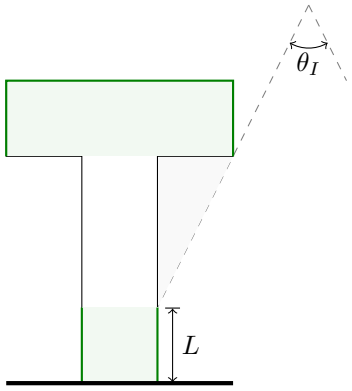

Figure 4.2: Representation of the sections of the coral morphology that receive light and so define the biomass. L the section of the base of the coral that receives light; and θ_I the spreading of the light. The coral surface-area contributing to the photosynthesis—i.e. the biomass—is accentuated with green; and the gray-shaded area represents the shading due to the morphology.

where L is the part of the base that is receiving light, visualised in Figure 4.2; $\theta_I(z)$ the spreading of light and so an indication of the diffusivity of light and a function of depth; and z is directed downwards with $z = 0$ at mean sea level.

The light distribution is wider higher in the water column and narrows down further down the water column [Jokiel, 2011b]. Therefore, this spreading is taken maximum at the top of the water column and it decays with the same rate as the light-intensity is attenuated; so according the Beer-Lambert law (*see* Eq. 4.1):

$$\theta_I(z) = \theta_I^{\max} \exp\left[-K_d z\right] \tag{4.5}$$

where $\theta_I^{\max}$ is the maximum spreading angle of light at the top of the water column, defined as $\theta_I^{\max} = 90°$—or $\theta_I^{\max} = \frac{1}{2}\pi$ [rad].

The spreading of light at the bottom of the plate is used to determine the section of the base of the coral that receives light for photosynthesis; i.e. $\theta_I(z)$ at $z = h - h_c + t_c$. The attenuation of the spreading is a continuous process, so there are no gaps or jumps between the upper and lower limits in the regime.

Representative light-intensity

The representative light-intensity is given by the biomass-averaged light-intensity. To include the morphology of corals, some modifications to the light-intensity have to be done to determine a representative light-intensity. This gives rise to the determination of the average light-intensity caught by the coral, which is the representative light-intensity for the photosynthesis:

$$\langle I_z \rangle = \frac{1}{B_c} \int I_z \, \mathrm{d}B_c \tag{4.6}$$

4.1.2 Flow structure

The hydrodynamics-related effects as discussed in Sections 4.2.2 and 4.3.1 on respectively the physiology and morphology of corals are driven by the in-canopy flow. The definition of this flow is

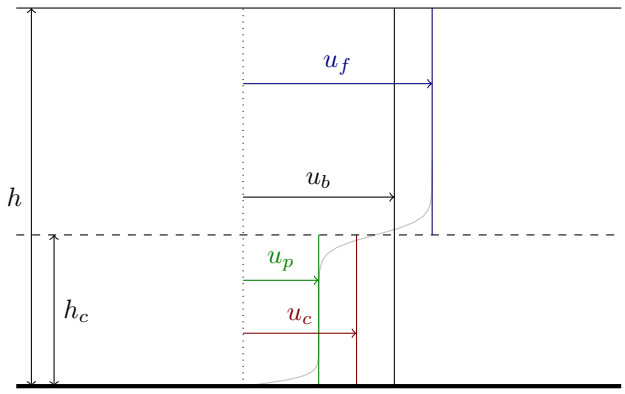

Figure 4.3: Schematisation of the flow-profile over a coral reef. u_b is the depth-averaged bulk flow velocity; u_f the above-canopy flow velocity averaged over the free flow regime, or free flow velocity; u_p the porous in-canopy flow velocity averaged over canopy height; u_c the constricted in-canopy flow velocity averaged over the canopy height; h the total water depth; and h_c the canopy or coral height. The light-gray line represents a more accurate flow profile due to the canopy's resistance.

discussed in this section. From the hydrodynamic forcing—i.e. waves and currents—to the in-canopy flow, different processes are encountered. For this, two length-scales are defined at which corals affect the flow-structure: (1) reef-scale; and (2) canopy-scale.

At the reef-scale, the canopy acts solely as friction on the flow of water over the reef; while at the canopy-scale, the water flowing over and through the canopy are taken separately. Where the canopy-scale is important in the determination of the in-canopy flow [Lowe et al., 2005a, 2008], which drives the coral's physiology and morphology [Hearn, 2001; Jimenez et al., 2008; Mass et al., 2010]; the reef-scale is leading in the determination of the water flux—and thereby the bulk flow—over the reef [Lowe et al., 2009], which is needed for the determination of the in-canopy flow [Lowe et al., 2005a, 2008].

In this section, four distinctive flow velocities are used. A visualisation of these flow velocities over the depth is given in Figure 4.3:

Bulk flow velocity (u_b) The bulk flow velocity is the depth-averaged flow velocity as solved at the reef-scale.

Above-canopy flow velocity (u_f) The above-canopy flow velocity—or free flow velocity—is the flow velocity above the canopy, which is not blocked by the canopy, and is taken averaged over the free flow regime; i.e. the water column above the canopy.

Porous in-canopy flow velocity (u_p) The porous in-canopy flow velocity—or in short porous flow velocity—is the spatially averaged flow velocity through the canopy in which the volume consumed by the canopy itself (i.e. the cylinders) is not taken into account.

Constricted in-canopy flow velocity (u_c) The constricted in-canopy flow velocity is the same as the porous flow velocity, except that it takes the volume occupied by the canopy into account. This reduces the conveyance area and so increases the flow velocity, relative to the porous flow velocity. This flow velocity is also taken averaged over the height of the canopy, just as the porous flow velocity.

This section consists of four topics: (1) waves; (2) bulk flow; (3) in-canopy flow; and (4) wave-current interaction. Thereby, it follows the path from the driving force—the waves—to the wave-induced

flow over a reef, which results in the in-canopy flow for which wave-current interactions are taken into account. The first two topics are discussed at the reef-scale—i.e. the canopy solely acts as a resisting force—and the in-canopy flow is given at the canopy-scale.

Waves

Flows over coral reefs are mainly driven by wave-breaking [Gourlay and Colleter, 2005; Monismith, 2007; Lowe et al., 2009; Falter et al., 2013], which results in a horizontal gradient in the radiation stress [Longuet-Higgins and Stewart, 1964] that gives rise to a wave set-up at the fore-reef [e.g. Hearn, 1999]. Other forcings—but often to a less extent [Lowe and Falter, 2015]—are wind [e.g. Atkinson et al., 1981] and buoyancy, which is due to a thermal gradient [e.g. Monismith et al., 2006] and/or because of the discharge of freshwater [e.g. Hoeke et al., 2013]. Due to the steep slopes of the fore reefs, the friction at the fore reef often plays a minor role [Gourlay and Colleter, 2005]. However, on the reef flat the friction is dominant, where the horizontal pressure gradient is balanced by the friction [e.g. Hearn et al., 2001; Lowe et al., 2009; Lowe and Falter, 2015]. Furthermore, the effects of waves have been shown to significantly influence the in-canopy flow [Lowe et al., 2005a,b, 2008]. Therefore, waves cannot be neglected in the determination of the in-canopy flow.

The dissipation of wave-energy over a (rough) surface is commonly given by the wave-energy dissipation factor as described by Jonsson [1966, 1980] and Jonsson and Carlsen [1976]. The commonly used description of this factor is given by [Swart, 1974]:

$$f_w = \begin{cases} 0.00251 \exp\left[5.21 \left(\dfrac{a_f}{k_s}\right)^{-0.19}\right] & \text{for } \dfrac{a_f}{k_s} > \dfrac{\pi}{2} \\ 0.3 & \text{for } \dfrac{a_f}{k_s} \leq \dfrac{\pi}{2} \end{cases} \tag{4.7}$$

where a_f is the wave orbital motion; and k_s the roughness length. Due to its maximum value of 0.3, it is not suitable for very rough reefs [Monismith et al., 2015; Rogers et al., 2016], where representative values exceed this maximum and even reach values of 1.8 [Monismith et al., 2015]. Therefore, the description as presented by Lowe et al. [2007] is preferred:

$$f_w = C_f + C_d \lambda_f \alpha_w^3 \tag{4.8}$$

where C_f is the friction coefficient; C_d the drag coefficient; λ_f the λ-parameter representing the rate of frontal area over the coral's footprint; and α_w the wave-attenuation coefficient (WAC), defined as the ratio of the in-canopy flow over the above-canopy flow [Lowe et al., 2005a]. These parameters are further elaborated on in a following paragraph (In-canopy flow, pp. 26–30), which focusses on the canopy-scale.

Studies have been dedicated to describe the roughness length of corals as function of their morphology and fractal dimensions [Hearn, 2011; Zawada and Brock, 2009; Zawada et al., 2010]. From these studies becomes clear that the roughness length of corals is significantly larger than other bottom covers; namely orders of magnitude [e.g. Nelson, 1996; Hearn et al., 2001]. The translation from these complex bathymetries towards a roughness indicator is still ambitious. Therefore, the aforementioned drag-related method is preferred. Moreover, this makes use of parameters that are readily available during the computations due to their need in other computations as well.

Bulk flow

Many studies have been done in which the geometry of the canopy is related to the in-canopy flow for which the above-canopy flow is known [Lowe et al., 2005a, 2007, 2008; van Rooijen et al., 2018].

This is, however, not the case with a two-dimensionally varying bathymetry in which the bottom friction and drag differ as well; due to the presence—or absence—of corals or other vegetation, such as seagrasses [e.g. Nepf and Vivoni, 2000; Nikora et al., 2013]. Therefore, the roughness of the reef as function of its geometry must be determined after which the distinction between the two aforementioned layers can be made.

In this study, the effect of the coral morphology is modified from Baptist [2005], who has done extensive research on this topic, focusing on vegetation in general. This study results in the formulation of a vegetation-based Chèzy coefficient:

$$C_v = \frac{1}{\sqrt{\frac{1}{C_b^2} + \frac{C_d \Phi h_c}{2g}}} + \frac{\sqrt{g}}{\kappa} \ln\left[\frac{h}{h_c}\right] \tag{4.9}$$

where C_b is the Chèzy coefficient of the non-vegetated bottom; C_d the drag coefficient of the vegetation (here, corals); κ the von Kármán constant; and Φ the vegetation density, defined as $\Phi = N_c d_c$ in which N_c is the number of stems per square metre. In the geometric parameters as described in Section 3.3 the vegetation density is given by:

$$\Phi = \frac{2\,\langle d_c \rangle}{a_c^2} \tag{4.10}$$

where $\langle d_c \rangle$ is the weighted-average of the diameter of the two-layer cylinder. Expressed in the defined morphological dimensions:

$$\langle d_c \rangle = \frac{b_c\,(h_c - t_c) + d_c t_c}{h_c} \tag{4.11}$$

In-canopy flow

The aim of this section is to determine the in-canopy flow and the associated drag coefficient, which are intertwined. Thereby, this paragraph starts with a short introduction on the qualitative effects due to the presence of a canopy after which the theories to quantify these effects are discussed. Next, the solution of the momentum balance including the canopy is presented in combination with the determination of the drag coefficient. Finally, the in-canopy flow structure is extended from a single layer canopy to a two layer canopy for which the same principles hold. These principles are first introduced using a single layer canopy for clarity.

Qualitative effects There are two main effects of the canopy on the flow structure: (1) the attenuation of the flow [e.g. Lowe et al., 2005a, 2008; Luhar et al., 2010; Nepf, 2012]; and (2) the increased turbulence at the top of the canopy [e.g. Hearn et al., 2001; Zeller et al., 2015], which enhances the mass transfer between corals and the ambient water [e.g. Lowe et al., 2005b; Reidenbach et al., 2006a; Shapiro et al., 2014]. How much the flow is attenuated within the canopy depends on three factors: (1) the degree of submergence; (2) the geometry of the canopy; and (3) the driving mechanism(s) of the flow, i.e. currents and/or waves [Nepf, 2012; Weitzman et al., 2015].

Whether the cylinders are submerged or emergent results in significant differences on the drag coefficient [McDonald et al., 2006]. The flow over submerged vegetation in general can be further categorised in depth-limited flow and unconfined flow [Nepf and Vivoni, 2000]. In the case of depth-limited flow, the horizontal pressure gradient is the dominant force driving the flow, while this changes to the turbulent shear stress at the top of the canopy for unconfined flow [McDonald et al., 2006; Nepf and Vivoni, 2000; Nikora et al., 2007a,b]. Moreover, the penetration of turbulence is

also dependent on the relative height of the coral compared to the total water depth [Ghisalberti and Nepf, 2002; Nepf and Vivoni, 2000]; increasing the ratio of water depth over the coral height, increases the penetration depth of turbulence into the canopy. In this study, the corals are assumed to be submerged at all times (*see* Sec. 3.3).

Theory The degree of attenuation can be described according to two theories: (1) the Canopy-Flow Theory (CFT) [Lowe et al., 2005a]; and (2) the Porous Media Theory (PMT) [Gu and Wang, 1991]. The PMT is especially beneficial for complex geometries such as corals [Lowe et al., 2008]. The momentum balances of the two theories show great similarities, but there are a threefold differences:

1. CFT includes shear stresses at the top of the canopy;
2. PMT includes laminar resistance within the canopy; and
3. CFT and PMT have different representations of the form drag.

The laminar resistance—included in the PMT—is often of limited influence for corals except for patches with very low flow velocities [Gu and Wang, 1991]. The drag representation as used in the PMT is preferred for real corals due to their complex structures. However, because the corals are represented as cylinders, the iterative process for submerged cylinders as described by van Rooijen et al. [2018] to determine the drag coefficient is preferred, which makes use of the CFT. Therefore, this study follows the CFT instead of the PMT.

The volume-averaged momentum equation in streamwise direction—i.e. x-direction—is given by [Finnigan, 2000; Zeller et al., 2015]:

$$\frac{\partial u}{\partial t} = -\frac{1}{\rho}\frac{\partial p}{\partial x} + \frac{1}{\rho}\frac{\partial \tau}{\partial z} - f_w \tag{4.12}$$

in which

$$f_w = f_d + f_i \tag{4.13}$$

where u is the flow velocity; ρ is the density of the water; p the pressure; τ the shear stress; f_d the drag force (per mass); and f_i the inertia force (per mass). In Equation (4.12), the vertical advection is not taken into account as its relevance is shown to be negligible [Zeller et al., 2015]. Furthermore, the resistance force (f_w) is given by the Morison equation (*see* Eq. 4.13).

Equation (4.12) is valid inside the canopy as well as above the canopy. Outside the region of influence of the canopy on the flow, Equation (4.12) reduces to:

$$\frac{\partial u_f}{\partial t} = -\frac{1}{\rho}\frac{\partial p}{\partial x} \tag{4.14}$$

which is in line with linear wave theory (*see* App. E.1).

Equation (4.14) is used to eliminate the pressure gradient from Equation (4.12) and the shear, drag and inertia forces are rewritten following the notation as in Lowe et al. [2005a] and Zeller et al. [2015] (*see* App. E.2), which results in the following formulation for the two-layer system as described by the CFT:

$$\frac{\partial\left(u_p - u_f\right)}{\partial t} = \frac{\left|u_f - u_p\right|\left(u_f - u_p\right)}{L_s} - \frac{\left|u_p\right| u_p}{L_d} - \frac{C_m \lambda_p}{1-\lambda_p}\frac{\partial u_p}{\partial t} \tag{4.15}$$

where the flow velocities are described as aforementioned and visualised in Figure 4.3: u_p is the porous in-canopy flow, which is defined as the average flow inside the canopy, and u_f the above-canopy flow; L_s and L_d are two length-scales associated with shear and drag, respectively; C_m is

the inertia coefficient, which value is within the range $C_m = 1.5 - 2.0$ [Dean and Dalrymple, 1998], where Lowe et al. [2005a] suggests $C_m = 1.7$; and λ_p is one of the λ-parameters. All parameters are discussed further below.

First, the λ-parameters describe morphological traits of the canopy and are given by [Britter and Hanna, 2003]:

$$\lambda_f = \frac{A_f}{A_T} \tag{4.16a}$$

$$\lambda_p = \frac{A_p}{A_T} \tag{4.16b}$$

in which

$$A_f = h_c d_c \qquad A_p = \frac{\pi}{4} d_c^2 \qquad A_T = \frac{1}{2} a_c^2$$

From the λ-parameters, the two aforementioned length-scales are determined; namely the shear length-scale [Zeller et al., 2015], and the drag length-scale [Coceal and Belcher, 2004], which are respectively defined by:

$$L_s = \frac{h_c}{C_s^2} \tag{4.17a}$$

$$L_d = \frac{2h_c\,(1 - \lambda_p)}{C_d \lambda_f} \tag{4.17b}$$

where C_s is the Smagorinsky coefficient [Smagorinsky, 1963]; and C_d the drag coefficient.

The use of the Smagorinsky coefficient instead of the friction coefficient [C_f, as used by Lowe et al., 2005a; Luhar et al., 2010; Weitzman et al., 2015] does not give rise to notable differences. However, the use of this Smagorinsky coefficient is more in line with the governing physics, namely turbulence (*see* App. E.2).

Solution To solve Equation (4.15), some modifications have to be done because Equation (4.15) is a non-linear differential equation. The method as proposed by Luhar et al. [2010] is used in which the flow velocities are represented by complex variables, and only the first Fourier harmonic is considered. The proposed representations of the flow velocities are:

$$u_p = \mathcal{R}e\left\{\beta \omega a_f \exp\left[i\omega t\right]\right\} \tag{4.18a}$$

$$u_f = \mathcal{R}e\left\{\omega a_f \exp\left[i\omega t\right]\right\} \tag{4.18b}$$

where ω is the wave frequency; a_f the wave-orbital motion of the above-canopy flow; and β gives the wave-attenuation coefficient (WAC) [Lowe et al., 2005a; Luhar et al., 2010]:

$$|\beta| = \alpha_w = \frac{u_p}{u_f} \tag{4.19}$$

In these definitions, ω and a_f are real and positive, while β may be complex [Luhar et al., 2010]. This gives the following solution to Equation (4.15) (*see* App. E.3):

$$i\,(\beta - 1) = \frac{8}{3\pi}\frac{a_f}{L_s}\,|1 - \beta|\,(1 - \beta) - \frac{8}{3\pi}\frac{a_f}{L_d}\,|\beta|\,\beta - i\frac{C_m \lambda_p}{1 - \lambda_p}\beta \tag{4.20}$$

Drag coefficient The determination of the drag coefficient is an iterative process [van Rooijen et al., 2018] due to the intertwined character with the flow and that all corals are assumed to be submerged (*see* Sec. 3.3). This iterative process is visualised in Figure 4.4. The steps in this iterative process are briefly described.

The two length-scales are calculated based on the geometry (*see* Eqs. 4.17a and 4.17b), where for the drag length-scale an assumption is made on the drag coefficient as a starting point. From there,

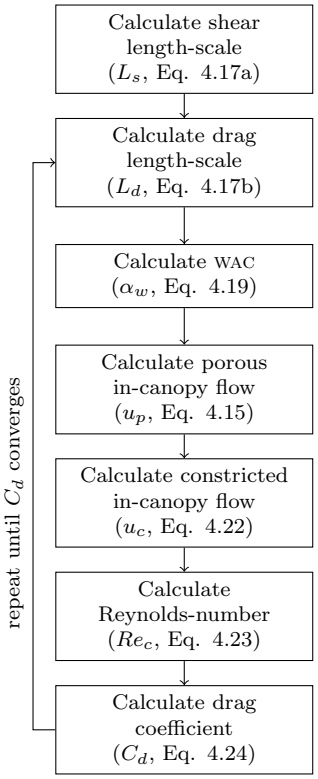

Figure 4.4: Scheme of the iterative process to determine the drag coefficient. Iterative process repeats until the drag coefficient converges. The formulations and details are presented and discussed in the text [modified from van Rooijen et al., 2018].

the WAC is determined by solving Equation (4.20). The porous in-canopy flow is determined based on the definition of the WAC (*see* Eq. 4.19) and the mass balance of water:

$$hu_b = (h - h_c)\, u_f + h_c u_p \tag{4.21}$$

where the flow velocities are as aforementioned and visualised in Figure 4.3: u_b is the bulk flow, u_f the above-canopy flow, and u_p the porous in-canopy flow. The unknown above-canopy flow is eliminated from Equation (4.21) using the definition of the WAC (*see* Eq. 4.19).

For the determination of the drag coefficient, the porous in-canopy flow has to be rewritten into the constricted in-canopy flow [Etminan et al., 2017, 2019; van Rooijen et al., 2018], where the constricted in-canopy flow accounts for the obstructions in the water column due to the canopy; i.e. it takes the reduction of the conveyance area into account:

$$u_c = \frac{1 - \lambda_p}{1 - \sqrt{\dfrac{4\lambda_p}{\psi\pi}}} u_p \tag{4.22}$$

in which:

$$\psi = \frac{s_{c,l}}{s_{c,s}}$$

where $s_{c,l}$ is the lateral distance between two consecutive corals; and $s_{c,s}$ the streamwise distance. In this study, $\psi = 2$ due to the uniformly staggered arrangement, while this parameter is included to account for randomly placed cylinders [Etminan et al., 2017].

The Reynolds-number based on the constricted in-canopy flow can directly be related to the drag coefficient [Etminan et al., 2017, 2019], where this Reynolds number is given by:

$$\mathrm{Re}_c = \frac{u_c d_c}{\nu} \tag{4.23}$$

and the drag coefficient is given by the relation between the Reynolds-number and the drag coefficient as for a single cylinder [Etminan et al., 2017, 2019; White, 2006]:

$$C_d = 1 + 10\mathrm{Re}_c^{-\frac{2}{3}} \tag{4.24}$$

With this drag coefficient the drag length-scale (Eq. 4.17b) is updated, and the cycle starts over again.

Two-layer canopy The physics associated with the single layer canopy are extended to a two-layer canopy—or a multi layer canopy for that matter—by connecting the layers via the shear stresses between them. For every canopy layer, a separate momentum balance is used:

$$\frac{\partial\left(u_{p,k}-u_f\right)}{\partial t} = \frac{|u_{p,k-1}-u_{p,k}|\left(u_{p,k-1}-u_{p,k}\right)}{L_{s,k}} - \frac{|u_{p,k}-u_{p,k+1}|\left(u_{p,k}-u_{p,k+1}\right)}{L_{s,k}} - \frac{|u_{p,k}|\,u_{p,k}}{L_{d,k}} - \frac{C_m\lambda_{p,k}}{1-\lambda_{p,k}}\frac{\partial u_{p,k}}{\partial t} \tag{4.25}$$

where k indicates the canopy layer, and $k = 0$ is the above-canopy flow.

The shear and drag length-scales are based on the thickness of the canopy layer:

$$L_{s,k} = \frac{\Delta h_k}{C_s^2} \tag{4.26}$$

$$L_{d,k} = \frac{2\Delta h_k\left(1-\lambda_{p,k}\right)}{C_{d,k}\lambda_{f,k}} \tag{4.27}$$

where Δh_k is the thickness of the canopy layer k.

The solution per canopy layer is given by:

$$i\left(\beta_k - 1\right) = \frac{8}{3\pi}\frac{a_f}{L_{s,k}}\Big(|\beta_{k-1}-\beta_k|\left(\beta_{k-1}-\beta_k\right) - |\beta_k-\beta_{k+1}|\left(\beta_k-\beta_{k+1}\right)\Big) - \frac{8}{3\pi}\frac{a_f}{L_{d,k}}|\beta_k|\,\beta_k - i\frac{C_m\lambda_{p,k}}{1-\lambda_{p,k}}\beta_k \tag{4.28}$$

Equation (4.28) is solved iteratively over the canopy layers. More details on the derivations are given in Appendix E.3.2.

Wave-current interaction

Waves result in a substantially larger WAC compared to currents only [Lowe et al., 2005a; Weitzman et al., 2015; Zeller et al., 2015]. Therefore, the WAC has to be determined separately after which the two components of the in-canopy flow are combined. Lowe et al. [2005a] found that the unidirectional

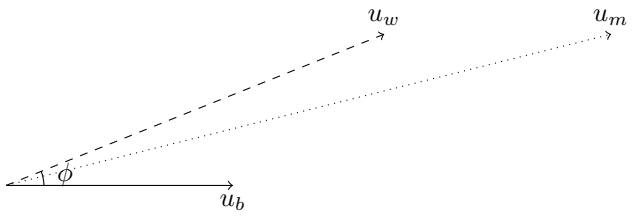

Figure 4.5: Schematisation of the mean flow due to wave-current interactions. u_m is the magnitude of the mean flow; u_b the magnitude of the unidirectional flow; u_w the magnitude of the wave orbital velocity; and ϕ the angle between the two flow components.

WAC is independent of the background wave field. However, this may not hold in all cases due to non-linear interactions [Grant and Madsen, 1986].

Nevertheless, in this study the independence between the unidirectional WAC and the wave field is assumed [as found by Lowe et al., 2005a]. The mean flow—combining both wave- and current-induced flows—gives [Bijker, 1967]:

$$u_m = \sqrt{u_b^2 + u_w^2 + 2u_b u_w \cos\phi} \tag{4.29}$$

where u_m is the magnitude of the mean flow; u_b the magnitude of the unidirectional flow, represented by the bulk flow; u_w the magnitude of the wave orbital velocity; and ϕ the angle between the two flow components (*see* Fig. 4.5).

Using the independence of the two flow components, Equation (4.29) can be rewritten such that it describes the mean in-canopy flow velocity:

$$u_{cm} = \sqrt{\alpha_c^2 u_b^2 + \alpha_w^2 u_w^2 + \alpha_c u_b \ \alpha_w u_w \cos\phi} \tag{4.30}$$

where α_c is the unidirectional WAC; and α_w the wave-induced WAC. The in-canopy flow as presented in Equation (4.30) is based on representative values of the WACs for the canopy as a whole.

4.1.3 Coral temperature

Due to the presence of a thermal boundary layer (TBL), the temperature at the coral tissue can reach values of 1°C above the ambient water temperature [Brodersen et al., 2014; Fabricius, 2006; Jimenez et al., 2011]. Because the temperature is such a key factor in the well-being of the coral (*see* Sec. 2.4) this process does not only include the efficiency of the coral-zooxanthellae symbiont due to water motion, but also represents the increased risk of bleaching due to limited flow.

As the thickness of the TBL is a function of the thickness of the velocity boundary layer (VBL), this section starts with the determination of the thickness of the VBL. Hereafter, the VBL is translated into the TBL and this section concludes with the description of the increased temperature at the coral tissue due to the presence of a TBL.

Velocity boundary layer

For cylinders in oscillatory flow, the ratio of the thickness of the VBL over the radius of the cylinder is commonly very small [Iwagaki and Ishida, 1974]. It is common practice to relate the boundary

sublayers to the wall coordinates, and so the VBL as well. In this study, the wall-coordinates are described as polar wall-coordinates and the thickness of the VBL is described as:

$$\frac{\delta u_*}{\nu} = r_\delta^+ \tag{4.31}$$

where δ is the thickness of the VBL; u_* the shear velocity and in this study related to the in-canopy flow (*see* Sec. 4.1.2), $u_* = \sqrt{C_f} u_{cm}$; ν is the kinematic viscosity of water; and r_δ^+ the wall-coordinate of the VBL. Its value is said to be $r_\delta^+ = \mathcal{O}\left(10^2\right)$ [Absi, 2009; Afzal, 2001; Bhaganagar et al., 2004; Frei, 2017; Iwagaki and Ishida, 1974]. Even though its value depends on the Reynolds number [Afzal, 2001, and references therein], it is assumed constant in this study and set to $r_\delta^+ = 500$. The effects of waves on the thickness of the VBL—the presence of waves results in a thinner VBL—is included in the magnitude of the in-canopy flow, which includes the morphology of the corals as well (*see* Sec. 4.1.2).

Thermal boundary layer

The thickness of the TBL is related to the VBL via the Prandtl-number [Incropera et al., 2007]:

$$\frac{\delta}{\delta_t} = \mathrm{Pr}^{\frac{1}{3}} \tag{4.32}$$

where δ_t is the thickness of the TBL; and Pr the Prandtl-number, which is defined by:

$$\mathrm{Pr} = \frac{\nu}{\alpha} \tag{4.33}$$

where α is the thermal diffusivity.

Increased temperature

According to Jimenez et al. [2011], there is a linear relation between the thickness of the TBL and the increased surface temperature at the coral-water interface; i.e. at the coral tissue. Moreover, this increase of the temperature at the coral tissue relative to the ambient seawater is also linearly related to the light-intensity:

$$\Delta T_c = \frac{\delta_t a_p}{k K_0} \langle I_z \rangle \tag{4.34}$$

where ΔT_c is the increase in coral temperature relative to the temperature of the ambient seawater; a_p the absorptivity of the coral; k the thermal conductivity; and K_0 a related constant [Jimenez et al., 2011]. In this study, this last parameter is kept constant and the effect of the morphology is taken into account via the magnitude of the in-canopy flow (*see* Sec. 4.1.2).

The combined effect of temperature, flow velocity, and light-intensity is argumentative due to its analogy to the feeling temperature humans are familiar with: out of the wind and in the sun, it *feels* warmer; in the wind and out of the sun, it *feels* colder. Furthermore, the combined effect of light and temperature is found more often [e.g. Coles and Jokiel, 1978; Fabricius, 2006; Houck et al., 1977].

CONCLUDING REMARKS

The influence of the corals on their environment is mainly via their effect on the hydrodynamics. However, also its growth determines the amount of light available for photosynthesis. The light-intensity used for photosynthesis—the representative light-intensity—is taken as the biomass-averaged light-intensity, which is based on the geometry of the coral.

The effects on the hydrodynamics are separated into five topics: (1) waves; (2) flow; (3) in-canopy flow; (4) wave-current interaction; and (5) multi layer canopy. The waves are the driving force of the hydrodynamics due to the wave set-up at the fore reef, which drives a wave-induced flow of the reef.

From here, a clear distinction is made between two length-scales: (1) the reef-scale; and (2) the canopy-scale. In the reef-scale, the bulk flow velocity over the reef is determined in which the geometry of the coral is translated into a Chèzy coefficient, where Equation (4.9) can be rewritten into:

$$C_v = \frac{1}{\sqrt{\frac{1}{C_b^2} + \frac{C_d \langle \lambda_f \rangle}{2g}}} + \frac{\sqrt{g}}{\kappa} \ln\left[\frac{h}{h_c}\right] \tag{4.35}$$

in which the vegetation density (Eq. 4.10) is rewritten into the average frontal λ-parameter ($\langle \lambda_f \rangle$, Eq. 4.16a), based on the average coral diameter (*see* Eq. 4.11).

The in-canopy flow is determined based on the Canopy-Flow Theory (CFT), which includes an iterative process to determine the drag coefficient as presented in Figure 4.4. In this iterative process, the partial differential equation associated with the CFT is solved by introducing the complex wave notation for the flow velocities (Eqs. 4.18a and 4.18b). This solution is presented in Equation (4.20).

The in-canopy flow velocity determines the thickness of the thermal boundary layer (TBL), which—in combination with the representative light-intensity—gives rise to increased thermal conditions at the coral tissue with respect to the ambient water.

4.2 Coral physiology

The growth rate is described as the calcification rate, which is the process of depositing calcium carbonate ($CaCO_3$) to build the calcareous skeleton of hermatypic corals [e.g. Allemand et al., 2004; Goreau, 1959; Jokiel, 2011a,b; McConnaughey and Whelan, 1997; Schneider and Erez, 2006b]. The deposition of aragonite—i.e. $CaCO_3$—results in reinforcement of the coral skeleton by increasing its density [e.g. Rico-Esenaro et al., 2019]; and in the extension of the skeleton [e.g. Edinger et al., 2000; Lough and Barnes, 1997, 2000; Lough, 2008; Lough et al., 2016; Scoffin et al., 1992; Tortolero-Langarica et al., 2016].

The relation of the calcification rate to the environmental conditions is described as a function of a proxy for the photosynthetic rate—because only light-enhanced calcification (LEC) is taken into account—and an aragonite dependency. This proxy of the photosynthesis describes the photosynthetic efficiency. The formulation of the calcification rate is modified from Evenhuis et al. [2015]:

$$\dot{G} = g_C \; C_{sp} \; P_H \; \gamma(\Omega_a) \; P(I, T, u) \tag{4.36}$$

where g_C is the calcification constant; C_{sp} the species constant; P_H the healthy coral cover; $\gamma(\Omega_a)$ the aragonite dependency; and $P(I, T, u)$ a proxy for photosynthesis that includes the photosynthetic

light, thermal and flow dependencies. Note that only the healthy coral population contributes to the calcification (moreover in Ch. 5). In this chapter, all of the coral cover is considered healthy; i.e. $P_H = 1$.

In Equation (4.36), the effects of the environmental conditions—light, hydrodynamics, temperature, and acidity—are taken into account via dependencies. These dependencies are scaled to a maximum of one, where a value of one indicates that the growth is independent of the parameter. All other values indicate the efficiency as based on the given parameter, and thus the limited growth—or productivity—due to the environmental factor. Both the photosynthetic rate and the calcification rate are given per coral biomass, which is the part of the coral in which photosynthesis takes place (*see* Sec. 4.1.1).

The main contributor to the calcification rate is the photosynthetic rate in which three of the four environmental factors are included: (1) light; (2) temperature; and (3) flow. The photosynthetic rate is based on the maximum photosynthetic rate multiplied by the efficiency of the coral-zooxanthellae symbiont. This efficiency includes a light, thermal, and flow dependency, which are denoted as $P(I)$, $P(T)$ and $P(u)$, respectively:

$$P(I, T, u) = P(I)\ P(T)\ P(u) \tag{4.37}$$

The elaboration on the physiology of corals is split in four sections in which all four environmental factors are discussed separately. The translation from light-intensity to photosynthesis is presented in Section 4.2.1. Thereafter, the photosynthetic flow dependency is discussed (Sec. 4.2.2). Next, the response of the coral-zooxanthellae symbiont to the thermal conditions is elaborated on in Section 4.2.3. The effect of the carbon-chemistry and acidity is given by the aragonite saturation state, which is dependent on the *p*H and the influence of the oceanic carbon system, on which more details in Section 4.2.4.

4.2.1 Light-intensity

As this study focusses on symbiotic corals, only light-enhanced calcification (LEC) is considered and thus the calcification is driven by photosynthesis [Goreau, 1959]. Thereby, light is an important factor in the growth of corals [e.g. Done, 2011a; Eyal et al., 2019]. This light dependency is based on the symbiosis of corals with zooxanthellae (*see* Sec. 2.4).

The influence of light on coral growth consists of two parts: (1) the photosynthetic rate induced by light; and (2) the acclimation of the coral-zooxanthellae symbiont to the light conditions, i.e. photo-acclimatisation. These parts also form the outline of this section, which concludes with a formulation of the photosynthetic light dependency.

Photosynthesis-irradiance curve

The relation between the light-intensity and the photosynthetic rate is commonly described by photosynthesis-irradiance curves [e.g. Anthony and Fabricius, 2000; Anthony et al., 2005; Chalker et al., 1983; Eyal et al., 2019; Silbiger et al., 2019]. The best representation is given by [Jassby and Platt, 1976]:

$$P_N = P_G^{\max} \tanh\left[\frac{I}{I_k}\right] - R \tag{4.38}$$

where P_N is the net photosynthesis; $P_G^{\max}$ the maximum gross photosynthesis; I the available light-intensity, in this case equal to the representative light-intensity, i.e. $I = \langle I_z \rangle$; and R is the dark respiration.

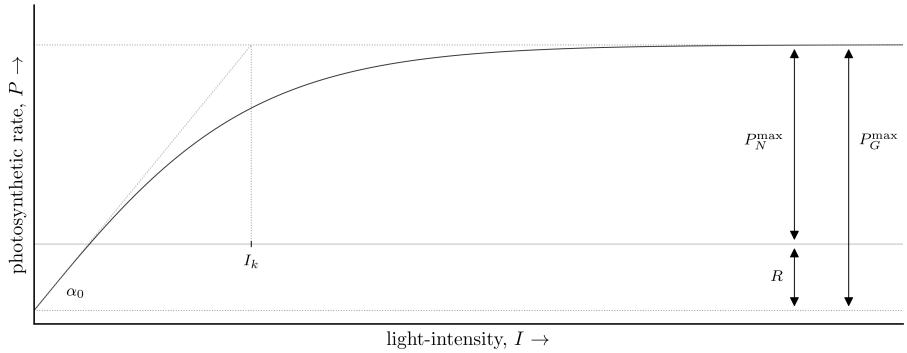

Figure 4.6: Schematic representation of a photosynthesis-irradiance curve including the definitions of its signifying parameters. P_N is the net photosynthesis; I the light-intensity; R the dark respiration; $P^G_{\max}$ the maximum gross photosynthesis; α_0 the initial slope of the curve; and I_k the saturation intensity, defined as the intersection of the initial slope with the curve's asymptote.

The dark respiration is set such that at the euphotic depth, the net photosynthetic rate equals zero. In this way, the effects of the euphotic zone on the coral growth is included as well, which can be of importance due to sea-level rise (SLR). The euphotic zone is defined as the zone in which more than one percent of the incoming light penetrates, and so the dark respiration is given as:

$$R = P_{\max} \tanh\left[\frac{0.01 I_0}{I_k}\right] \tag{4.39}$$

A visualisation of a PI-curve is given in Figure 4.6, labelling the key parameters just mentioned. The PI-curve indicates the efficiency of a plant—in this case the zooxanthellae—for a given light-intensity. This efficiency is capped at a maximum, and decreases again when photodamage and photo-inhibition occurs at too high intensities [e.g. Hoegh-Guldberg and Jones, 1999; Platt et al., 1975]. In this study, it is assumed that photodamage does not occur due to the fast acclimation of corals to their light-environment [Anthony and Hoegh-Guldberg, 2003a]; i.e. due to photo-acclimatisation.

Photo-acclimation

The key parameters of the PI-curve are not fixed, but change due to their light-environment [Chalker et al., 1983; Hennige et al., 2008, 2010; Mass et al., 2007]. The coral-zooxanthellae symbiotic system can adapt its PI-curve to such an extent that the net photosynthesis becomes almost independent of light-intensity [Anthony and Hoegh-Guldberg, 2003b; Hennige et al., 2008]. There are, however, limitations to these adaptations.

This dynamic behaviour of the PI-curve due to changes in light-environment—i.e. photo-acclimatisation—is described by Anthony and Hoegh-Guldberg [2003a], who showed that the saturation intensity is the main driver of the kinetics of the photo-acclimatisation. Nevertheless, also the maximum photosynthesis is influenced by the light-environment and thus is part of the photo-acclimatisation. Both mechanisms are caught by the same first-order differential equation [Anthony and Hoegh-Guldberg, 2003a]:

$$\frac{\mathrm{d}X(t)}{\mathrm{d}t} = -\iota\left[X^S - X(t)\right] \tag{4.40}$$

where ι is the acclimatisation exponent; X represents either the saturation intensity (I_k), or the maximum photosynthetic rate ($P_{\max}$); and X^S is the quasi steady-state value of X.

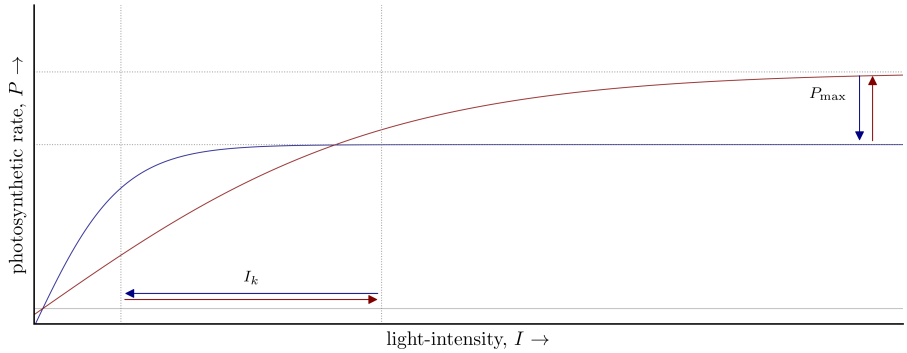

Figure 4.7: Effects of photo-acclimation on the photosynthesis-irradiance curve. The red line represent the PI-curve at high light-intensity, and the red arrows the direction of the photo-acclimatisation when the light-intensity increases; and vice versa for the blue line and arrows.

Table 4.1: The empirically determined parameters of the photo-acclimation. Estimates are given as mean ± standard error (data from Anthony and Hoegh-Guldberg [2003a].

X	$X^{\max}$	β_X	unit
I_k	372.32 ± 40.10	0.34 ± 0.05	μmol photons $s^{-1}m^{-2}$
$P_{\max}$	3.96 ± 0.52	0.09 ± 0.05	μmol O_2 $s^{-1}m^{-2}$

The quasi steady-state solution of both parameters is based on the light conditions, but also includes the limitations of the photosynthetic apparatus of the zooxanthellae. The quasi steady-state solutions of both parameters is based on the findings of Chalker et al. [1983] and is given by [Anthony and Hoegh-Guldberg, 2003a]:

$$X^S = X^{\max}\left(\frac{\overline{\langle I_z\rangle}^d}{\overline{I_0}^d}\right)^{\beta_X} \tag{4.41}$$

where $X^{\max}$ is the maximum steady-state value for X, determined empirically; $\overline{X}^d$ denotes the daily averaged value of X; and β_X is a constant exponent, also determined empirically. In Table 4.1, the empirical parameters are presented including their uncertainties.

Especially the wide spreading of the maximum steady-state saturation intensity [Anthony et al., 2005, and references therein], and the close to insignificant acclimation exponent for the maximum photosynthetic rate [Chalker et al., 1983] are points of attention. The effects of photo-acclimatisation on the PI-curve are visualised in Figure 4.7.

Light dependency

Thus, the photosynthetic response of the symbiont to light-intensity is determined based on the PI-curve (Eqs. 4.38 and 4.39) in which the representative light-intensity is defined as in Section 4.1.1. This results in the photosynthetic light dependency to be given by:

$$P(I) = P_{\max}\left(\tanh\left[\frac{\langle I_z\rangle}{I_k}\right] - \tanh\left[\frac{0.01I_0}{I_k}\right]\right) \tag{4.42}$$

where the saturation intensity follows variations in the light-environment with a time lag (Eqs. 4.40 and 4.41). The maximum of the photosynthetic rate also follows the mechanisms of the photo-

acclimatisation as given by Equations (4.40) and (4.41). However, the effects of photo-acclimatisation on this parameter are less pronounced.

4.2.2 Hydrodynamics

The health and dynamics of coral reefs are highly interlinked with the hydrodynamics of the reef; wave-induced flows refresh the water surrounding the corals and thereby supply the corals with their food and remove the waste products [Dennison and Barnes, 1988; Hearn et al., 2001; Schutter et al., 2011]. Mass et al. [2010] found that the major role of this flushing of the reefs is due to the reduction of oxidative stress of corals; in line with the Oxidative Theory of Coral Bleaching (*see* Sec. 2.4). The exact effects of flow on the growth of corals are still under debate and assigned to the removal of oxygen (O_2) [e.g. Mass et al., 2010; Schutter et al., 2011]; the supply of dissolved inorganic carbon (DIC) for photosynthesis [e.g. Osinga et al., 2017]; the supply of nutrients [e.g. Atkinson and Bilger, 1992; Hearn et al., 2001]; and reducing the thermal stress [e.g. Jimenez et al., 2008, 2011, 2012a,b].

All effects show comparable mechanisms: an increased flow reduces the thickness of the boundary layer around the coral colony. In the case of the removal and supply of molecules this is the diffusion boundary layer (DBL); and in the case of reducing the thermal stress this is the thermal boundary layer (TBL) (*see* Sec. 4.1.3). Both mechanisms are taken into account as they influence different processes. However, the removal and supply of molecules are taken as one, whereas the mechanism behind them is the same: enhancement of diffusive transport due to a reduction of the DBL.

Just as the TBL, the DBL is also a function of the velocity boundary layer (VBL), which is described in Section 4.1.3. This section focusses on the DBL and its effects on the photosynthetic flow dependency. It does so by elucidating on the process of diffusion limited transport and the description of the DBL. Finally, the photosynthetic flow dependency is presented.

Diffusion limited transport

Even though the removal of oxygen (O_2) fits best in the Oxidative Theory of Coral Bleaching (*see* Sec. 2.4), it is hard to determine the limitations of the photosynthesis based on the removal of O_2. Therefore—as the principle is the same—the supply of dissolved inorganic carbon (DIC) is taken as leading mechanism. For the diffusion of solutes through the diffusion boundary layer (DBL), Fick's first law is used:

$$F_\delta = -D \int_{\tilde{\zeta}=0}^{\delta_c} \frac{\partial \phi}{\partial \tilde{\zeta}} \, \mathrm{d}\tilde{\zeta} \tag{4.43}$$

where F_δ is the flux through the DBL; D the diffusion coefficient; δ_c the thickness of the DBL; ϕ the concentration; and $\tilde{\zeta}$ the axis in the DBL, directed away form the coral tissue with $\tilde{\zeta} = 0$ at the coral tissue (*see* Fig. 4.8).

Because the DBL is very small, a linear concentration gradient over the DBL can be assumed [Jimenez et al., 2011; Mass et al., 2010]. Thereby, Equation (4.43) simplifies to:

$$F_\delta = -\frac{D}{\delta_c} (\phi_\delta - \phi_0) \tag{4.44}$$

where ϕ_δ is the concentration of the ambient water, i.e. at the outer edge of the DBL; and ϕ_0 the concentration at the coral tissue.

When assuming that the photosynthesis is limited by the supply of DIC—or by nutrients for that matter—the concentration at the coral tissue can be set to zero, as everything is used for the photosynthesis. Thereby, the photosynthesis-induced flux is also equal to the flux through the DBL;

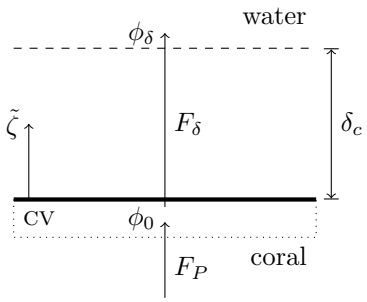

Figure 4.8: Schematisation of the fluxes at the coral-water interface. F_p is the photosynthesis-induced flux; F_δ the flux through the DBL; δ_c the thickness of the DBL; $\tilde{\zeta}$ the coordinate system at the coral surface, directed outwards. The concentration in the control volume (CV) is given by ϕ_0; and the concentration outside the DBL—i.e. the ambient water—by ϕ_δ.

i.e. $F_P = F_\delta$. Therefore, the photosynthetic rate can be related to the diffusion limited transport through the DBL:

$$P \propto \frac{D}{\delta_c}\phi_\delta$$

Diffusion boundary layer

The thickness of the DBL is related to the velocity boundary layer (VBL) via the Schmidt-number [Incropera et al., 2007]:

$$\frac{\delta}{\delta_c} = Sc^{\frac{1}{3}} \tag{4.45}$$

where Sc is the Schmidt-number, which is defined as:

$$\mathrm{Sc} = \frac{\nu}{D} \tag{4.46}$$

where ν is the kinematic viscosity of water; and D the molecular diffusivity.

Flow dependency

As the thickness of the VBL is inversely related to the flow velocity (*see* Eq. 4.31), and the photosynthetic rate is inversely related to the thickness of the DBL—and thereby also to the VBL (*see* Eqs. 4.45 and 4.31)—the photosynthetic rate is linearly related to the flow velocity. This is also found in literature [e.g. Comeau et al., 2014; Lenihan et al., 2015]. Furthermore, as the photosynthetic rate is not limited by the flow anymore for $u_{cm} \geq 0.10\ ms^{-1}$ [Hurd, 2000], the flow-related efficiency is (approximately) optimal for $u_{cm} \geq 0.10\ ms^{-1}$. The best continuous representation of a capped linear expression is the tangent-hyperbolic function, and so the flow-efficiency is given by:

$$P(u) = P_u^{\min} + \left(1 - P_u^{\min}\right) \tanh\left[a\frac{|\mathbf{u}_{cm}|}{u_{cr}}\right] \tag{4.47}$$

where $P_u^{\min}$ is the minimum efficiency at which there is no flow; a the linear slope around no flow, which is chosen such that the efficiency approaches one at u_{cr}: $a = 2$; and u_{cr} is the critical flow velocity at which the efficiency is (close to) 100%.

4.2.3 Temperature

One of the best known effects on coral growth is the temperature; especially in relation to coral bleaching [e.g. Berkelmans, 2002; Comeau et al., 2016; Dias et al., 2018; Vásquez-Bedoya et al., 2012]. Therefore, this is one of the most researched parameters influencing the coral health and growth, largely in combination with climate change [e.g. Berkelmans and Oliver, 1999; Harley et al., 2006; Hoegh-Guldberg, 1999; Kleypas et al., 2001]. The thermal stress on corals is commonly related to heat waves, but corals can also bleach due to cold stress [Evenhuis et al., 2015; Howells et al., 2013; Jokiel and Coles, 1977; Marshall and Clode, 2004].

The response of corals to high temperatures differs from the response to low temperatures; the response is more severe to high temperatures [Al-Horani, 2005; Buddemeier et al., 2008; Edmunds, 2005; Evenhuis et al., 2015]. Nevertheless, low temperatures result in more mortality when time progresses, which is the other way around for high temperatures [Jokiel and Coles, 1977]. In this sense, the thermal response of corals follows the analogy of flooding and drying.

The temperature influences the growth of corals in two ways:

1. The symbiosis between the coral and the zooxanthellae is very sensitive to thermal conditions [Al-Horani, 2005; Buddemeier et al., 2008; Edmunds, 2005].
2. The oceanic carbon chemistry—and thus the aragonite saturation state of the surrounding seawater—is influenced by the temperature (among others) [Mucci, 1983; Roy et al., 1993; Weiss, 1974], which can lead to undersaturation of aragonite that results in lower calcification rates. This can even lead to dissolution of the calcium carbonate ($CaCO_3$) skeleton of the corals [Guinotte et al., 2003; Kleypas et al., 1999, 2001; Silverman et al., 2009].

The latter is discussed in Section 4.2.4 and the focus of this section is on the first; the photosynthetic thermal dependency of corals and the possible thermal stresses. The relation as described by Evenhuis et al. [2015] is used for the coral response to temperature changes, which is in line with findings of others [e.g. Buddemeier et al., 2008; Edmunds, 2005; Jokiel and Coles, 1977]. Evenhuis et al. [2015] split the effects of temperature on the photosynthetic rate in two factors, which address two different biochemical mechanisms:

1. the adapted temperature response in which the temperature range of the coral species determines its calcification rate; and
2. the thermal envelope in which the fact that chemical reactions are faster at higher temperatures is included, following the Arrhenius equation.

The product of these two factors is taken as the thermal response of coral growth [Evenhuis et al., 2015]:

$$P(T) = f_1(T_c, T_{opt}, \Delta T) \cdot f_2(T_{opt}, E_a) \tag{4.48}$$

where f_1 is the function for the adapted temperature response; and f_2 the function for the thermal envelope. Both functions are elaborated on in the following paragraphs. In these formulations, the coral temperature is given by the summation of the water temperature and the increased temperature at the coral tissue due to the thermal boundary layer (TBL) (*see* Eq. 4.34) as discussed in Section 4.2.2:

$$T_c = T_w + \Delta T_c \tag{4.49}$$

where T_w is the sea surface temperature (SST).

This section starts with the thermal response of corals in which the adapted temperature response and the thermal envelope are discussed separately. In their discussion, the effects of the key param-

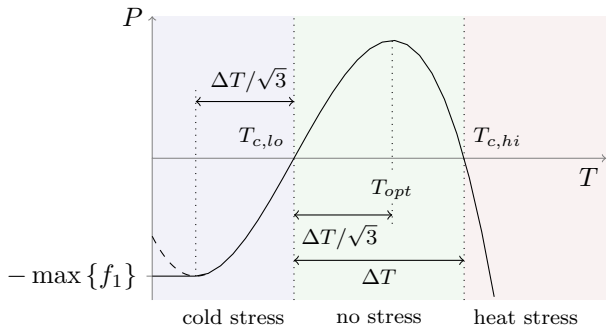

Figure 4.9: Visualisation of the adapted temperature response. The asymmetry between heat and cold stress is clearly visible and the key parameters are illustrated: T_{opt} is the optimum temperature for photosynthesis; ΔT the thermal range; T_{lo} the lower limit of the thermal range; and T_{hi} the upper limit of the thermal range.

eters on the thermal response are presented as well for a better understanding on the mechanisms. Finally, the method used to include the thermal-acclimatisation is presented.

Adapted temperature response

The coral-zooxanthellae symbiosis works within a temperature range [e.g. Evenhuis et al., 2015; Hoegh-Guldberg, 1999; Silverman et al., 2007] with an optimal temperature. Because the effects of lower temperatures than the optimum are less severe than those of higher temperatures [Al-Horani, 2005; Jokiel and Coles, 1977], the response is commonly given as a cubic polynomial [e.g. Buddemeier et al., 2008; Edmunds, 2005] and is modified from Evenhuis et al. [2015]:

$$f_1(T_c, T_{lo}, \Delta T) = \begin{cases} -\left(T_c - T_{lo}\right)\left(\left(T_c - T_{lo}\right)^2 - \left(\Delta T\right)^2\right)\mathrm{spec}(\Delta T) & T_c > T_{lo} - \dfrac{1}{\sqrt{3}}\Delta T \\ -f_1^{\max} & T_c \leq T_{lo} - \dfrac{1}{\sqrt{3}}\Delta T \end{cases} \tag{4.50}$$

where T_c is the coral temperature; ΔT the difference between the lower and upper limit of the thermal range, in short the thermal range; T_{lo} is the lower limit of the thermal range; and $\mathrm{spec}(\Delta T)$ the specialisation term, which describes the normalisation of Equation (4.50) to the area under the curve. Equation (4.50) and its characteristics are visualised in Figure 4.9.

The limits of the thermal range are based on temperature history and are further discussed later on in this section as part of the thermal-acclimatisation. The relation between the thermal key parameters are displayed in Figure 4.9 and given by:

$$\Delta T = T_{hi} - T_{lo} \tag{4.51a}$$

$$T_{opt} = T_{lo} - \frac{1}{\sqrt{3}}\Delta T \tag{4.51b}$$

where T_{hi} is the upper limit of the thermal range; and T_{opt} the optimum temperature for photosynthesis, and thus calcification.

Furthermore, the specialisation term—$\mathrm{spec}(\Delta T)$ in Equation (4.50)—is included to reward the coral for the specialisation to a smaller thermal range; and penalise for a wide thermal range as presented in Figure 4.10a in which the thermal range is varied. Evenhuis et al. [2015] suggests the following formulation:

$$\mathrm{spec}_E(\Delta T) = 4 \cdot 10^{-4} \exp\left[-0.33\left(\Delta T - 10\ [K]\right)\right] \tag{4.52}$$

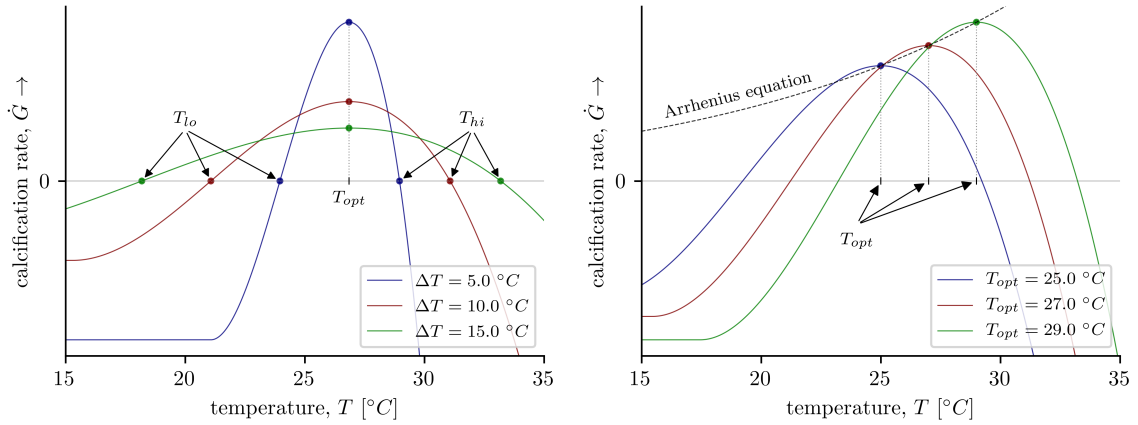

(a) Thermal range, ΔT.

(b) Optimum temperature, T_{opt}.

Figure 4.10: Visualisation of the effects of the thermal key-parameters. In both plots, the specialisation term is given by Equation (4.53). T_{lo} is the lower limit of the thermal range; T_{hi} the upper limit of the thermal range; ΔT the thermal range; and T_{opt} the optimum temperature. **(a)** The adapted temperature response curve flattens as the thermal range increases, indicating that the coral becomes more 'all-round' considering its tolerance to temperature. **(b)** The maximum of the adapted temperature response follows the Arrhenius equation, which results in an amplification of the adapted temperature response curve.

However, this results in a mathematically incorrect normalisation and is a modification from a normalisation of the area underneath the polynomial between the limits of the thermal range. Especially for smaller thermal ranges, there is a clear difference between the two formulations. The mathematically correct specialisation term is the following:

$$\mathrm{spec}_M(\Delta T) = \frac{1}{\int_{T_{lo}}^{T_{hi}} f_1(T_c)\ \mathrm{d}T_c} = \frac{4}{(\Delta T)^4} \tag{4.53}$$

As clearly demonstrated in Figure 4.11a, the formulation by Evenhuis et al. [2015] does not fully reward corals with a smaller range as the area underneath the adapted temperature response curve rapidly decreases for smaller thermal ranges (see Fig. 4.11b). This results in the same efficiency at the optimum temperature for $\Delta T = 5°\mathrm{C}$ and $\Delta T = 15°\mathrm{C}$ (*see* Fig. 4.11a).

Evenhuis et al. [2015] modified the specialisation term as presented in Equation (4.53) to Equation (4.52) due to its unrealistic behaviour. In this study, both versions of the specialisation term are considered and the results are compared to each other.

Thermal envelope

All chemical reactions are faster at higher temperatures because particles move faster, which is described by the Arrhenius equation. This behaviour is taken into account by the thermal envelope, which is given by [Evenhuis et al., 2015]:

$$f_2(T_{opt}, E_a) = \exp\left[\frac{E_a}{\overline{R}}\left(\frac{1}{300} - \frac{1}{T_{opt}}\right)\right] \tag{4.54}$$

where E_a is the activation energy, which has to be fitted; and $\overline{R}$ is the gas constant.

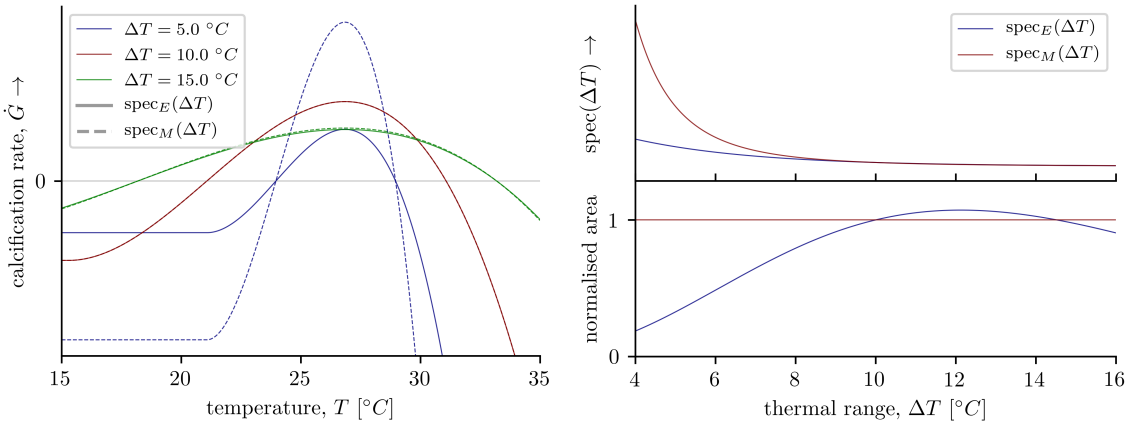

(a) Effect on the adapted temperature response.

(b) Specialisation term with normalised area.

Figure 4.11: Visualisation of the differences between two normalisation methods. $\text{spec}_E(\Delta T)$ follows the normalisation as suggested by Evenhuis et al. [2015] (*see* Eq. 4.52); and $\text{spec}_M(\Delta T)$ normalises the area under the adapted temperature response curve in a mathematically sound way (*see* Eq. 4.53). **(a)** The different specialisation terms result in significantly different results for smaller thermal ranges, but are comparable for larger thermal ranges. **(b)** The area underneath the modified specialisation term ($\text{spec}_E(\Delta T)$, Eq. 4.52) is not constant for all thermal ranges, while $\text{spec}_M(\Delta T)$ is defined as such.

The optimal temperatures will follow the Arrhenius equation, which is thereby the upper limit of the thermal response of corals (*see* Fig. 4.10b). The thermal envelope is such calibrated that $f_2 = 1.0$ at $T_{opt} = 300\ K\ (\approx 27°C)$, which is the ambient temperature at which the model of Evenhuis et al. [2015] was calibrated. This term, therefore, allows for the use of the model at other locations as well.

The inclusion of the effect as described by the Arrhenius equation results in an amplification of the adapted temperature response (*see* Eq. 4.50). This amplification also increases the area underneath the adapted temperature response curve and is visualised in Figure 4.10b. That the area increases can be explained by the fact that corals become more productive at higher temperatures—as long as they are resistant to the temperature—due to the increased reaction rates.

Thermal-acclimation

Just as with photo-acclimatisation (*see* Sec. 4.2.1), corals are also able to acclimatise to their thermal environment; i.e. thermal-acclimatisation [Hughes et al., 2003; Gibbin et al., 2018; Logan et al., 2014; Maynard et al., 2008; Middlebrook et al., 2008]. Even though this mechanism is said to be very slow [Hoegh-Guldberg et al., 2007], there are multiple suggestions in literature on a faster thermal-acclimatisation [Ainsworth et al., 2016; Howells et al., 2012; Palumbi et al., 2014]. The exact mechanisms behind the acclimatisation are still highly debated [Baird and Maynard, 2006; Oliver and Palumbi, 2011] as well as the borderline between acclimatisation, genetic adaptation and phenotypic plasticity [Edmunds and Gates, 2008; Gibbin et al., 2018]. The three most pronounced mechanisms are thought to be switching of zooxanthellae [Howells et al., 2012; Jones et al., 2008]; changes in bacterial communities [Reshef et al., 2006]; and due to the coral itself [Puisay et al., 2018].

For this study, the exact mechanism does not matter, but the fact of thermal-acclimatisation does. The thermal-acclimatisation of corals due to sub-lethal pre-stressing results in significantly higher

thermal resistance [Bellantuono et al., 2012; Gibbin et al., 2018; Middlebrook et al., 2008] and can alter the long-term outcomes of the existence of corals significantly [Ainsworth et al., 2016]. The order of magnitude over which thermal-acclimatisation is believed to take place is decades [Donner, 2011; Logan et al., 2014; Gibbin et al., 2018] instead of the days as for photo-acclimatisation [Anthony and Hoegh-Guldberg, 2003a].

The thermal-acclimatisation is taken into account via dynamic limits of the thermal range, which are based on historic sea surface temperature (SST) time-series [e.g. Donner, 2011; Lantz et al., 2019; Logan et al., 2014; McClanahan, 2017]. The method used is based on the work of Donner [2011] in which the commonly used degree heating week (DHW) [e.g. Eakin et al., 2019; Liu et al., 2003] is translated to the limits of the thermal range of the corals—as is used in this study.

This relation is based on the statistics of the thermal record. Every year, the maximum and minimum monthly mean are extracted from the time-series. From these, the mean and standard deviation are taken over n years:

$$\mu_T^{\min} = \overline{\min_y \left\{ \overline{T_c}^m \right\}}^n \tag{4.55a}$$

$$\sigma_T^{\min} = \sqrt{\frac{\sum_{i=1}^n \left(\min_y \left\{ \overline{T_c}^m \right\}_i - \overline{\min_y \left\{ \overline{T_c}^m \right\}}^n \right)}{n-1}} \tag{4.55b}$$

$$\mu_T^{\max} = \overline{\max_y \left\{ \overline{T_c}^m \right\}}^n \tag{4.55c}$$

$$\sigma_T^{\max} = \sqrt{\frac{\sum_{i=1}^n \left(\max_y \left\{ \overline{T_c}^m \right\}_i - \overline{\max_y \left\{ \overline{T_c}^m \right\}}^n \right)}{n-1}} \tag{4.55d}$$

where n is the amount of years influencing the thermal-acclimatisation; T_c the daily-averaged coral temperature; $\min_y \{X\}$ and $\max_y \{X\}$ are the annual minimum and maximum value of X, respectively; and $\overline{X}^m$ and $\overline{X}^n$ the average value of X over one month and n years, respectively.

Based on these statistics, the limits of the thermal range are given by [Donner, 2011]:

$$T_{lo} = \mu_T^{\min} - K_{var}\sigma_T^{\min} \tag{4.56a}$$

$$T_{hi} = \mu_T^{\max} + K_{var}\sigma_T^{\max} \tag{4.56b}$$

where K_{var} is the thermal-acclimatisation coefficient with $K_{var} = 2.45$ [Donner, 2011].

The thermal-acclimatisation is taken into account by the amount of years on which the upper and lower limits are based; i.e. the parameter n. Due to a lack of studies on the value, which is partly due to the species dependent response, the time-scale of the thermal-acclimatisation is given by:

$$n = \frac{n'}{C_{sp}} \tag{4.57}$$

where n' is assumed to be $n' = 60\ yrs$ [based on Logan et al., 2014, and references therein]. The thermal-acclimatisation coefficient is an empirical factor that depends on the variability, and must be used with caution [Donner, 2011]; there are locations with low variability in SST [Kleypas et al., 2008], but with high variability as well [Ateweberhan and McClanahan, 2010; McClanahan et al., 2007].

Note that Equation (4.49) is needed to correct for the difference between the temperature of the coral and the ambient sea water. For this correction, the representative hydrodynamic climate is used in combination with the average light-intensity over the same period as the SST time-series; i.e. n years. Thereby, the whole historic SST time-series is modified by the relative increase at the coral tissue (Eq. 4.49) after which the above statistics are retrieved from these modified time-series.

4.2.4 Acidity

The effects of the acidity are viewed via the response of the aragonite saturation state on the dissolved concentration of carbon dioxide (CO_2) in the oceanic waters. This involves the full chain of dissolved inorganic carbon (DIC) in which the concentrations are based on temperature, salinity, and pH [Roy et al., 1993; Weiss, 1974]; this makes it a complex, intertwined chain, because pH is influenced by the DIC composition of the water; and vice versa. As mentioned in Section 1.3, this iterative pH model is not included but the processes influencing the aragonite saturation state are.

In literature, the process of light-enhanced calcification (LEC) is often related to bicarbonate (HCO_3^-) [Allemand et al., 2004; Goreau, 1959; Jokiel, 2011b; McConnaughey and Whelan, 1997] in which HCO_3^- is the source for the photosynthesis as well as for the calcification process. These descriptions and models are on the molecular level in which many parameters play a role, and are unproven theories. Therefore, the calcification rate is related to the aragonite saturation state, which is common practice [e.g. Albright et al., 2008; Andersson et al., 2009; Buddemeier et al., 2008; Langdon et al., 2000; Ohde and Hossain, 2004; Shamberger et al., 2011] and does not require lots of detailed information.

In this section, first the oceanic carbon system is highlighted, since it forms the basis of the aragonite saturation state. Thereafter, it concludes with the formulation of the aragonite dependency of the calcification rate.

Oceanic carbon system

The oceanic carbon system is used for which the atmospheric carbon dioxide (CO_2) pressure—beside the temperature, salinity, and pH—is the forcing. The exchange between the atmospheric CO_2 and the oceanic dissolved CO_2 is given as:

$$[\,{CO_2}^*\,] = K_0^* \cdot pCO_2 \tag{4.58}$$

where $[{CO_2}^*]$ is the summation of the dissolved concentrations of CO_2 and carbonic acid (H_2CO_3), which are chemically inseparable [Zeebe and Wolf-Gladrow, 2001]; pCO_2 is the atmospheric CO_2 pressure; and K_0^* the solubility constant of CO_2, which is a function of salinity and temperature [Weiss, 1974]; as presented in Table 4.2.

When the CO_2 is dissolved in water, a couple of reactions take place, where the various dissolved inorganic carbon (DIC)s are related to each other via two—the first and second—stoichiometric equilibrium constants [Zeebe and Wolf-Gladrow, 2001]:

$${CO_2}^* + H_2O \overset{K_1^*}{\rightleftharpoons} {HCO_3}^- + H^+ \overset{K_2^*}{\rightleftharpoons} {CO_3}^{2-} + 2\,H^+ \tag{4.59}$$

where K_1^* and K_2^* are the stoichiometric equilibrium constants, which depend on temperature, pressure, and salinity (*see* Tab. 4.2).

Next, the aragonite saturation state can be determined, which depends on the concentration of carbonate (${CO_3}^{2-}$) as well as calcium-ions [e.g. Kleypas et al., 1999; Mucci, 1983]:

$$\Omega_a = \frac{[\,{Ca}^{2+}\,]\,[\,{CO_3}^{2-}\,]}{K_a'} \tag{4.60}$$

where K_a^* is the stoichiometric solubility product of aragonite, which depends on temperature as well as salinity (*see* Tab. 4.2); and $[\,{Ca}^{2+}\,]$ is the concentration of calcium-ions, which is given by [Millero, 1982, 1995]:

$$[\,{Ca}^{2+}\,] = 0.01028\frac{S}{35} \tag{4.61}$$

Table 4.2: Thermal and saline dependency of chemical reactions in seawater. Constants of (1) the solubility constant, K_0^*; (2) the first and second stoichiometric equilibrium constants, K_1^* and K_2^*; and (3) the stoichiometric solubility constant of aragonite, K_a^*. In the formulae, S is the salinity; and T_w the temperature of the seawater.

	$i=1$	$i=2$	$i=3$	$i=4$	Source
$\ln K_0^* = a_1 + a_3 \frac{100}{T_w} + a_4 \ln\left[\frac{T_w}{100}\right] + \left(c_1 + c_2 \frac{T_w}{100} + c_3 \left(\frac{T_w}{100}\right)^2\right) S$					
a_i	-60.2409	–	93.4517	23.3585	Weiss [1974]
b_i	–	–	–	–	
c_i	0.023517	-0.023656	0.0047036	–	
d_i	–	–	–	–	
$\ln K_1^* = a_1 + \frac{a_3}{T_w} + a_4 \ln T_w + \left(b_1 + \frac{b_3}{T_w}\right) S^{0.5} + c_1 S + d_1 S^{1.5}$					
a_i	2.83655	–	2307.1266	-1.5529413	Roy et al. [1993]
b_i	-0.20760841	–	4.0484	–	
c_i	0.08468345	–	–	–	
d_i	-0.00654208	–	–	–	
$\ln K_2^* = a_1 + \frac{a_3}{T_w} + a_4 \log T_w + \left(b_1 + \frac{b_3}{T_w}\right) S^{0.5} + c_1 S + d_1 S^{1.5}$					
a_i	-9.226508	–	3351.6106	-0.2005743	Roy et al. [1993]
b_i	-0.106901773	–	23.9722	–	
c_i	0.1130822	–	–	–	
d_i	-0.00846934	–	–	–	
$\log K_a^* = a_1 + a_2 T_w + \frac{a_3}{T_w} + a_4 \log T_w + \left(b_1 + b_2 T_w + \frac{b_3}{T_w}\right) S^{0.5} + c_1 S + d_1 S^{1.5}$					
a_i	-171.945	-0.077995	2909.298	71.595	Mucci [1983]
b_i	-0.068393	0.0017276	88.135	–	
c_i	-0.10018	–	–	–	
d_i	0.0059415	–	–	–	

where S is the salinity of seawater. The aragonite saturation state is mainly determined by the concentration of CO_3^{2-} due to an abundance of calcium-ions in the waters [Done, 2011b; Kleypas et al., 1999].

Aragonite dependency

The effect of the aragonite saturation state on the calcification rate—i.e. the aragonite dependency—is based on the Michaelis-Menten equation. This formulation is modified, as the calcification is commonly reduced to zero at $\Omega_a = 1$ in literature [e.g. Langdon and Atkinson, 2005; Ohde and Hossain, 2004]. This is based on the process that dissolution of the coralline skeleton takes place when the surrounding water is undersaturated in aragonite. However, this should not be taken too strict as it does not seem to hold in general [e.g. Albright et al., 2008; de Putron et al., 2011], which could be assigned to the difference in micro-environment inside the coral compared to the ambient water that is actively controlled by the coral [Allemand et al., 2004; Goreau, 1959; Jokiel, 2011b; McConnaughey and Whelan, 1997]. Therefore, the Michaelis-Menten equation is modified as follows:

$$\gamma(\Omega_a) = \frac{\Omega_a - \Omega_0}{\kappa_a + (\Omega_a - \Omega_0)} \tag{4.62}$$

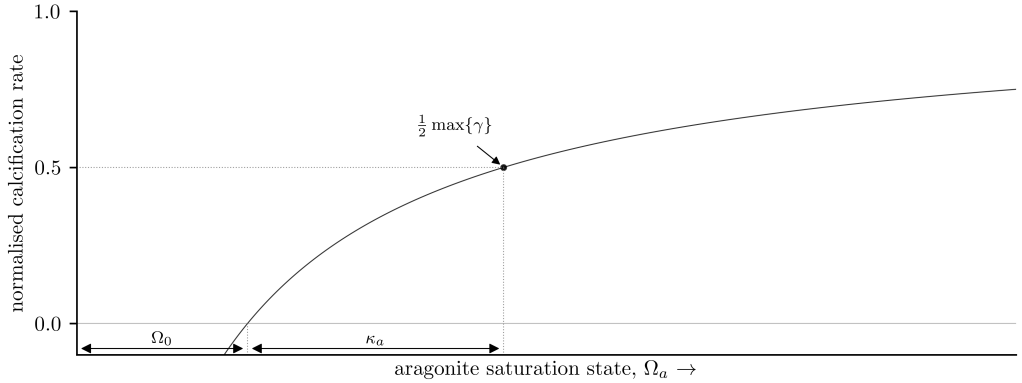

Figure 4.12: Visualisation of the aragonite dependency. The key parameters and there definitions are illustrated: the calcification is half of its maximum at $\Omega_a = \Omega_0 + \kappa_a$. The normalised calcification rate is taken as solely dependent on the aragonite saturation state, and thus is represented by the aragonite dependency, $\gamma(\Omega_a)$.

where κ_a is a measure for the half-rate, at which the calcification rate is half of the maximum; and Ω_0 is the aragonite saturation state at which the calcification rate is zero; i.e. the dilution saturation. Due to the shift at which the calcification rate is zero, the calcification rate is half-maximum at $\Omega_a = \Omega_0 + \kappa_a$ instead of at $\Omega_a = \kappa_a$. A visualisation of this dependency including the key parameters is given in Figure 4.12.

However, a linear aragonite dependency is found in multiple studies [e.g. Albright et al., 2008; Langdon et al., 2000]. Such a linear dependency is not capped—or a discontinuous function must be used—which is ambitious, as for high aragonite saturation states the calcification rate is no longer limited by this saturation state [Done, 2011b].

CONCLUDING REMARKS

The physiology of corals is described by dependencies on (1) light; (2) hydrodynamics; (3) temperature; and (4) acidity. The first three affect the photosynthetic efficiency, and the last only influences the calcification rate.

The impact of the environmental factors on the coral physiology are summarised into:

1. The light-intensity is translated into photosynthesis via a photosynthesis-irradiance curve. One of the key parameters of this photosynthesis-irradiance curve is the saturation intensity, which fluctuates due to the light-environment (*see* Eq. 4.40); so-called photo-acclimatisation. Note that for these computations the representative light-intensity is used (*see* Sec. 4.1.1).
2. The flow conditions influence the thickness of the velocity boundary layer (VBL), which is directly related to the thickness of the diffusion boundary layer (DBL). The diffusion boundary layer (DBL) affects the photosynthetic efficiency by limiting the diffusive transport of food and waste.
3. The thermal response of the coral is twofold: (1) the adapted temperature response, which takes into account the thermal specialisation of the coral (*see* Eqs. 4.50, 4.52 and

4.53); and (2) the thermal envelope, which accounts for the Arrhenius equation (*see* Eq. 4.54). Furthermore, corals have shown to acclimatise to their thermal environment as well—i.e. thermal-acclimatisation—which is, however, at a much slower pace than the photo-acclimatisation; days versus decades.

4. The effects of the acidity—enforced by a chain reaction due to the atmospheric pressure of CO_2 (*see* Eqs. 4.58 to 4.60)—results in changes in the saturation state of aragonite, which is one of the building blocks for calcification. Its effect on the calcification rate is based on the modified Michaelis-Menten equation (*see* Eq. 4.62).

4.3 Coral morphology

The morphological development is based on the optimal morphology as function of the environment, and the effective change of morphology based on the calcification rate as well as the morphology itself. First, the optimal morphological ratios based on the environmental conditions are discussed in Section 4.3.1, which are used for the eventual morphological development (Sec. 4.3.2).

4.3.1 Optimal morphology

The main environmental factors that play a role in the coral morphology are light and flow [e.g. Jaubert, 1977; Chappell, 1980; Lesser et al., 1994; Kruszyński et al., 2007], which effects are discussed in this section. Next to these two factors, sedimentation is also believed to influence the morphology of corals [Chappell, 1980; Hoogenboom et al., 2008, and references therein]. Beside the effect of the sediment concentration on the light-intensity, sediments are not taken into account.

The optimal morphology is given as the set of optimal morphological ratios. The combined effects are given by the product of the ratios as the functions of the light-intensity and the flow-environment in combination with a proportionality constant, i.e.:

$$r_{f,opt} = \chi_f \; r_{f,I} \; r_{f,u} \quad (4.63a) \qquad r_{p,opt} = \chi_p \; r_{p,I} \; r_{p,u} \quad (4.63b) \qquad r_{s,opt} = \chi_s \; r_{s,I} \; r_{s,u} \quad (4.63c)$$

where the subscript I denotes the dependency on light; the subscript u denotes the dependency on flow; and χ_f, χ_p and χ_s are the overall proportionality constants of the form, plate and spacing ratios, respectively.

The effects of the two stressors differ in mechanism: the effects of the light-availability on the shape of the coral are first elaborated on; and the effects of the driving transport mechanisms—advection or diffusion—as a function of the flow conditions are discussed next.

Light distribution

The light availability mainly influences the direction of growth of the coral [Graus and Macintyre, 1976]; vertical versus horizontal. High in the water column—where there is plenty of light—the light is multidirectional and corals grow upwards; while down the water column, the light originates mainly from above resulting in more horizontal directed growth [Graus and Macintyre, 1976; Jaubert, 1977]. At depth, all the light has to be captured, thus plates are formed to capture as much light as possible [Jokiel, 2011b]. Higher up the water column, the light-intensity can be such, that corals create branches to diffuse the light [Stambler and Dubinsky, 2005]. Otherwise, the light-intensity is too high for the photosynthetic apparatus, which results in photo-damage [Hoogenboom et al.,

2008]. There are no—quantitative or qualitative—relations found in the literature between the light-intensity and the width of the base, which sounds reasonable and so the plate ratio is solely based on the flow conditions.

Not much quantitative research has been done on the effects of light on the morphology of corals. Some of the main features agreed upon are the morphologies at high and at low light-intensities, which are branches and plates, respectively [Jaubert, 1977; Stambler and Dubinsky, 2005].

Recent studies have tried to quantify the morphology based on simplified geometries of corals [Muko et al., 2000; Anthony et al., 2005; Hoogenboom et al., 2008; Kaniewska et al., 2014; Ow and Todd, 2010]. These studies optimised the coral morphology to the acquisition of light in two-dimensional models [Muko et al., 2000; Anthony et al., 2005] and a three-dimensional model [Hoogenboom et al., 2008]. This optimalisation results in distinct morphologies for low and high light-intensities, but at intermediate intensities no clear optimal morphology exists. Therefore, at these light conditions, the morphology is not constrained by light as much.

Due to a lack of quantitative research in the effects of light-intensity on the morphology of corals—without the use of laborious models—this aspect is solely determined qualitatively. Increasing the depth, reduces the light-intensity (*see* Eq. 4.1), which reduces the height of the coral [Jaubert, 1977; Chappell, 1980; Jokiel, 2011b]. The height of the coral is therefore positively related to the light-intensity:

$$\langle I_z \rangle \uparrow \quad \rightarrow \quad \frac{h_c}{d_c} \uparrow$$

where $\langle I_z \rangle$ is the representative light-intensity (*see* Sec. 4.1.1).

This reasoning is in line with the quantitative models developed so far, where a clear flattening of the coral is computed for lower light-intensities at depth [Graus et al., 1984; Muko et al., 2000; Hoogenboom et al., 2008]. An important note to this reasoning is that the morphology of corals are determined by light-intensity, not depth.

High light-intensities support the formation of branches; to diffuse the incoming light to prevent photodamage of the zooxanthellae population in the coral tissue [Stambler and Dubinsky, 2005]. Therefore, the relative spacing is linked to the light-intensity as follows:

$$\langle I_z \rangle \uparrow \quad \rightarrow \quad \frac{d_c}{a_c} \downarrow$$

Thus, there are two main drivers in the determination of the coral morphology as function of the light-intensity: (1) diffusion of incoming light [Stambler and Dubinsky, 2005]; and (2) capture enough light for photosynthesis [e.g. Hoogenboom et al., 2008]. Protection against the high light-intensities can be achieved by creating spots of shadow, which is done most effectively by forming branches. This branch-formation at high light-intensity also enhances the collection of light for photosynthesis as there is more biomass per reef area. Deeper in the water column, the first aspect on protecting the photosynthetic apparatus [Stambler and Dubinsky, 2005] no longer is an issue. The capture of light on the other hand is. Because the light is mainly directed downwards further down in the water column [Jokiel, 2011b], corals form plates to capture as much light as possible. These mechanisms result in the following formulations to describe the optimal coral morphology as function of light-intensity:

$$r_{f,I} = \frac{\langle I_z \rangle}{I_0} \tag{4.64a}$$

$$r_{p,I} = 1 \tag{4.64b}$$

$$r_{s,I} = 1 - \tanh\left[\chi_{s,I}\frac{\langle I_z\rangle}{I_0}\right] \tag{4.64c}$$

where I_0 is the incoming light-intensity at the surface water; and $\chi_{s,I}$ the light proportionality constant of the spacing ratio.

Flow environment

The hydrodynamics surrounding the coral determines the strategy of the coral to obtain nutrients; advective transport versus diffusive transport [e.g. Kaandorp et al., 1996]. When the flow-velocities around the coral are low, the main method of transport is via diffusion; and vice versa. Diffusive transport is enhanced by creating more surface area, thus branches [Kaandorp and Sloot, 2001]. These branches enhance turbulent motions [Helmuth et al., 1997], which increase the uptake of nutrients and the removal of waste [Atkinson and Bilger, 1992; Hearn et al., 2001]. It, nevertheless, also increases the fragility of the coral, as the drag force on this type of morphology is larger [Helmuth and Sebens, 1993; Madin, 2005; Osorio-Cano et al., 2019].

Again, there is a lack in quantitative research on the effects of the flow on the coral morphology, but there is a clear trend: the higher the flow velocity, the more compact the coral morphology becomes [Helmuth and Sebens, 1993; Lesser et al., 1994; Kaandorp et al., 1996; Helmuth et al., 1997; Kruszyński et al., 2007]. This translates into:

$$|\mathbf{u}_{cm}|\uparrow \quad \rightarrow \quad \frac{d_c}{a_c}\uparrow$$

where $|\mathbf{u}_{cm}|$ is the magnitude of the in-canopy flow (*see* Sec. 4.1.2).

Furthermore, the tendency to lower the drag force on the coral, the coral changes its morphology such that it sticks out less [Kaandorp et al., 1996]. Reducing its height results in a more streamlined shape, which reduces the drag [Madin, 2005]:

$$|\mathbf{u}_{cm}|\uparrow \quad \rightarrow \quad \frac{h_c}{d_c}\downarrow$$

Finally, the increasing resistance of a wide base rewards corals in hydrodynamic violent locations [Madin and Connolly, 2006]:

$$|\mathbf{u}_{cm}|\uparrow \quad \rightarrow \quad \frac{b_c}{d_c}\uparrow$$

The resulting formulations of the characteristic ratios of the optimal morphology as function of the flow velocity are as follows:

$$r_{f,u} = \frac{u_{cr}}{|\mathbf{u}_{cm}|} \tag{4.65a}$$

$$r_{p,u} = 1 + \tanh\left[\chi_{p,u}\frac{|\mathbf{u}_{cm}| - u_{cr}}{u_{cr}}\right] \tag{4.65b}$$

$$r_{s,u} = 1 + \tanh\left[\chi_{s,u}\frac{|\mathbf{u}_{cm}| - u_{cr}}{u_{cr}}\right] \tag{4.65c}$$

where u_{cr} is a critical flow velocity that has to be fitted; $\chi_{p,u}$ the flow proportionality constant of the plate ratio; and $\chi_{s,u}$ the flow proportionality constant of the spacing ratio.

Beside the magnitude of the flow, the morphology of the coral is also shaped by the direction of the flow: (1) unidirectional flow leads to an elliptical shape [Kaandorp and Sloot, 2001]; and (2)

bi-directional flow to a radial symmetrical shape [Kaandorp and Sloot, 1999]. These findings are in line with the optimisation of a coral colony to the uptake of nutrients, by increasing its surface parallel to the flow direction [Kaandorp, 1995]. However, this variability is not taken into account in this study in which the corals are represented as symmetrical two-layered cylinders (*see* Fig. 3.6b).

4.3.2 Morphological development

The morphological development is based on phenotypic plasticity (*see* Sec. 3.3). Thereby, the calcification adds to the coral volume as more calcium carbonate ($CaCO_3$)—or aragonite—is accumulated to the coral skeleton. This addition of material is located such that the morphology moves towards its optimal morphology. In this study, this is represented as changing the morphological ratios towards the optimal morphological ratios (*see* Sec. 4.3.1).

Furthermore, as the calcification rate is given by biomass, the calcification rate per coral depends on the coral morphology itself. Therefore, the rate of change of the coral volume is described by a differential equation based on the following mass balance:

$$\frac{\partial V_c}{\partial t} = \frac{\dot{G}}{\rho_c} B_c(V_c; r_f, r_p) \tag{4.66}$$

where V_c is the volume of the coral colony; B_c the biomass, which is a function of the coral volume and the morphological ratios (*see* Sec. 4.1.1); $\dot{G}$ is the calcification rate, given per surface biomass; and ρ_c is the coral density.

The rate of change of the morphological ratios are given by the rate of change in coral volume. Therefore, the morphological development is described by a set of partial differential equations. All these equations have the same format and are based on Equation (4.66):

$$\frac{\partial \left(V_c r_i\right)}{\partial t} = \frac{\dot{G}\ r_{i,opt}}{\rho_c}\ B_c(V_c; r_f, r_p) \tag{4.67}$$

where r_i is the morphological ratio i; and $r_{i,opt}$ the optimal morphological ratio i.

Thereby, Equation (4.67) is the average of the previous morphological ratios and the optimal morphological ratios, weighted by the previous coral volume and the added volume due to calcification, respectively. Hereby, the mass balance of Equation (4.66) is conserved and the rate of change of the coral volume is used to describe the rate of change of the morphological ratios.

CONCLUDING REMARKS

The morphological development uses the definition of optimal morphologies, which are defined by the light and flow conditions These combined effects are given by:

$$r_{f,opt} = \chi_f \frac{\langle I_z \rangle}{I_k^{\max}} \frac{u_{cr}}{|\mathbf{u}_{cm}|} \tag{4.68a}$$

$$r_{p,opt} = \frac{1}{2}\left(1 + \tanh\left[\chi_{p,u} \frac{|\mathbf{u}_{cm}| - u_{cr}}{u_{cr}}\right]\right) \tag{4.68b}$$

$$r_{s,opt} = \frac{1}{2\sqrt{2}}\left(1 - \tanh\left[\chi_{s,I} \frac{\langle I_z \rangle}{I_0}\right]\right)\left(1 + \tanh\left[\chi_{s,u} \frac{|\mathbf{u}_{cm}| - u_{cr}}{u_{cr}}\right]\right) \tag{4.68c}$$

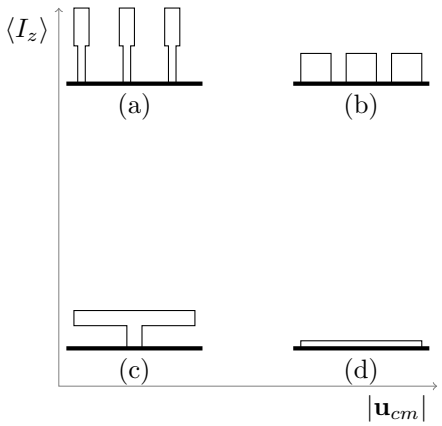

Figure 4.13: Schematic representation of the influence of the environment on the coral morphology. Coral morphologies are simplified to cylindrical shapes, as used in this study. **(a)** branching; **(b)** fingered, columnar; **(c)** tabular; **(d)** massive, encrusting.

where the overall proportionality constants for the plate and spacing ratios are based on the defined limitations given in Section 3.3: $\chi_p = 1/2$ and $\chi_s = 1/(2\sqrt{2})$.

With these three ratios and a given volume of the coral, all morphological dimensions can be determined by using the geometry of a two-layered cylinder. The rate of change of the morphology towards this optimal morphology depends on the calcification rate. Because the added volume due to the calcification is related to the coral morphology, this gives rise to a partial differential equation (*see* Eq. 4.67) describing the morphological development.

Figure 4.13 shows a qualitative representation of the coral morphologies over the considered environmental gradients; i.e. light and flow.

4.4 Summary

Summarising this chapter, the cycle of environmental conditions, coral physiology, and coral morphology are all encountered and discussed. Thereby, the basis of the biophysical model framework (BMF) is set.

Environment The coral environment describes the representative light-intensity for photosynthesis, the in-canopy flow structure and the coral "feeling" temperature. The representative light-intensity is based on the biomass-averaged light-intensity, where the biomass is defined as the surface of the coral colony receiving light.

The in-canopy flow is based on the canopy structure, which is split in two layers. In the determination, linear wave theory is used to determine the wave-attenuation coefficient (WAC) per canopy layer. The WAC is defined as the porous in-canopy flow over the above-canopy flow (*see* Fig. 4.3). The drag coefficient is determined based on the *constricted* in-canopy flow, which is a function of the canopy structure and the *porous* in-canopy flow.

The in-canopy flow is used to determine the thickness of the thermal boundary layer (TBL). The presence of a TBL results in a temperature increase as perceived by the coral; i.e. the feeling

temperature of the coral. This coral temperature is—among others—a function of the thickness of the TBL and the light-intensity.

Physiology The coral physiology describes the dependencies of the coral growth rate on the four included environmental factors: (1) light; (2) flow; (3) temperature; and (4) acidity. The first three factors are included via their effect on the photosynthesis, and the latter via the calcification.

The photosynthetic light dependency is given by the photosynthesis-irradiance curve. The two signifying parameters of this PI-curve—the maximum photosynthetic rate and the saturation intensity—are based on the dynamics of photo-acclimatisation.

The photosynthetic flow dependency is based on the presence of a diffusion boundary layer (DBL). Following Fick's first law, there is a linear relation between the photosynthesis limited by the diffusive transport and the flow velocity. As the photosynthesis is only flow-limited for low flow velocities, the flow dependency is given as a capped function; a tangent-hyperbolic function.

The photosynthetic thermal dependency is twofold: (1) the adapted temperature response; and (2) the thermal envelope. The first describes the efficiency of the coral-zooxanthellae symbiont based on the thermal limits in which this symbiosis works. The latter includes the principle of higher biochemical reactions at higher temperatures as formulated by the Arrhenius equation. The thermal limits of the symbiont are determined on long-term historic temperature time-series to which the corals are acclimatised; i.e. thermal-acclimatisation.

The implementation of the acidity is simplified to the aragonite saturation state, which is based on the oceanic carbon system. Thereby, the calcification includes an aragonite dependency. This dependency is based on the Michaelis-Menten equation, which describes the rate of biochemical reactions based on the concentrations of the biochemical components included.

Morphology The optimal morphology of corals is based on the light and flow conditions, where higher light-intensities result in the formation of branches to diffuse the light. Low flow velocities result in the same preference of branch-formation, but this is driven by the need to reduce the thickness of the velocity boundary layer (VBL)—and so the DBL and TBL. Moreover, the branches increase the coral surface compared to its volume, which is beneficial in the acquisition of food.

Lower light-intensities result in the formation of plates to be able to capture as much light as possible; and the increase in hydrodynamic stresses give rise to more compact morphologies, which are less susceptible to destruction. This translates in the formation of lower morphologies and a wider base diameter, respectively.

The morphological development is based on phenotypic plasticity in which the coral is able to change its morphology due to the environmental conditions. This rate of change of the morphology is based on the calcification rate, where new material for the skeleton is used to change the morphology towards the optimal morphology. This optimal morphology is based on the two aforementioned environmental conditions. Therefore, the morphological development is described by a set of partial differential equations.

Chapter 5

Coral bleaching

This chapter focusses on the bleaching of corals and how they recover. Corals bleach due to thermal stresses [e.g. Hoegh-Guldberg et al., 2007; Jokiel and Coles, 1977; Spalding et al., 2001]. When the temperature is out of the thermal range (*see* Sec. 4.2.3) the coral bleaches [e.g. Buddemeier et al., 2008; Evenhuis et al., 2015], which is due to both cold and heat stresses (*see* Fig. 4.9). Often, coral bleaching is solely related to the heat stresses [e.g. Harley et al., 2006; Hoegh-Guldberg et al., 2007; Hughes et al., 2019] due to global warming as part of climate change [e.g. Kleypas et al., 2001; Lough and Barnes, 2000; Wilkinson and Souter, 2008].

This chapter is on the population dynamics associated with coral bleaching, and therefore starts with introducing the framework of population states in Section 5.1. These population states are also presented in Figure 3.2 of which the part of interest for this chapter is highlighted in Figure 5.1. Thereafter, the dynamics associated with these population states is discussed in Section 5.2.

5.1 Population states

The health of corals is often described by population states [e.g. Baird and Marshall, 2002; Lough et al., 1999; Siebeck et al., 2006]. These states are phases of the coral from being healthy through being "ill" and laying on its "deathbed" up to being dead. Commonly, three population states are used to describe the coral health [e.g. Jokiel and Coles, 1977; Marshall and Baird, 2000] in which the dead population is not taken into account. In this study, however, a fourth is added [as suggested by Evenhuis et al., 2015]. The resulting four population states are the following:

Healthy Corals considered as healthy grow, reproduce, and calcify as normal. When biochemical stresses increase, healthy corals turn pale.

Pale The first phase of coral bleaching, results in pale corals. They have stopped growing and calcifying due to a loss of zooxanthellae, and can be called "ill". When the stresses continue, pale corals bleach; otherwise the corals start recovering.

Bleached Corals that are bleached also do not grow, reproduce, nor calcify and have lost most of their zooxanthellae. Bleached corals can be said to be on their "deathbed". From this state, the corals die if the stresses continue; if the stresses stop, the bleached corals turn pale after which they recover.

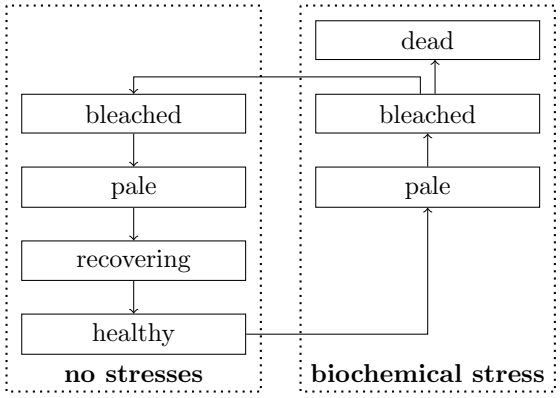

Figure 5.1: Pathways of loss and decay of corals due to biochemical stresses. When the coral is released from the stresses while in its pale state, it does not pass the bleached state before recovering. This arrow is left out for clarity of the scheme [based on Evenhuis et al., 2015].

Recovering When the thermal stresses cease, corals recover. Recovering corals have attracted some zooxanthellae, but do not grow, reproduce, nor calcify yet. When the stresses do not return, the corals become healthy again.

These states and their dynamics are visualised in Figure 5.1. The population states are described as fraction of surface—i.e. as percentage cover—and are denoted as P_H for healthy population; P_P for pale population; P_B for bleached population; and P_R for recovering population. Added to this list is the dead population—denoted as P_D—because the dead population of corals still contributes to the bottom roughness. Thereby, it is of interest for the hydrodynamics.

5.2 Population dynamics

The population dynamics are dependent on the photosynthesis, which relation to the environmental conditions is described in Sections 4.2.1 to 4.2.3. In this study, whether bleaching occurs or not depends on the coral temperature in which light-intensity, seawater temperature, and hydrodynamics are included (*see* Sec. 4.1.3). The set of differential equations as described by Evenhuis et al. [2015] is used as a basis for the population dynamics:

For $T_{lo} \leq T_c \leq T_{hi}$ (thus $P(I,T,u) \geq 0$):

$$\begin{bmatrix} \dot{P}_H \\ \dot{P}_R \\ \dot{P}_P \\ \dot{P}_B \end{bmatrix} = r_G P(I,T,u) C_{sp} \left(1 - \frac{P_T}{K}\right) \begin{bmatrix} 1 & 0 & 0 & 0 \\ 0 & 0 & 0 & 0 \\ 0 & 0 & 0 & 0 \\ 0 & 0 & 0 & 0 \end{bmatrix} \begin{bmatrix} P_H \\ P_R \\ P_P \\ P_B \end{bmatrix} \quad \textit{(growth)} \tag{5.1a}$$

$$+ \quad r_R P(I,T,u) \begin{bmatrix} 0 & \frac{1}{2}C_{sp} & 0 & 0 \\ 0 & -\frac{1}{2}C_{sp} & C_{sp} & 0 \\ 0 & 0 & -C_{sp} & 8/C_{sp} \\ 0 & 0 & 0 & -8/C_{sp} \end{bmatrix} \begin{bmatrix} P_H \\ P_R \\ P_P \\ P_B \end{bmatrix} \quad \textit{(recovery)} \tag{5.1b}$$

$$+ \quad r_M C_{sp} \begin{bmatrix} 0 & 0 & 0 & 0 \\ 0 & 0 & 0 & 0 \\ 0 & 0 & 0 & 0 \\ 0 & 0 & 0 & -1 \end{bmatrix} \begin{bmatrix} P_H \\ P_R \\ P_P \\ P_B \end{bmatrix} \quad \textit{(mortality)} \tag{5.1c}$$

For $T_c < T_{lo}$ or $T_c > T_{hi}$ (thus $P(I,T,u) < 0$):

$$\begin{bmatrix} \dot{P}_H \\ \dot{P}_R \\ \dot{P}_P \\ \dot{P}_B \end{bmatrix} = r_B P(I,T,u) C_{sp} \begin{bmatrix} 1 & 0 & 0 & 0 \\ 0 & 1 & 0 & 0 \\ -1 & -1 & \frac{1}{2} & 0 \\ 0 & 0 & -\frac{1}{2} & \frac{1}{4} \end{bmatrix} \begin{bmatrix} P_H \\ P_R \\ P_P \\ P_B \end{bmatrix} \quad \textit{(bleaching)} \tag{5.1d}$$

where $\dot{P}_i$ describes the rate of change of population state i; r_j are empirically determined rates for the four processes; K is the carrying capacity; and P_T the total living population, which is the sum of all four aforementioned population states ($P_T = P_H + P_R + P_P + P_B$). The lower and upper bound—T_{lo} and T_{hi}, respectively—describe the thermal range of corals in which corals do not experience thermal stresses (*see* Sec. 4.2.3).

The carrying capacity is the portion of the area that is suitable for coral colonisation, which consists of the existing coral patches—alive or dead—and also other (hard) suitable substratum [Riegl and Purkis, 2009]. Thus the carrying capacity is given by:

$$K = P_T + P_D + A_S \tag{5.2}$$

where P_D is the dead coral cover; and A_S the (hard) substratum suitable for coral colonisation.

Chapter 6

Coral dislodgement

Corals experience mechanical stresses beside the biochemical stresses as discussed in the previous chapter (*see* Ch. 5). Where biochemical stresses are size-independent [e.g. Baird and Marshall, 2002], mechanical stresses are size-dependent [Denny, 1995; Madin, 2005; Madin and Connolly, 2006; Hongo et al., 2012]. Moreover, there are four other important factors in the dislodgement and breakage of corals beside size [Denny, 1995; Madin, 2005]: (1) morphology; (2) flow velocity; (3) gravity; and (4) strength.

The removal of corals is mainly induced by the hydrodynamics. However, other environmental factors play a role as well: ocean acidification (OA) weakens the calcium carbonate ($CaCO_3$) skeleton and the reef substrate [Hoegh-Guldberg et al., 2007; Kleypas et al., 1999; Manzello et al., 2008; Marshall, 1985]; and a low calcification rate decreases the density of corals and thereby its strength [Chamberlain, 1978; Cooper et al., 2008; Madin, 2004; Madin et al., 2008]. Due to this dependency of the strength on the calcification rate, all physiological environmental factors—as discussed in Chapter 4—have implicitly a role to play in the mechanical resistance of corals.

This chapter is dedicated to the inclusion of storm damage in the framework as discussed in Chapter 3. First, the processes concerning storm damage on coral reefs are explored in Section 6.1. Thereafter, the modelling approach to include the storm damage to corals is presented in Section 6.2, which focusses on the left hand side of Figure 3.2 of which the section of interest is given by Figure 6.1. Finally, the post-storm recovery is discussed in Section 6.3.

6.1 Coral destruction

Corals can be destroyed (1) directly, due to the wave load [Madin, 2005; Madin and Connolly, 2006; Woodley et al., 1981]; and (2) indirectly, due to tumbling corals and fragments [Knowlton et al., 1981; Smith and Hughes, 1999]. The direct destruction is again split in two mechanisms: (1) breakage of the coral skeleton [Chamberlain, 1978; Schuhmacher and Plewka, 1981]; and (2) dislodgement of the whole coral colony [Hongo et al., 2012; Madin, 2005; Madin and Connolly, 2006].

The strength of corals is in general an order of magnitude higher than that of the substratum [Macintyre and Marshall, 1988; Madin, 2005; Madin et al., 2013]. Therefore, the limiting factor of coral resistance against hydrodynamic loads is the substratum [Hongo et al., 2012; Madin and

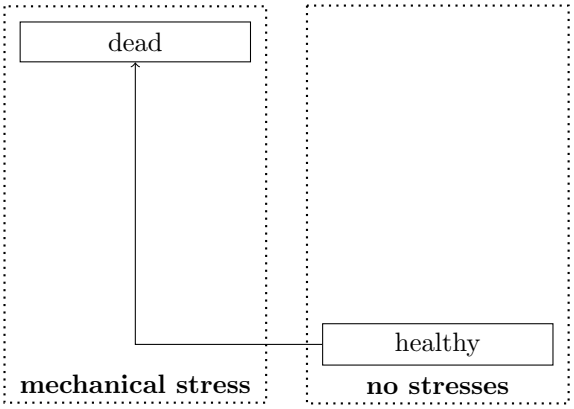

Figure 6.1: Pathways of loss and decay of corals due to mechanical stresses. When the coral is dislodged, it is removed and so the area turns into no coral cover, and the coral is dead. Also corals from other population states than healthy can be dislodged; these arrows are left out for clarity.

Connolly, 2006]. This leads to the schematisation of total removal of corals when the load exceeds the resistance and no partial removal—i.e. breakage—is taken into account. Thereby, the coral destruction is a binary process—the coral is healthy, or dead—as shown in Figure 6.1.

However, broken fragments and dislodged corals can survive [Knowlton et al., 1981] and reattach [Smith and Hughes, 1999]. For fragile corals, this is even thought of as the main reproduction mechanism [Lirman, 2000; Roth et al., 2013; van Dongen-Vogels and Mallefet, 2006]. Nevertheless, this requires the coral (fragment) to be stabilised and cemented to the substratum [Rasser and Riegl, 2002], which does not always succeed. Furthermore, dislodged and fragmented corals will destroy others as they move along with the flow; i.e. the indirect destruction [Knowlton et al., 1981; Smith and Hughes, 1999]. As the exact effects of the two mechanisms are still unknown, these two processes are not taken into account.

6.2 Dislodgement formulation

In this study, the dislodgement model by Madin and Connolly [2006] is used, which consists of two dimensionless parameters: (1) the dislodgement mechanical threshold (DMT) relates the strength to the load; and (2) the colony shape factor (CSF) includes the effect of the coral morphology. The model of Madin and Connolly [2006] is used due to its simplicity, but still proven robustness [e.g. Hongo et al., 2012]. The dislodgement criterion is modified[1] from Madin and Connolly [2006]:

$$\underbrace{\frac{\sigma_t}{\rho C_d \left|\mathbf{u}_m^{\max}\right|^2}}_{\text{DMT}} \leq \underbrace{\frac{16}{\pi b_c^3} \int_{h-h_c}^{h} (h-z)\, w_c(z)\, \mathrm{d}z}_{\text{CSF}} \tag{6.1}$$

where σ_t is the tensile strength of the substratum, which is assumed to be weaker than the coral skeleton [Madin, 2005; Madin et al., 2008, 2013]; ρ is the density of water; C_d the drag coefficient; $|\mathbf{u}_m^{\max}|$ the magnitude of the maximum flow velocity; b_c the width of the base by which the coral is attached to the substratum; $w_c(z)$ the width of the coral varying over its height; and z is directed downwards with $z = 0$ at mean sea level.

[1] The drag coefficient is assumed to be equal to one in the original formulation [Madin and Connolly, 2006]. In this formulation, it is included to show the full picture.

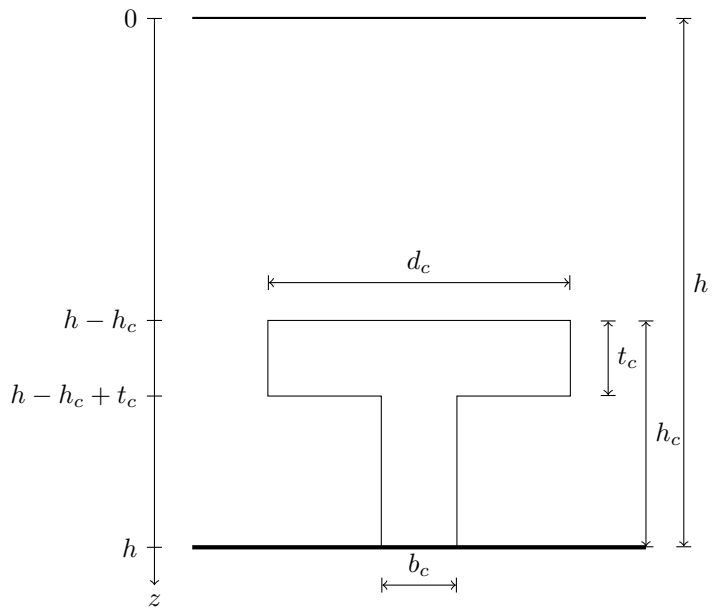

Figure 6.2: Representation of the coral morphology. The representation of the coral morphology is repeated here from Section 3.3 for convenience highlighting the description given in Equation (6.2).

For the width as function of the height, a simple formulation holds in this study due to the simple morphological representation (*see* Fig. 3.6a):

$$w_c(z) = \begin{cases} b_c & \text{for } h - h_c + t_c < z \leq h \\ d_c & \text{for } h - h_c \leq z \leq h - h_c + t_c \\ 0 & \text{for } z < h - h_c \end{cases} \tag{6.2}$$

where z is the vertical coordinate, which is positive directed downwards with $z = 0$ at mean sea level. Equation (6.2)—including the water depth marks—is visualised in Figure 6.2 for clarification.

Due to the fact that the coral morphology is homogeneous per grid cell, all corals are removed due to a storm; or all corals stay put. This feedback—of full removal, or not—is included into the biophysical model framework (BMF) via the coral cover and the coral morphology (*see* Sec. 3.1): the coral cover is reduced to zero when the dislodgement criterion is met; and the coral volume—and thereby the coral itself—is reduced to zero as well. This binary nature of the results of the dislodgement is due to the homogeneous representation of the coral morphology.

6.3 Recolonisation

As the formulations on the dislodgement result in a binary outcome—full dislodgement, or full survival—the aspect of recolonisation has to be included. If not, an area that complied with the dislodgement criterion will never be recolonised by corals in the biophysical model framework (BMF). Therefore, an extra term to include the recolonisation of the area is included, which is based on the coral recruitment. The full recruitment dynamics—coral spawning [Guest et al., 2005; Mangubhai and Harrison, 2008], larval dispersion [Bradbury and Snelgrove, 2001; Cowen et al., 2006; Cowen and Sponaugle, 2009], larval mortality [Connolly and Baird, 2010; Graham et al., 2008], larval

competence to settle [Miller and Mundy, 2003; Nozawa and Harrison, 2008; Connolly and Baird, 2010], and larval settlement [Harii et al., 2002; Harii and Kayanne, 2003; Tay et al., 2011]—are not included.[2] Instead, a constant contribution due to the annual spawning of corals [Vize, 2006] is included.

This annual spawning is related to the healthy coral cover and the coral volume. From these two parameters, the coral can regrow and repopulate the substrate. To best represent the coral recruitment dynamics without addition of many new parameters and calculations, two aspects are included: (1) the healthy population cover of the reef; and (2) the logistic bottleneck. The first represents the reduced recovery potential for far degraded reefs; and the latter the space available for settlement of larvae.

Therefore, the additions in healthy coral cover and coral volume are given by respectively:

$$\Delta P_H = S_P \langle P_H \rangle \left(1 - \frac{P_T}{K}\right) \tag{6.3a}$$

$$\Delta V_c = S_V \langle P_H \rangle \left(1 - \frac{P_T}{K}\right) \tag{6.3b}$$

where S_P and S_V are predefined constants on the potential of coral recruitment due to mass spawning events on the coral cover and volume, respectively; $\langle P_H \rangle$ is the average healthy coral cover of the whole reef; P_T the total living coral (healthy, recovering, pale and bleached); and K the carrying capacity of the area.

These potentials of coral recruitment are related and show great similarities:

$$S_P = p_s N_l d_l^2 \tag{6.4a}$$

$$S_V = p_s N_l d_l^3 \tag{6.4b}$$

where p_s is the probability of settlement; N_l the number of larvae due to the mass spawning event; and d_l the diameter of one larva.

[2] However, a suggestion on how the full recruitment dynamics of corals can be incorporated into the BMF developed in this study is presented in Appendix F. Here, formulations are derived for all aforementioned processes.

Chapter 7

Verification and validation

The results of the developed biophysical model framework (BMF) are presented in the form of a verification and validation to the available data, and a sensitivity analysis (*see* Ch. 8). Unfortunately, the coverage of the available data is limited and it does not address all aspects together as in this BMF. Therefore, parts of the BMF are validated separately. Another limitation to the validation is the limited amount of data, where most studies based their statistical work on a couple of tens of species; commonly, ten to twenty corals are investigated per study [e.g. Howells et al., 2013; Jokiel and Coles, 1977] or even less [e.g. Langdon and Atkinson, 2005]. This limited amount of data results in large spreading and uncertainty.

Furthermore, certain aspects of the BMF are the result of recent developments and there are no data sets whatsoever to validate them with. Therefore, the description on the dislodgement (*see* Ch. 6) is not validated in this report. Especially the lack of the width of the base of the coral colony results in disqualification of data as only the height and diameter are listed [e.g. Marks, 2007; Viehman et al., 2018]. However, this description has not been modified compared to the validated formulation in literature [Madin and Connolly, 2006], which shows good agreement with the data.

The coral morphology as function of its environment cannot be validated as well, due to a lack of useful data. In literature, only qualitative descriptions of the morphology and/or the environment are given on which no validation can be based. However, there are large data sets on the coral morphology in Florida, USA. Unfortunately, there are two downsides to these data sets for validation: (1) the morphology is solely described by the coral height and maximum diameter [Marks, 2007; Viehman et al., 2018]; and (2) the reefs are degrading and so might not be representative [pers. comm. L.T. Toth and M. Colella]. The results are presented in Figure 7.1 the two large data sets—AGRRA and CREMP—on the coral reefs in Florida, USA.[1]

This chapter starts with the verification of the coral environment (Sec. 7.1). Thereafter, the validation of the physiological processes are presented (Sec. 7.2), which first addresses every environmental factor separately. The physiology as a whole is presented at the end of Section 7.2 and is validated by means of comparison between model and measured calcification rates. Finally, the population dynamics are validated using bleaching reports and laboratory experiments on bleaching (Sec. 7.3).

[1] The attenuation of light is based on satellite data on the light-attenuation of blue light [NASA Goddard Space Flight Center Ocean Biology Processing Group, 2018]. The attenuation of blue light is rewritten to representative values for the photosynthetically active radiation (PAR) according Saulquin et al. [2013].

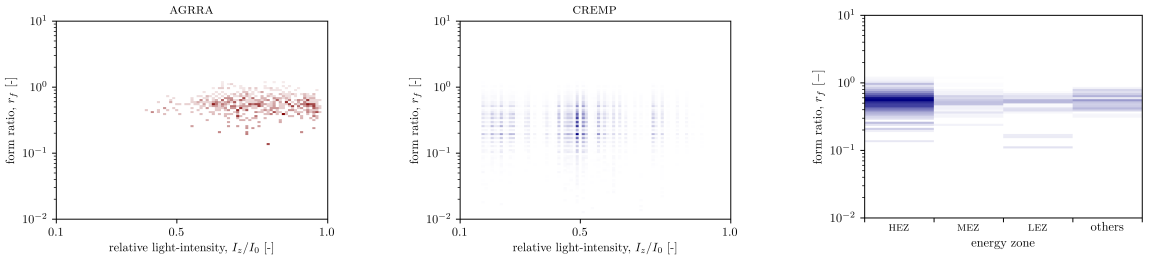

(a) Light conditions (AGRRA, $N = 627$).

(b) Light conditions (CREMP, $N = 82,398$).

(c) Flow conditions (AGRRA, $N = 627$).

Figure 7.1: Morphological dependency on environmental conditions. **(a)** and **(b)** The form ratio as function of relative light-intensity according two different data sets presented as density plots in which a higher opacity indicates a higher density. **(c)** The form ratio as function of wave energy. The reef zones are categorised by wave energy level: HEZ, high energy zone; MEZ, mid energy zone; LEZ, low energy zone; and 'others' includes descriptions of the reef that cannot be placed under one of the energy levels. Data is presented as a density plot of the form ratio as function of the zonation of the wave energy level. Sources: CREMP, Coral Reef Evaluation and Monitoring Project [provided by M. Colella]; AGRRA, Atlantic and Gulf Rapid Reef Assessment [Marks, 2007].

When the formulations of the BMF require data fitting, all of the limited data is used for this data fitting. Thereby, no independent data set is left to correctly validate with. This holds for (1) the photosynthetic flow dependency (Sec. 7.2.2); (2) the aragonite dependency (Sec. 7.2.4); and (3) the calcification rate (Sec. 7.2.5).

7.1 Coral canopy environment

The verification of the coral feedback only considers the effects of corals on the hydrodynamics, as the catchment of light as a function of the coral morphology is purely based on geometry (*see* Sec. 4.1.1). Moreover, the attenuation of light is commonly described by the Beer-Lambert law (*see* Eq. 4.1) and its validity is proven over and again.

Furthermore, the focus of this section is on the wave-attenuation coefficient (WAC) as the accuracy of the drag coefficient is considered negligible (*see* App. D.2.2); either the flow is very low so the risk of dislodgement is non-existing, or the drag coefficient approaches one for larger flow velocities and so is flow-independent. Therefore, assuming the drag coefficient to equal unity in the dislodgement calculations is reasonable, and common practice [Hongo et al., 2012; Madin and Connolly, 2006]. The effect of the drag coefficient on the WAC is taken into account by the assessment of the WAC.

In Figure 7.2, the model predictions and the measured values of the WAC are plotted against each other. From the four data sets used, only the data of Weitzman et al. [2015] covered a two-layer canopy; all other sources contain single-layer canopies. This is also where the data points with the high transparency and the large error come from; the predicted WAC is around 70%, while the measured data result in approximately 10% [Weitzman et al., 2015]. This mismatch is due to the numerical solver used (*see* App. A.2.1), which has not converged to an answer for these combinations of canopy and flow conditions. Increasing the number of iterations, does not solve the problem. All in all, the solution of the Canopy-Flow Theory (CFT) (*see* Eq. 4.28) shows great agreement with the data.

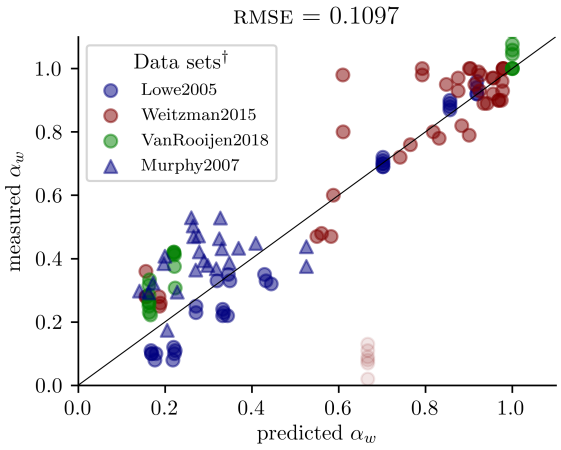

Figure 7.2: Verification of the wave-attenuation coefficient. The root-mean-squared errer (RMSE) is given on top of the plot. The iterations associated with the data points with high transparency as part of the settings according Weitzman et al. [2015] did not converge, and therefore are not included in the determination of the RMSE. † Sources: Lowe2005, Lowe et al. [2005a]; Weitzman2015, Weitzman et al. [2015]; VanRooijen2018, van Rooijen et al. [2018]; Murphy2007, Murphy et al. [2007].

7.2 Physiological processes

The validation of the physiological processes associated with the growth of corals has been described by their corresponding dependencies; i.e. all other conditions are taken constant and the parameter of interest is isolated. This means that for mixed studies—studies in which multiple environmental factors are investigated—the changes due to the parameter of interest is isolated as far as possible.

This section starts by validating the four environmental factors that are taken into account in the biophysical model framework (BMF): (1) light; (2) hydrodynamics; (3) temperature; and (4) acidity (Secs. 7.2.1 to 7.2.4, resp.). It concludes with the validation of the BMF to in-situ studies on the long-term calcification rates.

7.2.1 Light dependency

As is proven many times, the relation between the photosynthetic rate and light-intensity for photosynthetic organisms can be described by a photosynthesis-irradiance curve [e.g. Anthony and Hoegh-Guldberg, 2003a; Chalker et al., 1983; Dubinsky and Stambler, 2011; Jassby and Platt, 1976; Jeans et al., 2013]. Due to the common acceptance and extensively proven fact of the *PI*-curve, the validation of this part of the BMF is not included and it is assumed that the photosynthetic dependency to light is correctly described by the *PI*-curve. The key parameters describing it, however, are presented in this section (*see* Fig. 7.3), where especially the saturation intensity shows a good fit (*see* Fig. 7.3b). The root-mean-squared errors (RMSEs) between the model output and the measurements from literature are presented on top of the sub-figures in Figure 7.3.

7.2.2 Flow dependency

The effects of the flow on the growth of corals are commonly investigated in combination with at least one of the other environmental factors that are part of this study—i.e. light, temperature and/or aragonite. In these studies, the flow dependency is not the main topic of investigation and its effect

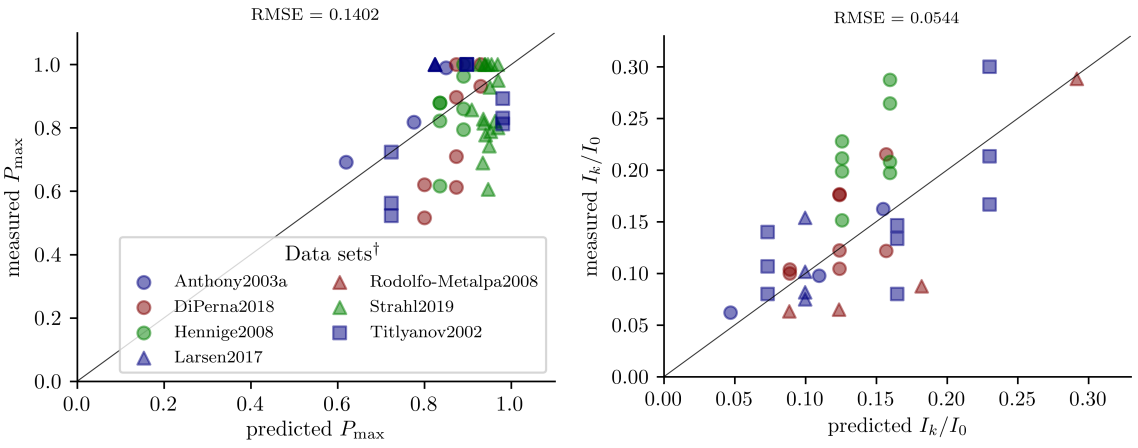

(a) maximum photosynthetic rate, P_{max}.

(b) relative saturation intensity, I_k/I_0.

Figure 7.3: Validation of photosynthetic light dependency. The root-mean-squared errors (RMSEs) for both plots are presented on top: **(a)** maximum photosynthetic rate, P_{max}; and **(b)** saturation intensity relative to the down welling light-intensity, I_k/I_0. The legend in **(a)** holds for both sub-figures. † Sources: Anthony2003a, Anthony and Hoegh-Guldberg [2003b]; DiPerna2018, DiPerna et al. [2018]; Hennige2008, Hennige et al. [2008]; Larsen2017, Larsen et al. [2017]; Rodolfo-Metalpa2008, Rodolfo-Metalpa et al. [2008]; Strahl2019, Strahl et al. [2019]; Titlyanov2002, Titlyanov and Titlyanova [2002] .

is commonly described qualitatively. As a result, in many studies the flow is considered as low flow versus high flow [e.g. Kuffner, 2002] or still water compared with at maximum two flow regimes [e.g. Comeau et al., 2014; Nakamura et al., 2005]. In combination with the various expressions on coral growth used in the various studies, validation of the photosynthetic flow dependency shows large spreading in the data; especially at low flow velocities (*see* Fig. 7.4).

Furthermore, most of the literature related the dependency of the coral growth—either photosynthetic rate or calcification rate—to the bulk flow. However, the formulation of the flow dependency relates the in-canopy flow to the photosynthetic efficiency via its effect on the velocity boundary layer (VBL) (*see* Eq. 4.47), which is physically more sound. Therefore, the in-canopy flow was reconstructed from the data if possible, and plotted against the resulting growth data; presented in Figure 7.4b. In case of too little data to fully reconstruct the in-canopy flow, a constant, representative wave-attenuation coefficient (WAC) is used based on the unidirectional limit; i.e. $\alpha_w = 0.3$. This because these studies are conducted inside a flume without waves and are therefore considered in the unidirectional domain.

Both fits—to the bulk and the in-canopy flow—do not show clear dependencies (*see* Fig. 7.4), which is due to (1) the units used to express the photosynthetic flow dependency differed per study in which commonly multiple species were investigated as well; and (2) the limited range of flow velocities investigated per study that have the same methodology of measuring, describing, etc. of the data. The fitted parameters are (1) for the bulk flow, $P_u^{\min} = 0.6889$ and $u_{cr} = 0.5173\ ms^{-1}$; and (2) for the in-canopy flow, $P_u^{\min} \approx 0.6889$ and $u_{cr} \approx 0.1716\ ms^{-1}$.

7.2.3 Thermal dependency

The thermal response of the calcification rate is often fitted to a cubic polynomial [Buddemeier et al., 2008; Edmunds, 2005], which makes sense as clearly visible in Figure 7.5. Herein, the thermal

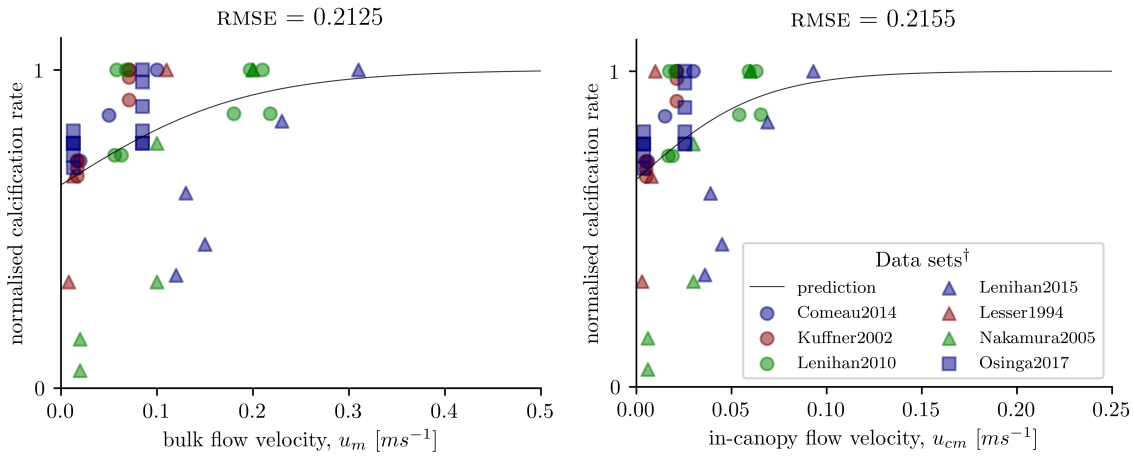

(a) Bulk flow, u_m.

(b) In-canopy flow, u_{cm}.

Figure 7.4: Validation of photosynthetic flow dependency. The root-mean-squared errors (RMSEs) for both plots are presented on top. The formulation on the dependency on flow is given as a function of the in-canopy flow (*see* Eq. 4.47). Because most literature based their findings on the bulk flow, both validations are presented: **(a)** bulk flow; and **(b)** in-canopy flow. When not enough data is available to reconstruct the in-canopy flow, a constant WAC is used; see text for further explanation. † Sources: Comeau2014, Comeau et al. [2014]; Kuffner2002, Kuffner [2002]; Lenihan2010, Lenihan and Edmunds [2010]; Lenihan2015, Lenihan et al. [2015]; Lesser1994, Lesser et al. [1994]; Nakamura2005, Nakamura et al. [2005]; Osinga2017, Osinga et al. [2017] .

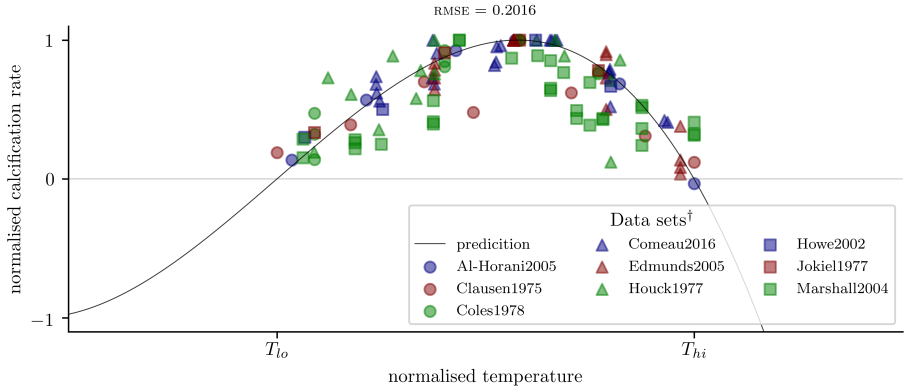

Figure 7.5: Validation of photosynthetic thermal dependency. The RMSE is given on top of the plot. All used data sets are both normalised for the calcification rate and for the thermal key parameters to be able to compare the various data sets within one plot. Temperatures are normalised to the thermal range between $T_{c,lo} = 20.0°C$ and $T_{c,hi} = 30.0°C$. † Sources: Al-Horani2005, Al-Horani [2005]; Clausen1975, Clausen and Roth [1975]; Coles1978, Coles and Jokiel [1978]; Comeau2016, Comeau et al. [2016]; Edmunds2005, Edmunds [2005]; Houck1977, Houck et al. [1977]; Howe2002, Howe and Marshall [2002]; Jokiel1977, Jokiel and Coles [1977]; Marshall2004, Marshall and Clode [2004] .

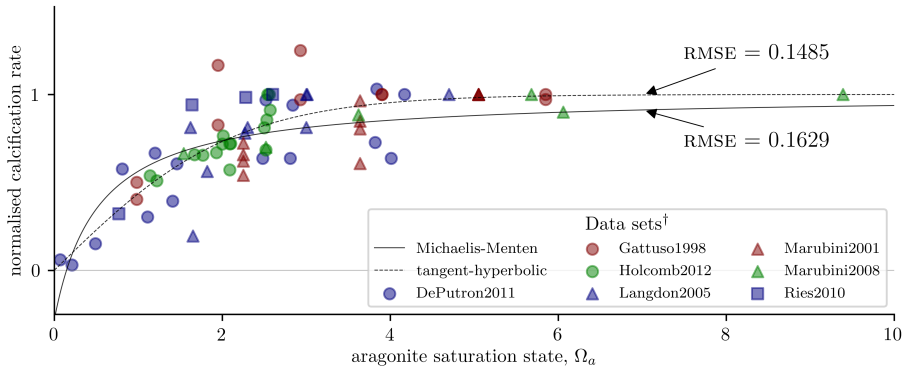

Figure 7.6: Validation of calcification aragonite dependency. The root-mean-squared errors (RMSEs) of both fits are presented near their fitting lines inside the plot. All used data sets are normalised for the calcification rate, which is often described in different units. † Sources: DePutron2011, de Putron et al. [2011]; Gattuso1998, Gattuso et al. [1998]; Holcomb2012, Holcomb et al. [2012]; Langdon2005, Langdon and Atkinson [2005]; Marubini2001, Marubini et al. [2001]; Marubini2008, Marubini et al. [2008]; Ries2010, Ries et al. [2010] .

key parameters—the limits of the thermal range—are normalised as well as the calcification rate to be able to compare the data sets with each other.

The data follows the shape of the formulations used; i.e. the existence of an optimal temperature and a thermal range. Not all follow the exact shape as drawn in black in Figure 7.5, but the validation gives confidence in the use of the formulation on the photosynthetic thermal dependency. Part of these discrepancies are attributed to the processing of the data, but also to the large spreading in the data itself—Figure 7.5 only includes the means presented in the data—as the number of corals measured is limited per study.

7.2.4 Aragonite dependency

Research on the aragonite dependency of the calcification rate is only of recent years, with the first publications at the end of the 1990s [Gattuso et al., 1998]. In this dependency, one must take into account (1) the high sensitivity of the aragonite to *p*H (*see* Eqs. 4.59 and 4.60); and (2) the fact that accurate *p*H measurements are hard to perform.

Even though the Michaelis-Menten equation (Eq. 4.62) is a process-based formulation, a comparable tangent-hyperbolic function seems to give a better fit to the data (*see* Fig. 7.6):

$$\gamma(\Omega_a) = \tanh\left[\frac{\Omega_a - \Omega_0}{\kappa_a}\right] \tag{7.1}$$

Nevertheless, the difference in accuracy is small in both cases. Part of the spreading of the data might be due to the normalisation of the calcification rate. On the other hand, substantial uncertainty is present in the measurements as well, and other aspects—e.g. temperature—could play a role.

7.2.5 Calcification rate

The specialisation term in the thermal response (*see* Sec. 4.2.3) has a substantial influence on the calcification rate for the cases in which the thermal range is narrow (*see* Fig. 7.7a versus Fig. 7.7b); the thermal conditions in Scoffin et al. [1992] resulted in thermal ranges below five degrees

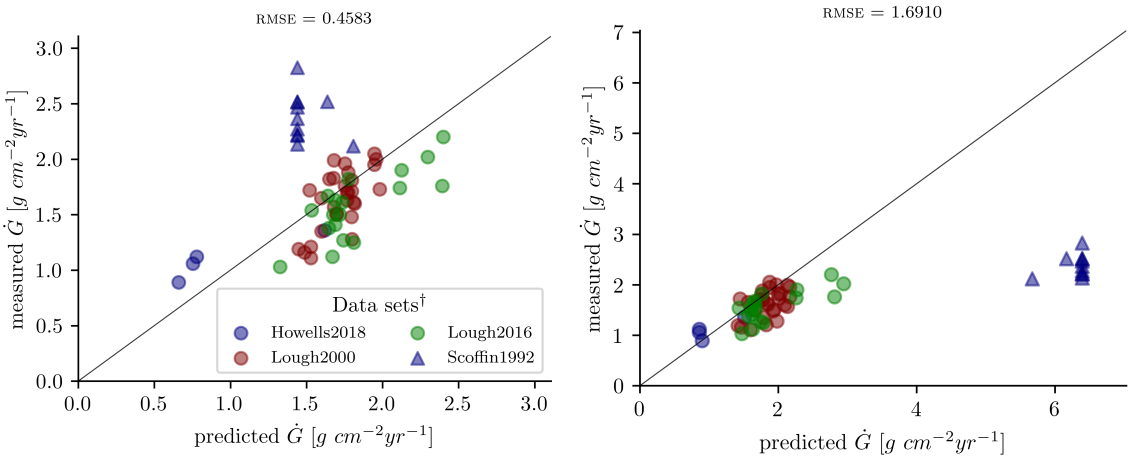

(a) According Evenhuis et al. [2015] (Eq. 4.52).

(b) According solely math (Eq. 4.53).

Figure 7.7: Validation of the calcification rate with literature. The root-mean-squared errors (RMSEs) of both plots are presented on top. The effects of the specialisation term in the adapted temperature response (Eq. 4.50) is included: **(a)** according the formulation of Evenhuis et al. [2015] (*see* Eq. 4.52); and **(b)** mathematically correct normalisation (*see* Eq. 4.53). Note the different scales of the two plots due to the mismatching model results with the data of Scoffin et al. [1992]. † Sources: Howells2018, Howells et al. [2018]; Lough2000, Lough and Barnes [2000]; Lough2016, Lough et al. [2016]; Scoffin1992, Scoffin et al. [1992] .

Centigrade ($\Delta T < 5°C$). Thereby, the thermal response is magnified considerably (*see* Fig. 7.7). Also note the different scales between Figures 7.7a and 7.7b.

The best fit of the calcification constant (g_C in Eq. 4.36) turns out to be $g_C = 0.52\ kg\ m^{-2}d^{-1}$ in case the specialisation term as suggested by Evenhuis et al. [2015] is used. Reducing the RMSE to a minimum in search of the best fit of the calcification constant based on the mathematical specialisation term (*see* Eq. 4.53) results in mainly adapting the constant such that the data of Scoffin et al. [1992] fits better. The differences between Figures 7.7a and 7.7b are fully related to the choice of the specialisation term. As a reminder, the specialisation term is in both cases a non-linear function of the thermal range (*see* Eqs. 4.52 and 4.53).

7.3 Population dynamics

The population dynamics represent the effects of a bleaching event. No studies include the recovering state, but the other states are in some way represented; the states between healthy and dead are commonly described as percentage dead [e.g. Edmunds, 2005], percentage bleached [e.g. Baird and Marshall, 2002], or other comparable ranking systems [e.g. Dias et al., 2018; Howells et al., 2013; Marshall and Baird, 2000].

Different studies, show different aspects of the population dynamics. To start with, Jokiel and Coles [1977] show the presence of heat stress as well as cold stress. This principle is also present in the study of Howells et al. [2013] effects of temperature history; presented in Figure 7.8. Studies on bleaching also include the recovery process in which the absence of the modelled recovery state is covered by the healthy population or the pale population.

The study of Howells et al. [2013] encompasses many aspects included in the biophysical model framework (BMF), and therefore it is discussed in more detail. First of all, it is an in-situ study that

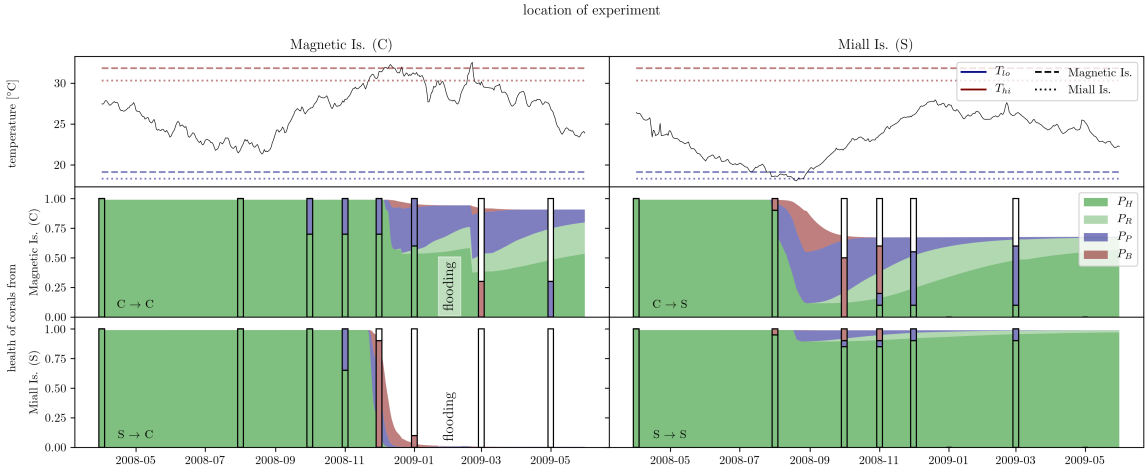

Figure 7.8: Validation of coral health data highlighting the difference between temperature history. Corals from two different locations at the Great Barrier Reef (GBR) were transplanted to illustrate the relevance of the temperature history on the response on thermal conditions, where Magnetic Island is located in Central GBR; and Miall Island in South GBR. Top plots present the in-situ measured sea surface temperature (SST) data. Other plots represent the response of the corals as the population dynamics. Bars indicate the measurements conducted during the experiments, and the continuous areas represent the model output; both following the same color scheme. More details are presented in the text (data from Howells et al. [2013]).

assess the responses of corals to a bleaching event. However, there is a twist to this study that makes it extra interesting; it takes the effects of temperature history into account. Therefore, it enables the validation of the determination of the thermal limits; i.e. the thermal-acclimatisation. In their study, Howells et al. [2013] transplanted corals from two different locations on the Great Barrier Reef hundreds of kilometres apart: Magnetic Island is located in Central Great Barrier Reef; and Miall Island is located in Southern Great Barrier Reef. Due to their different temperature histories, their thermal limits differ and so their responses to the thermal conditions.

During the study period, a bleaching event occurred at Magnetic Island due to heat stress (*see* Fig. 7.8, left column); and a bleaching event occurred at Miall Island due to cold stress (*see* Fig. 7.8, right column). As the corals from Miall Island are used to colder temperatures, the damage due to the bleaching event at Magnetic Island is substantially more severe. The cold water bleaching event at Miall Island is resulting in almost no bleaching for the corals from Miall Island—which are more adapted to colder temperatures—while severe bleaching occurs among the corals originating from Magnetic Island.

Unfortunately, Central Great Barrier Reef was affected by flooding during the study period, resulting in significant coral mortality [Howells et al., 2013]. This flooding event is marked in Figure 7.8. The data from Howells et al. [2013] after this flooding event is not taken into account in the assessment of the model validation.

Comparable assessments to the in detail described study of Howells et al. [2013] are performed with other studies encompassing bleaching. These assessments show that the BMF largely follows the dynamics of the coral population as described by these studies [e.g. Baird and Marshall, 2002; Dias et al., 2018; Edmunds, 2005; Jokiel and Coles, 1977; Marshall and Baird, 2000]. The root-mean-squared errors (RMSEs) of model validations on the population dynamics are presented in Table 7.1.

Table 7.1: The root-mean-squared errors for the validation of the population dynamics. Both specialisation terms are used: spec_M normalises the area under the curve (*see* Eq. 4.53); and spec_E follows the normalisation by Evenhuis et al. [2015] (*see* Eq. 4.52). The RMSEs for the healthy population are denoted under e_H; the healthy and recovering population combined as the healthy population under e_{H+R}; and the total population under e_T.

Source	spec_M			spec_E		
	e_H	e_{H+R}	e_T	e_H	e_{H+R}	e_T
Baird and Marshall [2002]	0.3498	0.2069	0.1292	0.3469	0.2026	0.1288
Bayraktarov et al. [2013]	0.1800	0.1623	0.0854	0.1835	0.1585	0.0552
Berkelmans and Van Oppen [2006]	0.1912	0.1961	0.1166	0.1911	0.1943	0.1156
Dias et al. [2018]	0.1333	0.1333	0.2074	0.1359	0.1359	0.2047
Howells et al. [2013][a]	0.1494	0.1649	0.0782	0.1511	0.1638	0.0883
Jokiel and Coles [1977]	0.1900	0.3282	0.4443	0.1806	0.2514	0.4122
Weighted average	0.1865	0.1824	0.2372	0.1862	0.1692	0.2268

[a] Data after flooding not included (*see* Fig. 7.8).

The RMSEs for predicting the healthy coral cover and the combination of healthy and recovering corals are both assessed (*see* Tab. 7.1). The reason is the inconsistent labelling of the recovering population state; this state is either labelled as healthy, or as pale (or a comparable label). Therefore, the data from the literature is both compared to the modelled healthy population and to the summation of healthy and recovering populations. Comparing the measured healthy population with the summation of the modelled healthy and recovering population seems to give a slightly better fit (*see* Tab. 7.1).

Chapter 8

Sensitivity analysis

The sensitivity analysis presented in this chapter consists of two focus points: the sensitivity of the biophysical model framework (BMF) on (1) the accuracy of the input parameters (Sec. 8.1); and (2) the in- and exclusion of certain processes (Sec. 8.2). The first is extensively covered in Appendix D of which the highlights are presented in this chapter. The latter assesses the potentials of input reduction and model reduction; as introduced in Section 3.2.

8.1 Input accuracy

This section focusses on the sensitivity of the biophysical model framework (BMF) to the input parameters. Thereby, determining the required accuracy of the input data. Because the fields of research covered in previous chapters (Chs. 4 to 6) are relatively young, most of the knowledge gaps need to be filled in. This sensitivity analysis functions as a guideline to prioritise where the need for more research and accurate data is most relevant in predicting the development of corals and coral reefs.

Due to the large amount of possible combinations and the complexity of the model, the sensitivity analysis is first analysed per module of the BMF [as suggested by Bellocchi et al., 2009]. This knowledge is used to assess the sensitivity of the full BMF to the resulting key processes.

The methodology of the modular sensitivity analysis differs from the full model analysis: in the modular analysis, the direct influence of changing the parameter in question is determined; while in the full model analysis, the effects of changes in value are compared over a time-span of hundred years. The reason is that in the modular analysis, the direct relation between input and output can be assessed; e.g. the sensitivity of the photosynthetic light dependency—and thereby the photosynthetic rate—can directly be related to the saturation intensity. This direct relation, however, cannot be assessed when looking at the full model due to the feedback loop included. Therefore, the set up is different.

The main findings of the modular analysis are presented in Section 8.1.1. Herein, not all modular analyses performed are covered as only the highlights are included; for the full set of analyses, one is referred to Appendix D. Based on the outcomes of these modular analyses, the sensitivity analysis of the full model is assessed and presented in Section 8.1.2.

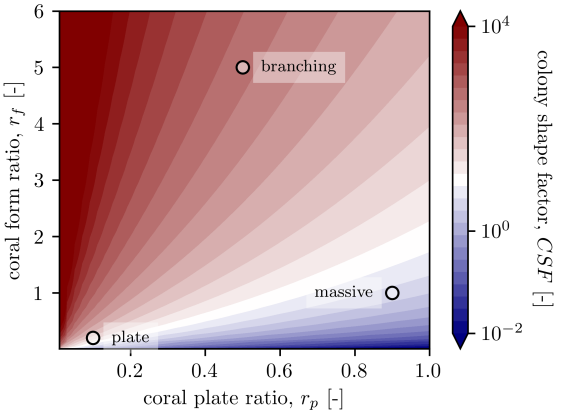

Figure 8.1: The colony shape factor as function of the morphological ratios. Three representative morphologies are added to the plot as reference cases: branching, massive and plate. These three are also shown in Section 3.3 (Fig. 3.5) as illustration of different morphologies. Note the logarithmic scale of the colorbar.

8.1.1 Modular analysis

The modular analysis shows that the BMF is mainly sensitive to three topics: (1) the coral morphology; (2) the bleaching susceptibility; and (3) the dislodgement susceptibility. The first is largely due to the unknown morphological development, which results in large uncertainty on the morphological representation and development. The latter two are based on the sensitivity of the BMF to the accurate prediction of the tipping point related to a stress event—bleaching or storm damage.

The sensitivity of the BMF to the processes related to the coral environment and the physiology are less pronounced compared to the three aforementioned topics. These three topics to which the BMF is most sensitive to are further highlighted below: (1) the coral morphology; (2) the bleaching susceptibility; and (3) the dislodgement susceptibility.

Coral morphology

The proportionality constants used in the formulations of the morphological ratios (*see* Sec. 4.3) are mostly unknown; only two constants are known based on the given constraints (*see* Sec. 3.3): namely, $\chi_p = 1/2$ and $\chi_s = 1/(2\sqrt{2})$. However, a mismatch of the other proportionality constants can have substantial influence on the optimal morphology of the coral as a function of the environmental conditions. Beside this affecting the determination of the in-canopy flow, it also greatly impacts the determination of the dislodgement criterion. The colony shape factor (CSF) is fully based on the morphological dimensions—as presented in Figure 8.1—and so a correct representation of the coral morphology determines the storm damage (moreover in a following paragraph: Coral dislodgement).

The sensitivity of the BMF to the proportionality constants is most pronounced for high light-intensities and/or low flow velocities. This because the formulations to determine the coral morphology—as given in Section 4.3.1—approach there asymptotes for low light-intensities and high flow velocities.

Coral bleaching

The bleaching of corals is related to the accuracy of the thermal limits. This is viewed as the bleaching susceptibility. What happens due to such a bleaching event is related to the population

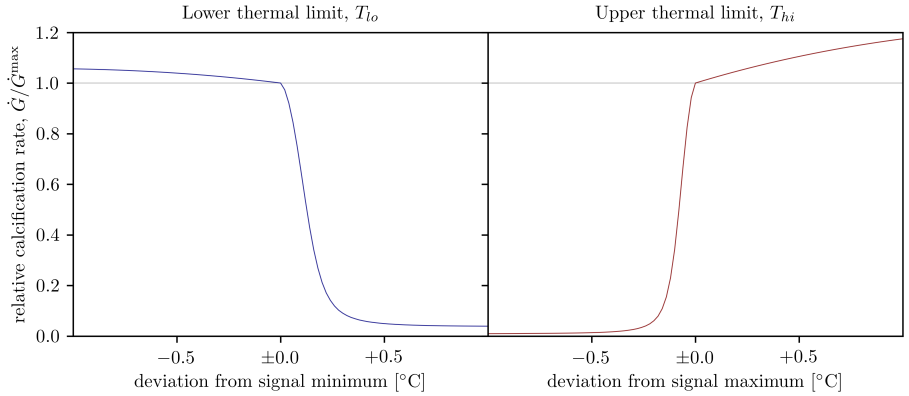

Figure 8.2: Sensitivity analysis of the bleaching susceptibility. The thermal signal is represented by a simple sine wave (*see* App. D.5.1 for more details on the approach).

dynamics. Therefore, there are two parts in the sensitivity analysis on coral bleaching: (1) the prediction of a bleaching event; and (2) the results of such a bleaching event. As the model results are more sensitive to correct predictions of the occurrence of a bleaching event than to the resulting population dynamics, only the first is highlighted here.

The inaccuracy of the determination of the thermal limits—i.e. the correctness of the thermal-acclimatisation formulation—has two possible outcomes: (1) a bleaching event is correctly predicted by the thermal limits; and (2) a bleaching event is incorrectly predicted by the thermal limits. The first results in limited dependency on accurate thermal limits. However, the latter is very sensitive to the correct determination of the thermal limits; as presented in Figure 8.2.

In Figure 8.2, the thermal signal is such that the extremes of the signal correspond to the thermal limits in the reference case (*see* App. D.5.1 for more details on the approach). When the thermal limits still correctly predict the occurrence of bleaching, the effects on the calcification rate are limited. Translated to this reference case: the modelled lower limit is below the actual lower limit and/or the modelled upper limit is above the actual upper limit (*see* Fig. 8.2). A mismatch in predicting the occurrence of a bleaching event—whether one is really occurring or not—results in substantial differences. Translated to this reference case: the modelled lower limit is above the actual lower limit and/or the modelled upper limit is below the actual upper limit.

Furthermore, there is a difference in response to cold stress versus heat stress. Due to the cubic polynomial (*see* Sec. 4.2.3), the gradient of the thermal dependency at the upper limit is larger than at the lower limit. This difference translates into a larger sensitivity of the outcomes to the correct upper limit; both for the responses if bleaching is correctly or incorrectly predicted.

Coral dislodgement

As with bleaching, dislodgement happens or not and predicting this tipping point correctly is essential in the determination of the dislodgement of corals. In Figure 8.3, this tipping point is plotted as function of flow velocity, tensile strength and morphology. The color scale in Figure 8.3 indicates the minimum tensile strength of the substratum (σ_t) for which the coral is not dislodged: a low value of the tensile strength (coloured blue in Fig. 8.3) indicates a low dislodgement susceptibility; while a high value of the tensile strength (coloured red in Fig. 8.3) indicates a high dislodgement susceptibility.

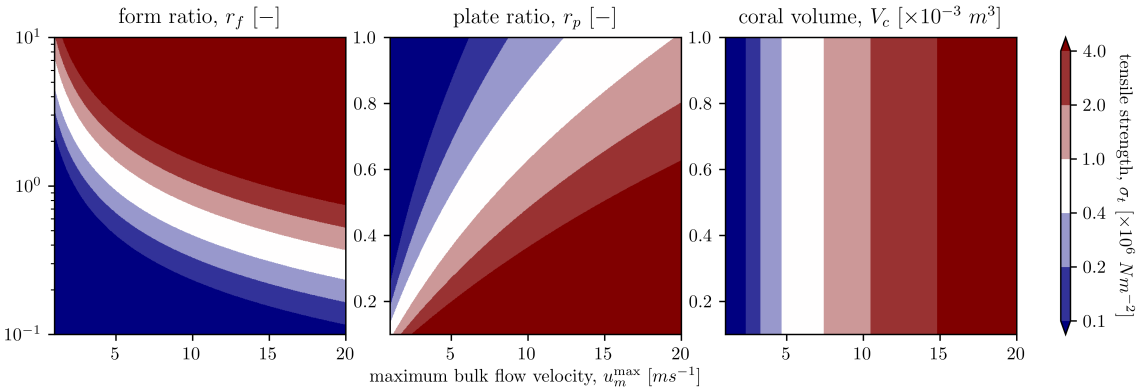

Figure 8.3: Sensitivity of the dislodgement criterion to the tensile strength of the substratum for different morphologies. The color scale indicates the tipping point of dislodgement for a range of tensile strengths. In every plot, one of the morphological parameters is taken over a range, while the others are kept constant. The constant values are: $r_f = 1.0$; $r_p = 0.5$; and $V_c = 0.5 \cdot 10^{-3}$ m^3. Note the logarithmic scale on the vertical axis of the left plot (form ratio).

Thus, the coral becomes more susceptible to dislodgement when (1) the flow velocity increases (horizontal axis of all three sub-plots in Fig. 8.3); (2) the form ratio increases, i.e. the coral becomes higher and narrower; and (3) the plate ratio decreases, i.e. a smaller base width. These findings are to be expected. The coral volume on the other hand does not affect the tipping point, as the colony shape factor (CSF) is independent of the coral volume; all the morphological dimensions are equally related to the coral volume and so the coral volume cancels out in the determination of the CSF (*see* App. D.6).

8.1.2 Full model analysis

The main contributors to the long term development of corals and coral reefs are the reactions on stresses; i.e. bleaching and storm events. Therefore, these two processes are assessed in the full model analysis. Furthermore, the recovery after such an event is of importance as well. Therefore, also the order of magnitude of coral recruitment is assessed. Because the sensitivity of the BMF to the recruitment process cannot be assessed modular, it is not included in the modular analysis, but is part of the full model analysis only.

The sensitivity of these processes are analysed via the following three parameters: (1) the thermal-acclimatisation coefficient (K_{var}) for bleaching; (2) the strength of the substratum (σ_t) for dislodgement; and (3) the probability of settlement of coral larvae (p_s) for recovery.

The sensitivity analysis of predicting the occurrence of coral bleaching is related to the thermal-acclimatisation coefficient as this parameter directly influences the thermal limits (*see* Eqs. 4.56a and 4.56b) without modifying the (long-term) sea surface temperature (SST) time-series. It is, therefore, a clear method to assess the complexity of predicting a bleaching event.

The sensitivity analysis of the coral dislodgement in the full model analysis is assessed based on the tensile strength of the substratum for two reasons: (1) there is a wide spreading in literature on its value [Madin, 2005]; and (2) there is a clear relation between the tensile strength and the dislodgement criterion (*see* Eq. 6.1), which is linear. Even though the dislodgement criterion is also highly dependent on the coral morphology (*see* Fig. 8.3), this relation is non-linear and so not

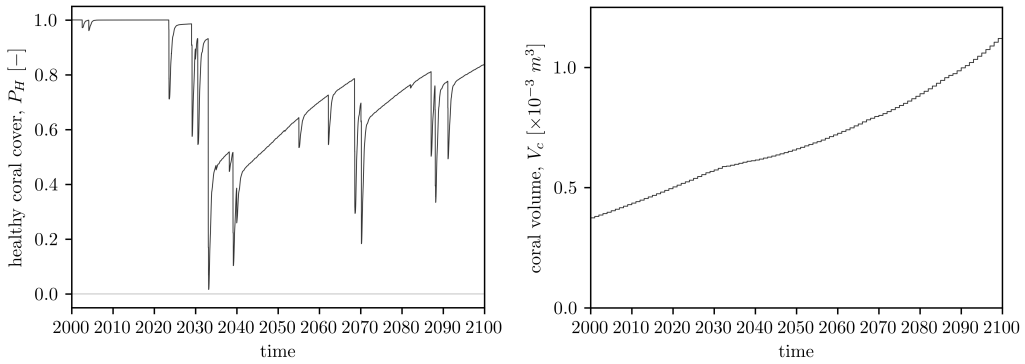

(a) Healthy coral cover.

(b) Coral volume.

Figure 8.4: Coral development over hundred years used as base case for the full model sensitivity analysis. The model results are presented on the reef flat, where the coral development is most pronounced. The coral development is presented as **(a)** healthy coral cover; and **(b)** coral volume.

as straightforward as the tensile strength. The goal of this sensitivity analysis is to indicate the sensitivity of the BMF to the prediction of the occurrence of dislodgement, and the linearly-related tensile strength suffices in achieving this goal.

The sensitivity analysis of the coral recovery—i.e. coral recruitment—in the full model analysis is based on the probability of settlement of coral larvae, as this parameter is similarly included in the recruitment formulations of both the coral cover and the coral volume (*see* Eqs. 6.4a and 6.4b, resp.). Furthermore, there is still much unknown about this process and so a wide spreading is legitimate. The range over which this parameter is assessed is based on a well-educated guess, as there is no data available in the literature.

The time-series of the environmental input factors include possible bleaching and storm events (*see* App. C). Because storm events have such a big impact—complete removal of all coral cover—the initial coral morphology is modified to control if coral dislodgement occurs or not. Beside the occurrence of coral dislodgement, these modifications have no substantial effect on the model results.

Base case

Before assessing the aforementioned full model sensitivity analyses, the model results based on the default values is presented and elaborated on for clarity: $K_{var} = 2.45$; $\sigma_t = 0.2 \cdot 10^6$ Nm^{-2}; and $p_s = 10^{-4}$. First of all, the sensitivity analyses are based on a prediction of coral development over hundred years. Next, the coral development is expressed in two parameters: (1) healthy coral cover; and (2) coral volume.

In Figure 8.4 the coral development of this 'base case' is presented. The bleaching events are clearly visible in Figure 8.4a by the downward peaks in healthy coral cover. The effects of the major bleaching event between 2030 and 2040 (*see* Fig. 8.4a) on the coral growth is also clearly visible in Figure 8.4b, where the increase in coral volume is suddenly halted after which it slowly increases again.

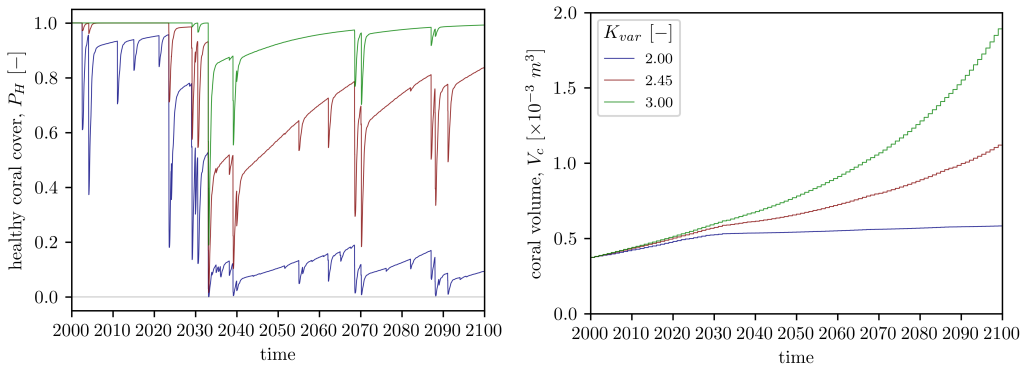

(a) Healthy coral cover.

(b) Coral volume.

Figure 8.5: Sensitivity of the coral development to the thermal-acclimation coefficient. The effects of the thermal-acclimatisation are presented for on the reef flat, where the effects are most pronounced: **(a)** healthy coral cover; and **(b)** coral volume.

Thermal-acclimation coefficient

The thermal-acclimatisation coefficient (K_{var}) has a substantial influence on the results of the BMF (*see* Fig. 8.5), as the bleaching susceptibility changes. For a smaller value of this coefficient, the thermal limits are closer together and so the thermal range reduces; and vice versa. The increased photosynthetic efficiency due to the specialisation term (*see* Sec. 4.2.3) does not weigh up to the increased bleaching susceptibility (*see* Fig. 8.5a). This is in line with Figure 8.2. The effects of the bleaching work through to the coral volume due to the reduced calcification as the healthy coral cover is reduced (*see* Fig. 8.5b).

Substratum strength

The strength of the substratum (σ_t) has a substantial influence on the results of the BMF (*see* Fig. 8.6), as the dislodgement mechanical threshold (DMT) reduces while the colony shape factor (CSF) remains the same. Thereby, the dislodgement criterion is met sooner. The effect of the strength of the substratum is equal to both the coral cover and volume (*see* Figs. 8.6a and 8.6b, resp.). As the strength increases, the load has to increase to invoke dislodgement, which is presented in the moving borderline of the tipping point of dislodgement in Figure 8.6c.

Probability of settlement

The sensitivity analysis of the probability of settlement is assessed in a scenario in which the corals are dislodged, as the contribution is largest when there is no living coral remaining. The recovery of the corals after such a storm event is substantially influenced by the probability of settlement (*see* Fig. 8.7). As the exact order of magnitude of the contribution of the coral spawning—assessed based on the probability of settlement—is unknown, a relatively large range is used: $p_s = 10^{-3} - 10^{-5}$. The sensitivity to the probability of settlement is largest for the coral volume (*see* Fig. 8.7b), but also substantial for the coral cover (*see* Fig. 8.7a).

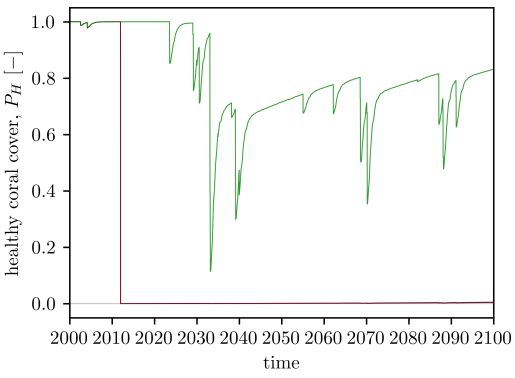

(a) Healthy coral cover.

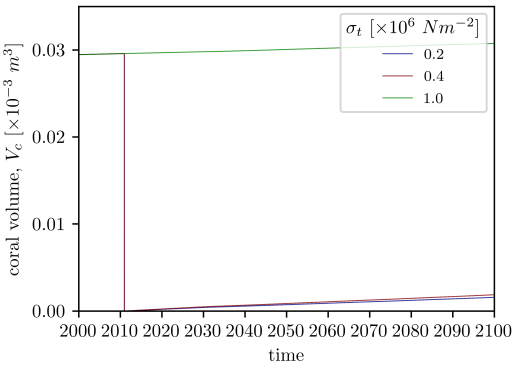

(b) Coral volume.

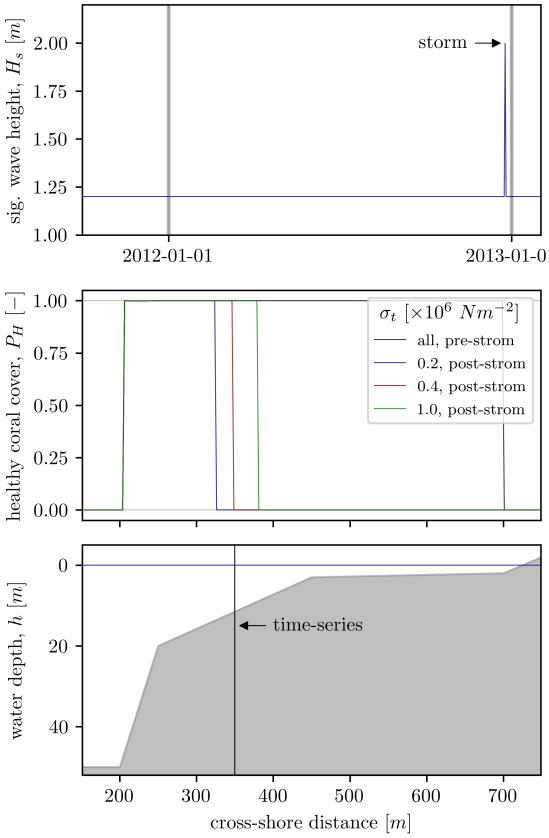

(c) Cross-shore coral cover distribution.

Figure 8.6: Sensitivity of the coral development to the strength of the substratum. **(a)** and **(b)** The time-series of the healthy coral cover and coral volume, respectively. **(c)** The movement of the tipping point due to the increasing tensile strength. The location of the time-series presented in **(a)** and **(b)** is marked in **(c)**.

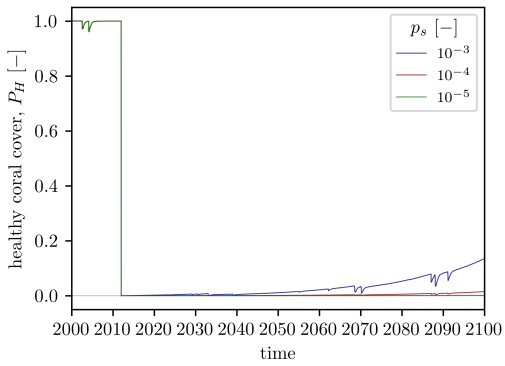

(a) Healthy coral cover.

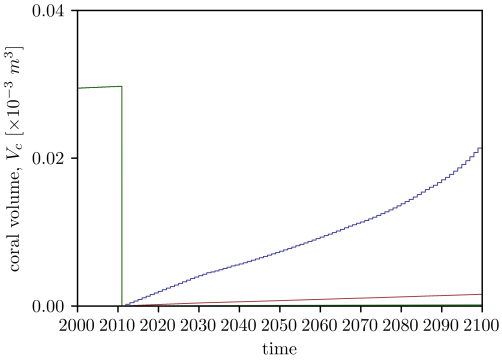

(b) Coral volume.

Figure 8.7: Sensitivity of the coral development to the probability of settlement of coral larvae. The effects of the probability of settlement are presented for on the reef flat, where the effects are most pronounced: **(a)** healthy coral cover; and **(b)** coral volume.

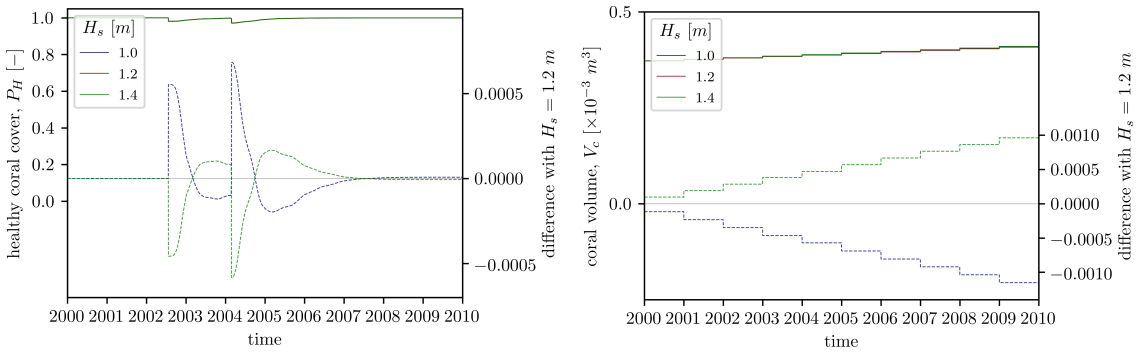

(a) Healthy coral cover.

(b) Coral volume.

Figure 8.8: Sensitivity of the coral development to the wave climate of the 'normal' conditions. The effects of the significant wave height as used for the 'normal' conditions on **(a)** healthy coral cover; and **(b)** coral volume. Note the different orders of magnitude between the absolute values (left axis) and differences (right axis).

8.2 Acceleration methods

Two of the four acceleration methods presented in Section 3.2 are treated as part of the sensitivity analysis: (1) input reduction; and (2) model reduction. The input reduction is taken to its extreme in which the wave climate is represented by one set of wave conditions representative for the full year (*see* App. C.2). In Section 8.2.1, the effects of this method on the model results in assessed. Thereafter, Section 8.2.2 highlights the benefits and the costs of the various processes included in the biophysical model framework (BMF).

8.2.1 Input reduction

The sensitivity of the BMF to the used input reduction is assessed by determining the model results for different wave conditions. When the differences in the outcomes are limited, reducing a full wave climate to one set of wave conditions representative for the whole year—as is done in this study—is resulting in representative model results. Note that this focusses on the 'normal' conditions, and so excludes the effects of storm conditions on the model results.

The representative wave climate for the 'normal' conditions—i.e. no-storm conditions—is characterised by a significant wave height of $H_s = 1.2$ m (*see* App. C.2). The sensitivity of the growth of corals to the exact wave conditions is limited as presented in Figures 8.8a and 8.8b for the coral cover and volume, respectively. Note the exacerbated differences, which are three to four orders of magnitude smaller than the absolute values.

The healthy coral cover shows only some deviations due to the wave conditions around a bleaching event (*see* Fig. 8.8a). For the coral volume holds that the differences grow every year—when the coral morphology is updated. Extrapolating the results presented in Figure 8.8b to hundred years results in differences two orders of magnitude smaller than the absolute value. However, the differences are so small, that these differences are negligible. Here, one has to keep in mind that the spreading in the data on the calcification rate is substantially more than the differences arising from the input reduction (*see* Fig. 7.7a).

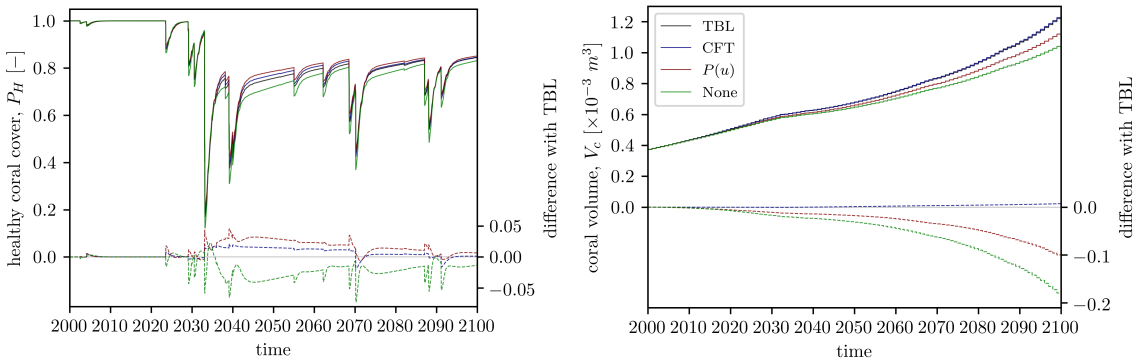

(a) Healthy coral cover.

(b) Coral volume.

Figure 8.9: Sensitivity of the coral development to the thermal micro-environment. TBL indicates the inclusion of the thermal boundary layer (TBL) and so the full assessment of the thermal micro-environment (simulation time: ±40 hours); CFT indicates solving the partial differential equations associated with the Canopy-Flow Theory (simulation time: ±12 hours); $P(u)$ indicates the inclusion of the photosynthetic flow dependency (simulation time: ±8 hours); and None indicates the exclusion of all; i.e. exclusion of the TBL, the CFT and the photosynthetic flow dependency (simulation time: ±1 hour). The solid lines represent the healthy coral cover, and the dashed lines the difference in coral cover compared to TBL. The most extreme effects are presented for **(a)** the coral cover, which is located in deep water; and **(b)** the coral volume, which is located in shallow water.

8.2.2 Model reduction

Beside the hydrodynamic model, there are two processes within the BMF that cost the most computational effort: (1) solving the Canopy-Flow Theory (CFT); and (2) including the effects of the thermal boundary layer (TBL) for which the CFT has to be solved. When these processes are not included, the bottleneck considering the computational time is reduced to only the hydrodynamic model simulation as the computational effort necessary for the rest of the BMF is negligible.

The simulation of hundred years of coral development including all processes took approximately 41.23 hours;[1] when the effects of the TBL are not taken into account, this reduced to approximately 12.67 hours; in case also the CFT is not included the computational time became approximately 8.54 hours; and excluding the flow entirely from the physiology resulted in a model run time of less than an hour. That means that the model is around five times faster when the computations considering the thermal and hydrodynamic micro-environments are not taken into account; and becomes approximately ten times faster again when the photosynthetic flow dependency is excluded as well. In the last case, the hydrodynamic model is only needed to simulate storms. Thus, there are four cases considered in the sensitivity of the BMF to the model reduction (*see* Fig. 8.9):

TBL The case labelled as TBL includes all processes; i.e. TBL, CFT and $P(u)$. Therefore, the duration of this simulation is the longest; approximately 40 hours.

CFT The case labelled as CFT includes all processes except determining the thermal micro-environment; i.e. CFT and $P(u)$. The simulation of this case takes approximately 12 hours to run.

[1] Computations were carried out on an external server at Deltares: 4 cores - 16 GB. When 8 GB of working memory was used, an error arose due to the lack of sufficient memory in case all processes were taken into account.

$P(u)$ The case labelled as $P(u)$ only includes the photosynthetic flow dependency; i.e. only $P(u)$. The related simulation takes approximately eight hours.

None The case labelled as None does not include any of the aforementioned processes. Therefore, the duration of this simulation is the shortest; approximately one hour.

The differences in the outcomes of the four cases are relatively small for the coral cover (*see* Fig. 8.9a), but more pronounced for the coral volume (*see* Fig. 8.9b). In all four cases, the bleaching events are captured correctly and there are only some small differences in the healthy coral cover during recovery. When the CFT is not solved, however, substantial discrepancies arise in coral volume; in the order of ten to twenty per cent. On the other hand, there is limited difference between solving the thermal micro-environment or not—i.e. TBL versus CFT in Figure 8.9. Furthermore, the discrepancies between solving the CFT or not—i.e. CFT versus $P(u)$ in Figure 8.9—are not notably present in case of the coral cover, except when the photosynthetic flow dependency is not included—i.e. None in Figure 8.9.

Chapter 9

Discussion

The discussion of this study starts with the set-up of the biophysical model framework (BMF) and its potential in Section 9.1. The remainder of the discussion focuses on the following three topics:

1. The computational efficiency of the BMF in which two of the in Section 3.2 introduced acceleration methods are discussed: (1) input reduction in Section 9.2; and (2) model reduction in Section 9.3.
2. The used morphological representation in combination with the dislodgement criterion results in some unrealistic outcomes concerning the damage inflicted by storms. This topic is addressed in Section 9.4 in which possible solutions are presented as well.
3. Section 9.5 discusses the agreement between the model restuls and both the deep reef refugia hypothesis (DRRH) and the turbid reef refugia hypothesis (TRRH) (*see* Sec. 2.5).

9.1 Setup biophysical model framework

The biophysical model framework (BMF) developed in this study includes a substantial number of processes essential for predicting the development of corals and coral reefs. Despite the limited available data, great agreement with the usable data is achieved (*see* Ch. 7). Nonetheless, the performance of the model can be improved by more validation for which further research is needed. Especially research on accurately predicting the occurrence of a stress event—bleaching or storm—is essential in modelling the coral development (*see* Sec. 8.1).

The BMF developed in this study is the first of its kind. It enables to combine the physiological processes—related to growth and bleaching—with the physical processes—mainly related to storms. Furthermore, this BMF enables the opportunity to run fast simulations to get insight in the future perspectives of a coral reef. Predictions of a hundred years take approximately one hour. On the other hand, the BMF is able to make more detailed predictions as well by including more processes; such as the thermal micro-environment. Therefore, this BMF may even assist in designing projects containing coral reefs; e.g. 'constructing' a coral reef to function as breakwater.

Even though many processes are already included in this first set-up, not all processes are embedded; e.g. the effects of nutrients [Atkinson and Bilger, 1992; Holcomb et al., 2012; Langdon and Atkinson, 2005] and sediment loads [Erftemeijer et al., 2012; Storlazzi et al., 2015].

Furthermore, the principle of bioerosion is not included in the BMF; i.e. the erosion of the coral skeleton due to biological activity such as grazers [Perry and Hepburn, 2008; Spencer and Viles, 2002]. In this study, the bioerosion is implicitly incorporated via the calcification constant. However, (1) the rate of bioerosion varies over the reef due to environmental conditions [Maher et al., 2018; Spencer and Viles, 2002]; and (2) does not reduce or stop when there is limited or no calcification. Therefore, the bioerosion may alter the future perspectives of coral reefs.

Such new processes are relatively easily added to the BMF due to its modular structure. Every module describes the dependency of the coral development in terms of efficiency based on the input parameter(s) of that specific module. This linear description forms the basis of the BMF. However, it does not limit the BMF to linear relations only; e.g. the combined effects of light, flow and thermal conditions are encapsulated in the BMF by the thermal boundary layer (TBL). Other non-linear processes can be added in a similar fashion.

Therefore the potential of the developed BMF is widespread. It enables the ability to (1) simulate the effects of climate projections on coral reefs; (2) test hypotheses on defence mechanisms for corals to survive; and (3) test protection and recovery programs beforehand to minimise possible negative side effects. Beside these possibilities the BMF is designed for, it also enables the use of corals and coral reefs in coastal protection projects.

9.2 Input reduction

The input reduction implemented in this study is mainly aimed at reducing the hydrodynamic simulation time, while still be able to proof the validity of the concept of the biophysical model framework (BMF) developed. The hydrodynamic model is one of the main contributors to the computational effort. This has lead to one representative wave climate for 'normal' conditions to which three storm categories—to represent storm conditions for the possible dislodgement of corals—are added (*see* App. C.2).

The exact flow conditions are not of importance for this study in which the focus is on the development of the BMF. Therefore, representing the wave climate to one set of wave conditions does not impose any concern on the validity of the BMF. First of all, a link between the biological part and the physical part of the model is established. This link also holds when a more complex representative wave climate is used, consisting of multiple wave conditions. The developed BMF does not loose its viability due to the single wave climate used in this study.

Furthermore, corals are not as susceptible to the exact wave conditions as is e.g. sand, and the correct estimate of the flow magnitudes as a result of the hydrodynamic forcing is sufficient (*see* Fig. 8.8). It is considered appropriate to use this hydrodynamic representation for studies on coral reefs and understanding their dynamics.

However, if there is a clear seasonality in the wave conditions, the seasonal wave-induced flow conditions can amplify or attenuate the effects of the thermal boundary layer (TBL). This might result in differences in bleaching susceptibility. Such conditions may invoke the need of the full model framework including all the processes with a more elaborate wave time-series. As this will considerably increase the computational effort, one has to consider the need for such detailed predictions.

Because climate projections often have a lower accuracy, it is redundant to produce such detailed predictions. Moreover, the accuracy of other biological processes included do not meet such accuracy. The added value of detailed hydrodynamic calculations only adds to the computational effort of the BMF without much benefit.

9.3 Model reduction

The model reduction focusses on reducing the amount of processes included in the simulation to accelerate the biophysical model framework (BMF). The main contributor to the computational time in the developed BMF is the determination of the thermal micro-environment; i.e. the effects due to the thermal boundary layer (TBL) (*see* Sec. 8.2.2). The reasoning is twofold: (1) the large amount of data handling required for the calculations associated with this process; and (2) the need to solve the flow micro-environment, hence solving the partial differential equation of the Canopy-Flow Theory (CFT).

The large amount of computational data comes from the fact that the thermal limits of the coral-zooxanthellae symbiont are based on the thermal history. Taking the thermal micro-environment taken into account results in the determination of the thermal history for every grid cell. As the thermal-acclimatisation is based on 60 years of thermal data, the resulting matrices are huge. Such data handling substantially slows down the model and requires a large working memory for the model to be able to work (*see* Sec. 8.2.2). This could be made more efficient, but the benefits would still be limited.

The substantial contribution to the computational time due to solving the CFT comes from the iterative process needed to find the complex-valued solution of the wave-attenuation coefficient (WAC). This has to be done twice per grid cell: once for the wave-induced WAC; and once for the current-induced WAC.

The exclusion of the effects of the TBL results in reef-wide bleaching when thermal conditions are outside the thermal range, while this does not necessarily need to be true [Fabricius, 2006; Johnston et al., 2019]. Nevertheless, the occurrence of bleaching is commonly related to the sea surface temperature (SST) instead of the thermal micro-environment [Silverman et al., 2007; Buddemeier et al., 2008; Evenhuis et al., 2015; Donner, 2011].

When the thermal micro-environment is not determined—i.e. the thermal conditions are solely based on the SST—there is no need for solving the CFT. The in-canopy flow is then only used for the photosynthetic flow dependency, which is equally well—if not better—fitted to the bulk flow velocity (*see* Sec. 7.2.2). Even though the relation with the in-canopy flow is process-based, the data fitting shows no benefit in using the in-canopy flow over the bulk flow (*see* Figs. 7.4b and 7.4a, resp.). This all is supported by the results presented in Section 8.2.2 in which the determination of the thermal and flow micro-environments do not result in different outcomes of the coral cover (*see* Fig. 8.9a).

However, discrepancies arise in the coral volume (*see* Fig. 8.9b). These differences may be due to the difference in fitting parameters for the in-canopy flow and the bulk flow. Due to the large spreading in the data, both fitted lines still show large root-mean-squared errors (RMSEs) (*see* Fig. 7.4). Therefore, the difference between both the predictions including the TBL and CFT and the predictions without these processes is most likely due to a mismatch in the photosynthetic flow dependency with the data. As there is no reason to value the fit with the in-canopy flow over the fit with the bulk flow, the results produced excluding the TBL and CFT are considered as representative.

Therefore, the benefits of including the effects of the TBL do not weigh up to the computational costs inflicted. By solely relying on the SST data for the thermal conditions, the computational time is almost fully determined by the hydrodynamic model as (1) the in-canopy flow does not need to be determined in detail; and (2) the large amount of data associated with the thermal micro-environment does not need to be handled and used. For further acceleration of the model, the hydrodynamic model has to be constructed more efficiently for which the methods and findings

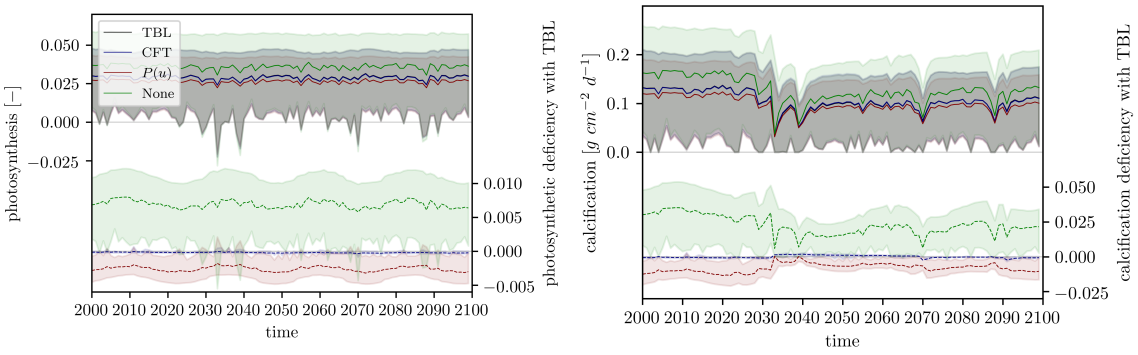

(a) Photosynthesis.

(b) Calcification.

Figure 9.1: Sensitivity of the photosynthesis and calcification to flow-related processes. TBL indicates the inclusion of the thermal boundary layer (TBL) and so the full assessment of the thermal micro-environment; CFT indicates solving the partial differential equations associated with the Canopy-Flow Theory; $P(u)$ indicates the inclusion of the photosynthetic flow dependency; and None indicates the exclusion of all; i.e. exclusion of the TBL, the CFT and the photosynthetic flow dependency. The solid lines represent the annual mean, and the dashed lines the difference in annual mean compared to TBL. The shading represents the spreading per year by filling the area between the annual minima and maxima. The most pronounced effects of the model reduction are presented for **(a)** the photosynthesis; and **(b)** the calcification.

from the field of morphodynamics form a great starting point [Li et al., 2018; Walstra et al., 2013; Lesser et al., 2004; Luijendijk et al., 2019, *see* Sec. 3.2].

One can argue if it is needed to include the photosynthetic flow dependency at all. As the error arising from it is (1) only present at low flow velocities where the flow limits the photosynthesis; and (2) smaller or equal to the RMSEs resulting from the data fitting (*see* Sec. 7.2.2, Fig. 7.4). Figures 9.1a and 9.1b present the photosynthesis and calcification for all four model configurations and the difference compared to the full model framework; i.e. including the thermal micro-environment.[1] Herein, the order of magnitude of the resulting errors is the same as of the data fitting of the photosynthetic flow dependency.

Even though the process of diffusion limited transport due to the diffusion boundary layer (DBL) and thereby limited photosynthetic capacity is shown to hold for corals [Mass et al., 2010; Schutter et al., 2011; Osinga et al., 2017; Atkinson and Bilger, 1992; Hearn et al., 2001], the data does not show a clear trend (*see* Fig. 7.4, Sec. 7.2.2). The latter is largely attributed to the limited range over which the effect of the flow on the photosynthetic rate is assessed in literature and the fact that it is often a secondary research objective. The positive relation between flow velocity and photosynthetic efficiency is a relation generally found and it is in line with the process of diffusion limited transport. Therefore, it is to be expected that further research on solely the relation between calcification and flow velocity would clarify the exact effects on the photosynthetic flow dependency. Until this point, the flow dependency can be excluded from the BMF and the coupling with the hydrodynamic model is only made to simulate the hydrodynamics due to a storm.

This undetermined relation between the flow conditions and the physiology of the coral-zooxanthellae symbiont might be the reason that previous models did not include this aspect [Evenhuis et al., 2015; Buddemeier et al., 2008; Silverman et al., 2007]. Nevertheless, these models only looked at the

[1] The labelling in Figure 9.1 is the same as presented in Section 8.2.2. In short: TBL includes all process (TBL, CFT and $P(u)$); CFT includes all except the thermal micro-environment (CFT and $P(u)$); $P(u)$ only includes the photosynthetic flow dependency ($P(u)$); and None excludes all these processes.

physiological processes, while the mechanical processes—i.e. storm events—are crucial in predicting the survival of corals and coral reefs [Madin and Connolly, 2006; Hongo et al., 2012]. This requires the connection with an hydrodynamic model—such as Delft3D Flexible Mesh—as is done in this study.

Again, when other processes that are more tightly related to the hydrodynamics—e.g. sediment dynamics and larval dispersion—are incorporated into the BMF, the need for detailed hydrodynamics is verified. However, the spreading in the available data behind the various micro-environments for which detailed hydrodynamics are needed is larger than the differences that arise when these processes are excluded from the framework. This exclusion has the large benefit of reducing the computational time tremendously; from the order of days to the order of minutes to hours.

The only pitfall remaining is the morphological development, which is also related to the flow conditions. As the coral development is very slow compared to all the other processes—and also still very inaccurate—an hydrodynamic update once every five or ten years will satisfy. Furthermore, using 'model morphologies'—further explained in Section 9.4—to determine the morphological preferences due to the environmental factors can solve this issue, as the morphological development in this formulation is related to natural selection instead of a direct function of the flow—and light—conditions.

9.4 Coral morphology and dislodgement

The morphological representation used in this study is able to correctly represent the effects of the coral on its surroundings [Lowe et al., 2005a; Murphy et al., 2007; van Rooijen et al., 2018; Weitzman et al., 2015, *see* Fig 7.2]. However, the formulations on the morphological development leave room for improvement. First of all, the calibration constants—i.e. the proportionality constants—are not based on research. This is because there is no useful data that relates the morphology to the environment; only qualitative suggestions [Chappell, 1980; Jokiel, 2011b].

Even though there are models developed to simulate the optimal morphology based on the light-conditions [Graus et al., 1984; Muko et al., 2000; Hoogenboom et al., 2008] and the flow-conditions [Kaandorp et al., 1996; Kaandorp and Sloot, 2001; Kaandorp et al., 2011; Kaandorp, 2013], they are too computationally expensive. These quantitative models are laborious and contain too much detail to fit in the biophysical model framework (BMF) developed in this study. There are more recent attempts to quantify the coral morphology [Zawada et al., 2019a,b], but these do not relate the morphology directly to its environment.

Furthermore, there is a downside to the morphological representation as used in this study in combination with the dislodgement criterion: when the dislodgement criterion is met, all the corals in the grid cell are removed. This is not in line with the partial dislodgement of corals found in reality [Madin and Connolly, 2006; Hongo et al., 2012]. The full removal when the dislodgement criterion is met, results in longer recovery periods after such a storm event because there is a linear log-log relation between the coral cover and the recovery rate [Hughes et al., 2019].

There are two possibilities to better represent the impact of storms: (1) partial dislodgement; and (2) model morphologies. The first keeps the morphological representation and its development as presented in Section 3.3; the latter redefines the morphological development and its distribution.

Partial dislodgement The possibility of partial dislodgement instead of full dislodgement is straightforward: a fraction of the corals that survive the storm event is defined. This fraction works

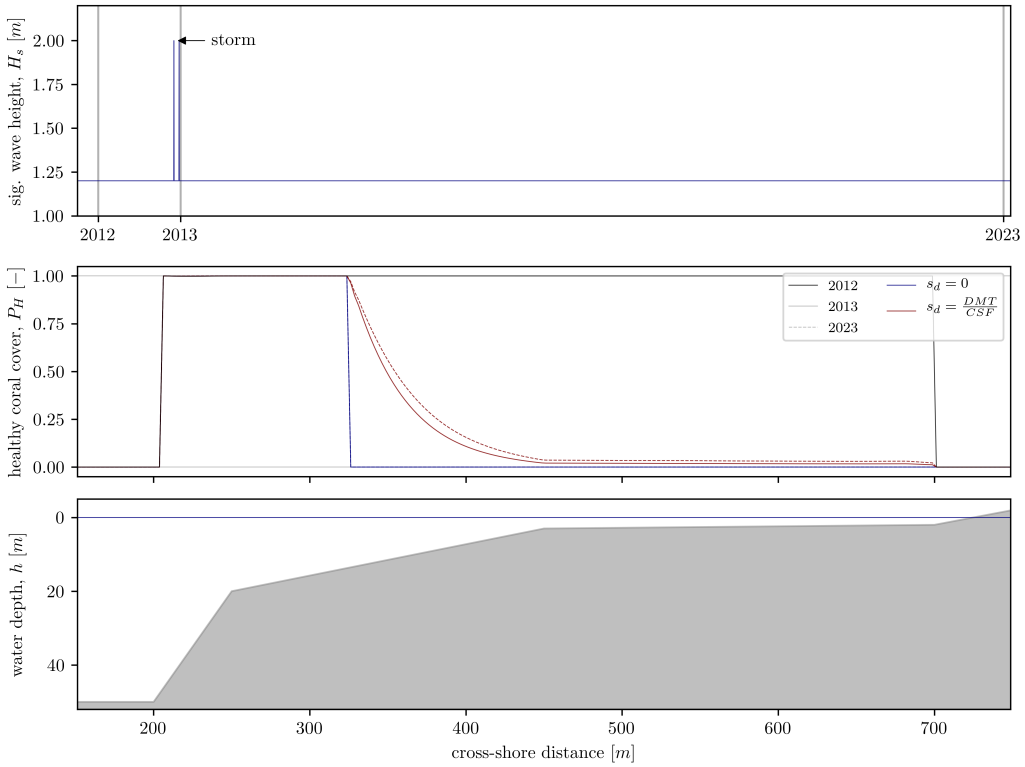

Figure 9.2: Indication of long-term effects of partial dislodgement compared to full dislodgement. The upper plot presents the hydrodynamic loading given as the significant wave height, H_s. The gray bars indicate the moments of pre- and post-storm and ten years after the storm event, which are presented in the middle plot. Here, dislodgement is represented by a reduction in the healthy population cover, P_H. The bottom plot presents the bathymetry.

both on the coral cover and on the coral volume:

$$P_T^{(n)} = s_d \; P_T^{(n-1)} \qquad \text{if } DMT \leq CSF \tag{9.1a}$$

$$V_c^{(n)} = s_d \; V_c^{(n-1)} \qquad \text{if } DMT \leq CSF \tag{9.1b}$$

where s_d is the fraction that survives the storm event when the dislodgement criterion is met; and (n) and $(n-1)$ are the time-steps at t_n and $t_n - \Delta t$ indicating pre- and post-storm, respectively.

This fraction surviving is preferably related to the severity of the storm compared to the robustness of the coral colony; i.e. to respectively the dislodgement mechanical threshold (DMT) and colony shape factor (CSF):

$$s_d = \tilde{s}_d \; \frac{DMT}{CSF} \leq 1 \tag{9.2}$$

where $\tilde{s}_d$ is a fitting parameter.

Figure 9.2 indicates the influence of using a partial dislodgement formulation against a full removal formulation. As there is more coral cover remaining, the recovery is faster [in line with

Hughes et al., 2019]. Therefore, a partial dislodgement of coral cover due to storms instead of a full dislodgement substantially changes the recovery time of the reef.

Model morphologies The second possibility is based on the principle of natural selection. A number of representative morphologies are used and distributed over the coral reef. Due to the environmental input, certain morphologies will do better than others at certain locations; or their might be limited differences between different morphologies. Over time—by natural selection—the morphologies representative for the environmental conditions will thrive and remain, while other morphologies have been out-competed.

The downside to this approach is that there are more variables per grid cell; all the coral-related parameters as used in this study times the number of model morphologies. Furthermore, all these morphologies have to be represented by just one canopy structure to couple with the hydrodynamic model. This representative morphology must result in a representative in- and above-canopy flow. However, the in-canopy flow does not need to be solved in the current set-up (*see* Sec. 9.3).

Beside the fact that this approach is more process-based—namely natural selection—there are also suggestions that there is a link between the morphological characteristics and (1) the physiological characteristics [Madin et al., 2016; Zawada et al., 2019b]; and (2) the strength of the coral skeleton [Madin, 2005]. The first includes traits such as bleaching susceptibility [Zawada et al., 2019b]. Such species dependent biological traits are easily tuned with the BMF developed in this study.

Zawada et al. [2019a,b] came up with seven groups based on their morphology and physiology: (1) arborescent; (2) laminar; (3) corymbose; (4) tabular; (5) digitate; (6) submassive; and (7) massive. This grouping shows great comparison with other studies [e.g. Marshall, 2000; Pratchett et al., 2015; Santodomingo et al., 2016]. Furthermore, sedimentation and burying susceptibility is also related to the morphology [Bak et al., 2005; Perry et al., 2012], and different morphologies indicate different strategies against sedimentation [Fricke and Schuhmacher, 1983; Sanders and Baron-Szabo, 2005; Stafford-Smith and Ormond, 1992].

The grouping of species is common in ecological studies [Shipley et al., 1989; Keddy, 1992; Lavorel et al., 1997; Tilman et al., 1997]. Herein, the grouping is based on similarities in biological traits [Poff et al., 2006; Merritt et al., 2010] of which the morphology is one. These traits are addressed as a result of natural selection [Southwood, 1977] and so it is reasonable to extend this methodology of terrestrial ecology into the marine environment as well.

In both cases, there is still large uncertainty about the exact development of the morphology over time. As briefly indicated in Section 1.3, this link with the coral morphology to close the feedback loop is not investigated in the same detail as the other parts of the feedback loop. The morphology in general has not received much attention in the literature. This does not acknowledge the key role it plays in the development of corals and coral reefs.

9.5 Reef refugia hypotheses

The aspects of the deep reef refugia hypothesis (DRRH) that can be assessed with the processes included in the biophysical model framework (BMF) so far are twofold (*see* Sec. 2.5): (1) the reduction in bleaching severity with depth; and (2) the reduction in storm damage with depth. Both principles are endorsed by the results of the BMF. On the other hand, only one aspect of

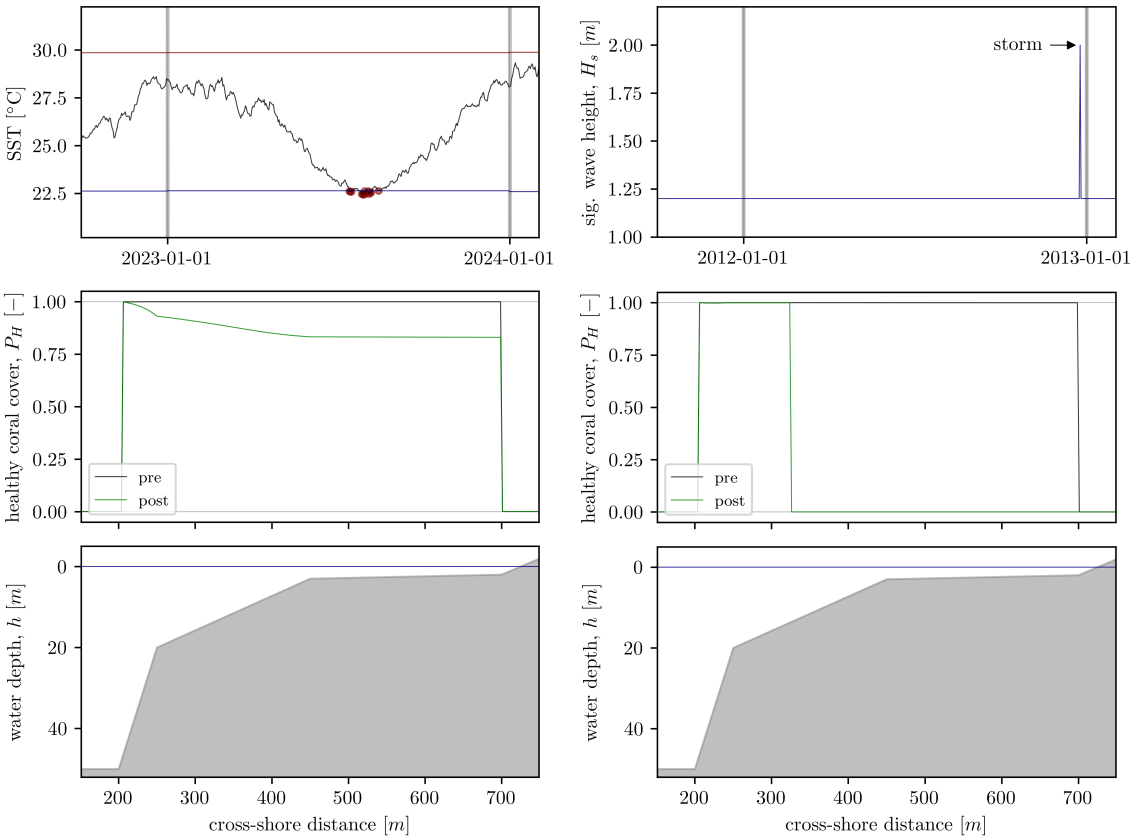

(a) Bleaching. **(b)** Dislodgement.

Figure 9.3: Spatially varying bleaching and dislodgement responses in correspondence with the deep reef refugia hypothesis. (a) The upper plot presents the snapshot of the sea surface temperature (SST) time-series considered, where the lower and upper limits of the thermal range are represented by the blue and red lines, respectively. **(b)** The upper plot presents the hydrodynamic loading given as the significant wave height, H_s. The gray bars in the top plots indicate the moments of pre- and post-stress presented in the middle plots. Here, bleaching and dislodgement are represented by a reduction in the healthy population cover, P_H. The bottom plot presents the bathymetry.

the turbid reef refugia hypothesis (TRRH) can be assessed: the reduction in bleaching severity with increasing turbidity.

First, the varying bleaching response over depth is modelled in line with the DRRH; as presented in Figure 9.3a. Deeper corals are not excluded from bleaching [Bak et al., 2005], but bleaching is more pronounced higher up the water column [Wilkinson and Souter, 2008].

Second, the effect of depth on the dislodgement is also modelled according the DRRH (*see* Fig. 9.3b) in which indirect damage is not taken into account. Such indirect influences would result in some damage of the deeper lying corals [Bak et al., 2005; Dollar, 1982], where Figure 9.3b is showing no reduction of (healthy) coral cover at all. Note the difference in impact of a bleaching event versus a storm event; a storm event results in complete removal, or no damage at all (*see* Sec. 9.4).

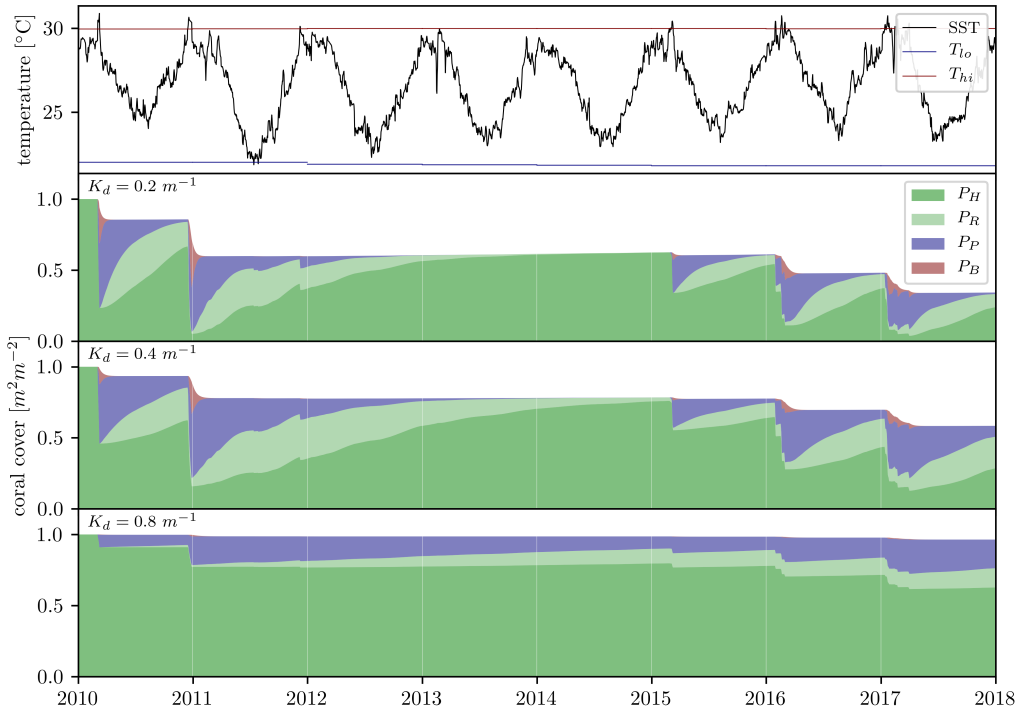

Figure 9.4: Differing bleaching response due to varying turbidity in agreement with the turbid reef refugia hypothesis. Top plot shows the thermal conditions including the thermal limits (T_{lo} and T_{hi}). Bottom three plots show the population dynamics for varying values of the light-attenuation coefficient (LAC), where the bleaching severity reduces for increasing LAC; i.e. increasing turbidity. P_H is the healthy coral cover; P_R the recovering coral cover; P_P the pale coral cover; P_B the bleached coral cover; and K_d the light-attenuation coefficient (LAC). The plots are not based on field measurements and are only illustrative to show the effect of the turbidity on the model results, which is in agreement with the turbid reef refugia hypothesis (TRRH).

In connecting the outcomes of the BMF with the DRRH, it is important to note that the BMF is developed independently from the DRRH. It is promising for both that there are similarities between the model restuls and the DRRH.

The most left and most right parts of the middle plots in Figures 9.3a and 9.3b with no coral cover are the result of unsustainable growing conditions at these locations: (1) the left hand side is to deep for photosynthesis—i.e. below the euphotic depth—and so does not support the living of symbiotic corals; and (2) the right hand side is the beach and so the substratum is considered unsuitable for coral growth.

Whether corals may thrive in turbid waters as suggested by the TRRH [Cacciapaglia and van Woesik, 2016; Perry et al., 2012; Santodomingo et al., 2016]—as was previously contradicted [Kleypas and Eakin, 2007, and references therein]—cannot yet fully be assessed with the developed model framework. Nonetheless, the hypothesis that the damage due to bleaching is reduced when sediment concentrations are higher is in line with results from the model; i.e. increasing the light-attenuation coefficient (LAC) [Storlazzi et al., 2015]. The aspect that an increased turbidity—i.e. LAC—reduces the bleaching severity is presented in Figure 9.4 for a hypothetical reef.

However, beside the LAC, other biophysical processes will also change due to the increased sediment concentration; e.g. the preferred morphology [Chappell, 1980; Fricke and Schuhmacher, 1983; Sanders and Baron-Szabo, 2005; Stafford-Smith and Ormond, 1992], and the physiology [Anthony, 2000; Anthony and Fabricius, 2000; Anthony et al., 2007]. These aspects are not taken into account in the assessment shown in Figure 9.4, nor in this study.

Why the reduction of light-intensity—due to greater depth or higher turbidity—decreases the severity of bleaching is still unclear. A possible reason might be found in the Oxidative Theory of Coral Bleaching (*see* Sec. 2.4): as the light-intensity is less, the photosynthetic production is less as well. Thereby, the production of reactive oxygen species (ROS) is also reduced and so the zooxanthellae produce less toxins. Due to the lower concentrations of ROS, the coral is less stressed and less zooxanthellae need to be expelled to lower the levels of ROS. Hence, there is less severe bleaching.

Chapter 10

Concluding remarks

The developed biophysical model framework (BMF) is able to make reliable predictions on the survival of corals and coral reefs under the threats of climate change. Thereby, it contributes to the goal of this study to contribute to the survival of corals in the following two ways:

1. The developed BMF enables the prediction of long-term coral development within the accuracy of climate projections. As it gives more insight in the complex world of corals, it supports the development of protection and recovery programs as the model enables the opportunity to test these programs in advance.
2. The developed BMF highlights the most important knowledge gaps on corals and coral reefs. As time is running out fast for corals if the status quo is maintained, these findings guide in the allocation of the limited resources and time towards the low-hanging fruits in the undiscovered world of coral reef biophysics.

This report finalises with some concluding remarks. The research questions—as defined in Section 1.2—are answered in Section 10.1. Sections 10.2 and 10.3 address the recommendations following from this research. As the BMF developed in this study is the first of its kind, it is inevitable that further progress is needed. Section 10.2 focusses on the recommendations for experimental studies to contribute to the limited amount of data; and Section 10.3 presents a set of recommendations on improvements on the BMF.

10.1 Research questions

First the defined sub-questions are answered after which a conclusion is drawn based on the research objective. The sub-questions are elaborately answered in the chapters dedicated to them (*see* Fig. 1.3, Sec. 1.5). This section provides brief, summarising answers to these questions:

1. *What are the biological characteristics of corals?*

   Corals in the euphotic zone are highly dependent on the zooxanthellae they host; almost all the energy the zooxanthellae produce goes to the coral host. The effectiveness and collaboration between the coral and the zooxanthellae is influenced by environmental conditions.

   The light conditions are important because of this symbiosis between corals and their zooxanthellae as light is key for photosynthesis. The energy production originating from the pho-

tosynthesis is used for the construction of the calcareous skeleton. This process is called light-enhanced calcification (LEC).

Furthermore, the thermal conditions determine the collaboration between the coral and the zooxanthellae. When the temperature gets too high—i.e. above the thermal limit—the coral ejaculates the zooxanthellae as they become poisonous to the coral. According the Oxidative Theory of Coral Bleaching, this is due to the overproduction of reactive oxygen species (ROS) by the zooxanthellae as a by-product of photosynthesis. The production of ROS during photosynthesis is common, and the coral and zooxanthellae have countermeasures. However, when temperatures are above the thermal limit, these countermeasures are not enough to keep the ROS below toxic levels.

2. *What are the components of the feedback loop between the coral and its environment?*

   The feedback loop between the coral—or coral-zooxanthellae symbiont—and its environment includes three items: (1) the coral environment; (2) the coral physiology; and (3) the coral morphology. The coral environment determines how the coral perceives the environmental input. For this, the transition has to be made from the macro-environment to the micro-environment. The coral physiology describes the response of the coral to this environmental input. Its response determines the coral cover and coral growth. The coral morphology is the important link that closes the feedback loop, which is nevertheless insufficiently studied. The morphology translates the growth of corals to the structure it forms, which is an important input factor for the coral environment; from macro- to micro-environment.

3. *What are the biophysical interactions between corals and their environment?*

   The biophysical interactions between the coral and its environment are complex and widespread. The feedback from the coral—as part of a coral reef—to its environment is mainly via the flow structure and pattern on and around a reef. The coral also highly influences its micro-environment in multiple aspects; e.g. the thermal micro-environment. The environment largely determines the growth rate of the coral, but also whether the coral bleaches or is dislodged.

   The growth rate as well as the bleaching and dislodgement susceptibilities are highly intertwined with multiple environmental factors. For the growth rate—i.e. the calcification—the light and thermal conditions are key for the photosynthesis, which is at the basis of the calcification; so-called LEC.

   The bleaching susceptibility is determined by the thermal conditions. Other environmental factors determine the severity of bleaching, where especially a strong connection is found with the light-intensity. Dislodgement susceptibility on the other hand is the combination of the flow conditions and the morphological complexity of the coral colony. Again, other environmental factors play a secondary role; e.g. the acidic conditions influence the density of the skeleton, which is an important factor for the strength of the skeleton.

4. *What are the main biophysical interactions determining the coral development?*

   As is commonly agreed upon, the leading environmental aspect determining the survival of corals is the temperature. This environmental factor largely determines whether the coral bleaches, which is an important aspect in the survival of corals. On the other hand, also the strength of the coral—beside the coral morphology and the hydrodynamic loading—is of importance for the survival of the coral, and the reef as a whole. As the coral skeleton becomes weaker—e.g. due to ocean acidification (OA) or reduced growth—the coral becomes more susceptible to dislodgement. Once the coral is gone, recolonisation of the area takes a

long period and highly depends on the health of the reef and nearby reefs for the supply of coral larvae.

As the decay and recovery mechanisms are the dominant processes on the long-term development of corals and coral reefs, these aspects largely determine the coral survival. The exact calcification rate of the corals is of less importance and can easily be tuned to fit the data. The correct prediction of damage—biochemical and mechanical—is key in making reliable predictions on the survival of corals and coral reefs as a whole. Mispredicting this damage substantially alters the modelled future perspectives of corals and coral reefs. Therefore, the determination of the tipping point associated with both the biochemical and mechanical damage—i.e. bleaching and dislodgement, respectively—is key in making long-term predictions on the survival of coral reefs.

For convenience, the research objective is repeated here:

How can the biophysical interactions between corals and the environment be modelled?

The biophysical interactions between corals and the environment can be modelled by integrating the biological responses of the coral-zooxanthellae symbiont—i.e. the coral physiology—with its morphology and the environment. The feedback loop between the coral and its environment is the core of the biophysical model framework (BMF). Even though not all interactions within this feedback loop are included, a trustworthy framework is developed that offers the opportunity to be extended by other processes.

Due to its linear basis, future developments in understanding the biophysical processes related to corals can easily be added to the BMF. Despite this linear basis, it does not rule out the incorporation of non-linear processes such as the thermal micro-environment, which is determined based on light, flow and thermal conditions.

Finally, even though not all aspects are (fully) incorporated, the developed BMF gives insight in the complex nature of the leading biophysics of corals and coral reefs. Because it is largely process-based, it is widely applicable. Furthermore, the BMF is based on open-source software—Python and Delft3D Flexible Mesh—and so can be used by everybody without financial constraints. As the core is written in Python, the connection with other hydrodynamic models is also be possible as only the connection for storm simulations are needed.

10.2 Data acquisition

As the biophysical model framework (BMF) developed in this study is the first of its kind, there are multiple areas in which improvements can be made. The availability of more data on the coral dynamics will result in better validation of the model. The results from this study are a good starting point for the prioritisation of future research objectives. The sensitivity analysis performed in this study (*see* Ch. 8) provides three main areas for future research:

Coral morphology The coral morphology—and especially its development—is mainly qualitatively addressed in the scientific literature [Chappell, 1980]. If addressed quantitatively, elaborate models are used to assess the best-fitting morphology [Hoogenboom et al., 2008; Kaandorp et al., 2011], which may take several hours to days to run [pers. comm. J.A. Kaandorp].

This component is essential in closing the feedback loop between the coral and its environment. More research is required to define morphological relations to its environment. The use of

model morphologies is another solution to fill up this knowledge gap (*see* Sec. 9.4). Future research can identify its efficiency and representation of reality.

Therefore, it is recommended to study the morphological development of corals due to the environmental conditions. In support of the suggested model morphologies (*see* Sec. 9.4), research has to be done on the topic of natural selection; why are certain morphological traits more beneficial than others under certain conditions.

Attachment strength The strength of the substratum is of substantial importance for the possible dislodgement of corals. As the dislodgement of corals highly alters the future of corals, the correctness of the strength is an important factor in making representative predictions. Herein, also the coral morphology plays a crucial role because it determines the other side of the dislodgement criterion (*see* Sec. 6.2). At the moment, there is a lot of spreading in the data on this strength [Madin, 2005]. Further research is needed on this parameter. As suggested in Section 9.4, the use of model morphologies can reduce the spreading found.

Coral recruitment The field of larval dispersion and recruitment in marine habitats is relatively young and much is still unknown. Nonetheless, the importance of the recruitment of larvae becomes more evident in recovery studies and is one of the key aspects of the deep reef refugia hypothesis (DRRH). In this study, the coral recruitment is incorporated in a very basic manner, partly due to knowledge gaps. The largest missing link in the coral recruitment dynamics is the process of settlement; e.g. the conditions that are favourable and unfavourable for coral larval settlement. Therefore, further research on the recruitment dynamics of corals is recommended with a special focus on the processes associated with the settlement of coral larvae.

10.3 Biophysical model framework improvements

Beside the fact that further research is needed to acquire more related data, the biophysical model framework (BMF) itself can be improved as well by (1) assessing the best morphological representation; (2) including more essential processes, such as coral recruitment dynamics and sediment dynamics; (3) switching from a deterministic approach—as used in this study—to a probabilistic approach; and (4) improving the numerical and computational efficiency. These improvements are further highlighted below.

Morphological representation Of the four main areas of improvement, the morphological representation is the most essential. When the model morphologies—as presented in Section 9.4—turn out to be a suitable morphological representation, spreading in biophysical parameters found may reduce as they can be grouped to the various model morphologies. Therefore, the use of model morphologies is most likely to contribute to improvements on the uncertainty in biophysical parameters and processes.

Furthermore, it eliminates the need to define morphologies as function of the environmental factors as it is based on natural selection. Therefore, correct descriptions on the responses of the various model morphologies will result in the correct morphological distribution across gradients. Moreover, the use of model morphologies also result in a better representation of storm damage; as discussed in Section 9.4.

All in all, changing the morphological representation to model morphologies has great potential to substantially improve the BMF: (1) a reduction in the spreading of physiological parameters; (2) a process-based relation between coral morphology and the environment without the need of extensive data acquisition on the morphological development; (3) a better representation

of storm damage; and (4) a better representation of reality, as differences in morphology are present unrelated to environmental gradients.

Biophysical processes Beside the four environmental factors that are included in this study, there are two other environmental dependencies commonly studied: (1) nutrient availability [Atkinson and Bilger, 1992; Holcomb et al., 2012; Langdon and Atkinson, 2005]; and (2) sediment concentration [Erftemeijer et al., 2012; Storlazzi et al., 2015]. The effects of these two factors on the photosynthetic efficiency can easily be added to this framework. Even though some studies have shown that there exist non-linear interactions between the nutrient availability and the response of the coral to the aragonite saturation state [Holcomb et al., 2012; Langdon and Atkinson, 2005]. This non-linearity would possibly result in reformulating the aragonite dependency.

Furthermore, the sediment concentration is believed to impact the coral morphology as well [Chappell, 1980], and so the coral morphology plays a substantial role in the physiology when sediment concentrations are added to the BMF [Fricke and Schuhmacher, 1983; Sanders and Baron-Szabo, 2005; Stafford-Smith and Ormond, 1992].

Next, the acidity of the water is taken into account via the aragonite saturation state in which the effect of coral growth on the pH is not incorporated [Allemand et al., 2004; Goreau, 1959; Jokiel, 2011b]. Future research must clarify the significance of the acidic micro-environment on the coral growth. As there is a high sensitivity of the aragonite saturation state to the acidity, this might result in better predictions under changing acidic conditions such as ocean acidification (OA).

Last but not least, the recruitment of coral larvae is included in a simplified manner (*see* Sec. 6.3), while more elaborate processes determine the fate of the coral larvae [Connolly and Baird, 2010; Cowen et al., 2006; Guest et al., 2005; Tay et al., 2011]. In Appendix F, an extensive recommendation is presented on how the full recruitment dynamics can be included in the developed BMF. This recommendation is not fully functional as certain parts of it are in need of more research to correctly represent the dynamics. Especially the probability of settlement of the larvae requires more attention. The added value of more elaborate recruitment dynamics incorporated in the BMF gives rise to better predictions of the recovery of a reef after a damaging event. It also provides the ability to assess possible recovery programs to help reefs regenerate after substantial damage; be it biochemical and/or mechanical.

Probabilistic approach The BMF developed in this study has a deterministic approach, while in nature a probabilistic approach is commonly more suitable [Denny, 2017]. As the values of all the parameters are varying and the responses of the organisms is typically non-linear, the physiological response under average conditions is typically different from the average response over a range of conditions [Jensen, 1906; Denny, 2017]. This is often called "the fallacy of the average", or "Jensen's inequality" [Jensen, 1906; Denny, 2017].

Furthermore, a probabilistic approach presents the outcomes as probabilities, which is more suitable to use in decision-making [Uusitalo et al., 2015; Moe et al., 2016]. Especially as biological processes have a varying nature, a deterministic approach does not cover the full picture [Uusitalo et al., 2015]. It is therefore increasingly used in for example environmental modelling [Aguilera et al., 2011, and references therein]; and modelling studies on ecosystem services [Landuyt et al., 2013, and references therein]. Such assessments aid in developing protection and recovering programs.

Therefore, extending the developed BMF towards a probabilistic nature enhances its use for decision-making in which risk assessments are key. This supports the development of protection and recovering programs with process-based model assessments.

There is, however, a large downside to the modification towards a probabilistic approach. This is the computational efficiency of the BMF. The deterministic BMF is able to predict with sufficient accuracy hundreds years into the future in the order of hours. The simulation time increases substantially when a probabilistic approach is used.

Numerical and computational efficiency Some biophysical processes require solving (partial) differential equations for which unconditionally stable numerical schemes are desired due to the varying input; especially for the population dynamics for which also a lower and upper limit are defined (*see* App. A.5). As the aim of this study was to develop a BMF, the focus has not been on the best fitting numerical schemes and their efficiency. In all cases, first order numerical schemes are used and so the accuracy is in the order of the spatial- and time-steps; $\mathcal{O}(\Delta x, \Delta y; \Delta t)$. This leaves room for improvements on both the numerical efficiency and accuracy.

Because aforementioned model improvements result in a higher computational effort, the exploration of acceleration of the BMF is recommended as well to keep the BMF computational valuable. As the computational time is mainly determined by the hydrodynamic model—if the micro-environments are not included, as suggested (*see* Sec. 9.3)—accelerating this part results in the largest returns. Furthermore, the applicability of a coral growth acceleration factor—in line with the morphological acceleration factor [Lesser et al., 2004; Roelvink, 2006]—is not assessed in this study, but only briefly addressed in Section 3.2. This coral growth acceleration factor shows great potential as the morphological acceleration factor has proven to substantially improve the model efficiency in morphodynamic modelling [Ranasinghe et al., 2011]. Therefore, the benefits and costs of such a coral growth acceleration factor have to be determined; especially when the hydrodynamics cannot be reduced to the extent as in this study—e.g. due to the inclusion of sediment loads.

Due to the many non-linear relations associated with the coral physiology, the leading assumption of linearity at the basis of the morphological acceleration factor will be the bottleneck. On the other hand, the changes due to the growth are small and so the non-linearities approximate linearities. This delicate balance needs further research as is done for the use of the morphological acceleration factor in morphodynamics.

Bibliography

Absi, R. (2009). A simple eddy viscosity formulation for turbulent boundary layers near smooth walls. *Comptes Rendus - Mecanique*, 337(4):158–165.

Ackleson, S. G. (2003). Light in shallow waters: A brief research review. *Limnology and Oceanography*, 48(1, part 2):323–328.

Afzal, N. (2001). Power law and log law velocity profiles in fully developed turbulent pipe flow: Equivalent relations at large Reynolds numbers. *Acta Mechanica*, 151(3-4):171–183.

Agrawal, D. C. (2010). Photosynthetic Solar constant. *Latin-American Journal of Physics Education*, 4(1):46–50.

Aguilera, P. A., Fernández, A., Fernández, R., Rumí, R., and Salmerón, A. (2011). Bayesian networks in environmental modelling. *Environmental Modelling and Software*, 26(12):1376–1388.

Ainsworth, T. D., Heron, S. F., Ortiz, J. C., Mumby, P. J., Grech, A., Ogawa, D., Eakin, C. M., and Leggat, W. (2016). Climate change disables coral bleaching protection on the Great Barrier Reef. *Science*, 352(6283):338–342.

Al-Horani, F. A. (2005). Effects of changing seawater temperature on photosynthesis and calcification in the scleractinian coral Galaxea fascicularis, measured with O2, Ca2+ and pH microsensors. *Scientia Marina*, 69(3):347–354.

Al-Horani, F. A., Tambutté, É., and Allemand, D. (2007). Dark calcification and the daily rhythm of calcification in the scleractinian coral, Galaxea fascicularis. *Coral Reefs*, 26(3):531–538.

Albright, R., Mason, B., and Langdon, C. (2008). Effect of aragonite saturation state on settlement and post-settlement growth of Porites astreoides larvae. *Coral Reefs*, 27(3):485–490.

Allemand, D., Ferrier-Pagès, C., Furla, P., Houlbrèque, F., Puverel, S., Reynaud, S., Tambutté, É., Tambutté, S., and Zoccola, D. (2004). Biomineralisation in reef-building corals: From molecular mechanisms to environmental control. *Comptes Rendus - Palevol*, 3(6-7):453–467.

Álvarez-Noriega, M., Baird, A. H., Dornelas, M., Madin, J. S., Cumbo, V. R., and Connolly, S. R. (2016). Fecundity and the demographic strategies of coral morphologies. *Ecology*, 97(12):3485–3493.

Andersson, A. J., Kuffner, I. B., MacKenzie, F. T., Jokiel, P. L., Rodgers, K. S., and Tan, A. (2009). Net Loss of CaCO3 from a subtropical calcifying community due to seawater acidification: Mesocosm-scale experimental evidence. *Biogeosciences*, 6(8):1811–1823.

Andréfouët, S. and Cabioch, G. (2011). Barrier Reef (Ribbon Reef). In Hopley, D., editor, *Encyclopedia of Modern Coral Reefs: Structure, Form and Process*, pages 102–107. Springer Netherlands, Dordrecht, the Netherlands.

Anthony, K. R., Connolly, S. R., and Hoegh-Guldberg, O. (2007). Bleaching, energetics, and coral mortality risk: Effects of temperature, light, and sediment regime. *Limnology and Oceanography*, 52(2):716–726.

Anthony, K. R., Hoogenboom, M. O., and Connolly, S. R. (2005). Adaptive variation in coral geometry and the optimization of internal colony light climates. *Functional Ecology*, 19(1):17–26.

Anthony, K. R., Kline, D. I., Diaz-Pulido, G., Dove, S., and Hoegh-Guldberg, O. (2008). Ocean acidification causes bleaching and productivity loss in coral reef builders. *Proceedings of the National Academy of Sciences of the United States of America*, 105(45):17442–17446.

Anthony, K. R., Maynard, J. A., Diaz-Pulido, G., Mumby, P. J., Marshall, P. A., Cao, L., and Hoegh-Guldberg, O. (2011). Ocean acidification and warming will lower coral reef resilience. *Global Change Biology*, 17(5):1798–1808.

Anthony, K. R. N. (2000). Enhanced particle-feeding capacity of corals on turbid reefs (Great Barrier Reef, Australia). *Coral Reefs*, 19(1):59–67.

Anthony, K. R. N. and Fabricius, K. E. (2000). Shifting roles of heterotrophy and autotrophy in coral energet-

ics under varying turbidity. *Journal of Experimental Marine Biology and Ecology*, 252(2):221–253.

Anthony, K. R. N. and Hoegh-Guldberg, O. (2003a). Kinetics of photoacclimation in corals. *Oecologia*, 134(1):23–31.

Anthony, K. R. N. and Hoegh-Guldberg, O. (2003b). Variation in coral photosynthesis, respiration and growth characteristics in contrasting light microhabitats: An analogue to plants in forest gaps and understoreys? *Functional Ecology*, 17(2):246–259.

Asher, S. and Shavit, U. (2019). The effect of water depth and internal geometry on the turbulent flow inside a coral reef. *Journal of Geophysical Research: Oceans*, 124(6):3508–3522.

Ateweberhan, M. and McClanahan, T. R. (2010). Relationship between historical sea-surface temperature variability and climate change-induced coral mortality in the western Indian Ocean. *Marine Pollution Bulletin*, 60(7):964–970.

Atkinson, M., Smith, S. V., and Stroup, E. D. (1981). Circulation in Enewetak Atoll lagoon (Marshall Islands). *Limnology and Oceanography*, 26(6):1074–1083.

Atkinson, M. J. and Bilger, R. W. (1992). Effects of water velocity on phosphate uptake in coral reef-hat communities. *Limnology and Oceanography*, 37(2):273–279.

Baird, A. H., Bhagooli, R., Ralph, P. J., and Takahashi, S. (2009a). Coral bleaching: The role of the host. *Trends in Ecology and Evolution*, 24(1):16–20.

Baird, A. H., Guest, J. R., and Willis, B. L. (2009b). Systematic and biogeographical patterns in the reproductive biology of scleractinian corals. *Annual Review of Ecology, Evolution, and Systematics*, 40(1):551–571.

Baird, A. H. and Marshall, P. A. (2002). Mortality, growth and reproduction in scleractinian corals following bleaching on the Great Barrier Reef. *Marine Ecology Progress Series*, 237:133–141.

Baird, A. H. and Maynard, J. A. (2006). Coral adaptation in the face of climate change. *Science*, 320:315–316.

Bak, R. P., Nieuwland, G., and Meesters, E. H. (2005). Coral reef crisis in deep and shallow reefs: 30 years of constancy and change in reefs of Curacao and Bonaire. *Coral Reefs*, 24(3):475–479.

Baptist, M. (2005). *Modelling floodplain biogeomorphology*. Phd, Delft University of Technology.

Bayraktarov, E., Pizarro, V., Eidens, C., Wilke, T., and Wild, C. (2013). Bleaching susceptibility and recovery of Colombian Caribbean corals in response to water current exposure and seasonal upwelling. *PLoS ONE*, 8(11):e80536.

Beck, M. W., Losada, I. J., Menéndez, P., Reguero, B. G., Díaz-Simal, P., and Fernández, F. (2018). The global flood protection savings provided by coral reefs. *Nature Communications*, 9(1):2186.

Bellantuono, A. J., Hoegh-Guldberg, O., and Rodriguez-Lanetty, M. (2012). Resistance to thermal stress in corals without changes in symbiont composition. *Proceedings of the Royal Society B: Biological Sciences*, 279(1731):1100–1107.

Bellocchi, G., Rivington, M., Donatelli, M., and Matthews, K. (2009). Validation of biophysical models: Issues and methodologies. In Lichtfouse, E., Navarrete, M., Debaeke, P., Véronique, S., and Alberola, C., editors, *Sustainable Agriculture*, volume 2, pages 577–603. Springer Netherlands, Dordrecht, the Netherlands.

Benedet, L., Dobrochinski, J. P., Walstra, D. J., Klein, A. H., and Ranasinghe, R. (2016). A morphological modeling study to compare different methods of wave climate schematization and evaluate strategies to reduce erosion losses from a beach nourishment project. *Coastal Engineering*, 112:69–86.

Berkelmans, R. (2002). Time-integrated thermal bleaching thresholds of reefs and their variation on the Great Barrier Reef. *Marine Ecology Progress Series*, 229:73–82.

Berkelmans, R. and Oliver, J. K. (1999). Large-scale bleaching of corals on the Great Barrier Reef. *Coral Reefs*, 18(1):55–60.

Berkelmans, R. and Van Oppen, M. J. (2006). The role of zooxanthellae in the thermal tolerance of corals: A 'nugget of hope' for coral reefs in an era of climate change. *Proceedings of the Royal Society B: Biological Sciences*, 273(1599):2305–2312.

Bhaganagar, K., Kim, J., and Coleman, G. (2004). Effect of roughness on wall-bounded turbulence. *Flow, Turbulence and Combustion*, 72:463–492.

Bijker, E. W. (1967). *Some Considerations About Scales for Coastal Models*. Phd, Delft University of Technology.

Bird, R. B., Stewart, W. E., and Lightfoot, E. N. (2002). *Transport Phenomena*. John Wiley & Sons, Hoboken, second edition.

Blanchon, P. (2011). Geomorphic zonation. In Hopley, D., editor, *Encyclopedia of Modern Coral Reefs: Structure, Form and Process*, pages 469–486. Springer Netherlands, Dordrecht, the Netherlands.

Böhm, M., Finnigan, J. J., Raupach, M. R., and Hughes, D. (2013). Turbulence structure within and above a canopy of bluff elements. *Boundary-Layer Meteorology*, 146(3):393–419.

Bongaerts, P., Ridgway, T., Sampayo, E. M., and Hoegh-Guldberg, O. (2010). Assessing the 'deep reef refugia' hypothesis: Focus on Caribbean reefs. *Coral Reefs*, 29(2):309–327.

Booij, N., Ris, R. C., and Holthuijsen, L. H. (1999). A third-generation wave model for coastal regions. 1. Model description and validation. *Journal of Geophysical Research: Oceans*, 104(C4):7649–7666.

Bosboom, J. and Stive, M. J. F. (2015). *Coastal Dynamics I*. Delft Academic Press, Delft, 0.5 edition.

Bradbury, I. R. and Snelgrove, P. V. (2001). Contrasting larval transport in demersal fish and benthic invertebrates: The roles of behaviour and advective processes in determining spatial pattern. *Canadian Journal of Fisheries and Aquatic Sciences*, 58(4):811–823.

Britter, R. E. and Hanna, S. R. (2003). Flow and dispersion in urban areas. *Annual Review of Fluid Mechanics*, 35:469–496.

Brodersen, K. E., Lichtenberg, M., Ralph, P. J., Kühl, M., and Wangpraseurt, D. (2014). Radiative energy budget reveals high photosynthetic efficiency in symbiont-bearing corals. *Journal of the Royal Society Interface*, 11(93).

Brown, J. H., Gupta, V. K., Li, B. L., Milne, B. T., Restrepo, C., and West, G. B. (2002). The fractal nature of nature: Power laws, ecological complexity and biodiversity. *Philosophical Transactions of the Royal Society B: Biological Sciences*, 357(1421):619–626.

Buddemeier, R. W., Jokiel, P. L., Zimmerman, K. M., Lane, D. R., Carey, J. M., Bohling, G. C., and Martinich, J. A. (2008). A modeling tool to evaluate regional coral reef responses to changes in climate and ocean chemistry. *Limnology and Oceanography: Methods*, 6(9):395–411.

Cabioch, G. (2011). Forereef/Reef Front. In Hopely, D., editor, *Encyclopedia of Modern Coral Reefs: Structure, Form and Process*, pages 422–423. Springer Netherlands, Dordrecht, the Netherlands.

Cacciapaglia, C. and van Woesik, R. (2015). Reef-coral refugia in a rapidly changing ocean. *Global Change Biology*, 21(6):2272–2282.

Cacciapaglia, C. and van Woesik, R. (2016). Climate-change refugia: Shading reef corals by turbidity. *Global Change Biology*, 22(3):1145–1154.

Carilli, J., Donner, S. D., and Hartmann, A. C. (2012). Historical temperature variability affects coral response to heat stress. *PLoS ONE*, 7(3):e34418.

Carilli, J. E., Godfrey, J., Norris, R. D., Sandin, S. A., and Smith, J. E. (2010). Periodic endolithic algal blooms in Montastraea faveolata corals may represent periods of low-level stress. *Bulletin of Marine Science*, 86(3):709–718.

Chalker, B. E., Dunlap, W. C., and Oliver, J. K. (1983). Bathymetric adaptations of reef-building corals at Davies Reef, Great Barrier Reef, Australia. II. Light saturation curves for photosynthesis and respiration. *Journal of Experimental Marine Biology and Ecology*, 73(1):37–56.

Chamberlain, J. A. (1978). Mechanical properties of coral skeleton: Compressive strength and its adaptive significance. *Paleobiology*, 4(4):419–435.

Chan, N. C., Connolly, S. R., Wangpraseurt, D., and Kühl, M. (2016). Flow and coral morphology control coral surface pH: Implications for the effects of ocean acidification. *Frontiers in Marine Science*, 3:10.

Chappell, J. (1980). Coral morphology, diversity and reef growth. *Nature*, 286(5770):249–252.

Chia, F. S., Buckland-Nicks, J., and Young, C. M. (1984). Locomotion of marine invertebrate larvae: A review. *Canadian Journal of Zoology*, 62(7):1205–1222.

Chindapol, N., Kaandorp, J. A., Cronemberger, C., Mass, T., and Genin, A. (2013). Modelling growth and form of the scleractinian coral Pocillopora verrucosa and the influence of hydrodynamics. *PLoS Computational Biology*, 9(1):e1002849.

Clausen, C. D. and Roth, A. A. (1975). Effect of temperature and temperature adaptation on calcification rate in the hermatypic coral Pocillopora damicornis. *Marine Biology*, 33(2):93–100.

Coceal, O. and Belcher, S. E. (2004). A canopy model of mean winds through urban areas. *Quarterly Journal of the Royal Meteorological Society*, 130:1349–1372.

Coles, S. L. and Jokiel, P. L. (1978). Synergistic effects of temperature, salinity and light on the hermatypic coral Montipora verrucosa. *Marine Biology*, 49(3):187–195.

Comeau, S., Carpenter, R. C., Lantz, C. A., and Edmunds, P. J. (2016). Parameterization of the response of calcification to temperature and pCO2 in the coral Acropora pulchra and the alga Lithophyllum kotschyanum. *Coral Reefs*, 35(3):929–939.

Comeau, S., Edmunds, P. J., Lantz, C. A., and Carpenter, R. C. (2014). Water flow modulates the response of coral reef communities to ocean acidification. *Scientific Reports*, 4.

Connolly, S. R. and Baird, A. H. (2010). Estimating dispersal potential for marine larvae: Dynamic models applied to scleractinian corals. *Ecology*, 91(12):3572–3583.

Cooper, T. F., De'ath, G., Fabricius, K. E., and Lough, J. M. (2008). Declining coral calcification in massive Porites in two nearshore regions of the northern Great Barrier Reef. *Global Change Biology*, 14(3):529–538.

Cowen, R. K., Paris, C. B., and Srinivasan, A. (2006). Scaling of connectivity in marine populations. *Science*, 311(5760):522–527.

Cowen, R. K. and Sponaugle, S. (2009). Larval dispersal and marine population connectivity. *Annual Review of Marine Science*, 1(1):443–466.

Darwin, C. R. (1842). *The structure and distribution of coral reefs*. London: Smith, Elder and Co, Cornhill.

de Putron, S. J., McCorkle, D. C., Cohen, A. L., and Dillon, A. B. (2011). The impact of seawater saturation state and bicarbonate ion concentration on calci-

fication by new recruits of two Atlantic corals. *Coral Reefs*, 30(2):321–328.

de Vriend, H. J., Capobianco, M., Chesher, T., de Swart, H. E., Latteux, B., and Stive, M. J. (1993). Approaches to long-term modelling of coastal morphology: A review. *Coastal Engineering*, 21(1-3):225–269.

Dean, R. G. and Dalrymple, R. A. (1998). *Water Wave Mechanics for Engineers and Scientists*. World Scientific, Singapore, advanced edition.

Deltares (2019a). D-Flow Flexible Mesh. Technical Reference Manual.

Deltares (2019b). D-Flow Flexible Mesh. User Manual.

Deltares (2019c). D-Waves. User Manual.

Dennison, W. C. and Barnes, D. J. (1988). Effect of water motion on coral photosynthesis and calcification. *Journal of Experimental Marine Biology and Ecology*, 115(1):67–77.

Denny, M. (2017). The fallacy of the average: On the ubiquity, utility and continuing novelty of Jensen's inequality. *The Journal of Experimental Biology*, 220(2):139–146.

Denny, M. W. (1995). Predicting physical disturbance: Mechanistic approaches to the study of survivorship on wave-swept shores. *Ecological Monographs*, 65(4):371–418.

Dias, M., Ferreira, A., Gouveia, R., Cereja, R., and Vinagre, C. (2018). Mortality, growth and regeneration following fragmentation of reef-forming corals under thermal stress. *Journal of Sea Research*, 141:71–82.

DiPerna, S., Hoogenboom, M., Noonan, S., and Fabricius, K. (2018). Effects of variability in daily light integrals on the photophysiology of the corals Pachyseris speciosa and Acropora millepora. *PLoS ONE*, 13(9):e0203882.

Dollar, S. J. (1982). Wave stress and coral community structure in Hawaii. *Coral Reefs*, 1(2):71–81.

Done, T. (2011a). Coral reef, definition. In Hopley, D., editor, *Encyclopedia of Modern Coral Reefs: Structure, Form and Process*, pages 261–267. Springer Netherlands, Dordrecht, the Netherlands.

Done, T. (2011b). Corals: Environmental Controls on Growth. In Hopley, D., editor, *Encyclopedia of Modern Coral Reefs: Structure, Form and Process*, pages 281–293. Springer Netherlands, Dordrecht, the Netherlands.

Donner, S. D. (2011). An evaluation of the effect of recent temperature variability on the prediction of coral bleaching events. *Ecological Applications*, 21(5):1718–1730.

Dubé, C. E., Mercière, A., Vermeij, M. J., and Planes, S. (2017). Population structure of the hydrocoral Millepora platyphylla in habitats experiencing different flow regimes in Moorea, French polynesia. *PLoS ONE*, 12(3):e0173513.

Dubinsky, Z. and Stambler, N. (2011). *Coral Reefs: An Ecosystem in Transition*. Springer Netherlands, Dordrecht, the Netherlands.

Eakin, C. M., Lough, J. M., and Heron, S. F. (2008). Climate variability and change: Monitoring data and evidence for increased coral bleaching stress. In Van Oppen, M. J. and Lough, J. M., editors, *Coral Bleaching: Patterns, Processes, Causes and Consequences*, chapter 4, pages 41–68. Springer-Verlag, Berlin, Germany.

Eakin, C. M., Sweatman, H. P. A., and Brainard, R. E. (2019). The 2014–2017 global-scale coral bleaching event: Insights and impacts. *Coral Reefs*, 38(4):539–545.

Edinger, E. N., Limmon, G. V., Jompa, J., Widjatmoko, W., Heikoop, J. M., and Risk, M. J. (2000). Normal coral growth rates on dying reefs: Are coral growth rates good indicators of reef health? *Marine Pollution Bulletin*, 40(5):404–425.

Edmunds, P. J. (2005). The effect of sub-lethal increases in temperature on the growth and population trajectories of three scleractinian corals on the southern Great Barrier Reef. *Oecologia*, 146(3):350–364.

Edmunds, P. J. and Gates, R. D. (2008). Acclimatization in tropical reef corals. *Marine Ecology Progress Series*, 361:307–310.

Erftemeijer, P. L., Riegl, B., Hoeksema, B. W., and Todd, P. A. (2012). Environmental impacts of dredging and other sediment disturbances on corals: A review. *Marine Pollution Bulletin*, 64(9):1737–1765.

Etminan, V., Lowe, R. J., and Ghisalberti, M. (2017). A new model for predicting the drag exerted by vegetation canopies. *Water Resources Research*, 53(4):3179–3196.

Etminan, V., Lowe, R. J., and Ghisalberti, M. (2019). Canopy resistance on oscillatory flows. *Coastal Engineering*, 152:103502.

Evenhuis, C., Lenton, A., Cantin, N. E., and Lough, J. M. (2015). Modelling coral calcification accounting for the impacts of coral bleaching and ocean acidification. *Biogeosciences*, 12(9):2607–2630.

Eyal, G., Cohen, I., Eyal-Shaham, L., Ben-Zvi, O., Tikochinski, Y., and Loya, Y. (2019). Photoacclimation and induction of light-enhanced calcification in the mesophotic coral Euphyllia paradivisa. *Royal Society Open Science*, 6(2):180527.

Fabricius, K. E. (2006). Effects of irradiance, flow, and colony pigmentation on the temperature microenvironment around corals: Implications for coral bleaching? *Limnology and Oceanography*, 51(1):30–37.

Fairbridge, R. W. (1950). Recent and Pleistocene coral reefs of Australia. *The Journal of Geology*, 58(4):330–401.

Falter, J. L., Lowe, R. J., Zhang, Z., and McCulloch, M. (2013). Physical and biological controls on the carbonate chemistry of coral reef waters: Effects of metabolism, wave forcing, sea level, and geomorphology. *PLoS ONE*, 8(1):e53303.

Ferrario, F., Beck, M. W., Storlazzi, C. D., Micheli, F., Shepard, C. C., and Airoldi, L. (2014). The effectiveness of coral reefs for coastal hazard risk reduction and adaptation. *Nature Communications*, 5(1):3794.

Finelli, C. M., Helmuth, B. S. T., Pentcheff, N. D., and Wethey, D. S. (2006). Water flow influences oxygen transport and photosynthetic efficiency in corals. *Coral Reefs*, 25(1):47–57.

Finnigan, J. (2000). Turbulence in plant canopies. *Annual Review of Fluid Mechanics*, 32:519–571.

Frei, W. (2017). Which Turbulence Model Should I Choose for my CFD Application?

Freitas, L. M., Oliveira, M. d. D. M., Leão, Z. M., and Kikuchi, R. K. P. (2019). Effects of turbidity and depth on the bioconstruction of the Abrolhos reefs. *Coral Reefs*, 38(2):241–253.

Fricke, H. W. and Schuhmacher, H. (1983). The depth limits of red sea stony corals: An ecophysiological problem (A deep diving survey by submersible). *Marine Ecology*, 4(2):163–194.

Gattuso, J. P., Frankignoulle, M., Bourge, I., Romaine, S., and Buddemeier, R. W. (1998). Effect of calcium carbonate saturation of seawater on coral calcification. *Global and Planetary Change*, 18(1-2):37–46.

Gaylord, B., Hodin, J., and Ferner, M. C. (2013). Turbulent shear spurs settlement in larval sea urchins. *Proceedings of the National Academy of Sciences of the United States of America*, 110(17):6901–6906.

Ghisalberti, M. and Nepf, H. M. (2002). Mixing layers and coherent structures in vegetated aquatic flows. *Journal of Geophysical Research*, 107(C2):3.

Gibbin, E. M., Krueger, T., Putnam, H. M., Barott, K. L., Bodin, J., Gates, R. D., and Meibom, A. (2018). Short-term thermal acclimation modifies the metabolic condition of the coral holobiont. *Frontiers in Marine Science*, 5:10.

Glynn, P. W. (1996). Coral reef bleaching: Facts, hypotheses and implications. *Global Change Biology*, 2(6):495–509.

Goreau, T. F. (1959). The physiology of skeleton formation in corals. I. A method for measuring the rate of calcium deposition by corals under different conditions. *The Biological Bulletin*, 116(1):59–75.

Gourlay, M. R. and Colleter, G. (2005). Wave-generated flow on coral reefs - An analysis for two-dimensional horizontal reef-tops with steep faces. *Coastal Engineering*, 52(4):353–387.

Graham, E. M., Baird, A. H., and Connolly, S. R. (2008). Survival dynamics of scleractinian coral larvae and implications for dispersal. *Coral Reefs*, 27(3):529–539.

Graham, N. A., Jennings, S., MacNeil, M. A., Mouillot, D., and Wilson, S. K. (2015). Predicting climate-driven regime shifts versus rebound potential in coral reefs. *Nature*, 518(7537):94–97.

Grant, W. D. and Madsen, O. S. (1986). The continental-shelf bottom boundary layer. *Annual Review of Fluid Mechanics*, 18:265–305.

Graus, R. R. and Macintyre, I. G. (1976). Light control of growth form in colonial reef corals: Computer simulation. *Science*, 193(4256):895–897.

Graus, R. R., Macintyre, I. G., and Herchenroder, B. E. (1984). Computer simultion of the reef zonation at Discovery Bay, Jamaica: Hurricane disruption and long-term physical oceanographic controls. *Coral Reefs*, 3(2):59–68.

Gu, Z. and Wang, H. (1991). Gravity waves over porous bottoms. *Coastal Engineering*, 15(5-6):497–524.

Guest, J. R., Baird, A. H., Goh, B. P., and Chou, L. M. (2005). Reproductive seasonality in an equatorial assemblage of scleractinian corals. *Coral Reefs*, 24(1):112–116.

Guinotte, J. M., Buddemeier, R. W., and Kleypas, J. A. (2003). Future coral reef habitat marginality: Temporal and spatial effects of climate change in the Pacific basin. *Coral Reefs*, 22(4):551–558.

Hall-Spencer, J. M., Rodolfo-Metalpa, R., Martin, S., Ransome, E., Fine, M., Turner, S. M., Rowley, S. J., Tedesco, D., and Buia, M. C. (2008). Volcanic carbon dioxide vents show ecosystem effects of ocean acidification. *Nature*, 454(7200):96–99.

Harii, S. and Kayanne, H. (2003). Larval dispersal, recruitment, and adult distribution of the brooding stony octocoral Heliopora coerulea on Ishigaki Island, southwest Japan. *Coral Reefs*, 22(2):188–196.

Harii, S., Kayanne, H., Takigawa, H., Hayashibara, T., and Yamamoto, M. (2002). Larval survivorship, competency periods and settlement of two brooding corals, Heliopora coerulea and Pocillopora damicornis. *Marine Biology*, 141(1):39–46.

Harii, S., Nadaoka, K., Yamamoto, M., and Iwao, K. (2007). Temporal changes in settlement, lipid content and lipid composition of larvae of the spawning hermatypic coral Acropora tenuis. *Marine Ecology Progress Series*, 346:89–96.

Harley, C. D. G., Hughes, A. R., Hultgren, K. M., Miner, B. G., Sorte, C. J. B., Thornber, C. S., Rodriguez, L. F., Tomanek, L., and Williams, S. L. (2006). The impacts of climate change in coastal marine systems. *Ecology Letters*, 9(2):228–241.

Harris, D. L., Rovere, A., Casella, E., Power, H., Canavesio, R., Collin, A., Pomeroy, A., Webster, J. M., and Parravicini, V. (2018). Coral reef structural complexity provides important coastal protection from waves under rising sea levels. *Science Advances*, 4(2):eaao4350.

Harrison, P. and Wallace, C. (1990). Reproduction, dispersal and recruitment of scleractinian corals. In Dubinsky, Z., editor, *Coral reef ecosystems*, chapter 7, pages 133–207. Elsevier, Amsterdam.

Hata, T., Madin, J. S., Cumbo, V. R., Denny, M., Figueiredo, J., Harii, S., Thomas, C. J., and Baird, A. H. (2017). Coral larvae are poor swimmers and require fine-scale reef structure to settle. *Scientific Reports*, 7(1):2249.

Hatcher, B. G. (1988). Coral reef primary productivity: A beggar's banquet. *Trends in Ecology and Evolution*, 3(5):106–111.

Hearn, C., Atkinson, M., and Falter, J. (2001). A physical derivation of nutrient-uptake rates in coral reefs: Effects of roughness and waves. *Coral Reefs*, 20(4):347–356.

Hearn, C. J. (1999). Wave-breaking hydrodynamics within coral reef systems and the effect of changing relative sea level. *Journal of Geophysical Research: Oceans*, 104(C12):30007–30019.

Hearn, C. J. (2001). Introduction to the special issue of Coral Reefs on "coral reef hydrodynamics". *Coral Reefs*, 20(4):327–329.

Hearn, C. J. (2011). Perspectives in coral reef hydrodynamics. *Coral Reefs*, 30(SUPPL. 1):1–9.

Hédouin, L. and Gates, R. D. (2013). Assessing fertilization success of the coral Montipora capitata under copper exposure: Does the night of spawning matter? *Marine Pollution Bulletin*, 66(1-2):221–224.

Helmuth, B. and Sebens, K. (1993). The influence of colony morphology and orientation to flow on particle capture by the scleractinian coral Agaricia agaricites (Linnaeus). *Journal of Experimental Marine Biology and Ecology*, 165(2):251–278.

Helmuth, B. S., Sebens, K. P., and Daniel, T. L. (1997). Morphological variation in coral aggregations: Branch spacing and mass flux to coral tissues. *Journal of Experimental Marine Biology and Ecology*, 209:233–259.

Hennige, S. J., Smith, D. J., Perkins, R., Consalvey, M., Paterson, D. M., and Suggett, D. J. (2008). Photoacclimation, growth and distribution of massive coral species in clear and turbid waters. *Marine Ecology Progress Series*, 369:77–88.

Hennige, S. J., Smith, D. J., Walsh, S. J., McGinley, M. P., Warner, M. E., and Suggett, D. J. (2010). Acclimation and adaptation of scleractinian coral communities along environmental gradients within an Indonesian reef system. *Journal of Experimental Marine Biology and Ecology*, 391(1-2):143–152.

Hinkel, J., Lincke, D., Vafeidis, A. T., Perrette, M., Nicholls, R. J., Tol, R. S. J., Marzeion, B., Fettweis, X., Ionescu, C., and Levermann, A. (2014). Coastal flood damage and adaptation costs under 21st century sea-level rise. *Proceedings of the National Academy of Sciences*, 111(9):3292–3297.

Hoegh-Guldberg, O. (1999). Climate change, coral bleaching and the future of the world's coral reefs. *Marine and Freshwater Research*, 50(8):839–866.

Hoegh-Guldberg, O. and Jones, R. J. (1999). Photoinhibition and photoprotection in symbiotic dinoflagellates from reef-building corals. *Marine Ecology Progress Series*, 183:73–86.

Hoegh-Guldberg, O., Mumby, P. J., Hooten, A. J., Steneck, R. S., Greenfield, P., Gomez, E., Harvell, C. D., Sale, P. F., Edwards, J. A., Caldeira, K., Knowlton, N., Eakin, C. M., Iglesias-Prieto, R., Muthiga, N., Bradbury, R. H., Dubi, A., and Hatziolos, M. E. (2007). Coral reefs under rapid climate change and ocean acidification. *Science*, 318(5857):1737–1742.

Hoeke, R. K., Storlazzi, C. D., and Ridd, P. V. (2013). Drivers of circulation in a fringing coral reef embayment: A wave-flow coupled numerical modeling study of Hanalei Bay, Hawaii. *Continental Shelf Research*, 58:79–95.

Holcomb, M., Cohen, A. L., and McCorkle, D. C. (2012). An investigation of the calcification response of the scleractinian coral Astrangia poculata to elevated pCO2 and the effects of nutrients, zooxanthellae and gender. *Biogeosciences*, 9(1):29–39.

Holthuijsen, L. H. (2007). *Waves in Oceanic and Coastal Waters*. Cambridge University Press, New York, NY.

Hongo, C., Kawamata, H., and Goto, K. (2012). Catastrophic impact of typhoon waves on coral communities in the Ryukyu Islands under global warming. *Journal of Geophysical Research: Biogeosciences*, 117(2).

Hoogenboom, M. O., Connolly, S. R., and Anthony, K. R. (2008). Interactions between morphological and physiological plasticity optimize energy acquisition in corals. *Ecology*, 89(4):1144–1154.

Hopley, D. (1982). *The Geomorphology of the Great Barrier Reef*. Wiley, New York.

Houck, J. E., Buddemeier, R. W., Smith, S. V., and Jokiel, P. L. (1977). The response of coral growth rate and skeletal strontium content to light intensity and water temperature. In Tayler, D. L., editor, *Proceedings of the 3rd International Coral Reef Symposium*, pages 425–431, Miami, Florida. Rosenstiel School of Marine and Atmospheric Science.

Howe, S. A. and Marshall, A. T. (2002). Temperature effects on calcification rate and skeletal deposition in the temperate coral, Plesiastrea versipora (Lamarck).

Journal of Experimental Marine Biology and Ecology, 275(1):63–81.

Howells, E. J., Beltran, V. H., Larsen, N. W., Bay, L. K., Willis, B. L., and Van Oppen, M. J. (2012). Coral thermal tolerance shaped by local adaptation of photosymbionts. *Nature Climate Change*, 2(2):116–120.

Howells, E. J., Berkelmans, R., Van Oppen, M. J., Willis, B. L., and Bay, L. K. (2013). Historical thermal regimes define limits to coral acclimatization. *Ecology*, 94(5):1078–1088.

Howells, E. J., Dunshea, G., McParland, D., Vaughan, G. O., Heron, S. F., Pratchett, M. S., Burt, J. A., and Bauman, A. G. (2018). Species-specific coral calcification responses to the extreme environment of the southern Persian Gulf. *Frontiers in Marine Science*, 5:56.

Hughes, T. P., Baird, A. H., Bellwood, D. R., Card, M., Connolly, S. R., Folke, C., Grosberg, R., Hoegh-Guldberg, O., Jackson, J. B., Kleypas, J., Lough, J. M., Marshall, P., Nyström, M., Palumbi, S. R., Pandolfi, J. M., Rosen, B., and Roughgarden, J. (2003). Climate change, human impacts, and the resilience of coral reefs. *Science*, 301(5635):929–933.

Hughes, T. P., Kerry, J. T., Baird, A. H., Connolly, S. R., Chase, T. J., Dietzel, A., Hill, T., Hoey, A. S., Hoogenboom, M. O., Jacobson, M., Kerswell, A., Madin, J. S., Mieog, A., Paley, A. S., Pratchett, M. S., Torda, G., and Woods, R. M. (2019). Global warming impairs stock–recruitment dynamics of corals. *Nature*, 568(7752):387–390.

Hughes, T. P. and Tanner, J. E. (2000). Recruitment failure, life histories, and long-term decline of Caribbean corals. *Ecology*, 81(8):2250–2263.

Hurd, C. L. (2000). Water motion, marine macroalgal physiology, and production. *Journal of Phycology*, 36(3):453–472.

Idso, S. B. and Gilbert, R. G. (1974). On the universality of the Poole and Atkins Secchi disk-light extinction equation. *The Journal of Applied Ecology*, 11(1):399.

Incropera, F. P., DeWitt, D. P., Bergman, T. L., and Lavine, A. S. (2007). *Fundamentals of Heat and Mass Transfer*. John Wiley & Sons, Hoboken, sixth edition.

IPCC (2014). *Climate Change 2014: Synthesis Report. Contribution of Working Groups I, II and III to the Fifth Assessment Report of the Intergovernmental Panel on Climate Change*. IPCC, Geneva, Switzerland.

ITACA (2018). The Sun As A Source Of Energy. Part 3: Calculating Solar Angles.

Iwagaki, Y. and Ishida, H. (1974). Laminar Boundary Layer around a Circular Cylinder under Oscillatory Waves. In *14th International Conference on Coastal Engineering*, pages 1848–1862, Copenhagen, Denmark. American Society of Civil Engineers.

James, D. W. (1968). The thermal diffusivity of ice and water between -40 and +60 oC. *Journal of Materials Science*, 3(5):540–543.

Jassby, A. D. and Platt, T. (1976). Mathematical formulation of the relationship between photosynthesis and light for phytoplankton. *Limnology and Oceanography*, 21(4):540–547.

Jaubert, J. (1977). Light, metabolism and growth forms of the hermatypic scleractinian coral Synarea convexa, Verrill, in the lagoon of Moorea, French Polynesia. In *Proceedings of the 3rd International Coral Reef Symposium*, volume 1, pages 483–488, Miami, Florida.

Jeans, J., Campbell, D. A., and Hoogenboom, M. O. (2013). Increased reliance upon photosystem II repair following acclimation to high-light by coral-dinoflagellate symbioses. *Photosynthesis Research*, 118(3):219–229.

Jensen, J. L. W. V. (1906). Sur les fonctions convexes et les inégalités entre les valeurs moyennes. *Acta Mathematica*, 30(1):175–193.

Jimenez, I. M., Kühl, M., Larkum, A. W., and Ralph, P. J. (2008). Heat budget and thermal microenvironment of shallow-water corals: Do massive corals get warmer than branching corals? *Limnology and Oceanography*, 53(4):1548–1561.

Jimenez, I. M., Kühl, M., Larkum, A. W. D., and Ralph, P. J. (2011). Effects of flow and colony morphology on the thermal boundary layer of corals. *Journal of the Royal Society Interface*, 8(65):1785–1795.

Jimenez, I. M., Larkum, A. W., Ralph, P. J., and Kühl, M. (2012a). In situ thermal dynamics of shallow water corals is affected by tidal patterns and irradiance. *Marine Biology*, 159(8):1773–1782.

Jimenez, I. M., Larkum, A. W., Ralph, P. J., and Kühl, M. (2012b). Thermal effects of tissue optics in symbiont-bearing reef-building corals. *Limnology and Oceanography*, 57(6):1816–1825.

Johnston, M. A., Hickerson, E. L., Nuttall, M. F., Blakeway, R. D., Sterne, T. K., Eckert, R. J., and Schmahl, G. P. (2019). Coral bleaching and recovery from 2016 to 2017 at East and West Flower Garden Banks, Gulf of Mexico. *Coral Reefs*, 38:787–799.

Jokiel, P. L. (2011a). Ocean acidification and control of reef coral calcification by boundary layer limitation of proton flux. *Bulletin of Marine Science*, 87(3):639–657.

Jokiel, P. L. (2011b). The reef coral two compartment proton flux model: A new approach relating tissue-level physiological processes to gross corallum morphology. *Journal of Experimental Marine Biology and Ecology*, 409(1-2):1–12.

Jokiel, P. L. and Coles, S. L. (1977). Effects of temperature on the mortality and growth of Hawaiian reef corals. *Marine Biology*, 43(3):201–208.

Jones, A. M., Berkelmans, R., Van Oppen, M. J., Mieog, J. C., and Sinclair, W. (2008). A community change in the algal endosymbionts of a scleractinian coral following a natural bleaching event: Field evidence of acclimatization. *Proceedings of the Royal Society B: Biological Sciences*, 275(1641):1359–1365.

Jonsson, I. G. (1966). Wave boundary layers and friction factors. In *Proceedings of the 10th International Conference on Coastal Engineering*, pages 127–148, New York, NY. American Society of Civil Engineers.

Jonsson, I. G. (1980). A new approach to oscillatory rough turbulent boundary layers. *Ocean Engineering*, 7(1):109–152.

Jonsson, I. G. and Carlsen, N. A. (1976). Experimental and theoretical investigations in an oscillatory turbulent boundary layer. *Journal of Hydraulic Research*, 14(1):45–60.

Kaandorp, J. A. (1995). Analysis and synthesis of radiate accretive growth in three dimensions. *Journal of Theoretical Biology*, 175(1):39–55.

Kaandorp, J. A. (2013). Macroscopic modelling of environmental influence on growth and form of sponges and corals using the accretive growth model. *ISRN Biomathematics*, 2013:1–14.

Kaandorp, J. A., Filatov, M., and Chindapol, N. (2011). Simulating and quantifying the environmental influence on coral colony growth and form. In Dubinsky, Z. and Stambler, N., editors, *Coral Reefs: An Ecosystem in Transition*, pages 177–185. Springer Netherlands, Dordrecht, the Netherlands.

Kaandorp, J. A., Koopman, E. A., Sloot, P. M., Bak, R. P., Vermeij, M. J., and Lampmann, L. E. (2003). Simulation and analysis of flow patterns around the scleractinian coral Madracis mirabilis (Duchassaing and Michelotti). *Philosophical Transactions of the Royal Society B: Biological Sciences*, 358(1437):1551–1557.

Kaandorp, J. A., Lowe, C. P., Frenkel, D., and Sloot, P. M. (1996). Effect of nutrient diffusion and flow on coral morphology. *Physical Review Letters*, 77(11):2328–2331.

Kaandorp, J. A. and Sloot, P. M. A. (1999). Growth and Form of Sponges and Corals in a Moving Fluid. In Carbone, A., Gromov, M., and Prusinkiewicz, P., editors, *Pattern Formation in Biology, Vision and Dynamics*, pages 24–41. World Scientific, Singapore.

Kaandorp, J. A. and Sloot, P. M. A. (2001). Morphological models of radiate accretive growth and the influence of hydrodynamics. *Journal of Theoretical Biology*, 209(3):257–274.

Kaniewska, P., Anthony, K. R., Sampayo, E. M., Campbell, P. R., and Hoegh-Guldberg, O. (2014). Implications of geometric plasticity for maximizing photosynthesis in branching corals. *Marine Biology*, 161(2):313–328.

Kaniewska, P., Magnusson, S. H., Anthony, K. R., Reef, R., Kühl, M., and Hoegh-Guldberg, O. (2011). Importance of macro- versus microstructure in modulating light levels inside coral colonies. *Journal of Phycology*, 47(4):846–860.

Keddy, P. A. (1992). Assembly and response rules: Two goals for predictive community ecology. *Journal of Vegetation Science*, 3(2):157–164.

King, A. T., Tinoco, R. O., and Cowen, E. A. (2012). A k-ϵ turbulence model based on the scales of vertical shear and stem wakes valid for emergent and submerged vegetated flows. *Journal of Fluid Mechanics*, 701:1–39.

Kleypas, J. A., Buddemeier, R. W., Archer, D., Gattuso, J. P., Langdon, C., and Opdyke, B. N. (1999). Geochemical consequences of increased atmospheric carbon dioxide on coral reefs. *Science*, 284(5411):118–120.

Kleypas, J. A., Buddemeier, R. W., and Gattuso, J. P. (2001). The future of coral reefs in an age of global change. *International Journal of Earth Sciences*, 90(2):426–437.

Kleypas, J. A., Danabasoglu, G., and Lough, J. M. (2008). Potential role of the ocean thermostat in determining regional differences in coral reef bleaching events. *Geophysical Research Letters*, 35(3):3613.

Kleypas, J. A. and Eakin, C. M. (2007). Scientists' perceptions of threats to coral reefs: Results of a survey of coral reef researchers. *Bulletin of Marine Science*, 80(2):419–436.

Knowlton, N., Lang, J. C., Christine Rooney, M., and Clifford, P. (1981). Evidence for delayed mortality in hurricane-damaged Jamaican staghorn corals. *Nature*, 294:251–252.

Koehl, M. A. and Hadfield, M. G. (2010). Hydrodynamics of larval settlement from a larva's point of view. *Integrative and Comparative Biology*, 50(4):539–551.

Kratzer, S., Håkansson, B., and Sahlin, C. (2003). Assessing Secchi and photic zone depth in the Baltic Sea from satellite data. *Ambio*, 32(8):577–585.

Kruszyński, K. J., Kaandorp, J. A., and Van Liere, R. (2007). A computational method for quantifying morphological variation in scleractinian corals. *Coral Reefs*, 26(4):831–840.

Kuffner, I. B. (2002). Effects of ultraviolet radiation and water motion on the reef coral, Porites compressa Dana: A transplantation experiment. *Journal of Experimental Marine Biology and Ecology*, 270(2):147–169.

Landuyt, D., Broekx, S., D'hondt, R., Engelen, G., Aertsens, J., and Goethals, P. L. (2013). A review of Bayesian belief networks in ecosystem service modelling. *Environmental Modelling and Software*, 46:1–11.

Langdon, C. and Atkinson, M. J. (2005). Effect of elevated pCO2 on photosynthesis and calcification of corals and

interactions with seasonal change in temperature/ irradiance and nutrient enrichment. *Journal of Geophysical Research C: Oceans*, 110(9):1–16.

Langdon, C., Takahashi, T., Sweeney, C., Chipman, D., Goddard, J., Marubini, F., Aceves, H., Barnett, H., and Atkinson, M. J. (2000). Effect of calcium carbonate saturation state on the calcification rate of an experimental coral reef. *Global Biogeochemical Cycles*, 14(2):639–654.

Lantz, C. A., Schulz, K. G., and Eyre, B. D. (2019). The effect of warming and benthic community acclimation on coral reef carbonate sediment metabolism and dissolution. *Coral Reefs*, 38(1):149–163.

Largier, J. L. (2003). Considerations in estimating larval dispersal distances from oceanographic data. *Ecological Applications*, 13(1 SUPPL.):71–89.

Larsen, T. C., Browne, N. K., Erichsen, A. C., Tun, K., and Todd, P. A. (2017). Modelling for management: Coral photo-physiology and growth potential under varying turbidity regimes. *Ecological Modelling*, 362:1–12.

Lavorel, S., McIntyre, S., Landsberg, J., and Forbes, T. D. (1997). Plant functional classifications: From general groups to specific groups based on response to disturbance. *Trends in Ecology and Evolution*, 12(12):474–478.

Lenihan, H. S. and Edmunds, P. J. (2010). Response of Pocillopora verrucosa to corallivory varies with environmental conditions. *Marine Ecology Progress Series*, 409:51–63.

Lenihan, H. S., Hench, J. L., Holbrook, S. J., Schmitt, R. J., and Potoski, M. (2015). Hydrodynamics influence coral performance through simultaneous direct and indirect effects. *Ecology*, 96(6):1540–1549.

Lesser, G. R., Roelvink, J. A., van Kester, J. A., and Stelling, G. S. (2004). Development and validation of a three-dimensional morphological model. *Coastal Engineering*, 51(8-9):883–915.

Lesser, M. P. (1997). Oxidative stress causes coral bleaching during exposure to elevated temperatures. *Coral Reefs*, 16(3):187–192.

Lesser, M. P. (2006). Oxidative stress in marine environments: Biochemistry and physiological ecology. *Annual Review of Physiology*, 68(1):253–278.

Lesser, M. P. (2011). Coral bleaching: Causes and mechanisms. In *Coral Reefs: An Ecosystem in Transition*, pages 405–419. Springer Netherlands, Dordrecht.

Lesser, M. P., Slattery, M., and Leichter, J. J. (2009). Ecology of mesophotic coral reefs. *Journal of Experimental Marine Biology and Ecology*, 375(1-2):1–8.

Lesser, M. P., Weis, V. M., Patterson, M. R., and Jokiel, P. L. (1994). Effects of morphology and water motion on carbon delivery and productivity in the reef coral, Pocillopora damicornis (Linnaeus): Diffusion barriers, inorganic carbon limitation, and biochemical plasticity. *Journal of Experimental Marine Biology and Ecology*, 178(2):153–179.

Li, L., Storms, J. E., and Walstra, D. J. (2018). On the upscaling of process-based models in deltaic applications. *Geomorphology*, 304:201–213.

Lincke, D. and Hinkel, J. (2018). Economically robust protection against 21st century sea-level rise. *Global Environmental Change*, 51:67–73.

Lirman, D. (2000). Fragmentation in the branching coral Acropora palmata (Lamarck): Growth, survivorship, and reproduction of colonies and fragments. *Journal of Experimental Marine Biology and Ecology*, 251(1):41–57.

Liu, G., Strong, A. E., and Skirving, W. (2003). Remote sensing of sea surface temperatures during 2002 barrier reef coral bleaching. *Eos*, 84(15):2002–2004.

Logan, C. A., Dunne, J. P., Eakin, C. M., and Donner, S. D. (2014). Incorporating adaptive responses into future projections of coral bleaching. *Global Change Biology*, 20(1):125–139.

Longuet-Higgins, M. S. and Stewart, R. w. (1964). Radiation stresses in water waves: A physical discussion, with applications. *Deep-Sea Research and Oceanographic Abstracts*, 11(4):529–562.

Lough, J. M. (2008). Coral calcification from skeletal records revisited. *Marine Ecology Progress Series*, 373:257–264.

Lough, J. M. and Barnes, D. J. (1997). Several centuries of variation in skeletal extension, density and calcification in massive Porites colonies from the Great Barrier Reef: A proxy for seawater temperature and a background of variability against which to identify unnatural change. *Journal of Experimental Marine Biology and Ecology*, 211(1):29–67.

Lough, J. M. and Barnes, D. J. (2000). Environmental controls on growth of the massive coral Porites. *Journal of Experimental Marine Biology and Ecology*, 245(2):225–243.

Lough, J. M., Barnes, D. J., Devereux, M. J., Tobin, B. J., and Tobin, S. (1999). Variability in growth characteristics of massive Porites on the Great Barrier Reef. Technical Report No. 28, CRC Reef Research Centre, Townsville.

Lough, J. M., Cantin, N. E., Benthuysen, J. A., and Cooper, T. F. (2016). Environmental drivers of growth in massive Porites corals over 16 degrees of latitude along Australia's northwest shelf. *Limnology and Oceanography*, 61(2):684–700.

Lowe, R. J. and Falter, J. L. (2015). Oceanic forcing of coral reefs. *Annual Review of Marine Science*, 7(1):43–66.

Lowe, R. J., Falter, J. L., Koseff, J. R., Monismith, S. G., and Atkinson, M. J. (2007). Spectral wave flow attenuation within submerged canopies: Implications for wave energy dissipation. *Journal of Geophysical Research: Oceans*, 112(5):5018.

Lowe, R. J., Falter, J. L., Monismith, S. G., and Atkinson, M. J. (2009). Wave-driven circulation of a coastal reef-lagoon system. *Journal of Physical Oceanography*, 39(4):873–893.

Lowe, R. J., Koseff, J. R., and Monismith, S. G. (2005a). Oscillatory flow through submerged canopies: 1. Velocity structure. *Journal of Geophysical Research: Oceans*, 110:C10016.

Lowe, R. J., Koseff, J. R., Monismith, S. G., and Falter, J. L. (2005b). Oscillatory flow through submerged canopies: 2. Canopy mass transfer. *Journal of Geophysical Research: Oceans*, 110:C10017.

Lowe, R. J., Shavit, U., Falter, J. L., Koseff, J. R., and Monismith, S. G. (2008). Modeling flow in coral communities with and without waves: A synthesis of porous media and canopy flow approaches. *Limnology and Oceanography*, 53(6):2668–2680.

Lugo-Fernández, A. and Roberts, H. H. (2011). Reef Front Wave Energy. In Hopley, D., editor, *Encyclopedia of Modern Coral Reefs: Structure, Form and Process*, pages 876–881. Springer Netherlands, Dordrecht, the Netherlands.

Luhar, M., Coutu, S., Infantes, E., Fox, S., and Nepf, H. (2010). Wave-induced velocities inside a model seagrass bed. *Journal of Geophysical Research: Oceans*, 115(12):1–15.

Luijendijk, A., Schipper, M., and Ranasinghe, R. (2019). Morphodynamic acceleration techniques for multi-timescale predictions of complex sandy interventions. *Journal of Marine Science and Engineering*, 7(3):78.

Luijendijk, A. P., Ranasinghe, R., de Schipper, M. A., Huisman, B. A., Swinkels, C. M., Walstra, D. J., and Stive, M. J. (2017). The initial morphological response of the Sand Engine: A process-based modelling study. *Coastal Engineering*, 119:1–14.

Macintyre, I. G. and Marshall, J. F. (1988). Submarine lithification in coral reefs: Some facts and misconceptions. In *Proceedings of the 6th International Coral Reef Symposium*, volume 1, pages 263–272.

Madin, J. S. (2004). *A mechanistic approach to understanding and predicting hydrodynamic disturbance on coral reefs*. Phd, James Cook University.

Madin, J. S. (2005). Mechanical limitations of reef corals during hydrodynamic disturbances. *Coral Reefs*, 24(4):630–635.

Madin, J. S. and Connolly, S. R. (2006). Ecological consequences of major hydrodynamic disturbances on coral reefs. *Nature*, 444(7118):477–480.

Madin, J. S., Dell, A. I., Madin, E. M. P., and Nash, M. C. (2013). Spatial variation in mechanical properties of coral reef substrate and implications for coral colony integrity. *Coral Reefs*, 32(1):173–179.

Madin, J. S., Hoogenboom, M. O., Connolly, S. R., Darling, E. S., Falster, D. S., Huang, D., Keith, S. A., Mizerek, T., Pandolfi, J. M., Putnam, H. M., and Baird, A. H. (2016). A trait-based approach to advance coral reef science. *Trends in Ecology and Evolution*, 31(6):419–428.

Madin, J. S., O'Donnell, M. J., and Connolly, S. R. (2008). Climate-mediated mechanical changes to post-disturbance coral assemblages. *Biology Letters*, 4(5):490–493.

Maher, R. L., Johnston, M. A., Brandt, M. E., Smith, T. B., and Correa, A. M. (2018). Depth and coral cover drive the distribution of a coral macroborer across two reef systems. *PLoS ONE*, 13(6):e0199462.

Mangubhai, S. and Harrison, P. L. (2008). Asynchronous coral spawning patterns on equatorial reefs in Kenya. *Marine Ecology Progress Series*, 360:85–96.

Manzello, D. P., Kleypas, J. A., Budd, D. A., Eakin, C. M., Glynn, P. W., and Langdon, C. (2008). Poorly cemented coral reefs of the eastern tropical Pacific: Possible insights into reef development in a high-CO2 world. *Proceedings of the National Academy of Sciences of the United States of America*, 105(30):10450–10455.

Marks, K. W. (2007). AGRRA Database, version (10/2007).

Marshall, A. T. and Clode, P. (2004). Calcification rate and the effect of temperature in a zooxanthellate and an azooxanthellate scleractinian reef coral. *Coral Reefs*, 23(2):218–224.

Marshall, J. F. (1985). Cross-shelf and facies related variations in submarine cementation in the Central Great Barrier Reef. In *Proceedings of the 5th International Coral Reef Congress*, volume 3, pages 221–226, Tahiti.

Marshall, P. A. (2000). Skeletal damage in reef corals: Relating resistance to colony morphology. *Marine Ecology Progress Series*, 200:177–189.

Marshall, P. A. and Baird, A. H. (2000). Bleaching of corals on the Great Barrier Reef: Differential susceptibilities among taxa. *Coral Reefs*, 19(2):155–163.

Marubini, F., Barnett, H., Langdon, C., and Atkinson, M. J. (2001). Dependence of calcification on light and carbonate ion concentration for the hermatypic coral Porites compressa. *Marine Ecology Progress Series*, 220:153–162.

Marubini, F., Ferrier-Pagès, C., Furla, P., and Allemand, D. (2008). Coral calcification responds to seawater acidification: A working hypothesis towards a physiological mechanism. *Coral Reefs*, 27(3):491–499.

Mass, T., Einbinder, S., Brokovich, E., Shashar, N., Vago, R., Erez, J., and Dubinsky, Z. (2007). Photoacclimation of Stylophora pistillata to light extremes: Metabolism and calcification. *Marine Ecology Progress Series*, 334:93–102.

Mass, T., Genin, A., Shavit, U., Grinstein, M., and Tchernov, D. (2010). Flow enhances photosynthesis in marine benthic autotrophs by increasing the efflux of oxygen from the organism to the water. *Proceedings of the National Academy of Sciences*, 107(6):2527–2531.

Massel, S. R. and Done, T. J. (1993). Effects of cyclone waves on massive coral assemblages on the Great Barrier Reef: Meteorology, hydrodynamics and demography. *Coral Reefs*, 12(3-4):153–166.

Maxwell, W. G. H. (1968). *Atlas of the Great Barrier Reef*. Elsevier, Amsterdam.

Maynard, J. A., Anthony, K. R. N., Marshall, P. A., and Masiri, I. (2008). Major bleaching events can lead to increased thermal tolerance in corals. *Marine Biology*, 155(2):173–182.

McClanahan, T. R. (2017). Changes in coral sensitivity to thermal anomalies. *Marine Ecology Progress Series*, 570:71–85.

McClanahan, T. R., Ateweberhan, M., Muhando, C. A., Maina, J., and Mohammed, M. S. (2007). Effects of climate and seawater temperature variation on coral bleaching and mortality. *Ecological Monographs*, 77(4):503–525.

McConnaughey, T. A. and Whelan, J. F. (1997). Calcification generates protons for nutrient and bicarbonate uptake. *Earth-Science Reviews*, 42(1-2):95–117.

McDonald, C. B., Koseff, J. R., and Monismith, S. G. (2006). Effects of the depth to coral height ratio on drag coefficients for unidirectional flow over coral. *Limnology and Oceanography*, 51(3):1294–1301.

Merritt, D. M., Scott, M. L., Leroy Poff, N., Auble, G. T., and Lytle, D. A. (2010). Theory, methods and tools for determining environmental flows for riparian vegetation: Riparian vegetation-flow response guilds. *Freshwater Biology*, 55(1):206–225.

Middlebrook, R., Hoegh-Guldberg, O., and Leggat, W. (2008). The effect of thermal history on the susceptibility of reef-building corals to thermal stress. *Journal of Experimental Biology*, 211(7):1050–1056.

Miller, K. and Mundy, C. (2003). Rapid settlement in broadcast spawning corals: Implications for larval dispersal. *Coral Reefs*, 22(2):99–106.

Millero, F. J. (1982). The thermodynamics of seawater at one atmosphere. *Ocean Science and Engineering*, 7:403–460.

Millero, F. J. (1995). Thermodynamics of the carbon dioxide system in the oceans. *Geochimica et Cosmochimica Acta*, 59(4):661–677.

Moberg, F. and Folke, C. (1999). Ecological goods and services of coral reef ecosystems. *Ecological Economics*, 29(2):215–233.

Moe, S. J., Haande, S., and Couture, R. M. (2016). Climate change, cyanobacteria blooms and ecological status of lakes: A Bayesian network approach. *Ecological Modelling*, 337:330–347.

Monismith, S. G. (2007). Hydrodynamics of coral reefs. *Annual Review of Fluid Mechanics*, 39(1):37–55.

Monismith, S. G., Genin, A., Reidenbach, M. A., Yahel, G., and Koseff, J. R. (2006). Thermally driven exchanges between a coral reef and the adjoining ocean. *Journal of Physical Oceanography*, 36(7):1332–1347.

Monismith, S. G., Rogers, J. S., Koweek, D., and Dunbar, R. B. (2015). Frictional wave dissipation on a remarkably rough reef. *Geophysical Research Letters*, 42(10):4063–4071.

Moya, A., Tambutté, S., Tambutté, É., Zoccola, D., Caminiti, N., and Allemand, D. (2006). Study of calcification during a daily cycle of the coral Stylophora pistillata: Implications for 'light-enhanced calcification'. *Journal of Experimental Biology*, 209(17):3413–3419.

Mucci, A. (1983). The solubility of calcite and aragonite in seawater at various salinities, temperatures, and one atmosphere total pressure. *American Journal of Science*, 283(7):780–799.

Muko, S., Kawasaki, K., Sakai, K., Takasu, F., and Shigesada, N. (2000). Morphological plasticity in the coral Porites sillimaniani and its adaptive significance. *Bulletin of Marine Science*, 66(1):225–239.

Murphy, E., Ghisalberti, M., and Nepf, H. (2007). Model and laboratory study of dispersion in flows with submerged vegetation. *Water Resources Research*, 43(5):1–12.

Nakamura, T., van Woesik, R., and Yamasaki, H. (2005). Photoinhibition of photosynthesis is reduced by water flow in the reef-building coral Acropora digitifera. *Marine Ecology Progress Series*, 301:109–118.

NASA Goddard Space Flight Center Ocean Biology Processing Group (2018). Moderate-resolution Imaging Spectroradiometer (MODIS) Aqua Downwelling Diffuse Attenuation Coefficient Data; 2018 Reprocessing.

Nelson, R. C. (1996). Hydraulic roughness of coral reef platforms. *Applied Ocean Research*, 18(5):265–274.

Nepf, H. M. (2012). Flow and transport in regions with aquatic vegetation. *Annual Review of Fluid Mechanics*, 44(1):123–142.

Nepf, H. M. and Vivoni, E. R. (2000). Flow structure in depth-limited, vegetated flow. *Journal of Geophysical Research: Oceans*, 105(C12):28547–28557.

Nicholls, R. J., Marinova, N., Lowe, J. A., Brown, S., Vellinga, P., De Gusmão, D., Hinkel, J., and Tol, R. S. (2011). Sea-level rise and its possible impacts

given a 'beyond 4 oC world' in the twenty-first century. *Philosophical Transactions of the Royal Society A: Mathematical, Physical and Engineering Sciences*, 369(1934):161–181.

Nielsen, D. A., Petrou, K., and Gates, R. D. (2018). Coral bleaching from a single cell perspective. *ISME Journal*, 12(6):1558–1567.

Nikora, N., Nikora, V., and O'Donoghue, T. (2013). Velocity profiles in vegetated open-channel flows: Combined effects of multiple mechanisms. *Journal of Hydraulic Engineering*, 139(10):1021–1032.

Nikora, V., McEwan, I., McLean, S., Coleman, S., Pokrajac, D., and Walters, R. (2007a). Double-averaging concept for rough-bed open-channel and overland flows: Theoretical background. *Journal of Hydraulic Engineering*, 133(8):873–883.

Nikora, V., Pokrajac, D., McEwan, I., Campbell, L., McLea, S., Coleman, S., Clunie, D., Aberle, J., and Koll, K. (2007b). Double-averaging concept for rough-bed open-channel and overland flows: Applications. *Journal of Hydraulic Engineering*, 133(8):884–895.

Nozawa, Y. and Harrison, P. L. (2008). Temporal patterns of larval settlement and survivorship of two broadcast-spawning acroporid corals. *Marine Biology*, 155(3):347–351.

Ohde, S. and Hossain, M. M. M. (2004). Effect of CaCO3 (aragonite) saturation state of seawater on calcification of Porites coral. *Geochemical Journal*, 38(6):613–621.

Oliver, T. A. and Palumbi, S. R. (2011). Do fluctuating temperature environments elevate coral thermal tolerance? *Coral Reefs*, 30(2):429–440.

Osinga, R., Derksen-Hooijberg, M., Wijgerde, T., and Verreth, J. A. J. (2017). Interactive effects of oxygen, carbon dioxide and flow on photosynthesis and respiration in the scleractinian coral Galaxea fascicularis. *The Journal of Experimental Biology*, 220(12):2236–2242.

Osorio-Cano, J. D., Osorio, A. F., Alcérreca-Huerta, J. C., and Oumeraci, H. (2019). Drag and inertia forces on a branched coral colony of Acropora palmata. *Journal of Fluids and Structures*, 88:31–47.

Ow, Y. X. and Todd, P. A. (2010). Light-induced morphological plasticity in the scleractinian coral Goniastrea pectinata and its functional significance. *Coral Reefs*, 29(3):797–808.

Palumbi, S. R., Barshis, D. J., Traylor-Knowles, N., and Bay, R. A. (2014). Mechanisms of reef coral resistance to future climate change. *Science*, 344(6186):895–898.

Pavlov, A. K., Granskog, M. A., Stedmon, C. A., Ivanov, B. V., Hudson, S. R., and Falk-Petersen, S. (2015). Contrasting optical properties of surface waters across the Fram Strait and its potential biological implications. *Journal of Marine Systems*, 143:62–72.

Perry, C. T. and Hepburn, L. J. (2008). Syn-depositional alteration of coral reef framework through bioerosion, encrustation and cementation: Taphonomic signatures of reef accretion and reef depositional events. *Earth-Science Reviews*, 86(1-4):106–144.

Perry, C. T., Smithers, S. G., Gulliver, P., and Browne, N. K. (2012). Evidence of very rapid reef accretion and reef growth under high turbidity and terrigenous sedimentation. *Geology*, 40(8):719–722.

Platt, T., Denman, K. L., and Jassby, A. D. (1975). The mathematical representation and prediction of phytoplankton productivity. Technical report, Research and Development Directorate Marine Ecology Laboratory Bedford Institute of Oceanography, Dartmouth, Nova Scotia.

Poff, N. L. R., Olden, J. D., Vieira, N. K., Finn, D. S., Simmons, M. P., and Kondratieff, B. C. (2006). Functional trait niches of North American lotic insects: Traits-based ecological applications in light of phylogenetic relationships. *Journal of the North American Benthological Society*, 25(4):730–755.

Poole, H. H. and Atkins, W. R. G. (1929). Photoelectric measurements of submarine illumination throughout the year. *Journal of the Marine Biological Association of the United Kingdom*, 16(1):297–324.

Pratchett, M. S., Anderson, K. D., Hoogenboom, M. O., Widman, E., Baird, A. H., Pandolfi, J. M., Edmunds, P. J., and Lough, J. M. (2015). Spatial, temporal and taxonomic variation in coral growth-implications for the structure and function of coral reef ecosystems. *Oceanography and Marine Biology: An Annual Review*, 53:215–295.

Principe, P. P., Bradley, P., Yee, S., Fisher, W., Johnson, E., Allen, P., and Campbell, D. (2012). Quantifying Coral Reef Ecosystem Services. Technical report, U.S. Environmental Protection Agency.

Puisay, A., Pilon, R., Goiran, C., and Hédouin, L. (2018). Thermal resistances and acclimation potential during coral larval ontogeny in Acropora pulchra. *Marine Environmental Research*, 135:1–10.

Ranasinghe, R., Swinkels, C., Luijendijk, A., Roelvink, D., Bosboom, J., Stive, M., and Walstra, D. J. (2011). Morphodynamic upscaling with the MORFAC approach: Dependencies and sensitivities. *Coastal Engineering*, 58(8):806–811.

Rasser, M. W. and Riegl, B. (2002). Holocene coral reef rubble and its binding agents. *Coral Reefs*, 21(1):57–72.

Rehman, A. U., Szabó, M., Deák, Z., Sass, L., Larkum, A., Ralph, P., and Vass, I. (2016). Symbiodinium sp. cells produce light-induced intra- and extracellular singlet oxygen, which mediates photodamage of the photosynthetic apparatus and has the potential to interact with the animal host in coral symbiosis. *The New phytologist*, 212(2):472–484.

Reidenbach, M. A., Koseff, J. R., Monismith, S. G., and Steinbuck, J. V. (2006a). The effects of waves and mor-

phology on mass transfer within branched reef corals. *Limnology and Oceanography*, 51(2):1134–1141.

Reidenbach, M. A., Monismith, S. G., Koseff, J. R., Yahel, G., and Genin, A. (2006b). Boundary layer turbulence and flow structure over a fringing coral reef. *Limnology and Oceanography*, 51(5):1956–1968.

Reshef, L., Koren, O., Loya, Y., Zilber-Rosenberg, I., and Rosenberg, E. (2006). The coral probiotic hypothesis. *Environmental Microbiology*, 8(12):2068–2073.

Reynolds, R. W., Smith, T. M., Liu, C., Chelton, D. B., Casey, K. S., and Schlax, M. G. (2007). Daily high-resolution-blended analyses for sea surface temperature. *Journal of Climate*, 20(22):5473–5496.

Rico-Esenaro, S. D., Sanchez-Cabeza, J. A., Carricart-Ganivet, J. P., Montagna, P., and Ruiz-Fernández, A. C. (2019). Uncertainty and variability of extension rate, density and calcification rate of a hermatypic coral (Orbicella faveolata). *Science of the Total Environment*, 650:1576–1581.

Riegl, B. M. and Purkis, S. J. (2009). Model of coral population response to accelerated bleaching and mass mortality in a changing climate. *Ecological Modelling*, 220(2):192–208.

Ries, J. B., Cohen, A. L., and McCorkle, D. C. (2010). A nonlinear calcification response to CO2-induced ocean acidification by the coral Oculina arbuscula. *Coral Reefs*, 29(3):661–674.

Rodolfo-Metalpa, R., Huot, Y., and Ferrier-Pagès, C. (2008). Photosynthetic response of the Mediterranean zooxanthellate coral Cladocora caespitosa to the natural range of light and temperature. *Journal of Experimental Biology*, 211(10):1579–1586.

Rodrigues, L. J. and Grottoli, A. G. (2006). Calcification rate and the stable carbon, oxygen, and nitrogen isotopes in the skeleton, host tissue, and zooxanthellae of bleached and recovering Hawaiian corals. *Geochimica et Cosmochimica Acta*, 70(11):2781–2789.

Roelvink, J. A. (2006). Coastal morphodynamic evolution techniques. *Coastal Engineering*, 53(2-3):277–287.

Rogers, J. S., Monismith, S. G., Koweek, D. A., and Dunbar, R. B. (2016). Wave dynamics of a Pacific Atoll with high frictional effects. *Journal of Geophysical Research: Oceans*, 121:350–367.

Roth, L., Muller, E. M., and Van Woesik, R. (2013). Tracking Acropora fragmentation and population structure through thermal-stress events. *Ecological Modelling*, 263:223–232.

Roy, R. N., Roy, L. N., Vogel, K. M., Porter-Moore, C., Pearson, T., Good, C. E., Millero, F. J., and Campbell, D. M. (1993). The dissociation constants of carbonic acid in seawater at salinities 5 to 45 and temperatures 0 to 45 oC. *Marine Chemistry*, 44(2-4):249–267.

Sanders, D. and Baron-Szabo, R. C. (2005). Scleractinian assemblages under sediment input: Their characteristics and relation to the nutrient input concept. *Palaeogeography, Palaeoclimatology, Palaeoecology*, 216(1-2):139–181.

Santodomingo, N., Renema, W., and Johnson, K. G. (2016). Understanding the murky history of the Coral Triangle: Miocene corals and reef habitats in East Kalimantan (Indonesia). *Coral Reefs*, 35(3):765–781.

Saulquin, B., Hamdi, A., Gohin, F., Populus, J., Mangin, A., and D'Andon, O. F. (2013). Estimation of the diffuse attenuation coefficient KdPAR using MERIS and application to seabed habitat mapping. *Remote Sensing of Environment*, 128:224–233.

Scheffer, M., Carpenter, S., Foley, J. A., Folke, C., and Walker, B. (2001). Catastrophic shifts in ecosystems. *Nature*, 413(6856):591–596.

Schneider, K. and Erez, J. (2006a). The effect of carbonate chemistry on calcification and photosynthesis in the hermatypic coral Acropora eurystoma. *Limnology and Oceanography*, 51(3):1284–1293.

Schneider, K. and Erez, J. (2006b). The effect of carbonate chemistry on calcification and photosynthesis in the hermatypic coral Acropora eurystoma. *Limnology and Oceanography*, 51(3):1284–1293.

Schuhmacher, H. and Plewka, M. (1981). Mechanical resistance of reefbuilders through time. *Oecologia*, 49:279–282.

Schutter, M., Kranenbarg, S., Wijffels, R. H., Verreth, J., and Osinga, R. (2011). Modification of light utilization for skeletal growth by water flow in the scleractinian coral Galaxea fascicularis. *Marine Biology*, 158(4):769–777.

Scoffin, T. P., Tudhope, A. W., Brown, B. E., Chansang, H., and Cheeney, R. F. (1992). Patterns and possible environmental controls of skeletogenesis of Porites lutea, South Thailand. *Coral Reefs*, 11(1):1–11.

Shamberger, K. E., Feely, R. A., Sabine, C. L., Atkinson, M. J., DeCarlo, E. H., Mackenzie, F. T., Drupp, P. S., and Butterfield, D. A. (2011). Calcification and organic production on a Hawaiian coral reef. *Marine Chemistry*, 127(1-4):64–75.

Shapiro, O. H., Fernandez, V. I., Garren, M., Guasto, J. S., Debaillon-Vesque, F. P., Kramarsky-Winter, E., Vardi, A., and Stocker, R. (2014). Vortical ciliary flows actively enhance mass transport in reef corals. *Proceedings of the National Academy of Sciences*, 111(37):13391–13396.

Shipley, B., Keddy, P. A., Moore, D. R. J., and Lemky, K. (1989). Regeneration and establishment strategies of emergent macrophytes. *The Journal of Ecology*, 77(4):1093.

Siebeck, U. E., Marshall, N. J., Klüter, A., and Hoegh-Guldberg, O. (2006). Monitoring coral bleaching using a colour reference card. *Coral Reefs*, 25(3):453–460.

Siegel, D. A., Mitarai, S., Costello, C. J., Gaines, S. D., Kendall, B. E., Warner, R. R., and Winters, K. B. (2008). The stochastic nature of larval connectivity among nearshore marine populations. *Proceedings of the National Academy of Sciences of the United States of America*, 105(26):8974–8979.

Silbiger, N. J., Goodbody-Gringley, G., Bruno, J. F., and Putnam, H. M. (2019). Comparative thermal performance of Orbicella franksi at its latitudinal range limits. *Marine Biology*, 166:126.

Silverman, J., Lazar, B., Cao, L., Caldeira, K., and Erez, J. (2009). Coral reefs may start dissolving when atmospheric CO2 doubles. *Geophysical Research Letters*, 36(5):L05606.

Silverman, J., Lazar, B., and Erez, J. (2007). Effect of aragonite saturation, temperature, and nutrients on the community calcification rate of a coral reef. *Journal of Geophysical Research: Oceans*, 112(5):C05004.

Smagorinsky, J. (1963). General circulation experiments with the primitive equations. *Monthly Weather Review*, 91(3):99–164.

Smith, C. L., Hill, A. E., Foreman, M. G., and Peña, M. A. (2001). Horizontal transport of marine organisms resulting from interactions between diel vertical migration and tidal currents off the west coast of Vancouver Island. *Canadian Journal of Fisheries and Aquatic Sciences*, 58(4):736–748.

Smith, L. D. and Hughes, T. P. (1999). An experimental assessment of survival, re-attachment and fecundity of coral fragments. *Journal of Experimental Marine Biology and Ecology*, 235:147–164.

Smithers, S. (2011). Fringing Reefs. In Hopley, D., editor, *Encyclopedia of Modern Coral Reefs: Structure, Form and Process*, pages 430–446. Springer Netherlands, Dordrecht, the Netherlands.

Solihuddin, T., Collins, L. B., Blakeway, D., and O'Leary, M. J. (2015). Holocene coral reef growth and sea level in a macrotidal, high turbidity setting: Cockatoo Island, Kimberley Bioregion, northwest Australia. *Marine Geology*, 359:50–60.

Southwood, T. R. E. (1977). Habitat, the templet for ecological strategies? *The Journal of Animal Ecology*, 46(2):336.

Spalding, M. D., Ravilious, C., and Green, E. P. (2001). *World atlas of coral reefs. Prepared at the UNEP World Conservation Monitoring Centre*. University of California Press, London, England.

Spencer, T. and Viles, H. (2002). Bioconstruction, bioerosion and disturbance on tropical coasts: Coral reefs and rocky limestone shores. *Geomorphology*, 48(1-3):23–50.

Stafford-Smith, M. G. and Ormond, R. F. (1992). Sediment-rejection mechanisms of 42 species of Australian scleractinian corals. *Marine and Freshwater Research*, 43(4):683–705.

Stambler, N. and Dubinsky, Z. (2005). Corals as light collectors: An integrating sphere approach. *Coral Reefs*, 24(1):1–9.

Stoddart, D. R. (1969). Ecology and morphology of recent coral reefs. *Biological Reviews*, 44(4):433–498.

Storlazzi, C. D., Norris, B. K., and Rosenberger, K. J. (2015). The influence of grain size, grain color, and suspended-sediment concentration on light attenuation: Why fine-grained terrestrial sediment is bad for coral reef ecosystems. *Coral Reefs*, 34(3):967–975.

Strahl, J., Rocker, M. M., and Fabricius, K. E. (2019). Contrasting responses of the coral Acropora tenuis to moderate and strong light limitation in coastal waters. *Marine Environmental Research*, 147:80–89.

Strahl, J., Stolz, I., Uthicke, S., Vogel, N., Noonan, S. H., and Fabricius, K. E. (2015). Physiological and ecological performance differs in four coral taxa at a volcanic carbon dioxide seep. *Comparative Biochemistry and Physiology -Part A : Molecular and Integrative Physiology*, 184:179–186.

Swart, D. H. (1974). *Offshore sediment transport and equilibrium beach profiles*. Phd, Delft University of Technology.

Tay, Y. C., Guest, J. R., Chou, L. M., and Todd, P. A. (2011). Vertical distribution and settlement competencies in broadcast spawning coral larvae: Implications for dispersal models. *Journal of Experimental Marine Biology and Ecology*, 409(1-2):324–330.

Tilman, D., Knops, J., Wedin, D., Reich, P., Ritchie, M., and Siemann, E. (1997). The influence of functional diversity and composition on ecosystem processes. *Science*, 277(5330):1300–1302.

Titlyanov, E. A. and Titlyanova, T. V. (2002). Reef-building corals - Symbiotic autotrophic organisms: 2. Pathways and mechanisms of adaptation to light. *Russian Journal of Marine Biology*, 28(Suppl. 1):S16–S31.

Todd, P. A. (2008). Morphological plasticity in scleractinian corals. *Biological Reviews*, 83(3):315–337.

Tortolero-Langarica, J. J., Rodríguez-Troncoso, A. P., Carricart-Ganivet, J. P., and Cupul-Magaña, A. L. (2016). Skeletal extension, density and calcification rates of massive free-living coral Porites lobata Dana, 1846. *Journal of Experimental Marine Biology and Ecology*, 478:68–76.

Uijttewaal, W. S. J. (2019). Turbulence in Hydraulics.

Uusitalo, L., Lehikoinen, A., Helle, I., and Myrberg, K. (2015). An overview of methods to evaluate uncertainty of deterministic models in decision support. *Environmental Modelling and Software*, 63:24–31.

van Dongen-Vogels, V. and Mallefet, J. (2006). Fragment growth-rates of six cultivated coral species: A reference framework for coral transplantation. *Mer*, 44(3-4):99–107.

van Rooijen, A., Lowe, R., Ghisalberti, M., Conde-Frias, M., and Tan, L. (2018). Predicting current-induced drag in emergent and submerged aquatic vegetation canopies. *Frontiers in Marine Science*, 5:449.

Van Woesik, R., Houk, P., Isechal, A. L., Idechong, J. W., Victor, S., and Golbuu, Y. (2012). Climate-change refugia in the sheltered bays of Palau: Analogs of future reefs. *Ecology and Evolution*, 2(10):2474–2484.

Van Woesik, R., Lacharmoise, F., and Köksal, S. (2006). Annual cycles of solar insolation predict spawning times of Caribbean corals. *Ecology Letters*, 9(4):390–398.

Vásquez-Bedoya, L. F., Cohen, A. L., Oppo, D. W., and Blanchon, P. (2012). Corals record persistent multidecadal SST variability in the Atlantic Warm Pool since 1775 AD. *Paleoceanography*, 27(3):PA3231.

Vermeij, M. J. and Bak, R. P. (2002). How are coral populations structured by light? Marine light regimes and the distribution of Madracis. *Marine Ecology Progress Series*, 233:105–116.

Veron, J. E. (2011). Corals: Biology, skeletal deposition, and reef-building. In Hopley, D., editor, *Encyclopedia of Modern Coral Reefs: Structure, Form and Process*, pages 275–281. Springer Netherlands, Dordrecht, the Netherlands.

Viehman, S., Gittings, S., Groves, S., Moore, J., Moore, T., and Stein, J. (2018). NCCOS Assessment: Coral Disturbance Response Monitoring (DRM) along the Florida Reef Tract following Hurricane Irma from 2017-10-09 to 2017-10-18 (NCEI Accession 0179071). Coral demographics. Technical report, NOAA National Centers for Environmental Information.

Vize, P. D. (2006). Deepwater broadcast spawning by Montastraea cavernosa, Montastraea franksi, and Diploria strigosa at the Flower Garden Banks, Gulf of Mexico. *Coral Reefs*, 25(1):169–171.

von Arx, W. S. (1948). The circulation systems of Bikini and Rongelap lagoons. *Eos, Transactions American Geophysical Union*, 29(6):861–870.

Vreman, B., Geurts, B., and Kuerten, H. (1997). Large-eddy simulation of the turbulent mixing layer. *Journal of Fluid Mechanics*, 339:357–390.

Vuik, C., Vermolen, F. J., van Gijzen, M. B., and Vuik, M. J. (2015). *Numerical Methods for Ordinary Differential Equations*. Delft Academic Press, Delft, The Netherlands, 2nd edition.

Walstra, D. J., Hoekstra, R., Tonnon, P. K., and Ruessink, B. G. (2013). Input reduction for long-term morphodynamic simulations in wave-dominated coastal settings. *Coastal Engineering*, 77:57–70.

Walther, G. R., Post, E., Convey, P., Menzel, A., Parmesan, C., Beebee, T. J., Fromentin, J. M., Hoegh-Guldberg, O., and Bairlein, F. (2002). Ecological responses to recent climate change. *Nature*, 416(6879):389–395.

Weiss, R. F. (1974). Carbon dioxide in water and seawater: the solubility of a non-ideal gas. *Marine Chemistry*, 2(3):203–215.

Weitzman, J. S., Zeller, R. B., Thomas, F. I., and Koseff, J. R. (2015). The attenuation of current- and wave-driven flow within submerged multispecific vegetative canopies. *Limnology and Oceanography*, 60(6):1855–1874.

White, F. M. (2006). *Viscous Fluid Flow*. McGraw-Hill Higher Education, New York, NY, 3rd edition.

Wilkinson, C. and Souter, D. (2008). Status of Caribbean Coral Reefs after Bleaching and Hurricanes in 2005. Technical report, Global Coral Reef Monitoring Network, and Reef and Rainforest Research Centre, Townsville, Queensland, Australia.

Willis, B. L., Babcock, R. C., Harrison, P. L., Oliver, J. K., and Wallace, C. C. (1985). Patterns in the mass spawning of corals on the Great Barrier Reef from 1981 to 1984. In *Proceedings of the Fifth International Coral Reef Congress*, pages 343–348, Tahiti, French Polynesia.

Wilson, J. R. and Harrison, P. L. (1998). Settlement-competency periods of larvae of three species of scleractinian corals. *Marine Biology*, 131(2):339–345.

Woodley, J. D., Chornesky, E. A., Clifford, P. A., Jackson, J. B., Kaufman, L. S., Knowlton, N., Lang, J. C., Pearson, M. P., Porter, J. W., Rooney, M. C., Rylaarsdam, K. W., Tunnicliffe, V. J., Wahle, C. M., Wulff, J. L., Curtis, A. S., Dallmeyer, M. D., Jupp, B. P., Koehl, M. A., Neigel, J., and Sides, E. M. (1981). Hurricane Allen's impact on Jamaican coral reefs. *Science*, 214(4522):749–755.

Woodroffe, C. D. and Biribo, N. (2011). Atolls. In Hopley, D., editor, *Encyclopedia of Modern Coral Reefs: Structure, Form and Process*, pages 51–71. Springer Netherlands, Dordrecht, the Netherlands.

Woodroffe, C. D. and Webster, J. M. (2014). Coral reefs and sea-level change. *Marine Geology*, 352:248–267.

Woods, R. M., Baird, A. H., Mizerek, T. L., and Madin, J. S. (2016). Environmental factors limiting fertilisation and larval success in corals. *Coral Reefs*, 35(4):1433–1440.

Wooldridge, S. A. (2009). Water quality and coral bleaching thresholds: Formalising the linkage for the inshore reefs of the Great Barrier Reef, Australia. *Marine Pollution Bulletin*, 58(5):745–751.

Zawada, D. G. and Brock, J. C. (2009). A multiscale analysis of coral reef topographic complexity using

lidar-derived bathymetry. *Journal of Coastal Research*, SI(53):6–15.

Zawada, D. G., Piniak, G. A., and Hearn, C. J. (2010). Topographic complexity and roughness of a tropical benthic seascape. *Geophysical Research Letters*, 37:L14604.

Zawada, K. J., Dornelas, M., and Madin, J. S. (2019a). Quantifying coral morphology. *Coral Reefs*, 38(6):1281–1292.

Zawada, K. J., Madin, J. S., Baird, A. H., Bridge, T. C., and Dornelas, M. (2019b). Morphological traits can track coral reef responses to the Anthropocene. *Functional Ecology*, 33(6):962–975.

Zeebe, R. E. and Wolf-Gladrow, D. (2001). Equilibrium. In Halpern, D., editor, *CO2 in Seawater: Equilibrium, Kinetics, Isotopes*, volume 65, chapter 1, pages 1–26. Elsevier Science B.V., Amsterdam, first edition.

Zeller, R. B., Zarama, F. J., Weitzman, J. S., and Koseff, J. R. (2015). A simple and practical model for combined wave-current canopy flows. *Journal of Fluid Mechanics*, 767:842–880.

Zheng, G. and DiGiacomo, P. M. (2017). Remote sensing of chlorophyll-a in coastal waters based on the light absorption coefficient of phytoplankton. *Remote Sensing of Environment*, 201:331–341.

Glossary

Acceleration factor A factor that accommodates the gap between different time-scales by multiplying the effects of the slower process with a predefined factor. This results in a reduction of the computational time of the model in which both processes are included.

Acclimatisation The phenotypic changes in the physiology and morphology of corals due to naturally changing conditions in which the genotype does not play a role [Edmunds and Gates, 2008]. In this study, this means that the coral acclimatise to the environmental conditions as it is "getting more used to" the changed environment.

Aragonite A synonym for calcium carbonate ($CaCO_3$) often used in relation to corals (*see* Calcium carbonate).

Bicarbonate One of the main building blocks for the calcification process as well as photosynthesis in corals; denoted as HCO_3^- (*see* Dissolved inorganic carbon).

Bioerosion The breakdown of biomass (e.g. corals) in a biological manner; e.g. due to algae, fungi, bacteria and/or fish.

Biophysical model framework A model (framework) in which both biological and physical processes are combined and interact with each other. Where in biological models the physics are considered as enforced input—and vice versa—in a biophysical model, these two types of models are coupled and give feedback to each other.

Calcium carbonate The calcareous material of which hermatypic corals are made; denoted as $CaCO_3$.

Canopy-Flow Theory The Canopy-Flow Theory describes the flow within a submerged canopy relative to the flow unaffected by the canopy—higher in the water column—as a balance of (1) the horizontal pressure gradient; (2) the shear stresses; (3) the form drag; and (4) the inertial force. This theory assumes the vegetation to be represented by constraints in the moving fluid, such as cylinders [Lowe et al., 2005a, 2008].

Carbon dioxide One of the most pronounced greenhouse gasses, which is a source for photosynthesis; denoted as CO_2 (*see* Dissolved inorganic carbon).

Carbonate In chemistry often referred to as the salt of carbonic acid (H_2CO_3), and forms in combination with calcium-ions the substance for coral's skeletons, namely aragonite, or calcium carbonate ($CaCO_3$); denoted as CO_3^{2-} (*see* Dissolved inorganic carbon).

Carbonic acid An inorganic carbon, also known as *dihydrogen carbonate* or *hydrogen bicarbonate* and chemically indistinguishable from dissolved carbon dioxide (CO_2); denoted as H_2CO_3 (*see* Dissolved inorganic carbon).

Climate change Changes in climate thought of to be enhanced by human activities, such as global warming and increased concentrations of carbon dioxide in the atmosphere due to burning of fossil fuels. This study focuses on the aspects of sea-level rise (SLR), global warming, increasing storm frequency, and ocean acidification (OA) (*see* Sea-level rise, Global warming, Ocean acidification).

Colony shape factor Dimensionless number describing the morphology (i.e. shape) of the coral colony. It is an indication of how top-heavy the morphology is, and a higher value is more easily dislodged. When its value exceeds a threshold, the coral colony is dislodged. This threshold relates the strength to the forcing; the so-called dislodgement mechanical threshold (DMT) (*see* Dislodgement mechanical threshold).

Coloured dissolved organic matter The optically measurable component of dissolved organic matter is called the coloured dissolved organic matter. With organic matter, carbon-based compounds are meant that come from the remains of organisms; e.g. plants.

Coral bleaching The biochemical process of corals dying due to thermal stresses. The symbiosis between the coral and the photosynthetic organisms—i.e. the zooxanthellae—they host is disturbed during such thermal stresses. At first, the coral turns pale as it is expelling its zooxanthellae. When the thermal stresses persist, the coral moves on to a bleached state, which leads to death if the stresses remain. The name 'bleaching' comes from the fact that the coral loses its pigment when it expels the zooxanthellae; the white calcareous skeleton is exposed.

Coral dislodgement The mechanical process of corals dying due to mechanical stresses. The whole coral colony is removed at once due to hydrodynamic stresses, which are often related to a storm event. Dislodgement of the whole coral colony is often the leading mechanism of storm damage—over coral breakage—

because the coral skeleton is in general stronger than the substratum.

Coral growth acceleration factor The acceleration factor that amplifies the coral growth with respect to the hydrodynamics and physiology (*see* Acceleration factor).

D-FLOW Hydrodynamic model in which the flow is determined [Deltares, 2019a,b]. It is part of Delft3D Flexible Mesh (*see* Delft3D Flexible Mesh).

D-WAVES Hydrodynamic model in which the waves are determined, based on SWAN [Booij et al., 1999; Deltares, 2019c]. It is part of Delft3D Flexible Mesh (*see* Delft3D Flexible Mesh and SWAN).

Deep reef refugia hypothesis The hypothesis that under the face of climate change, deep reefs can function as refugia for shallow reefs. Deep reefs are defined as coral reefs between 30 metres of depth and the euphotic depth; shallow reefs are coral reefs with a depth less than 30 metres. The deep reefs are considered as possible refugia due to the reduced damage by bleaching as well as storms. [Bongaerts et al., 2010; Glynn, 1996] (*see* Euphotic depth).

Degree heating week A method in describing the onset of bleaching as used by the NOAA Coral Reef Watch program [Eakin et al., 2008; Liu et al., 2003]. One degree heating week is defined as that the temperature of the water is one week one degree Celsius higher than the maximum monthly mean; and has the unit of $°C-wk$. $2°C-wk$ means two weeks of one degree Celsius above the maximum monthly mean; or one week of two degrees Celsius above the maximum monthly mean.

Delft3D Flexible Mesh Hydrodynamic model developed by Deltares [2019a,b,c]. More details on Delft3D Flexible Mesh are presented in Appendix B.

Diffusion boundary layer The boundary layer over which the transport is solely based on diffusion due to the increased relevance of the viscosity.

Dislodgement mechanical threshold Dimensionless number on the strength (resistance) and the hydrodynamic forcing (load) on a coral colony; defined as the resistance over the load. When its value falls below a critical value, the coral colony is dislodged. This critical value is based on the shape of the coral colony; the so-called colony shape factor (CSF) (*see* Colony shape factor).

Dissolved inorganic carbon The summation of all inorganic carbon dissolved in water; thus the sum of the concentrations of carbon dioxide (CO_2), carbonic acid (H_2CO_3), bicarbonate (HCO_3^-), and carbonate (CO_3^{2-}) in water. These inorganic carbons are used as a source for photosynthesis.

Energy Flux Method Reduction of the wave climate by subdividing in representative wave cases. This subdivision is based on a predefined number of wave classes. Every wave class is defined such that they all contain the same amount of cumulative wave energy flux. The representative wave case is given as the wave height, wave period and wave direction of the mean wave energy flux per wave class (*see* Input reduction).

Energy Flux with Extreme Wave Conditions Method Reduction of the wave climate by subdividing in representative wave cases. This subdivision is based on a predefined number of wave classes. Every wave class is defined such that they all contain the same amount of cumulative wave energy, except one wave class per directional bin. This wave class contains the twelve data points within the directional bin with the highest wave energy flux and form a separate wave class. This wave class represents an *extreme wave class*. The representative wave case is given as the wave height, wave period and wave direction of the main wave energy flux per wave class. Thereby, this method highly corresponds with the Energy Flux Method (EFM), with the addition of the *extreme wave class* per directional bin (*see* Energy Flux Method, Input reduction).

Euphotic depth The depth until which the euphotic zone reaches; i.e. the borderline of the euphotic zone (*see* Euphotic zone).

Euphotic zone The zone of the water column that is exposed to sunlight, where a light-intensity of 1% relative to the surface intensity is the lower boundary; i.e. the euphotic depth. Outside the euphotic zone, photosynthesis is not profitable.

Fixed Bins Method Reduction of the wave climate by subdividing in representative wave cases. This subdivision is based on a predefined directional bin and a predefined number of bins over the wave height. The representative wave case is given as the mean wave height, wave period and wave direction per wave class (*see* Input reduction).

Genetic adaptation Evolutionary adaptation to a changing climate by changing the genetic composition via offspring [Edmunds and Gates, 2008].

Global warming Worldwide temperature rise due to higher concentrations of atmospheric carbon dioxide (CO_2) and other greenhouse gasses. Global warming affects the climate and also results in sea-level rise (*see* Climate change and Sea-level rise).

Hermatypic coral Kind of coral that deposits calcareous material to construct its skeleton, thereby forming the stony framework of a reef.

Input reduction Methods to reduce the computational time of a model by reducing the amount of input.

Light-attenuation coefficient The coefficient describing the attenuation of light when it passes the water column. The light-attenuation coefficient is mainly based on salinity, suspended particulate matter, and coloured dissolved organic matter. This factor can be determined based on two methods: (1) using a Secchi disk [Idso and Gilbert, 1974; Poole and Atkins, 1929]; or (2) using remote-sensing data [e.g. Freitas et al., 2019; Kratzer et al., 2003; Zheng and DiGiacomo, 2017].

Light-enhanced calcification Coral calcification due to the energy surplus produced by zooxanthellae via photosynthesis, which needs the energy of the light to produce the energy surpluses.

Mean sea level The average sea level when fluctuations due to wind-waves and tidal waves are averaged over time.

Model reduction Methods to reduce the computational time of a model by (1) reducing the amount of processes, scales and/or dimensions; and/or (2) simplifying the processes included in the model.

Morphological acceleration factor The acceleration factor that amplifies the morphological development with respect to the hydrodynamics (*see* Acceleration factor).

Morphology The structure and form of a living organism. Translated to the topic of this study, the morphology indicates the structure and form of the coral colony. This should not be mistaken with the commonly used term morphology in the study of morphodynamics, which indicates the structure and form of the (sand/mud) bed. In this study, the term morphology is related to the structure of the coral colony; unless explicitly stated otherwise.

Ocean acidification Acidification of the oceans due to higher concentrations of dissolved carbon dioxide (CO_2). Thereby, it results in changes in the oceanic carbon budget and thus the composition of dissolved inorganic carbon (DIC). Ocean acidification is related to the more general trend of climate change (*see* Climate change, Carbon dioxide, Dissolved inorganic carbon).

Oxidative Theory of Coral Bleaching The theory states that coral bleaching is caused by the expel of zooxanthellae due to overproduction of oxygen, and thereby reactive oxygen species as well. By expelling the zooxanthellae form the coral tissue, the source of the reactive oxygen species is removed and so the concentration of reactive oxygen species drops as well. Nevertheless, by expelling the zooxanthellae, the symbiosis is disrupted and the coral will die when these disruptive environmental conditions will remain for longer periods of time. [Lesser, 2006; Nielsen et al., 2018].

Oxygen The source of life for many, but a waste product for corals and to much can lead to toxic levels, which is commonly thought to be the driving mechanism behind bleaching; denoted as O_2 (*see:* Oxidative Theory of Coral Bleaching).

Phenotypic plasticity Changes in the phenotype of the lifetime of the coral due to changing environmental conditions [Todd, 2008]. The degree of phenotypic plasticity is species dependent [Edmunds and Gates, 2008]. Translated to this study: due to phenotypic plasticity, the coral changes its morphology over its lifetime due to the environmental conditions.

Photo-acclimatisation Acclimatisation to changing light-conditions (*see:* Acclimatisation).

Photosynthate Energy-rich product of the photosynthesis, also commonly known as sugars; often denoted as CH_2O.

Photosynthesis-irradiance curve The photosynthetic production rate as function of the incoming irradiance (i.e. light-intensity) is described as a photosynthesis-irradiance curve. This curve has the shape of a tangent-hyperbolic, giving rise to a maximum photosynthesis.

Photosynthetically active radiation The part of the solar radiation spectrum that drives the process of photosynthesis, which is given by the visible range of the light spectrum: wavelengths of $400 - 700\ nm$.

Physiology The biological processes of a living organism. Translated to the topic of this study, the physiology indicates the biological processes associated with the coral development; e.g. the photosynthesis of the zooxanthellae and the calcification of the coral animal. Note that in this study, the physiology of the coral includes both the coral animal and the photosynthetic organisms it hosts; i.e. its zooxanthellae. Thereby, with coral physiology the biological processes associated with the coral-zooxanthellae symbiont are meant.

Porous Media Theory The Porous Media Theory describes the flow within a submerged canopy relative to the flow unaffected by the canopy—higher in the water column—as a balance of (1) the horizontal pressure gradient; (2) the laminar resisting force; (3) the form drag; and (4) the inertial force. The laminar resisting force and the form drag in this theory follow the Forchheimer equation. This theory assumes the vegetation to be represented by a certain porosity [Gu and Wang, 1991; Lowe et al., 2008].

Reactive oxygen species As a by-product of photosynthesis, reactive oxygen species are produced as well. These chemicals are toxic for the cells of the zooxanthellae and reduce the photosynthesis. At low concentrations, the organism produces enough defences (e.g. superoxide dismutase) to counteract the toxicity and keep it below critical levels. When concentration get too high for any reason, reactive oxygen species will damage the lipids, proteins, and even DNA of the cell. There are four reactive oxygen species: (1) singlet oxygen, $^1O_2$; (2) superoxide radicals, $O_2^{\bullet -}$; (3) hydrogen peroxide, H_2O_2; and (4) hydroxyl radical, $HO^{\bullet}$. [Lesser, 2006].

Representative Concentration Pathway Projection of the climate based on a possible anthropogenic emission scenario of greenhouse gasses used and described by the IPCC [2014].

Root-mean-squared error The root mean squared value of the error between model and data, where the error is given by the difference between the modelled value and the data point. The root mean squared value of an array is calculated based on three steps: (1) square all the numbers in the array; (2) sum the squared values of the array; and (3) take the root of this mean value first.

Sea surface temperature The temperature at the surface of the water.

Sea-level rise Rising of the sea-level due to climate change, which is due to a combination of factors: (1) melting of the ice-caps; and (2) expansion of water due to temperature increase. Both are driven by the worldwide temperature rise (*see* Global warming, Climate change).

Suspended particulate matter Particles suspended in the water column, mainly consisting of sediments, which settle during calm conditions forming a layer of silt at the bottom.

SWAN Hydrodynamic model in which the evolution of short-crested wind-generated waves is simulated; Simulating WAves Nearshore [Booij et al., 1999]. This model is used in Delft3D Flexible Mesh via the wave module D-WAVES (*see* Delft3D Flexible Mesh and D-WAVES).

Symbiont Organism that is part of a symbiosis. The coral-zooxanthellae symbiont is the combination of the coral and zooxanthellae that live in mutualistic symbiosis (*see* Symbiosis, Zooxanthellae).

Symbiosis The close and long-term interaction between two or more organisms. There are different types of symbiosis: mutualistic, commensalistic and parasitic. In mutualistic symbiosis, all parties benefit from the collaboration; in commensalistic symbiosis, one party benefits and the other neither benefits, nor is harmed; and in parasitic symbiosis, one party benefits but by doing so harms the other party. The symbiosis between corals and their zooxanthellae is a mutualistic symbiosis (*see* Zooxanthellae).

Thermal boundary layer The boundary layer over which temperature is transported via conduction, whereas convection is limited by the viscosity.

Thermal-acclimatisation Acclimatisation to changing temperatures (*see* Acclimatisation).

Time-scale compression Compression of an input time-series with a constant—or varying—factor to reduce computational time. This compression includes all forcing time-series except the tidal forcing, which would result in unrealistic tidal flow velocities.

Turbid reef refugia hypothesis The hypothesis that under the face of climate change, turbid reefs can function as refugia. Turbid reefs are considered as possible refugia due to the reduced damage due to bleaching. [Cacciapaglia and van Woesik, 2015].

Velocity boundary layer The boundary layer in which the kinematic viscosity is significant and enhances shear stresses is the flow.

Wave-attenuation coefficient The coefficient describing the attenuation of flow due to the presence of obstacles in the water column, such as corals. The wave-attenuation coefficient depends on the characteristics of the forcing—i.e. the flow—and the geometric properties of the canopy [Lowe et al., 2005a, 2008].

Zooxanthellae Zooxanthellae are single-celled, photosynthetic organisms, which contain chlorophyll *a* and chlorophyll *c*, as well as other pigments. These organisms live in symbiosis with corals and other marine life.

Appendix

Appendix A

Model description

This appendix is about the translation of the natural processes—as discussed extensively in Chapters 4 to 6—into a model for which numerical approaches are used. Thereby, it goes more into detail compared to the discussed model approach in Chapter 3. The common thread of the appendix is visualised in Figure A.1, which is a compressed version of Figure 3.1. This appendix follows the boxes as presented in Figure A.1 and thereby goes through the feedback loop step-by-step. The boxes "*water temperature*" and "*acidity*" are not discussed as they represent only forcings to the system, and thereby not considered as part of the feedback loop.

The biophysical model framework (BMF) constructed for this study does not incorporate a full elaboration on the hydrodynamics for which good-working models already exist. Nevertheless, a brief discussion on the modifications associated with the presence of a canopy is included; as discussed in Section 4.1.2.

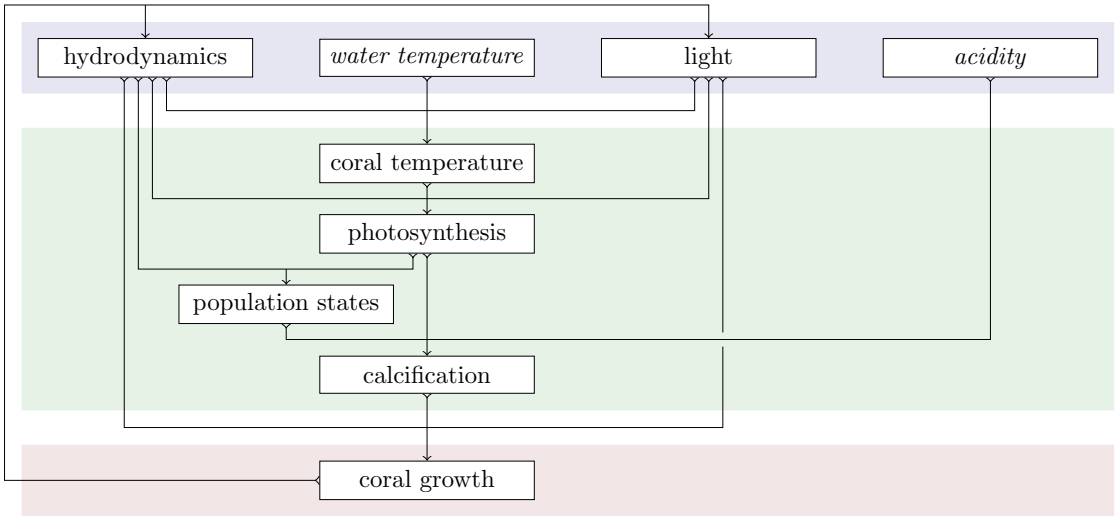

Figure A.1: Design of the biophysical model framework. The blue-shaded section indicates the environment of the corals; the green-shaded section indicates the physiology of corals; and the red-shaded section indicates the morphology of corals. The water temperature and the acidity are written in italics as they are not part of the feedback loop.

Every section discusses one of the boxes as presented in Figure A.1 in which three sets of parameters are given: (1) the forced input parameters; (2) the dynamically included input parameters; and (3) the output parameters. All parameters are not shown in Figure A.1 for clarity. The three coloured areas indicate the three main processes consisting of (1) the environment of the coral (blue); (2) the physiology of the coral (green); and (3) the morphology of the coral (red). The time-step starts at the environment—i.e. the blue area—from which the physiological response is determined. This results in changes in the morphology to close the cycle.

The notation used for the descriptions of the formulae as numerical input are subscripts for the spatial indication; and a superscript for the temporal indication. The x, y-coordinates are given by spatial steps in (i, j), where one spatial step is defined as Δx and Δy, respectively. The discretisation of the z-coordinate is not taken into account as it is a depth-averaged approach. However, the layers associated with the canopy are included and denoted by the letter k in which $k = 1$ is the top layer of the canopy and $k = 2$ the bottom layer. This notation is only necessary in case of the in-canopy flow structure.

The time-step is indicated by the letter n, and one time-step is defined as Δt. In case the time-notation includes an asterisk—i.e. n^*—it indicates that the time dependent parameters remains constant throughout the year; hence is updated annually ($\Delta t^* = 1\ yr$).

All numerical notations are placed within brackets to distinguish from algebraic operators; e.g. $X_{(i,j)}^{(n+1)}$ is the parameter X at $(x, y; t+\Delta t)$. For clarity, the absence of the numerical notation indicates the spatially and/or temporally independence of that parameter. The numerical notation is also left out when all parameters are within the same spatial- and/or time-step.

The structure of this appendix follows the flowchart as presented in Figure A.1 and starts with the modelling approach of the light-intensity as captured by the coral based on the solar radiation reaching the coral and the effects of its morphology on the representative light-intensity (App. A.1). Next, the effects of the morphology on the forced hydrodynamic conditions are presented (App. A.2) in which the flow structure and the thickness of the thermal boundary layer (TBL) are determined. This includes the solution to the Canopy-Flow Theory (App. A.2.1); and the iterative process in determining the drag coefficient (App. A.2.2). Thereafter, the temperature at the coral's tissue is discussed (App. A.3).

Based on the light, flow and thermal conditions, the rate of photosynthesis is determined (App. A.4). From thereon, the well-being of the corals are viewed (App. A.5)—i.e. the population dynamics—in which the effects of bleaching and dislodgement are included. Based on the aforementioned, the end result of the physiological response of the corals is determined (App. A.6); i.e. the calcification rate. This calcification rate results in the growth of corals in which the light and flow conditions play an important role in the resulting morphology of the corals (App. A.7), where also the impact of storms is included. Hereby, the feedback loop is closed.

A.1 Light

As clearly visible in Figure A.1, the representative light-intensity is of substantial importance for further steps in the process. The input consists of the morphological dimensions, the water depth, the incoming solar radiation, and the light-attenuation coefficient (LAC) for photosynthetically active radiation (PAR). As output, there is only the biomass-averaged light-intensity. All is visualised in Figure A.2.

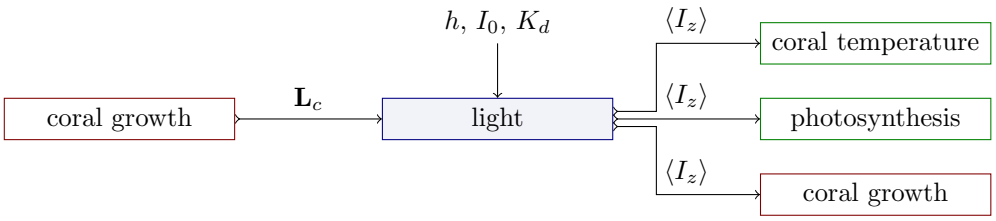

Figure A.2: Detailed visualisation of the in- and output parameters for the box 'light' as presented in Figure A.1. $\mathbf{L}_c$ is the vector containing the morphological dimensions, $\mathbf{L}_c = [d_c\ h_c\ b_c\ t_c\ a_c]$; h the water depth; I_0 the incoming light-intensity; K_d the LAC for PAR; and $\langle I_z \rangle$ the representative light-intensity.

The representative light-intensity is determined as given by Equation (4.6). This expression includes the integral of an exponential function, and rewritten in solely in- and output parameters gives:

$$\begin{aligned}\langle I_z \rangle^{(n)} = \frac{\pi I_0^{(n)}}{B_c^{(n)}} \Bigg\{ &\frac{1}{4}\left(d_c^{(n^*)}\right)^2 \exp\left[-K_d^{(n)}\left(h^{(n)} - h_c^{(n^*)}\right)\right] \\ &+ \frac{d_c^{(n^*)}}{K_d^{(n)}}\left(\exp\left[-K_d^{(n)}\left(h^{(n)} - h_c^{(n^*)}\right)\right] - \exp\left[-K_d^{(n)}\left(h^{(n)} - h_c^{(n^*)} + t_c^{(n^*)}\right)\right]\right) \\ &+ \frac{b_c^{(n^*)}}{K_d^{(n)}}\left(\exp\left[-K_d^{(n)}\left(h^{(n)} - L^{(n)}\right)\right] - \exp\left[-K_d^{(n)} h^{(n)}\right]\right)\Bigg\} \end{aligned} \tag{A.1}$$

in which

$$B_c^{(n)} = \pi\left(\frac{1}{4}\left(d_c^{(n^*)}\right)^2 + d_c^{(n^*)} t_c^{(n^*)} + b_c^{(n^*)} L^{(n)}\right) \tag{A.2a}$$

$$L^{(n)} = h_c^{(n^*)}\left(1 - \frac{b_c^{(n^*)}}{d_c^{(n^*)}}\right)\left(1 - \frac{d_c^{(n^*)}}{2h_c^{(n^*)} \tan\left[\frac{1}{2}\theta_I^{(n)}\right]}\right) \tag{A.2b}$$

$$\theta_I^{(n)} = \theta_I^{\max} \exp\left[-K_d^{(n)}\left(h^{(n)} - h_c^{(n^*)} + t_c^{(n^*)}\right)\right] \tag{A.2c}$$

A.2 Hydrodynamics

This section elaborates on the numerical approaches for solving the effects of the coral canopy as discussed in Section 4.1.2. A brief elaboration on the hydrodynamic model incorporated in determining the wave length, wave set-up, the wave-induced flow, etc. is given in Appendix B. This section focusses on the effects of the resulting hydrodynamics on the canopy flow structure.

The input of this box consists of the morphological dimensions of the coral, the water depth, the wave characteristics, and the flow characteristics. The wave and flow characteristics are determined using the just-mentioned hydrodynamic model. The output parameters are the thickness of the TBL and the magnitude of the in-canopy flow. Note that the thickness of the TBL is based on the in-canopy flow as well. All the hydrodynamic computations are performed using the morphology of the previous time-step and the hydrodynamic loads of the current time-step; as a new time-step is started after the coral growth is updated.

The determination of the in-canopy flow includes solving the differential equation associated with the Canopy-Flow Theory (CFT), and going through the iterative process of determining the drag coefficient. First, the method used in solving the CFT is discussed in Appendix A.2.1 after which the iterative cycle for the drag coefficient is highlighted in Appendix A.2.2. Finally, the determination of the thickness of the TBL is covered (App. A.2.3).

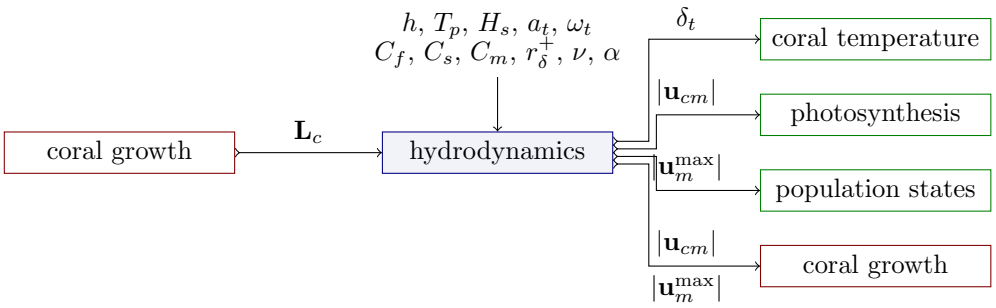

Figure A.3: Detailed visualisation of the in- and output parameters for the box 'hydrodynamics' as presented in Figure A.1. $\mathbf{L}_c$ is the vector containing the characteristic length-scales of the coral structure, $\mathbf{L}_c = [d_c\ h_c\ b_c\ t_c\ a_c]$; h the water depth; T_p the peak wave-period; H_s the significant wave height; a_t the tidal range; ω_t the tidal frequency; C_f the friction coefficient; C_s the Smagorinsky coefficient; C_m the inertia coefficient; $r_\delta{}^+$ the wall coordinate of the velocity boundary layer (VBL); ν the kinematic viscosity of water; α the thermal diffusivity; δ_t the thickness of the thermal boundary layer (TBL); and $|\mathbf{u}_m^{\max}|$ and $|\mathbf{u}_{cm}|$ the magnitude of the maximum bulk and in-canopy flow, respectively.

A.2.1 In-canopy flow

This section elaborates on the numerical implementation of the solution of the partial differential equation, which is derived in Appendix E.3. The solution of the multi-layer canopy (*see* Eq. E.33) is rewritten so it holds for a two-layer canopy in which the bottom shear stress is assumed to be zero as well as the shear stress at the top of the canopy:

$$f_1 = i\left(\beta_1 - 1\right) - \frac{8}{3\pi}\frac{a_f}{L_{s,1}}\Big(\left|1-\beta_1\right|\left(1-\beta_1\right) - \left|\beta_1-\beta_2\right|\left(\beta_1-\beta_2\right)\Big) + \frac{8}{3\pi}\frac{a_f}{L_{d,1}}\left|\beta_1\right|\beta_1 + i\frac{C_m\lambda_{p,1}}{1-\lambda_{p,1}}\beta_1 \tag{A.3a}$$

$$f_2 = i\left(\beta_2 - 1\right) - \frac{8}{3\pi}\frac{a_f}{L_{s,2}}\left|\beta_1-\beta_2\right|\left(\beta_1-\beta_2\right) + \frac{8}{3\pi}\frac{a_f}{L_{d,2}}\left|\beta_2\right|\beta_2 + i\frac{C_m\lambda_{p,2}}{1-\lambda_{p,2}}\beta_2 \tag{A.3b}$$

This set of equations has to be solved iteratively in which both the solutions to Equations (A.3a) and (A.3b) separately are calculated by an iterative method as well. For this, built-in functions exist. As Equations (A.3a) and (A.3b) are complex valued functions, the Newton-Raphson method is used. This function is part of the package `scipy.optimize` in Python.[1] However, for this solver to work, the derivatives of both functions are needed (*see* App. E.3.3). This results in the following expressions of these derivatives for the two-layer canopy:

$$\frac{\partial f_1}{\partial \beta_1} = i - \frac{8}{3\pi}\frac{a_f}{L_{s,1}}\left(\frac{\left(1-\beta_1\right)^2}{\left|1-\beta_1\right|} - \left|1-\beta_1\right| - \frac{\left(\beta_1-\beta_2\right)^2}{\left|\beta_1-\beta_2\right|} - \left|\beta_1-\beta_2\right|\right) + \frac{8}{3\pi}\frac{a_f}{L_{d,1}}\left(\frac{\beta_1^2}{\left|\beta_1\right|} + \left|\beta_1\right|\right) + i\frac{C_m\lambda_{p,1}}{1-\lambda_{p,1}} \tag{A.4a}$$

$$\frac{\partial f_2}{\partial \beta_2} = i - \frac{8}{3\pi}\frac{a_f}{L_{s,2}}\left(\frac{\left(\beta_1-\beta_2\right)^2}{\left|\beta_1-\beta_2\right|} - \left|\beta_1-\beta_2\right|\right) + \frac{8}{3\pi}\frac{a_f}{L_{d,2}}\left(\frac{\beta_2^2}{\left|\beta_2\right|} + \left|\beta_2\right|\right) + i\frac{C_m\lambda_{p,2}}{1-\lambda_{p,2}} \tag{A.4b}$$

To save computational time, the CFT is not incorporated during the modelling of waves and thus these processes are decoupled. Nevertheless, the effects of the presence of waves on the wave-attenuation coefficient (WAC) is substantial [Lowe et al., 2005a] and thus cannot be neglected.

[1] More information on the function: https://docs.scipy.org/doc/scipy/reference/generated/scipy.optimize.newton.html (retrieved January 23, 2020).

A.2.2 Drag coefficient

This section presents the iterative process on the determination of the drag coefficient as introduced in Section 4.1.2 (Fig. 4.4). The solution to the partial differential equation of the CFT as elaborated on in Appendix A.2.1 is used in the iterations for the drag coefficient. For convenience, Figure 4.4 is extended and presented in Figure A.5. The iteration step is indicated by the superscript (m), and the canopy layer is indicated by the subscript k.

The iteration starts with the definition of characteristic parameters of the morphology—namely the λ-parameters (Eqs. 4.16a and 4.16b) and the shear length-scales (Eq. 4.17a) for both canopy layers—and a well-educated guess on the free above-canopy flow and the drag coefficients themself. From there, the drag length-scales are calculated (Eq. A.7), which depend on their corresponding drag coefficient.

With the estimated above-canopy flow velocity, and the wave and morphological characteristics, the WAC is determined (Eq. A.8). The porous in-canopy flow velocities are used to calculate the constricted in-canopy flow velocities (Eq. A.10). With this flow velocity, the corresponding drag coefficient is determined (Eq. A.12) via its Reynolds number (Eq. A.11). Convergence of the drag coefficients is checked, and when it is not converged enough, both the drag coefficients and the above-canopy flow are updated. To accelerate the conversion, the above-canopy flow is partly updated to reduce wiggles. This is accomplished by using a weighted average.

This cycle continues until the drag coefficient is within a pre-defined margin of the previous value of the drag coefficient; i.e. until the drag coefficient has converged sufficiently.

A.2.3 Thermal boundary layer

The thickness of the TBL can be readily calculated from Equations (4.31) to (4.33) in which the determined in-canopy flow is used as input; note that the in-canopy flow is the combination of current- and wave-induced in-canopy flows. Rewritten into one formulation gives:

$$\delta_t = \frac{r_\delta^+ \nu}{\sqrt{C_f}\,|\mathbf{u}_{cm}|}\left(\frac{\alpha}{\nu}\right)^{\frac{1}{3}} \tag{A.5}$$

where only the in-canopy flow varies over time; and all other parameters remain constant throughout.

A.3 Coral temperature

The determination of the temperature at the coral tissue is a relatively short one, which depends on the light-intensity, the thickness of the thermal boundary layer (TBL) and the ambient temperature; as presented in Figure A.4. As output is the temperature of the coral, which determines the thermal response of the photosynthesis.

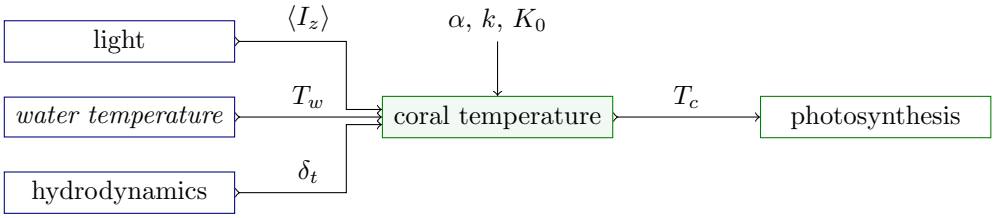

Figure A.4: Detailed visualisation of the in- and output parameters for the box 'coral temperature' as presented in Figure A.1. $\langle I_z \rangle$ is the coral surface-averaged light-intensity; δ_t the thickness of the TBL; T_w the daily-averaged sea surface temperature (SST); K_0 the species related constant on the TBL; and T_c the temperature at the coral tissue.

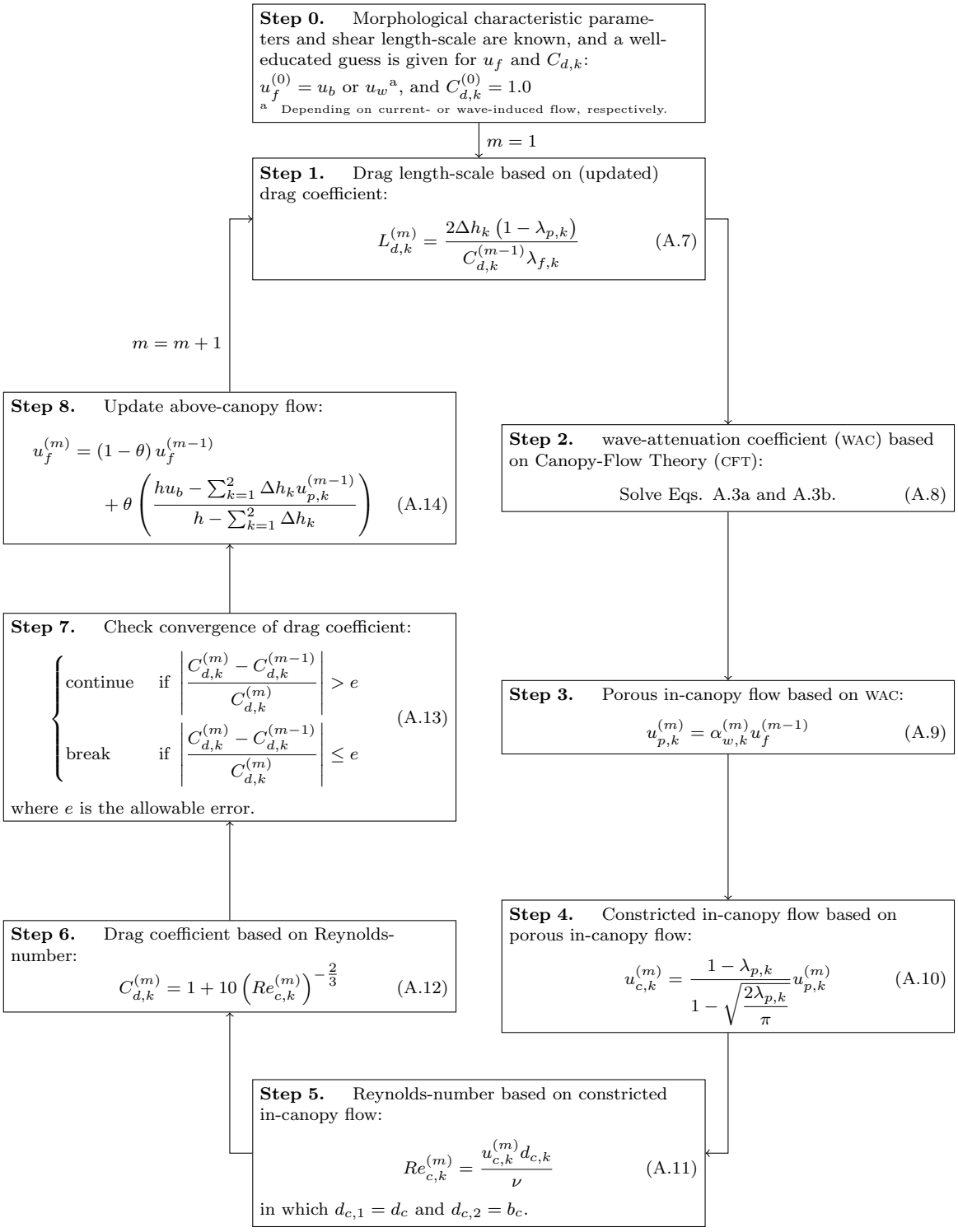

Figure A.5: Extensive scheme of the iterative process to determine the drag coefficient. Iteration-step is denoted as (m), and all parameters without the iteration-step in the superscript are constant throughout the iteration. The iteration process covers all canopy layers at the same time as is needed to systematically solve the in-canopy flow (Step 2). The iterative process repeats until the drag coefficients converge [modified from van Rooijen et al., 2018].

This step can be summarised into one formulation in which Equations (4.34) and (4.49) are combined:

$$T_c = T_w + \frac{\delta_t a_p}{kK_0} \langle I_z \rangle \tag{A.6}$$

In this formulation, the temperature of the ambient seawater is given by the daily-averaged SST ($T_w = \overline{SST}^d$), which is not part of the feedback loop (*see* Fig. A.1). Furthermore, note that the light, thermal and flow conditions vary over time, but are all in the same time-step in Equation (A.6).

A.4 Photosynthesis

The photosynthetic part places all the physiological responses together and includes the acclimatisation of the corals. As clearly visible in Figure A.6, there are a lot of input parameters of which not all are fully static; the incoming light-intensity (I_0) is a forcing. This section starts with the elucidation of the two acclimatisation responses: (1) photo-acclimatisation; and (2) thermal-acclimatisation (Secs. A.4.1 and A.4.2, resp.). Thereafter, the photosynthetic response to the environment is presented in Appendix A.4.3.

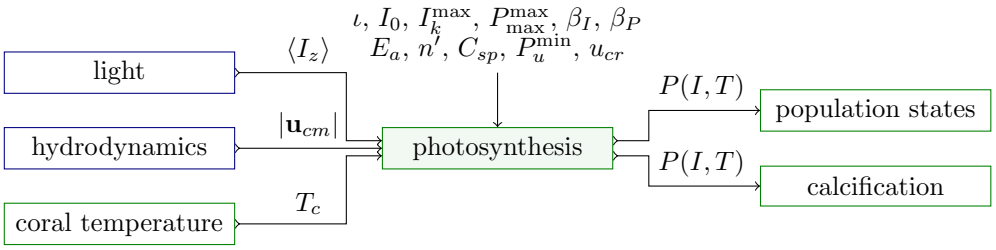

Figure A.6: Detailed visualisation of the in- and output parameters for the box 'photosynthesis' as presented in Figure A.1. $\langle I_z \rangle$ the coral surface-averaged light-intensity; T_c the temperature at the coral tissue; $|\mathbf{u}_{cm}|$ the magnitude of the in-canopy flow; ι the acclimation exponent; I_0 the light-intensity at the surface water; $I_k^{\max}$ and $P_{\max}^{\max}$ the maximum steady-state values of the saturation intensity and the maximum photosynthetic rate, respectively; β_I and β_P the quasi steady-state constants of the saturation intensity and the maximum photosynthetic rate, respectively; E_a the activation energy; n' the acclimation period; C_{sp} the species constant; $P_u^{\min}$ the minimum photosynthetic flow dependency; u_{cr} the critical flow velocity; and $P(I,T,u)$ the photosynthetic rate.

A.4.1 Photo-acclimation

The photo-acclimatisation is described by one differential equation (Eq. 4.40) for both the maximum photosynthetic rate and the saturation intensity. The general solution is given by:

$$X^{(n)} = X^{S(n)} + \left(X^{(n-1)} - X^{S(n)} \right) \exp\left[-\iota \Delta t \right] \tag{A.15}$$

where X represents the maximum photosynthetic rate ($P_{\max}$), or the saturation intensity (I_k); and X^S the quasi steady-state solution of X. This quasi steady-state solution is time-dependent as well, whereas it is based on the incoming light-intensity and the coral surface-averaged light-intensity as given by:

$$X^S = X^{\max} \left(\frac{\langle I_z \rangle}{I_0} \right)^{\beta_X} \tag{A.16}$$

A.4.2 Thermal-acclimation

The thermal-acclimatisation is based on a long sea surface temperature (SST) time-series of preferable at least N^* years.[2] If the time-series of SST data is shorter, the thermal characteristics are based on this shorter time-series; for lack of better. Note that thereby corals acclimatise faster.

The limits of the thermal range are based on long-term statistics of the thermal environment, where for the upper limit the annual maximum monthly mean is used; and for the lower limit the annual minimum monthly mean [Donner, 2011]. The mean and standard deviation are taken from these monthly means:

$$\mu_T^{\min} = \overline{\min_y \left\{\overline{T_c}^m\right\}}^{N^*} \tag{A.17a}$$

$$\sigma_T^{\min} = \sqrt{\frac{\sum_{n^*=1}^{N^*}\left(\min_y \left\{\overline{T_c}^m\right\}_{n^*} - \overline{\min_y \left\{\overline{T_c}^m\right\}}^{N^*}\right)}{N^*-1}} \tag{A.17b}$$

$$\mu_T^{\max} = \overline{\max_y \left\{\overline{T_c}^m\right\}}^{N^*} \tag{A.17c}$$

$$\sigma_T^{\max} = \sqrt{\frac{\sum_{n^*=1}^{N^*}\left(\max_y \left\{\overline{T_c}^m\right\}_{n^*} - \overline{\max_y \left\{\overline{T_c}^m\right\}}^{N^*}\right)}{N^*-1}} \tag{A.17d}$$

on which the limits of the thermal range are based:

$$T_{lo} = \mu_T^{\min} - K_{var}\sigma_T^{\min} \tag{A.18a}$$

$$T_{c,hi} = \mu_T^{\max} + K_{var}\sigma_T^{\max} \tag{A.18b}$$

where $\mu_T^{\min}$ and $\mu_T^{\max}$ are respectively the mean of the minimum and maximum annual monthly means; K_{var} is the thermal-acclimatisation coefficient with $K_{var} = 2.45$; and $\sigma_T^{\min}$ and $\sigma_T^{\max}$ are the associating standard deviations.

The SST time-series solely used for the thermal-acclimatisation must be corrected for the influence of the thermal boundary layer (TBL); the SST time-series must be rewritten into a time-series of the coral temperature. The effects of the TBL are taken into account by representative values of the light, flow and morphology parameters, and is taken constant over the pre-model period; i.e. n years before the start time of the model run.

Due to the annual statistics needed for the computations on the thermal-acclimatisation, and the slow changes in the limits of the thermal range, the effects of the thermal-acclimatisation are updated annually. Furthermore, the time-scale associated with the thermal-acclimatisation is rounded to whole years due to the use of annual statistics.

A.4.3 Photosynthetic rate

The photosynthetic rate consists of three mains terms: (1) the photosynthetic light dependency, which changes due to the photo-acclimatisation; (2) photosynthetic the thermal dependency, which response is characterised by the thermal-acclimatisation; and (3) the photosynthetic flow dependency. For convenience, the presented formulation of the photosynthetic rate (Eq. 4.37) is repeated in this section:

$$P(I,T,u) = \underbrace{P(I)}_{(1)}\ \underbrace{P(T)}_{(2)}\ \underbrace{P(u)}_{(3)} \tag{A.19}$$

where the aforementioned terms are numbered accordingly.

[2] The definition of N^* is given in Equation (4.57) and is the number of years taken into account in the thermal-acclimatisation; i.e. the number of years on which the thermal key parameters are based. In the main text, this parameter is given as n, but for clarity is here substituted by N^*.

Photo dependency

The photosynthetic light dependency follows the shape of the photosynthesis-irradiance curve and can be taken directly from Equation (4.42):

$$P(I) = P_{\max}\left(\tanh\left[\frac{\langle I_z\rangle}{I_k}\right] - \tanh\left[\frac{0.01 I_0}{I_k}\right]\right) \tag{A.20}$$

where the maximum photosynthetic rate and saturation intensity follow the formulations of the photo-acclimatisation (*see* Eqs. A.15 and A.16).

Thermal dependency

All thermal key parameters are updated annually as part of the thermal-acclimatisation. Thereby, the adapted temperature response is given by:

$$f_1^{(n)} = \begin{cases} -\left(T_c^{(n)} - T_{lo}^{(n^*)}\right)\left(\left(T_c^{(n)} - T_{lo}^{(n^*)}\right)^2 - \left(\Delta T^{(n^*)}\right)^2\right)\operatorname{spec}\left(\Delta T^{(n^*)}\right) & T_c^{(n)} > T_{lo}^{(n^*)} - \frac{1}{\sqrt{3}}\Delta T^{(n^*)} \\ -\max\{f_1\} & T_c^{(n)} \leq T_{lo}^{(n^*)} - \frac{1}{\sqrt{3}}\Delta T^{(n^*)} \end{cases} \tag{A.21}$$

and the thermal envelope by:

$$f_2^{(n)} = \exp\left[\frac{E_a}{\overline{R}}\left(\frac{1}{300} - \frac{1}{T_{opt}^{(n^*)}}\right)\right] \tag{A.22}$$

where the superscript (n^*) indicates the annually updating of the parameter; and the specialisation term as suggested by Evenhuis et al. [2015] is used:

$$\operatorname{spec}_E(\Delta T^{(n^*)}) = 4 \cdot 10^{-4} \exp\left[-0.33\left(\Delta T^{(n^*)} - 10\ [K]\right)\right] \tag{A.23}$$

Flow dependency

The photosynthetic flow dependency can readily be used from Equation (4.47):

$$P(u) = P_u^{\min} + \left(1 - P_u^{\min}\right)\tanh\left[a\frac{|\mathbf{u}_{cm}|}{u_{cr}}\right] \tag{A.24}$$

where the best fit through the data gives: (1) to the in-canopy flow $P_u^{\min} \approx 0.689$, and $u_{cr} \approx 0.172\ ms^{-1}$; and (2) to the bulk flow $P_u^{\min} = 0.689$, and $u_{cr} = 0.517\ ms^{-1}$ (*see* Sec. 7.2.2).

A.5 Population states

The population states determine the well-being of the corals and translates the possible stresses into decay. The main contributor to this step is the photosynthetic response in the absence of storms. Its output for further steps consists solely of the healthy coral cover as presented in Figure A.7, but the distribution of population states is of substantial importance for the determination of the population states in the next time-step.

For the population dynamics, the set of partial differential equations as given in Chapter 5 has to be solved (Eqs. 5.1a to 5.1d) to which the addition originating from the coral dislodgement must be added (*see* Sec. 6.2). The inclusion of the effects due to dislodgement are binary: (1) nothing happens; or (2) all coral cover is removed from the cell. For the population dynamics, this is represented as:

$$P_i^{(n)} = \begin{cases} 0 & \text{if } DMT \leq CSF \\ \text{solve Eqs. 5.1a to 5.1d} & \text{if } DMT > CSF \end{cases} \tag{A.25}$$

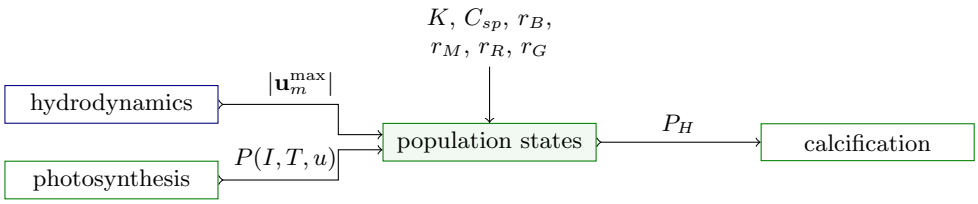

Figure A.7: Detailed visualisation of the in- and output parameters for the box 'population states' as presented in Figure A.1. $|\mathbf{u}_m^{\max}|$ is the maximum flow velocity; $P(I,T,u)$ the representation of the photosynthetic rate; C_{sp} the species constant; r_B the bleaching rate; r_M the mortality rate; r_R the recovery rate; r_G the growth rate; and P_H the healthy population.

where DMT is the dislodgement mechanical threshold (DMT); and CSF the colony shape factor (CSF).

When the dislodgement criterion is not met, the partial differential equations associated with the population dynamics have to be solved (*see* Eqs. 5.1a to 5.1d). These formulae are repeated here in scalar-form for convenience:

For $T_{lo} \leq T_c \leq T_{hi}$ (i.e. $P(I,T,u) \geq 0$):

$$\frac{\partial P_H}{\partial t} = r_G\ P(I,T,u)\ C_{sp}\ \left(1 - \frac{P_T}{K}\right) P_H + \tfrac{1}{2} r_R\ P(I,T,u)\ C_{sp} P_R \tag{A.26a}$$

$$\frac{\partial P_R}{\partial t} = r_R\ P(I,T,u)\ \left(-\tfrac{1}{2} C_{sp} P_R + C_{sp} P_P\right) \tag{A.26b}$$

$$\frac{\partial P_P}{\partial t} = r_R\ P(I,T,u)\ \left(-C_{sp} P_P + \frac{8}{C_{sp}} P_B\right) \tag{A.26c}$$

$$\frac{\partial P_B}{\partial t} = -\frac{8 r_R\ P(I,T,u)}{C_{sp}} P_B - r_M C_{sp} P_B \tag{A.26d}$$

For $T_c < T_{lo}$ or $T_c > T_{hi}$ (i.e. $P(I,T,u) < 0$):

$$\frac{\partial P_H}{\partial t} = r_B\ P(I,T,u)\ C_{sp} P_H \tag{A.27a}$$

$$\frac{\partial P_R}{\partial t} = r_B\ P(I,T,u)\ C_{sp} P_R \tag{A.27b}$$

$$\frac{\partial P_P}{\partial t} = r_B\ P(I,T,u)\ C_{sp}\left(-P_H - P_R + \tfrac{1}{2} P_P\right) \tag{A.27c}$$

$$\frac{\partial P_B}{\partial t} = r_B\ P(I,T,u)\ C_{sp}\left(-\tfrac{1}{2} P_P + \tfrac{1}{4} P_B\right) \tag{A.27d}$$

where one has to keep in mind that the photosynthetic rate is negative for temperatures outside the thermal range, and vice versa; i.e. $P(I,T,u) \geq 0$ for $T_{lo} \leq T_c \leq T_{hi}$, and $P(I,T,u) < 0$ for $T_c < T_{lo}$ or $T_c > T_{hi}$.

Because the population states describe the coral coverage per area, the solution of the population states are bounded by limits for every population state and for the total population as well; i.e. $0 \leq P_i \leq 1$ and $0 \leq P_T \leq 1$. Furthermore, the rates of change are time-dependent due to the dependence on the proxy of the photosynthetic rate. Therefore, an unconditionally stable scheme is needed to ensure stability [Vuik et al., 2015]. The simplest implicit scheme is used—the implicit Euler scheme—which is given by:

$$\frac{\partial y}{\partial t} = f(t,y) \quad \rightarrow \quad \frac{y^{(n)} - y^{(n-1)}}{\Delta t} \approx f\left(t_n, y^{(n)}\right) \tag{A.28}$$

Because the implicit Euler scheme is an implicit method, it results in a set of equations that has to be solved. This is the largest disadvantage of implicit schemes. Fortunately, the set of differential equations are easily

rewritten in an explicit form. In this process, the order of solving the explicit expressions does matter due to their partial dependencies.

In the case of growth, the order is (1) bleached population; (2) pale population; (3) recovering population; and (4) healthy population; i.e. from Eq. A.26d to Eq. A.26a. In the case of bleaching, the order is opposite; i.e. Eq. A.27a to Eq. A.27d. Furthermore, the photosynthetic rate is determined before the computations on the population states. Thereby, this parameter is known at the time-step under consideration and is denoted as $PS^{(n)}$ (at time-step $t = t_n$).

During growth—i.e. the coral temperature is within its thermal range—the following explicit expressions of the differential equations have to be solved in the following order:

1. Bleached population:

$$P_B^{(n)} = \frac{P_B^{(n-1)}}{1 + \Delta t \left(\frac{8 r_R P S^{(n)}}{C_{sp}} + r_M C_{sp} \right)} \tag{A.29a}$$

2. Pale population:

$$P_P^{(n)} = \frac{P_P^{(n-1)} + \frac{8 \Delta t \; r_R P S^{(n)}}{C_{sp}} P_B^{(n)}}{1 + \Delta t \; r_R P S^{(n)} C_{sp}} \tag{A.29b}$$

3. Recovering population:

$$P_R^{(n)} = \frac{P_R^{(n-1)} + \Delta t \; r_R P S^{(n)} C_{sp} P_P^{(n)}}{1 + \frac{1}{2} \Delta t \; r_R P S^{(n)} C_{sp}} \tag{A.29c}$$

4. Healthy population:

$$P_H^{(n)} = \frac{-b + \sqrt{b^2 - 4ac}}{2a} \tag{A.29d}$$

in which

$$a = \frac{\Delta t \; r_G P S^{(n)} C_{sp}}{K}$$
$$b = 1 - \Delta t \; r_G P S^{(n)} C_{sp} \left(1 - \frac{P_R^{(n)} + P_P^{(n)} + P_B^{(n)}}{K} \right)$$
$$c = - \left(P_H^{(n-1)} + \tfrac{1}{2} \Delta t \; r_R P S^{(n)} C_{sp} P_R^{(n)} \right)$$

Note that the *abc*-rule is used for solving the healthy population due to the non-linearity of Equation (A.26a). This non-linearity originates from the inclusion of the healthy population in the total population: $P_T = P_H + P_R + P_P + P_B$ (*see* Sec. 5).

During a bleaching event—i.e. the coral temperature is outside its thermal range—the following explicit expressions of the differential equations have to be solved in the following order:

1. Healthy population:

$$P_H^{(n)} = \frac{P_H^{(n-1)}}{1 - \Delta t \; r_B P S^{(n)} C_{sp}} \tag{A.30a}$$

2. Recovering population:

$$P_R^{(n)} = \frac{P_R^{(n-1)}}{1 - \Delta t \; r_B P S^{(n)} C_{sp}} \tag{A.30b}$$

3. Pale population:

$$P_P^{(n)} = \frac{P_P^{(n-1)} - \Delta t \; r_B P S^{(n)} C_{sp} \left(P_H^{(n)} + P_R^{(n)} \right)}{1 - \frac{1}{2} \Delta t \; r_B P S^{(n)} C_{sp}} \tag{A.30c}$$

4. Bleached population:

$$P_B^{(n)} = \frac{P_B^{(n-1)} - \frac{1}{2} \Delta t \; r_B P S^{(n)} C_{sp} P_P^{(n)}}{1 - \frac{1}{4} \Delta t \; r_B P S^{(n)} C_{sp}} \tag{A.30d}$$

A.6 Calcification

This section elaborates on the calcification as a result of the photosynthesis, the population states, and the acidity; shown in Figure A.8. The input parameters consist of the proxy of the photosynthetic rate, the healthy coral cover and the aragonite saturation state as well as the characteristic parameters for the aragonite saturation state, the growth constant, and the species constant. The output is the calcification rate, which determines how much the coral will grow.

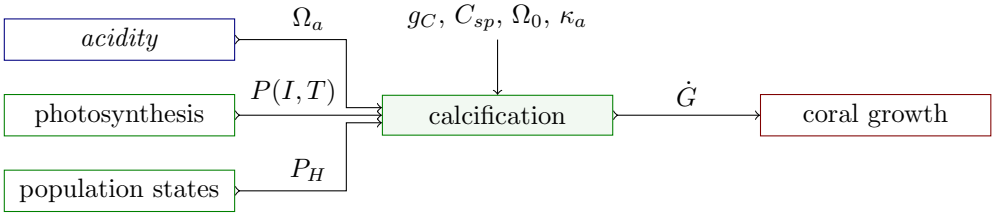

Figure A.8: Detailed visualisation of the in- and output parameters for the box 'calcification' as presented in Figure A.1.

The calculations concerning the calcification are rather straightforward, as there are no differential equations or whatsoever involved. Therefore, the calcification rate is calculated by filling in the values of the parameters into Equation (4.36), repeated here for convenience:

$$\dot{G} = g_C \; C_{sp} \; P_H \; \gamma(\Omega_a) \; P(I,T,u) \tag{A.31}$$

where the dependency on the aragonite saturation state is given by the Michaelis-Menten equation. This formulation is repeated here for convenience as well:

$$\gamma(\Omega_a) = \frac{\Omega_a - \Omega_0}{\kappa_a + (\Omega_a - \Omega_0)} \tag{A.32}$$

in which the best fit of this curve through the data gives: $\Omega_0 \approx 0.146$, and $\kappa_a \approx 0.662$ (*see* Sec. 7.2.4).

The effects of the aragonite saturation state are not dynamically incorporated—as aforementioned—and the aragonite is determined outside the model based on (1) changes in temperature and carbon dioxide (CO_2) concentrations; or (2) literature on predictions of future aragonite saturation states for various Representative Concentration Pathways (RCPs). Whereat the latter is preferred as in these studies more aspects are included, such as accurate predictions on ocean acidification (OA).

A.7 Coral growth

This last section elaborates on the last set of calculations of a time-step and focusses on the morphological development as function of the light- and flow conditions, and the calcification rate (*see* Fig. A.9). The result is the description of the size and spacing of the cylinders; combined in one vector parameter denoted as $\mathbf{L}_c = [d_c\ h_c\ b_c\ t_c\ a_c]$.

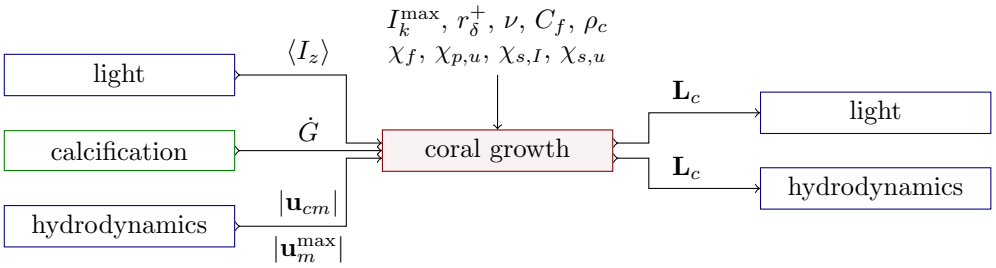

Figure A.9: Detailed visualisation of the in- and output parameters for the box 'coral growth' as presented in Figure A.1. $\langle I_z \rangle$ is the coral surface-averaged light-intensity; $|\mathbf{u}_{cm}|$ the magnitude of the in-canopy flow; $\dot{G}$ the calcification rate; $I_k^{\max}$ the maximum saturation intensity; r_δ^+ the wall coordinate of the thickness of the velocity boundary layer (VBL); ν the kinematic viscosity of water; C_f the friction coefficient; ρ_c the density of the coral; and $\mathbf{L}_c$ the vector containing the characteristic length-scales of the coral structure: $\mathbf{L}_c = [d_c\ h_c\ b_c\ t_c\ a_c]$.

For the coral growth, the partial differential equation as given in Section 4.3.2 has to be solved (Eq. 4.67) to which the addition originating from the coral dislodgement must be added (*see* Sec. 6.2). The inclusion of the effects due to dislodgement are binary: (1) nothing happens; or (2) all coral cover is removed from the cell (*see* Sec. 6.2). For the coral growth, this is represented as:

$$V_c^{(n)} = \begin{cases} 0 & \text{if } DMT \leq CSF \\ V_c^{(n-1)} + \Delta V_c^{(n)} & \text{if } DMT > CSF \end{cases} \tag{A.33}$$

where DMT is the dislodgement mechanical threshold (DMT); and CSF the colony shape factor (CSF) (*see* Sec. 6.2).

The effect of the environment on the morphology is given by three ratios (*see* Sec. 3.3): r_f, r_p and r_s. These three ratios are also used in the determination of the changes of them over time due to changes of environmental conditions. The rate of change of the morphology is given by the calcification rate (*see* Eq. 4.67). The discretisation of Equation (4.67) gives:

$$r_i^{(n^*)} = \frac{V_c^{(n^*-1)} r_i^{(n^*-1)} + \Delta V_c^{(n^*)} r_{i,opt}^{(n^*)}}{V_c^{(n^*-1)} + \Delta V_c^{(n^*)}} \tag{A.34}$$

in which

$$\Delta V_c^{(n^*)} = \frac{\left(a_c^{(n^*-1)}\right)^2}{2} \frac{1}{\rho_c \Delta t^*} \sum_{n=1}^{n^*} B_c^{(n)} \dot{G}^{(n)} \Delta t \tag{A.35}$$

where V_c is the coral volume; ΔV_c the increase in volume due to calcification; ρ_c the density of the coral's skeleton;[3] B_c the coral biomass as given in Equation (A.2a); and $r_{i,opt}$ the optimal morphological ratio i as given by Equations (4.63a) to (4.63c).

[3]The density of the coral is assumed to be $\rho_c = 1,600\ kg\ m^{-3}$.

Next, the new coral dimensions are computed by using the new volumes for which simple geometry will do the job:

$$d_c = \sqrt[3]{\frac{4V_c}{\pi r_f \left(r_p + r_p^2 - r_p^3\right)}} \tag{A.36a}$$

$$h_c = \sqrt[3]{\frac{4V_c r_f^2}{\pi \left(r_p + r_p^2 - r_p^3\right)}} \tag{A.36b}$$

$$b_c = \sqrt[3]{\frac{4V_c r_p^2}{\pi r_f \left(1 + r_p - r_p^2\right)}} \tag{A.36c}$$

$$t_c = \sqrt[3]{\frac{4V_c r_f^2 r_p^2}{\pi \left(1 + r_p - r_p^2\right)}} \tag{A.36d}$$

$$a_c = \frac{1}{r_s} \sqrt[3]{\frac{4V_c}{\pi r_f \left(r_p + r_p^2 - r_p^3\right)}} \tag{A.36e}$$

Appendix B

Hydrodynamic model: Delft3D Flexible Mesh

The hydrodynamic model is Delft3D Flexible Mesh (D3D-FM) from which the modules D-FLOW and D-WAVES are used. This hydrodynamic model has an option to include the effects of vegetation [Deltares, 2019a,b]. This appendix presents the basic formulations of D-FLOW and D-WAVES, and the settings used in this study (App. B.1). Thereafter, the online-coupling between the three components—D-FLOW, D-WAVES and the biophysical model developed in this study—are presented in Appendix B.2. Finally, the design of the hydrodynamic model as in this study is drawn in Appendix B.3.

B.1 Governing equations

This section is based on the user manuals and technical reference manuals of D-FLOW [Deltares, 2019a,b] and D-WAVES [Deltares, 2019c].

B.1.1 D-Flow

The water motion is described by the Navier-Stokes equations and the continuity equation, where the Navier-Stokes equations are derived from the momentum balance equations in all three directions:

$$\frac{\partial u}{\partial t} + u\frac{\partial u}{\partial x} + v\frac{\partial u}{\partial y} + w\frac{\partial u}{\partial z} = -\frac{1}{\rho}\frac{\partial p}{\partial x} + \frac{\partial}{\partial x}\left(\nu_H \frac{\partial u}{\partial x}\right) + \frac{\partial}{\partial y}\left(\nu_H \frac{\partial u}{\partial y}\right) + \frac{\partial}{\partial z}\left(\nu_V \frac{\partial u}{\partial z}\right) + fv + F_x \quad \text{(B.1a)}$$

$$\frac{\partial v}{\partial t} + u\frac{\partial v}{\partial x} + v\frac{\partial v}{\partial y} + w\frac{\partial v}{\partial z} = -\frac{1}{\rho}\frac{\partial p}{\partial y} + \frac{\partial}{\partial x}\left(\nu_H \frac{\partial v}{\partial x}\right) + \frac{\partial}{\partial y}\left(\nu_H \frac{\partial v}{\partial y}\right) + \frac{\partial}{\partial z}\left(\nu_V \frac{\partial v}{\partial z}\right) - fu + F_y \quad \text{(B.1b)}$$

$$\frac{\partial w}{\partial t} + u\frac{\partial w}{\partial x} + v\frac{\partial w}{\partial y} + w\frac{\partial w}{\partial z} = -\frac{1}{\rho}\frac{\partial p}{\partial z} + \frac{\partial}{\partial x}\left(\nu_H \frac{\partial w}{\partial x}\right) + \frac{\partial}{\partial y}\left(\nu_H \frac{\partial w}{\partial y}\right) + \frac{\partial}{\partial z}\left(\nu_V \frac{\partial w}{\partial z}\right) - g + F_z \quad \text{(B.1c)}$$

where u, v, w are the flow velocities in respectively x, y, z-direction; f is the Coriolis parameter; ρ the water density; p the pressure; ν_H and ν_V respectively the horizontal and the vertical eddy viscosity coefficients; g the gravitational acceleration; and M_i the contributions due to external sources or sinks of momentum in i-direction, e.g. Reynolds stresses and wave stresses.

The continuity equation for incompressible fluids—which water is assumed to be—is derived from the mass balance:

$$\frac{\partial u}{\partial x} + \frac{\partial v}{\partial y} + \frac{\partial w}{\partial z} = 0 \quad \text{(B.2)}$$

In the depth-averaged two-dimensional approach—as in this study—the vertical accelerations are neglected. This reduces the vertical momentum equation (Eq. B.1c) to the hydrostatic pressure balance:

$$\frac{\partial p}{\partial z} = -\rho g \tag{B.3}$$

For small density differences with respect to the absolute values—i.e. $\Delta\rho \ll \rho$—it does not affect the horizontal momentum balance to assume a constant density; the so-called Boussinesq approximation. When Reynolds averaging is applied, one gets the following set of equations:

$$\frac{\partial \zeta}{\partial t} + \frac{\partial hu}{\partial x} + \frac{\partial hv}{\partial y} = 0 \tag{B.4a}$$

$$\frac{\partial \overline{u}}{\partial t} + \overline{u}\frac{\partial \overline{u}}{\partial x} + \overline{v}\frac{\partial \overline{u}}{\partial y} = \frac{\overline{F}_x}{\rho h} \tag{B.4b}$$

$$\frac{\partial \overline{v}}{\partial t} + \overline{u}\frac{\partial \overline{v}}{\partial x} + \overline{v}\frac{\partial \overline{v}}{\partial y} = \frac{\overline{F}_y}{\rho h} \tag{B.4c}$$

where $\overline{F}_i$ is the forcing term in i-direction in which all forcing terms are combined: pressure gradient; bottom friction; wave stresses; etc.

In this study, two types of boundary conditions are used: (1) water level boundary; and (2) Neumann boundary. Therefore, only these two boundary types are highlighted here. Nevertheless, there are more possible boundary types in D-Flow.

Water level boundary The water level boundary is used to simulate the tide. In this case, the water level boundary in D-Flow is the sum of the tidal constituents:

$$\zeta = \sum_{i=1}^{N} \hat{\zeta}_i \cos\left(\omega_i t - \phi_i\right) \tag{B.5}$$

where ζ is the water level elevation with respect to the reference level, here mean sea level; $\hat{\zeta}_i$ the water level elevation of tidal component i; ω_i the angular frequency of component i; and ϕ_i the phase of constituent i.

Neumann boundary The Neumann boundary condition specifies the water level gradient perpendicular to the open boundary it is imposed on. This results in a flexible boundary condition through which water is allowed to flow, and the water level moves freely along the boundary. The Neumann boundary condition in this study is specified as:

$$\frac{\partial \zeta}{\partial \mathbf{n}} = 0 \tag{B.6}$$

where $\mathbf{n}$ is the inward-positive normal vector.

B.1.2 D-Waves

In Delft3D Flexible Mesh (D3D-FM), D-Waves is the wave module that is used to simulate the evolution of short-crested wind-generated waves. This module makes use of SWAN—Simulating WAves Nearshore—that is developed by Delft University of Technology [Booij et al., 1999]. This section briefly highlights the governing equations of D-Waves; i.e. SWAN.

In SWAN, the wave energy is translated to the wave action:

$$N = \frac{E}{\omega} \tag{B.7}$$

where N is the wave action; E the wave energy; and ω the wave frequency.

The evolution of the wave spectrum is described by the spectral action balance in which the wave action is conserved:

$$\frac{\partial N}{\partial t} + \frac{\partial c_x N}{\partial x} + \frac{\partial c_y N}{\partial y} + \frac{\partial c_\sigma N}{\partial \sigma} + \frac{\partial c_\theta N}{\partial \theta} = \frac{S}{\sigma} \tag{B.8}$$

where c_i is the propagation velocity in i-direction: x and y propagation in geographical space, σ depth- and current-induced shifting of the relative frequency, and θ refraction due to depth and current variations; and S is the source term in which the effects of generation, dissipation and non-linear wave-wave interactions are included. The source term is the summation of all three contributors:

$$S = S_{in}(\sigma, \theta) + S_{ds}(\sigma, \theta) + S_{nl}(\sigma, \theta) \tag{B.9}$$

where S_{in} is the contribution of wind input; S_{ds} the contribution due to wave dissipation; and S_{nl} the contribution due to non-linear wave-wave interactions.

The dissipation of waves consists of three different processes: (1) white-capping; (2) bottom friction; and (3) depth-induced wave breaking. These contributions are also summed:

$$S_{ds}(\sigma, \theta) = S_{ds,w}(\sigma, \theta) + S_{ds,b}(\sigma, \theta) + S_{ds,br}(\sigma, \theta) \tag{B.10a}$$

where $S_{ds,w}$ represents the white-capping; $S_{ds,b}$ the bottom friction; and $S_{ds,br}$ the wave breaking. These contributions are given by:

$$S_{ds,w}(\sigma, \theta) = -\Gamma \tilde{\sigma} \frac{k}{\tilde{k}} E(\sigma, \theta) \tag{B.10b}$$

where Γ is the steepness dependent coefficient; k the wave number; and $\tilde{\sigma}$ and $\tilde{k}$ the mean frequency and wave number, respectively.

$$S_{ds,b}(\sigma, \theta) = -C_{bottom} \frac{\sigma^2}{g^2 \sinh^2(kh)} E(\sigma, \theta) \tag{B.10c}$$

where C_{bottom} is a bottom friction coefficient.

$$S_{ds,br}(\sigma, \theta) = -\frac{D_{tot}}{E_{tot}} E(\sigma, \theta) \tag{B.10d}$$

where D_{tot} is the rate of dissipation of the total energy due to wave breaking, which heavily depends on the breaking parameter that is defined as:

$$\gamma = \frac{H_{\max}}{h} \tag{B.11}$$

where $H_{\max}$ is the maximum wave height.

B.2 Online coupling

The coupling between D-Flow and D-Waves occurs within the Delft3D Flexible Mesh (D3D-FM) environment. Both modules write essential output to the communication file. The effects of waves on the flow are included by adding the wave-induced forces to the horizontal momentum equations. These wave-induced forces are based on the so-called radiation stresses:

$$F_x = -\frac{\partial S_{xx}}{\partial x} - \frac{\partial S_{xy}}{\partial y} \tag{B.12a}$$

$$F_y = -\frac{\partial S_{yy}}{\partial y} - \frac{\partial S_{yx}}{\partial x} \tag{B.12b}$$

where S_{ij} are the radiation stresses.

The online-coupling between the different modules—D-Flow, D-Waves and the biophysical model framework (BMF) developed in this study—are made via a Python-script. For all packages and functions to work correctly, a special environment is created in Python in which the following settings are used:

- Python version 3.6.5
- NumPy version 1.14.3
- SciPy version 1.1.0
- NetCDF4 version 1.4.2
- Matplotlib version 2.2.2
- BMI-Python

Other versions might result in errors and thus should not be used. For BMI-Python to work, the `bmi.wrapper` package has to be downloaded[1] and installed. In some cases, the NetCDF4 package has to be downloaded[2] and installed as well; if not done by default.

B.3 Hydrodynamic model design

B.3.1 Bathymetry

The design of the hydrodynamic model represents a fringing reef, which is uniform in the alongshore direction. The bathymetry of the D-Flow domain is extended and used in the full D-Waves domain, which is much larger. The domain of D-Waves is much wider to limit the influence of the boundaries in the region of interest; because the waves have a spreading, the waves flattens at the boundaries of the domain. There are two solutions to counteract this problem: (1) impose the same boundary conditions at these boundaries as at the boundary at open sea; and (2) make the domain of D-Waves sufficiently wide that this effect dampens out in the region of interest.

Due to the shallowness of the reef flat, the boundary conditions could not be added to all boundaries of the domain as this would result in instabilities during storm events. Therefore, the domain of the D-Waves must be widened sufficiently to reduce the effect of the boundaries to a minimum.

Inside the region of interest—i.e. the domain of D-Flow—nine observation stations are placed at equal distance in the centre (*see* Fig. B.1).

B.3.2 Boundary conditions

The boundary conditions are specified by three types: (1) the tide via fluctuations in the water level in D-Flow; (2) Neumann boundary condition in D-Flow; and (3) a wave-spectrum in D-Waves. Both the tidal boundary condition and the wave spectrum are imposed on the southern boundary, and the northern boundary is closed; i.e. a land boundary. The tide is simplified to a simple tidal signal consisting of only the M_2-component with a tidal range of two metres. The wave spectrum differs due to storms, and the characteristic values are specified in Appendix C.2.

On both the western and eastern boundaries the Neumann boundary condition is imposed; as defined in Equation (B.6). This boundary condition is used to reduce the effects of nesting the D-Flow domain into the D-Waves domain.

[1] Download the `bmi.wrapper` package from https://github.com/openearth/bmi-python.
[2] Download the `netcdf4` package from http://www.ldf.uci.edu/~gohlke/pythonlibs/#netcdf4.

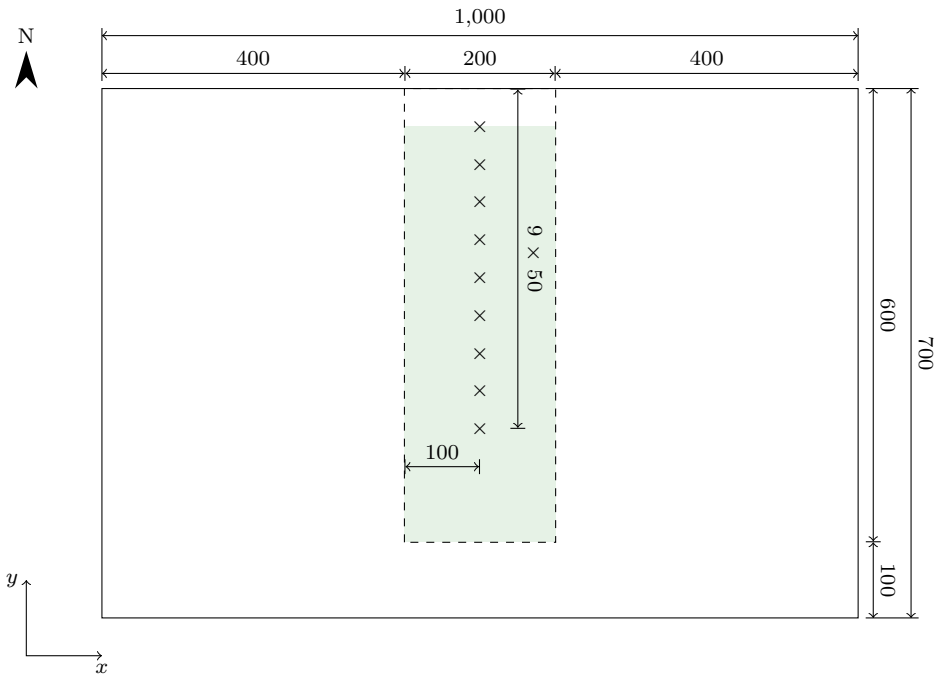

(a) Plan view.

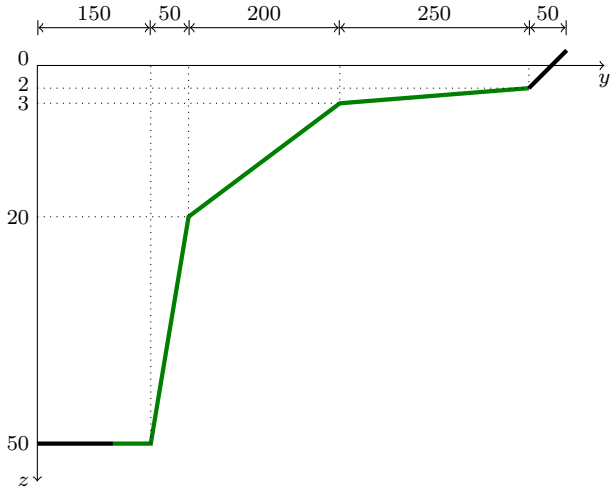

(b) Side view.

Figure B.1: Design of the hydrodynamic model. All measures are given in metres. **(a)** Plan view of the hydrodynamic model design. The observation stations are indicated by a cross (×) and are labelled ascending from South to North. The smaller domain marked with the dashed lines is the domain of D-Flow, and the larger domain is of D-Waves. The area in which corals can grow is shaded green. **(b)** Side view of the hydrodynamic model. The bottom profile is represented by the thick, black and green line, where the green line indicates the section on which corals can grow; the water level follows the y-axis. The bottom profile is uniform in alongshore direction; i.e. in x-direction.

Appendix C

Artificial time-series

The coral development is modelled using artificial time-series, which are partly based on the statistics of time-series of coral reef sites; partly on literature. There are multiple time-series, which are all discussed here. Every environmental factor included in the biophysical model framework (BMF) has its corresponding time-series.

All four time-series are presented in Figure C.1 and elaborated on in:

- Appendix C.1: Light conditions
- Appendix C.2: Hydrodynamic conditions
- Appendix C.3: Thermal conditions
- Appendix C.4: Acidic conditions

C.1 Light conditions

This section is largely based on ITACA [2018]. The incoming light is based on the orbit of the Earth and is a function of the latitude, ϕ. The function on the solar insolation is used:

$$\overline{Q}^d = \frac{S_0}{\pi}\frac{R_0^2}{R_E^2}\left[h_0 \sin(\phi)\sin(\delta) + \cos(\phi)\cos(\delta)\sin(h_0)\right] \tag{C.1}$$

in which

$$\delta = \epsilon \sin(\theta) \tag{C.2}$$

where θ depends on the time of the *vernal equinox*, which is on March 20 or 21. Therefore, one could say it is on "March 20.5". This is day number 79.75 of the year[1] and is defined to give $\theta = 0$. Therefore, the inclination of the sun can be rewritten as function of the number of the day of the year:

$$\delta = \epsilon \sin\left(2\pi\left[\frac{n - n_0}{365.25}\right]\right) \tag{C.3}$$

where n_0 is the day number of the vernal equinox (i.e. $n_0 = 79.75$). Thus, one could state that the polar angle of the Earth's surface is given by:

$$\theta = 2\pi\left(\frac{n - n_0}{365.25}\right) \tag{C.4}$$

[1] Assuming February has 28.25 days, which takes the effects of leap years into account as well.

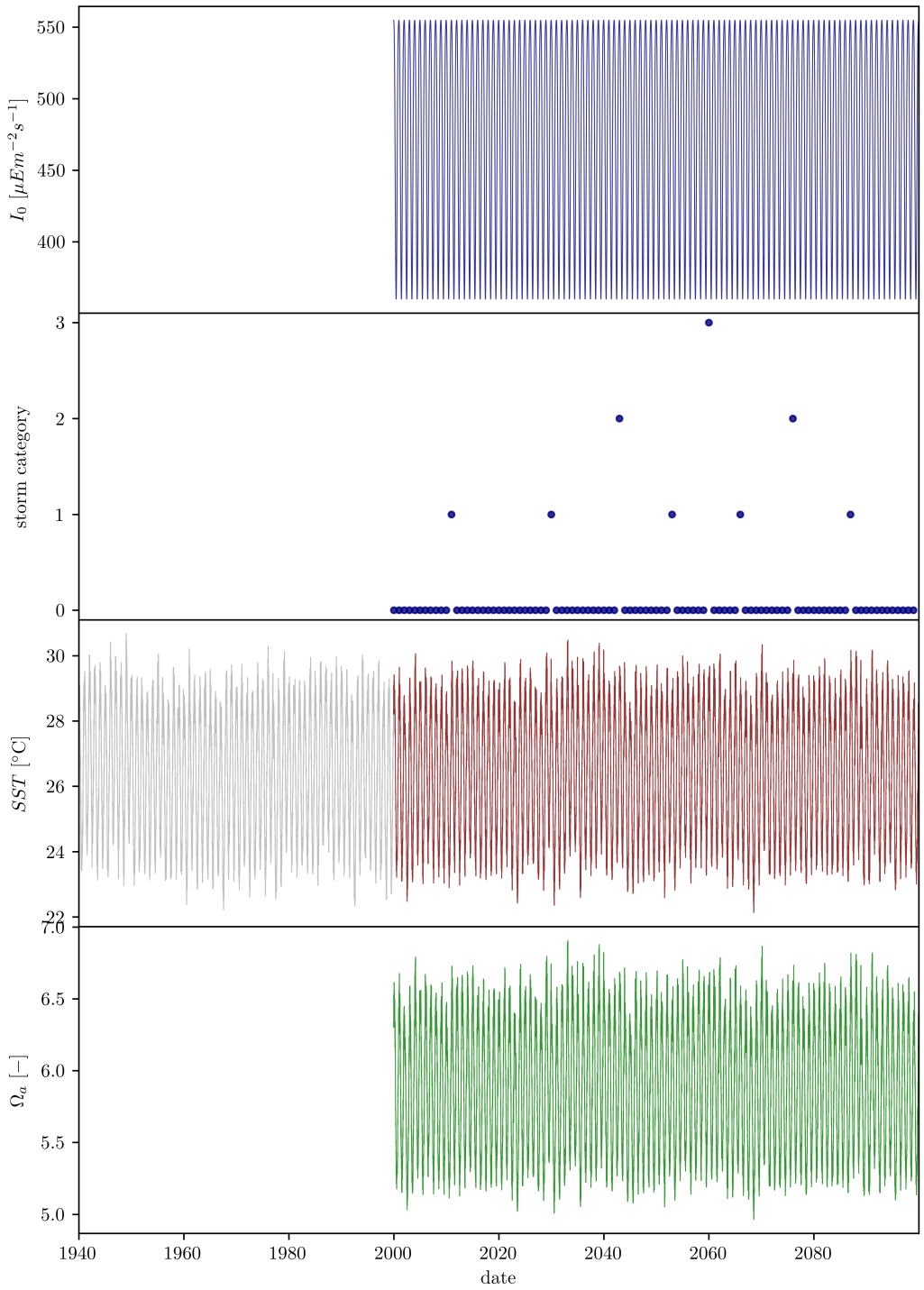

Figure C.1: Artificial time-series for environmental factors. In color are the time-series over the period simulated. In gray, the time-series needed for the thermal-acclimatisation. The storm categories are defined in Table C.1.

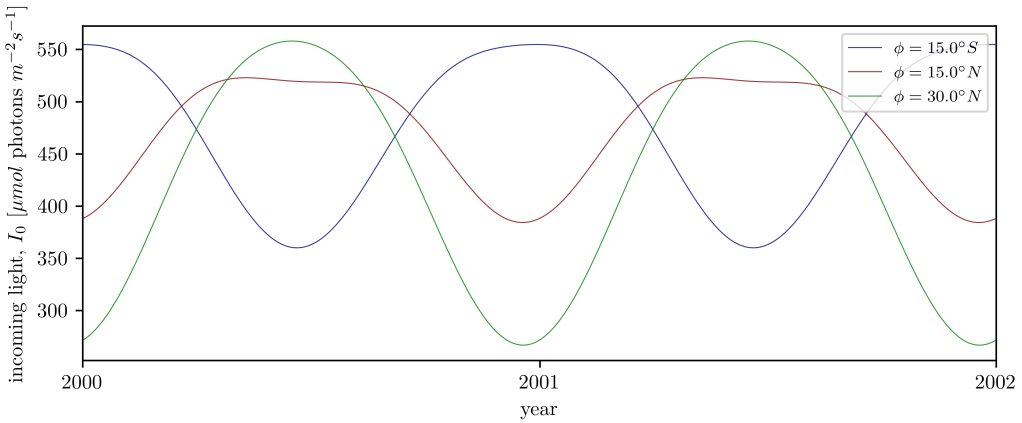

Figure C.2: Artificial light time-series for different latitudes. Three latitudes are presented in which the difference between northern and southern hemisphere is shown, and the difference between the absolute value of the latitude.

Furthermore, $\epsilon = 23.4398°$ and for the elliptical orbit holds:

$$\frac{R_0}{R_E} = 1 + e\cos(\theta - \overline{\omega}) \tag{C.5}$$

where e is the eccentricity ($e = 0.016704$); and $\overline{\omega}$ the longitude of perihelion ($\overline{\omega} = 282.895°$). Moreover, the hour angle is given by:

$$h_0 = \begin{cases} 0 & \text{for } \tan(\phi)\tan(\delta) < -1 \\ \cos^{-1}\left[-\tan(\phi)\tan(\delta)\right] & \text{for } -1 \leq \tan(\phi)\tan(\delta) \leq 1 \\ \pi & \text{for } \tan(\phi)\tan(\delta) > 1 \end{cases} \tag{C.6}$$

Note that the obliquity (ϵ) and the eccentricity (e) vary over time as well, in the order of centuries to millennia. This relatively small change is not taken into account as only a time-series of 100 years is used.

Finally, the solar constant is translated into the photosynthetically active radiation (PAR) solar constant. This value is approximately $S_0 \approx 350.0\ Wm^{-2}$ [Agrawal, 2010]; rewritten to the unit used in this study yields $S_0 \approx 1600\ \mu mol$ photons $m^{-2}s^{-1}$. As indication of the fluctuating light-conditions, Figure C.2 presents the annual fluctuations of incoming light at three different latitudes.

C.2 Hydrodynamic conditions

As the dislodgement criterion is only met during storm conditions, the hydrodynamics of the 'no-storm' conditions—i.e. the 'normal' conditions—are based on one representative wave climate. This wave climate is representative for the hydrodynamics throughout the year with the exception of storms. The storm conditions are categorised based on their severity.

The hydrodynamic conditions are described in terms of offshore wave conditions and the tide. The tide consists only of a simple M_2-tide, which is maintained under both 'normal' conditions and storm conditions. The offshore wave conditions are expressed in terms of significant wave height and the peak period.

The different representative wave conditions for coral reefs are based on literature [e.g. Madin, 2004, 2005; Massel and Done, 1993; Hongo et al., 2012] and ranked by their return period as presented in Table C.1.

Table C.1: Offshore wave conditions per return period. The return period of the 'normal' conditions is left empty as these are the wave conditions in the absence of storms.

Storm category		Return period R $[yrs]$	Significant wave height H_s $[m]$	Peak wave period T_p $[s]$
0	normal	n/a	1.2	4.0
1	severe storm	10	2.0	4.0
2	tropical storm	50	3.5	5.0
3	extreme storm	100	4.0	6.0

These return periods are used to determine whether a storm hits the reef, or not. For this, the return period is rewritten in a probability of occurrence:

$$P_i = \frac{1}{R_i} \tag{C.7}$$

where P_i is the probability of storm i to occur with the return period R_i. Note that the 'normal' conditions prevail in the absence of storms and so has a probability of occurrence of 100%.

A storm hits the reef when a random sampled number between zero and one is below the determined probability of the storm. The largest storm is leading and smaller category storms are not modelled as corals surviving the larger storm, will also remain attached during a smaller storm:

$$[H_s, T_p] = [H_{s,i}, T_{p,i}] \quad \text{if} \quad P_{i+1} < \mathcal{U}(0,1) \leq P_i \tag{C.8}$$

where $[H_{s,i}, T_{p,i}]$ are the offshore wave conditions of storm i; $i = 0$ indicates the 'normal' conditions; $\mathcal{U}(0,1)$ is the Uniform distribution between zero and one; and the upper and lower limits are given by $P_0 = 1$ and $P_{N+1} = 0$ with N storm types.

After every storm, the 'normal' conditions are used to determine the new flow and wave fields in which the morphology is modified including the storm damage. This results in a time-series of storm categories. In case a storm hits the coast—i.e. a storm category of 1 or higher—it is always followed by a storm category 0; the normal conditions. Therefore, the time-series consists in general of more wave specifications than the amount of years it covers.

The time-series consisting of the storm categories is translated to a time-series on the wave conditions, as specified in Table C.1. These conditions are fed to the hydrodynamic model. The hydrodynamic model simulates twelve hours to get a representative flow field. Reducing the simulation time results in substantial discrepancies for the mean water depth (*see* Fig. C.3) and the mean and maximum bulk flow velocity (*see* Fig. C.3) on the reef flat. Both are assigned to the fact that the M_2 tidal signal results in approximately a full tidal wave every twelve hours. This tidal signal mainly determines the mean water depth. As the flow velocity is related to the water depth, these mismatches are translated to the flow velocities as well.

However, a small bias towards lower values for the maximum bulk flow velocity comes in when a model run time of twelve hours is used. Therefore, storms are simulated for a full day—i.e. 24 hours—and for the 'normal' conditions, a simulation period of twelve hours is used. As the maximum bulk flow velocity is only of importance for the dislodgement criterion, the 'normal' conditions are based on the model run time of twelve hours to accelerate the model.

C.3 Thermal conditions

The thermal conditions are based on sea surface temperature (SST) data from the NOAA OI SST V2 High Resolution Dataset[2] (hereafter referred to as "NOAA data set") [Reynolds et al., 2007]. This data set covers daily mean SST values from September 1981 onwards and has a spatial resolution of $0.25° \times 0.25°$.

[2]NOAA High Resolution SST data provided by the NOAA/OAR/ESRL PSD, Boulder, Colorado, USA, from their Web site at https://www.esrl.noaa.gov/psd/.

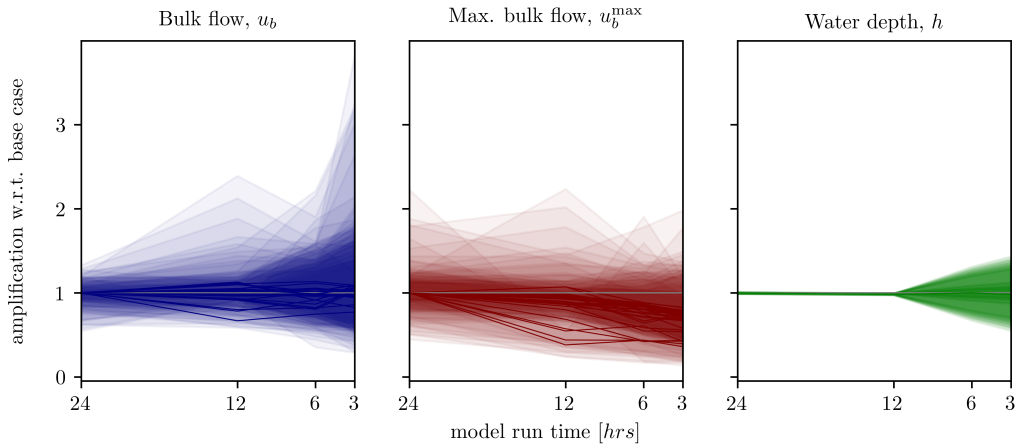

(a) Relative difference with respect to base case.

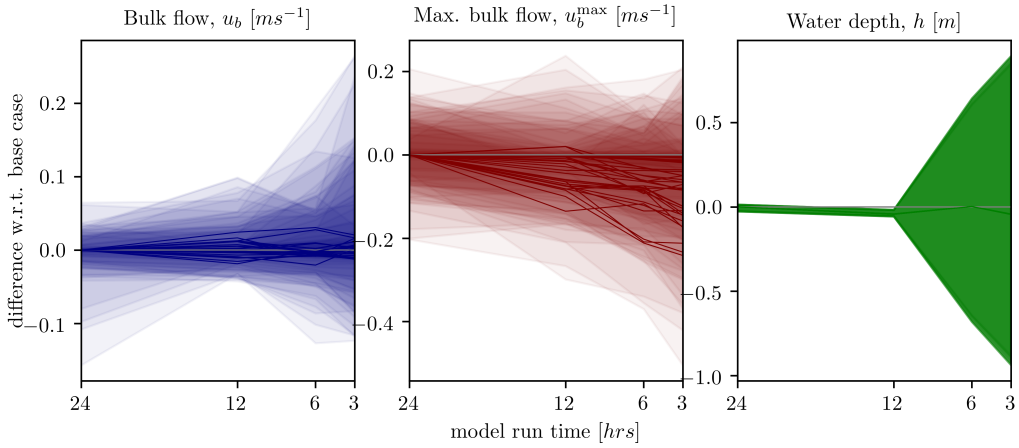

(b) Absolute difference with respect to base case.

Figure C.3: Hydrodynamic output differences due to representative hydrodynamic model run time. Solid lines represent the mean values per observation station (*see* Fig. B.1a) and the shadings indicate the minimum and maximum values at those stations.

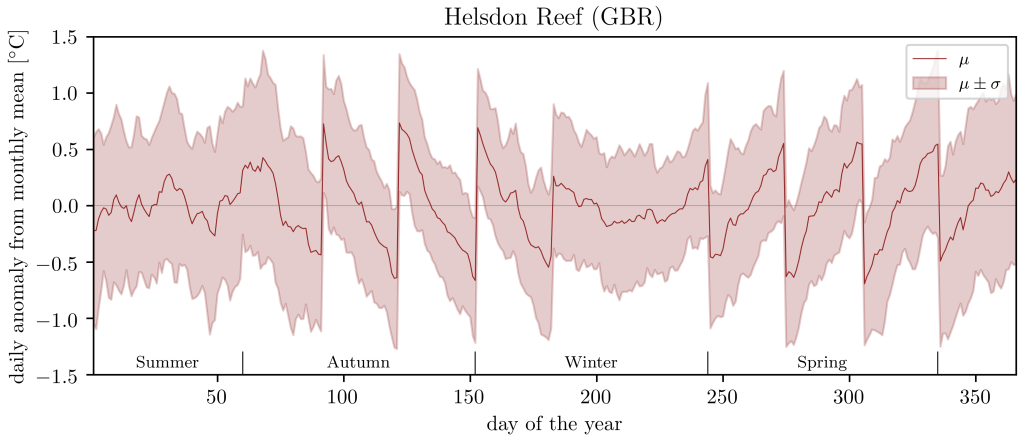

Figure C.4: Daily anomalies with respect to the monthly mean at Helsdon Reef, Great Barrier Reef. The reference temperature (i.e. the monthly mean) changes every month resulting in clear differences in the daily statistics with respect to the monthly means.

From this daily data, statistics are retrieved on which the artificial time-series is based. The artificial time-series for a given latitude and longitude follows the following principle:

$$\widetilde{T} = \underbrace{\mu_T + \mathcal{N}\left(\mu'_y, \sigma'_y\right)}_{\text{annual}} + \underbrace{\mathcal{N}\left(\mu'_m, \sigma'_m\right)}_{\text{monthly}} + \underbrace{\mathcal{N}\left(\mu'_d, \sigma'_d\right)}_{\text{daily}} \tag{C.9}$$

where $\widetilde{T}$ is the predicted SST; μ_T the average temperature throughout the NOAA data set; and $\mathcal{N}$ a normal distribution based on:

- μ'_y and σ'_y, which are the mean and standard deviation of the annual fluctuations to the overall mean. Herein, the first two terms on the right-hand side are combined in the script, representing the annual fluctuations of annual mean temperature as the mean of the annual fluctuations is equal to zero; i.e. $\mu'_y = 0$, and the annual fluctuations are given by $\mathcal{N}\left(\mu_T, \sigma'_y\right)$.
- μ'_m and σ'_m, which are the mean and standard deviation of the monthly fluctuations to the annual mean. Note that the monthly anomalies are based on the difference between the monthly means of year Y and the annual mean of year Y. Based on this, for every month in the year a match of mean and standard deviation is derived.
- μ'_d and σ'_d, which are the mean and standard deviation of the daily fluctuations to the monthly means. Note that the daily anomalies are based on the difference between the daily means of month M and year Y and the monthly mean of month M and year Y. Based on this, for every day of the year a match of mean and standard deviation is derived. That there is a daily bias compared to the monthly mean is shown in Figure C.4.

This method is used to include consistency throughout the year and month on the thermal conditions. Thereby, the seasons are well-represented in the artificial SST time-series.

For this, the statistics as given in Equation (C.9) have to be retrieved from the NOAA data set. This is accomplished by decomposing the SST signal step by step:

1. The annual means are calculated of which the mean and standard deviation are determined.
2. The monthly means are calculated for all years of the NOAA data set. The annual means are subtracted from the monthly means, which results in a monthly time-series of monthly SST anomalies

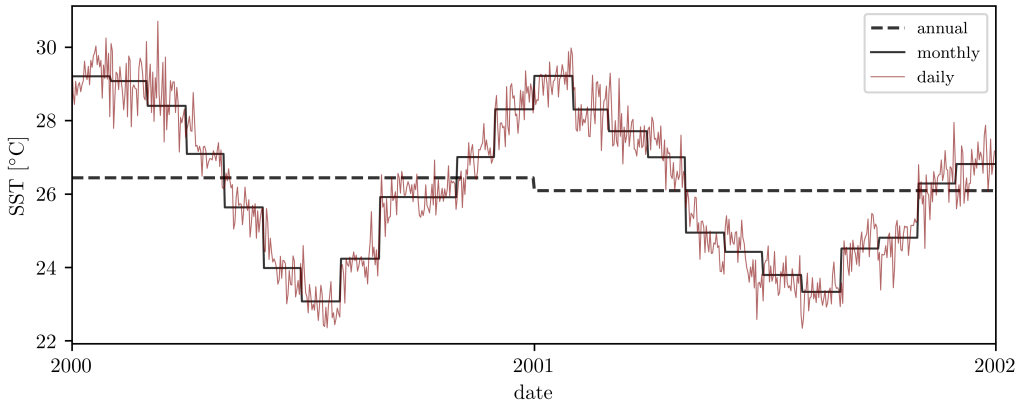

Figure C.5: Construction method of the artificial SST time-series. The various components from Equation (C.9) are plotted separately. Note that the time-series is applicable to the southern hemisphere as summer is around new year.

with respect to their corresponding annual mean. Based on this time-series, the mean and standard deviation per month are determined.

3. The NOAA data set consists of daily means, which are subtracted by their corresponding monthly means to retrieve the daily anomalies with respect to the monthly fluctuations. Based on these anomalies, daily means and standard deviations are determined for every day of the year as these change within the month (*see* Fig. C.4).

The construction of the artificial SST time-series follows comparable steps:

1. The annual means are based on the annual Normal distribution ('annual' in Eq. C.9).
2. The monthly anomalies with respect to the annual mean are based on the monthly Normal distribution ('monthly' in Eq. C.9) and added to the annual means.
3. The daily anomalies with respect to the monthly mean are based on the daily Normal distribution ('daily' in Eq. C.9) and added to the monthly absolute means.

The contribution of every step is visualised in Figure C.5 for two years. This methodology shows good comparison between the artificial SST time-series and the original SST time-series from the NOAA data set.

C.4 Acidic conditions

The acidic conditions are expressed in a time-series of the aragonite saturation state. The acidity of the water is kept constant at levels representative for today: $p\mathrm{H} = 8.0$ [e.g. Chan et al., 2016; Hall-Spencer et al., 2008; Manzello et al., 2008]. Also the salinity and the atmospheric carbon dioxide (CO_2) pressure are kept constant ($S = 35\ PSU$ and $p\mathrm{CO}_2 = 400$ ppm [e.g. Anthony et al., 2011]), and so the aragonite saturation state becomes a function of the temperature alone (*see* Eqs. 4.58 to 4.60, and Tab. 4.2). As the aragonite saturation state is reduced to a function to the thermal conditions alone, the associated time-series follows the same pattern as well (*see* Fig. C.1).

Appendix D

Sensitivity analysis

The sensitivity analysis addresses the separate processes individually to define the dominant parameters. These dominant parameters are eventually used for a sensitivity analysis of the full model. This screening of the parameters is (1) to reduce computational time; and (2) to retrieve a clear overview of the importance of all the parameters contributing to the dynamics associated with corals.

The sensitivity analyses are performed systematically in which uniformity is preserved throughout for better comparison between the modular analyses. This includes the same formatting of the figures throughout and additional clarifications are provided if need be.

This appendix starts with a brief description on the method used for the sensitivity analysis (App. D.1) after which the modular analyses are discussed (Apps. D.2 to D.6). This appendix concludes with the sensitivity analysis of the full model on key parameters (App. D.7).

D.1 Methodology

Two types of parameters are used for the sensitivity analysis: (1) model parameters; and (2) input parameters. The sensitivity of the model parameters are assessed over a range of the input parameters because of many non-linear relationships. Thereby, the sensitivity analysis is not (partly) determined by the choice of environmental conditions, which can change the results.

The sensitivity of the input parameters can be assessed based on the gradient over which they are presented. This gives an indication of the required data accuracy for these parameters. The sensitivity of model parameters is determined based on a deviation of ten per cent from the estimate.

The outcomes are expressed in relative sense and in absolute sense if clarifying. The relative difference is defined by:

$$\Delta_R = \frac{\widetilde{E} - E}{E} \tag{D.1}$$

where $\widetilde{E}$ is the estimate based on the 10% deviation (added or subtracted); and E the estimate.

The absolute differences—if taken into account—are defined by the difference between the result based on the 10% deviation and the result based on the estimates:

$$\Delta_A = \widetilde{E} - E \tag{D.2}$$

Table D.1: Representative coral morphologies used in the sensitivity analysis. Both methods to describe the morphologies are used: (1) the morphological ratios in combination with the coral volumes; and (2) the absolute morphological dimensions.

morphology	Ratios				Dimensions			
	r_f [−]	r_p [−]	r_s [−]	V_c [m^3]	d_c [m]	h_c [m]	b_c [m]	t_c [m]
branching	5.0	0.5	0.3	0.005	0.1	0.6	0.05	0.3
massive	1.0	0.9	0.6	0.050	0.4	0.4	0.36	0.36
plate	0.2	0.1	0.5	0.050	1.4	0.3	0.14	0.03

Table D.2: Parameters determining the representative light-intensity. r_f is the coral form ratio, or the height-to-diameter ratio; r_p the plate ratio, or the base-to-diameter ratio; V_c the volume of the coral, which is a proxy of its size; K_d the light-attenuation coefficient (LAC); I_0 the incoming light-intensity; and h the water depth.

	Parameter	Estimate	Deviation	Unit
model	r_f	*see* Tab. D.1	10%	−
	r_p			−
	V_c			m^3
input	K_d	0.10–0.90	n/a	m^{-1}
	I_0	400–800		μmol photons $m^{-2}s^{-1}$
	h	2.0–40.0		m

D.2 Coral environment

Three representative morphologies are used for the assessment on the coral environment: (1) branching; (2) massive; and (3) plate. Table D.1 lists the morphological ratios as well as the dimensions. The morphologies analysed are relatively large to amplify the effects of the morphology, as deviations of the morphologies of smaller corals do not result in notable changes. Orders of magnitude of the sizes of the morphologies used in this sensitivity analysis are decimetres to metres (*see* Tab. D.1).

This section contains the modular sensitivity analyses of:

- the representative light-intensity in Appendix D.2.1;
- the in-canopy flow structure in Appendix D.2.2; and
- the thermal micro-environment in Appendix D.2.3.

D.2.1 Representative light-intensity

The estimates of all considered parameters are presented in Table D.2. Figure D.1 presents the results for all three morphologies.

From Figure D.1 becomes clear that the representative light-intensity is most sensitive to deviations for branching coral colonies, which cover a larger vertical gradient. This also explains the sensitivity of the representative light-intensity for higher values of the light-attenuation coefficient (LAC). For high LACs, the gradient in light-intensity over depth steepens and thus deviations on the height of the coral result in larger differences (*see* Figs. D.1a to D.1c, top rows).

A comparable effect is visible for the plate ratio—i.e. base-to-diameter ratio—where the error grows for increasing values of the LAC (*see* Figs. D.1a to D.1c, middle rows). This is related to the definition included in the spreading of the light (*see* Eq. 4.5), which exponentially decays over depth.

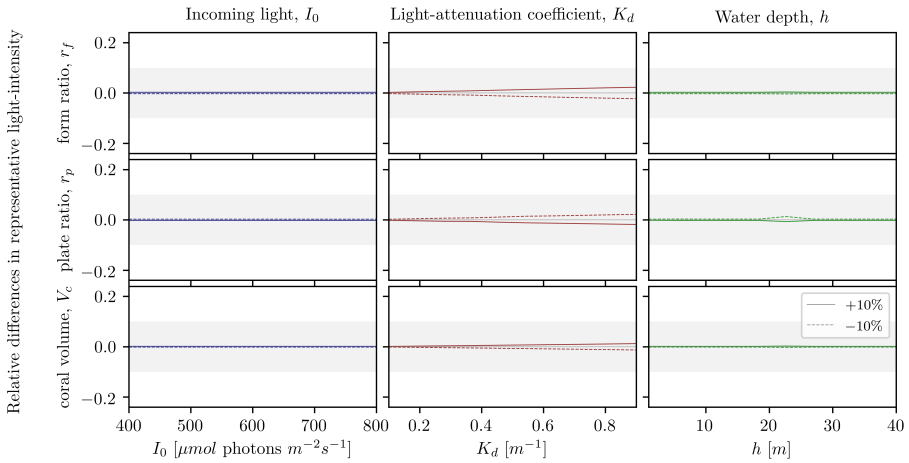

(a) Branching morphology.

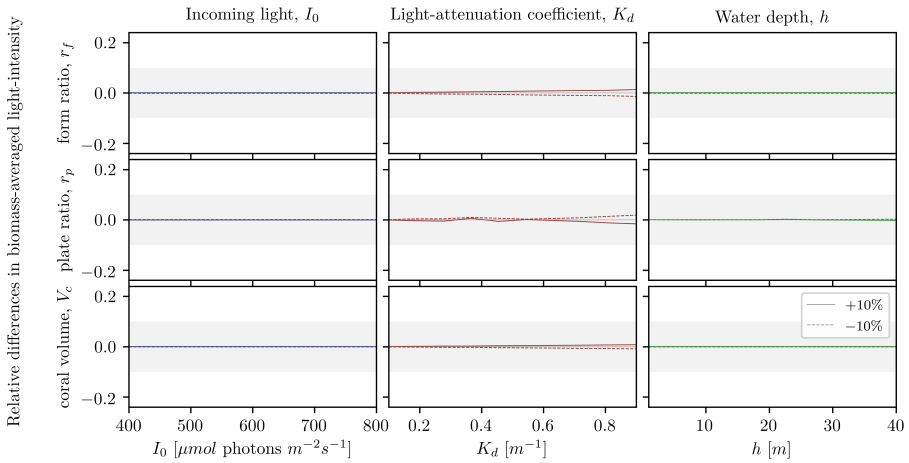

(b) Massive morphology.

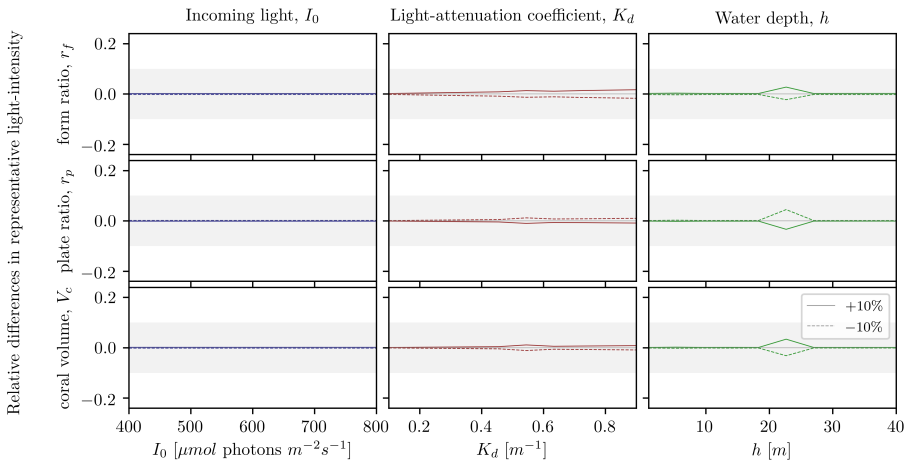

(c) Plate morphology.

Figure D.1: Sensitivity analysis of the representative light-intensity for three morphologies. (a) branching; **(b)** massive; and **(c)** plate. The sensitivity of the parameters is expressed as relative difference in representative light-intensity compared to the estimate (*see* Eq. D.1 and Tab. D.2). The gray-shaded area marks the threshold difference comparable to the imposed deviation; i.e. the 10% mark.

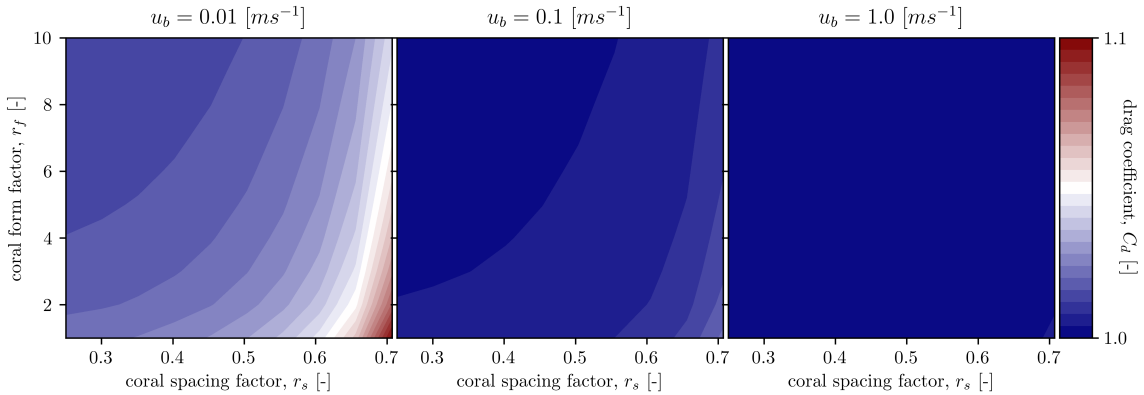

Figure D.2: The drag coefficient as a result of flow velocity and coral morphology. The bulk flow velocities increase logarithmic (given as plot-titles), and the morphological ratios are given on the axes: the coral spacing ratio (r_s) on the horizontal axis; and the coral form ratio (r_f) on the vertical axis.

All in all, the representative light-intensity is relatively insensitive to the morphological ratios and is mainly determined based on (1) the incoming light; (2) the light-attenuation coefficient (LAC); and (3) the water depth.

D.2.2 Flow structure

The drag coefficient as determined following van Rooijen et al. [2018] is close to one for cylinders in higher Reynolds numbers (*see* Eq. 4.24) [White, 2006]. These higher Reynolds numbers are easily achieved as an effect of the canopy. Furthermore, when the drag coefficient is high, the flow velocities are low and so the drag force is low as well, which is dominated by the flow velocity. Hence, the drag force is described as a quadratic function of the flow velocity (*see* App. E.2.2).

The close to independency of the drag coefficient to the staggered arrangement of the cylinders is clearly visible in Figure D.2, where only for very low bulk flow velocities the drag coefficient increases for certain morphological ratios. Moreover, even when the drag coefficient differs from one, it is a small deviation of around ten per cent ($\approx 10\%$). These small changes in the drag coefficient as a function of the canopy structure also hold for the two-layer canopy, where the drag coefficients computed to determine the layered wave-attenuation coefficient (WAC) are all in the same range as in Figure D.2.

The sensitivity analysis of the WAC is taken as function of the above-canopy flow (u_f), and the wave period (T). As model parameters, the morphological ratios, the coral volume and the two of the three coefficients are used: (1) inertia coefficient; and (2) Smagorinsky coefficient. The determination of the drag coefficient is part of the iterative search to the WAC. An overview of the used values and ranges is presented in Table D.3.

The results of the sensitivity analysis are displayed in Figure D.3 (pp. 147–149) from which it becomes clear that the spacing ratio (r_s) is the most important parameter in the determination of the WAC, and so the flow structure in the canopy. This is most pronounced for the massive morphology and then the plate morphology (*see* Figs. D.3b and D.3c, third row), while the branching morphology's deviation of the WAC due to the spacing ratio remains within agreeable limits (*see* Fig. D.3a); i.e. the deviation is less than 10%. The other two morphological ratios are of less importance; except for the massive morphology in which the plate ratio plays a major role on the WAC as well (*see* Fig. D.3b, second row).

From this, it becomes clear that the WAC is largely dependent on the space available in the canopy for the flow, whereas the combination of the spacing ratio and the plate ratio describes this void ratio. The height of the canopy does not play a significant role on the attenuation directly, but implicitly it does via the above-canopy flow. As the relative canopy height—relative to the water depth—increases, less space

Table D.3: Parameters determining the wave-attenuation coefficient. r_f is the coral form ratio, or the height-to-diameter ratio; r_p the plate ratio, or the base-to-diameter ratio; r_s the spacing ratio, or the diameter-to-axial distance ratio; V_c the volume of the coral, which is a proxy of its size; C_m the inertia coefficient; C_s the Smagorinsky coefficient; u_b the bulk flow velocity; T the wave period; and h the water depth.

	Parameter	Estimate	Deviation	Unit
model	r_f	*see* Tab. D.1	10%	–
	r_p			–
	r_s			–
	V_c			m^3
	C_m	1.7		–
	C_s	0.1		–
input	u_b	0.01–1.00	n/a	ms^{-1}
	T	3.0–90.0		s
	h	2.0–20.0		m

becomes available above the canopy, which forces more water through the canopy and the above-canopy flow velocity increases as well.

Furthermore, the sensitivity of the WAC to the coral volume is negligible (*see* Fig. D.3, fourth row). Deviations in the inertia coefficient result in some errors in the WAC as well (*see* Fig. D.3, fifth row). This difference in sensitivity of the WAC indicates an inertia-dominated situation. When the wave period is taken over a larger range[1]—e.g. up to two minutes—the change from inertia dominated towards the unidirectional domain becomes clear as the WAC becomes more sensitive to the Smagorinsky coefficient, which is negligible for short waves. Nevertheless, the sensitivity of the WAC on both coefficients is limited as the relative deviation of the WAC is less than the imposed deviation on this coefficient.

The sensitivity of the WAC on the model parameters remains constant over the ranges of the input parameters—i.e. the bulk flow velocity, the wave period and the water depth—in most cases (*see* Figs. D.3a to D.3c). This is rather illusive—especially in case of the flow velocity and the wave period—as Figure D.3 presents the *relative* differences. The *absolute* differences over the ranges of these input parameters result in substantial deviations (not shown). Thus, the WAC does change as a function of the above-canopy flow as well as the wave period, but the relative error due to deviations in the model parameters is close to insensitive to these quantities; i.e. there is an insignificant non-linearity between the input parameters and the model parameters.

The water depth does not impose substantial changes on the in-canopy flow structure until the canopy gets close to be emergent instead of submerged. It is then that the form ratio (r_f) starts to play a minor role as well, for the same reason; deviations in the form ratio result in deviations in the level of submergence of the canopy, which affects the in-canopy flow structure when close to emergence.

D.2.3 Thermal micro-environment

The relative increase in temperature at the coral-water interface is based on the presence of a thermal boundary layer (TBL). The thickness of the TBL is again related to the thickness of the velocity boundary layer (VBL) (*see* Eq. 4.32). Herein, also three 'constants' are included, which are officially dynamic: (1) the kinematic viscosity of water, ν; (2) the thermal diffusivity of water, α; and (3) the thermal conductivity of water, k. Therefore, these constants are also taken into account. An overview of all the parameters included in the sensitivity analysis is presented in Table D.4.

[1]The longer waves pose problems as the iterative solver of the complex equations for the determination of the WAC (*see* App. E.3) does not unconditionally converge. The solver used is the `newton` function of the package `scipy` with the sub-package `optimize` in Python 3.7. The iterations are solved according the Newton-Raphson method (more information: https://docs.scipy.org/doc/scipy/reference/generated/scipy.optimize.newton.html). This method is very powerful, especially for complex functions. Unfortunately, it does not always converge. This problem of converges is not present for a single-layer canopy, but only for the multi-layer canopy forced with long waves.

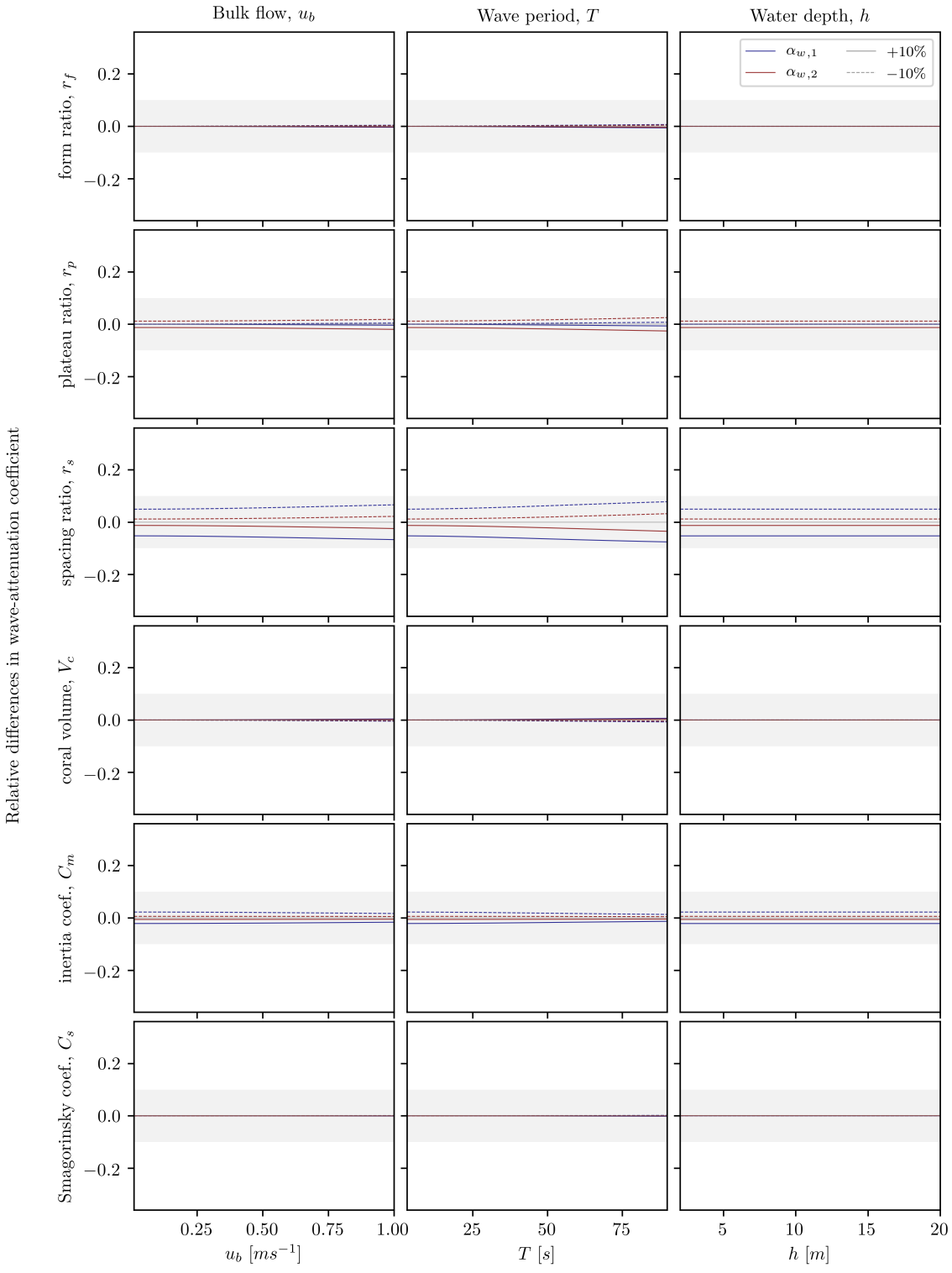

(a) Branching morphology.

Figure D.3: Sensitivity analysis of the flow structure for three morphologies represented by the wave-attenuation coefficient. (a) branching; **(b)** massive; and **(c)** plate. The sensitivity analysis of the parameters is expressed as relative difference in wave-attenuation coefficient (WAC) compared to the estimate (*see* Eq. D.1 and Tab. D.3). Difference between the two layers in the canopy is made by the opacity of the lines (*see* legend). The gray-shaded area marks the threshold difference comparable to the imposed deviation; i.e. the 10% mark.

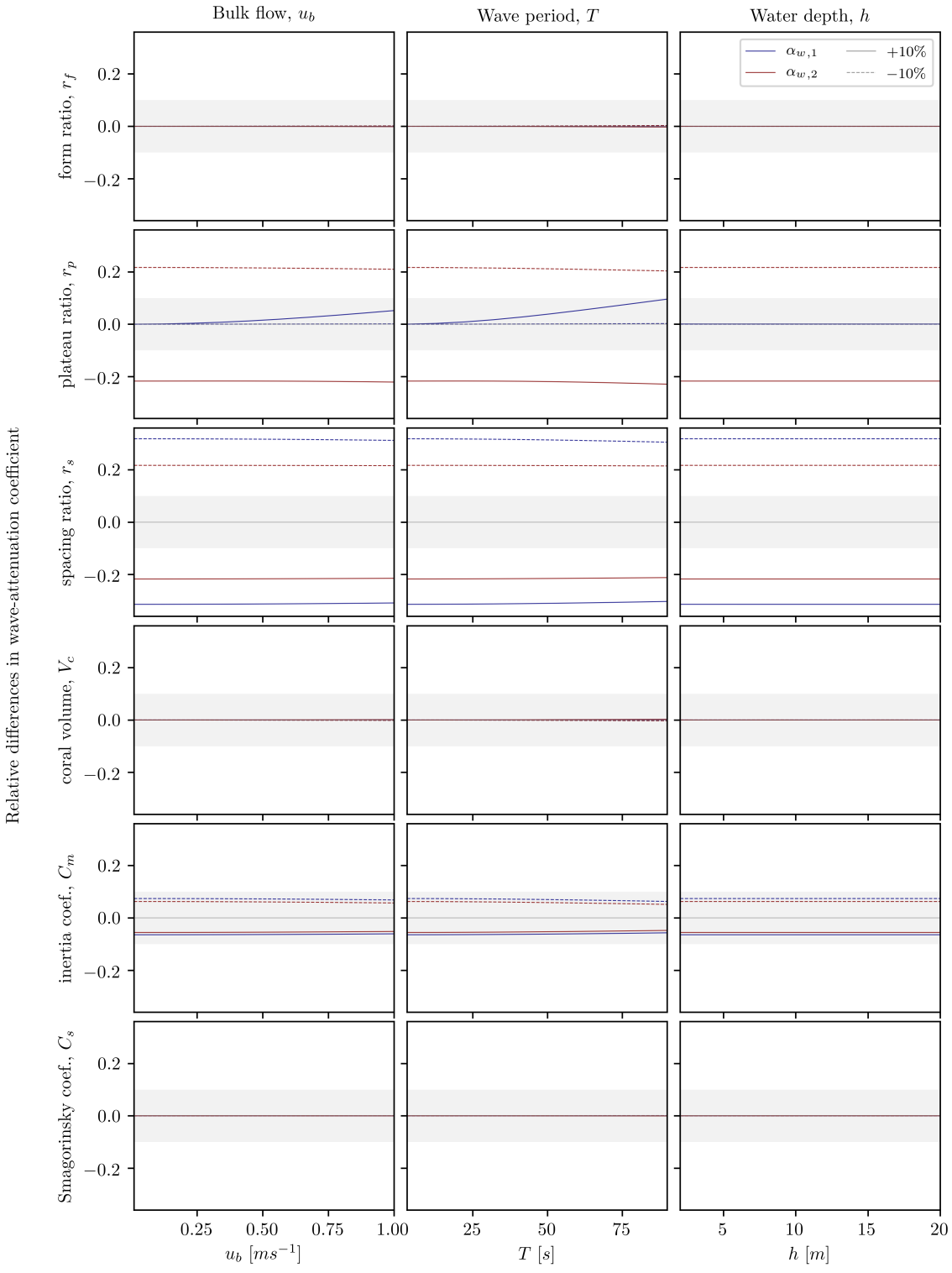

(b) Massive morphology.

Figure D.3: Sensitivity analysis of the flow structure for three morphologies represented by the wave-attenuation coefficient (cont.). (a) branching; **(b)** massive; and **(c)** plate. The sensitivity analysis of the parameters is expressed as relative difference in wave-attenuation coefficient (WAC) compared to the estimate (*see* Eq. D.1 and Tab. D.3). Difference between the two layers in the canopy is made by the opacity of the lines (*see* legend). The gray-shaded area marks the threshold difference comparable to the imposed deviation; i.e. the 10% mark.

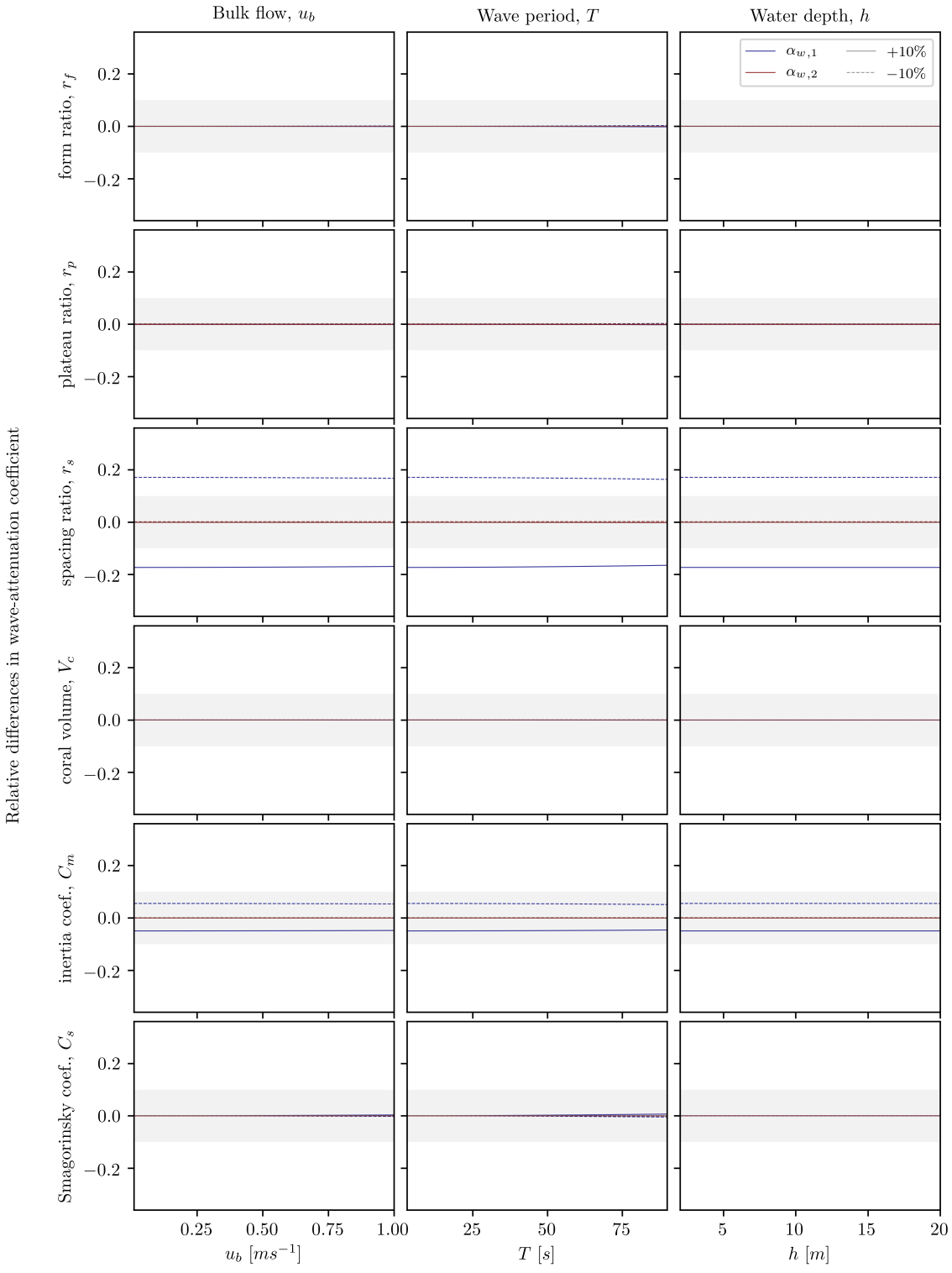

(c) Plate morphology.

Figure D.3: Sensitivity analysis of the flow structure for three morphologies represented by the wave-attenuation coefficient (cont.). (a) branching; **(b)** massive; and **(c)** plate. The sensitivity analysis of the parameters is expressed as relative difference in wave-attenuation coefficient (WAC) compared to the estimate (*see* Eq. D.1 and Tab. D.3). Difference between the two layers in the canopy is made by the opacity of the lines (*see* legend). The gray-shaded area marks the threshold difference comparable to the imposed deviation; i.e. the 10% mark.

Table D.4: Parameters determining the thermal flow dependency. C_f is the friction coefficient; r_δ^+ the radial wall coordinate that specifies the thickness of the VBL; K_0 a constant; a_p the absorptivity of the coral; ν the kinematic viscosity of water; α the thermal diffusivity; k the thermal conductivity; u_{cm} the in-canopy flow velocity; and $\langle I_z \rangle$ the biomass-averaged light-intensity.

	Parameter	Estimate	Deviation	Unit
model	C_f	0.01		–
	r_δ^+	200.0		–
	K_0[a]	80.0		–
	a_p	0.4	10%	–
	ν	$1.0 \cdot 10^{-6}$		$m^2 s^{-1}$
	α[b]	$1.0 \cdot 10^{-7}$		$m^2 s^{-1}$
	k[c]	0.6089		$J m^{-1} s^{-1} K^{-1}$
input	u_{cm}	0.00–1.00	n/a	$m s^{-1}$
	$\langle I_z \rangle$	0.01–600.0		μmol photons $m^{-2} s^{-1}$

[a] Estimate based on measurements at which the increase in temperature at the coral surface was around 1°C for flow velocities around zero [e.g. Jimenez et al., 2011].
[b] James [1968].
[c] Bird et al. [2002].

The results of the sensitivity analysis are presented in Figure D.4 for the absolute differences only, as the relative differences remain constant over the range of the input parameters (not shown). The relative difference is easily determined from the formulations expressing the thermal flow dependency (*see* Eqs. 4.32 to 4.34).

From Figure D.4 becomes clear that the increased temperature is most pronounced for the combination of low flow velocities and high light-intensities. Furthermore, the absolute errors are relatively small and only differs at maximum around 0.05 K with the estimation. Moreover, the increased temperature due to the presence of the TBL under normal conditions does not exceed 0.10 K.

Furthermore, none of the imposed deviations are amplified, which is in line with the expectations from the formulation of the effects of the TBL on the thermal conditions (*see* Eq. 4.34). Herein, all parameters have a power of one or less, which indicates that the imposed deviations are in no case amplified. As all model as well as input parameters are not related to each other, there are also no non-linearities.

Nevertheless, there is large uncertainty in the value of the constant K_0. Thereby, there is also large uncertainty on the outcomes of the determined thermal micro-environment as the magnitude of the error in this constant results in an equally relative error in the determination of the increased temperature at the coral-water interface.

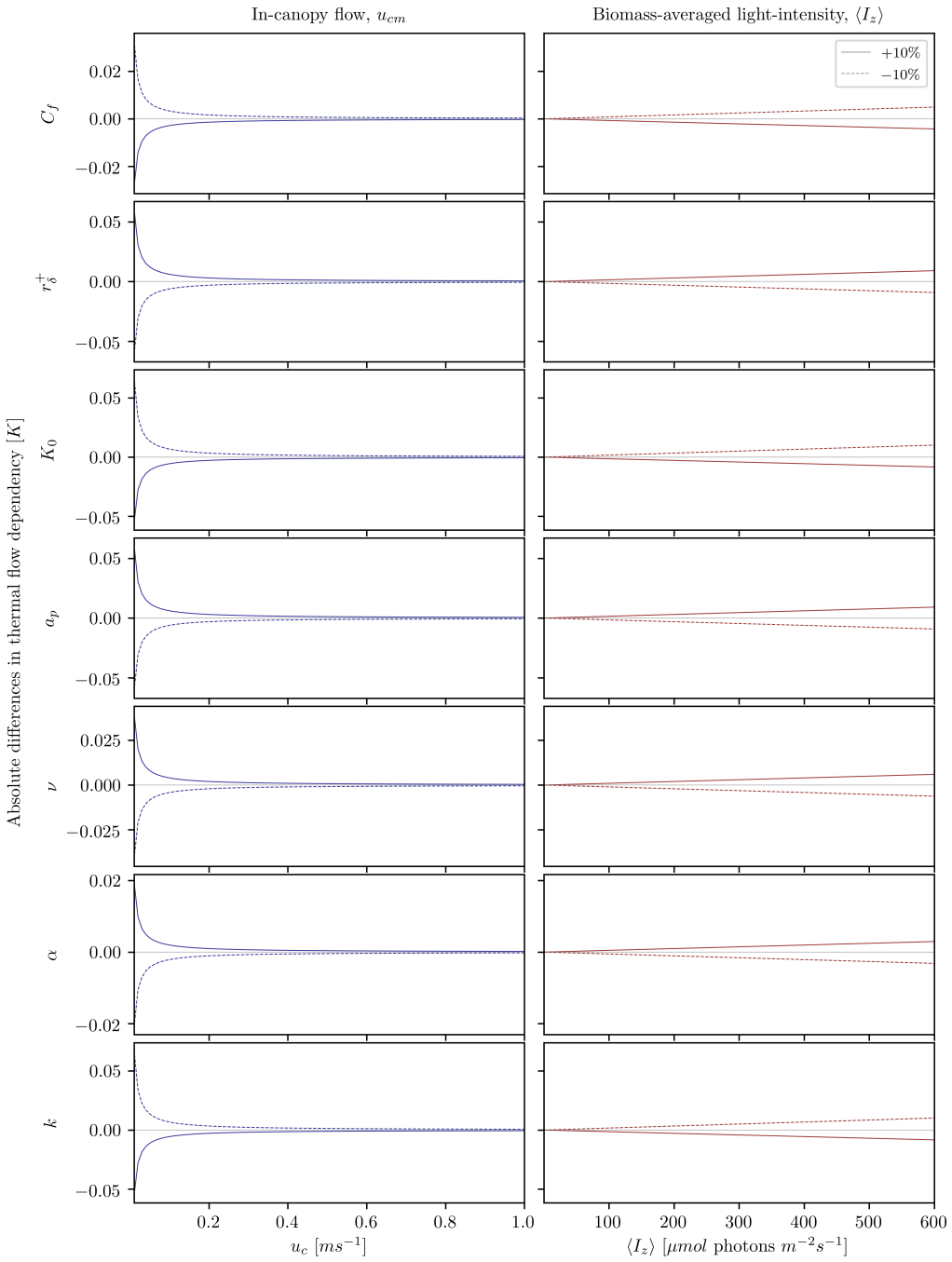

Figure D.4: Sensitivity analysis of the thermal flow dependency expressed as absolute differences. The absolute differences are determined by determining the difference between the estimate and the 10% deviation from that estimate (*see* Tab. D.4).

Table D.5: Parameters determining the photosynthetic light dependency. $I_k^{\max}$ is the maximum saturation intensity; ι the acclimatisation exponent; β_{I_k} and $\beta_{P_{\max}}$ the steady-state exponents for the saturation intensity and the maximum photosynthetic rate, respectively; K_d the light-attenuation coefficient (LAC); I_0 the incoming light-intensity; and h' the representative water depth that results in the same light-intensity as the representative light-intensity.

	Parameter	Estimate	Deviation	Unit
model	$I_k^{\max}$	370.0	10%	μmol photons $m^{-2}s^{-1}$
	ι	0.6		d^{-1}
	β_{I_k}	0.34		$-$
	$\beta_{P_{\max}}$	0.09		$-$
input	K_d	0.10–0.90	n/a	m^{-1}
	I_0	400–800		μmol photons $m^{-2}s^{-1}$
	h'	2.0–40.0		m

D.3 Coral physiology

The sensitivity analysis on the coral physiology assesses every environmental factor separately:

- photosynthetic light dependency in Appendix D.3.1;
- photosynthetic flow dependency in Appendix D.3.2;
- photosynthetic thermal dependency in Appendix D.3.3; and
- aragonite dependency in Appendix D.3.4.

All these dependencies are compared via their effects on the calcification rate, which is determined via the photosynthesis for the first three environmental factors.

D.3.1 Light dependency

The sensitivity to the light conditions is based on the photosynthetic light dependency. Table D.5 lists the parameters assessed in this sensitivity analysis. Note that the water depth is given as the representative water depth, which is the water depth that results in the same light-intensity as the representative light-intensity. This way, the morphology does not need to be taken into account. Within this section, the representative water depth is mentioned the water depth for readability and an apostrophe is added to the symbol; i.e. h' instead of h.

The results of the sensitivity analysis of the photosynthetic light dependency are given in Figures D.5 and D.6 for the steady-state solution and for the inclusion of time-varying light-conditions, respectively. In the steady-state assessment, the sensitivity of the acclimation exponent is none (*see* Fig. D.5) because this parameter only plays a role over time. The steady-state assessment gives a clear insight in the sensitivity of the other model parameters based on the input parameters. Therefore, both the assessments are included; steady-state as well as time-varying.

The effect of the description of the dark respiration (*see* Eq. 4.39) is clearly visible in both the assessments over the ranges of LAC and water depth (Figs. D.5 and D.6, respectively in the second and third column); in both cases the zero-line is crossed. The differences switch signs when the input parameters align with the euphotic depth because the dark respiration is defined such that the photosynthetic light dependency equals zero at the euphotic depth.

Furthermore, deviations in the model parameters are slightly amplified in the time-varying assessment around the euphotic depth (*see* Fig. D.6, second and third column). The settings of the other input parameters are set such that the focus remains on the area within the euphotic zone because (1) this is the area of interest, as net photosynthesis is negative outside the euphotic zone; and (2) the differences due to the

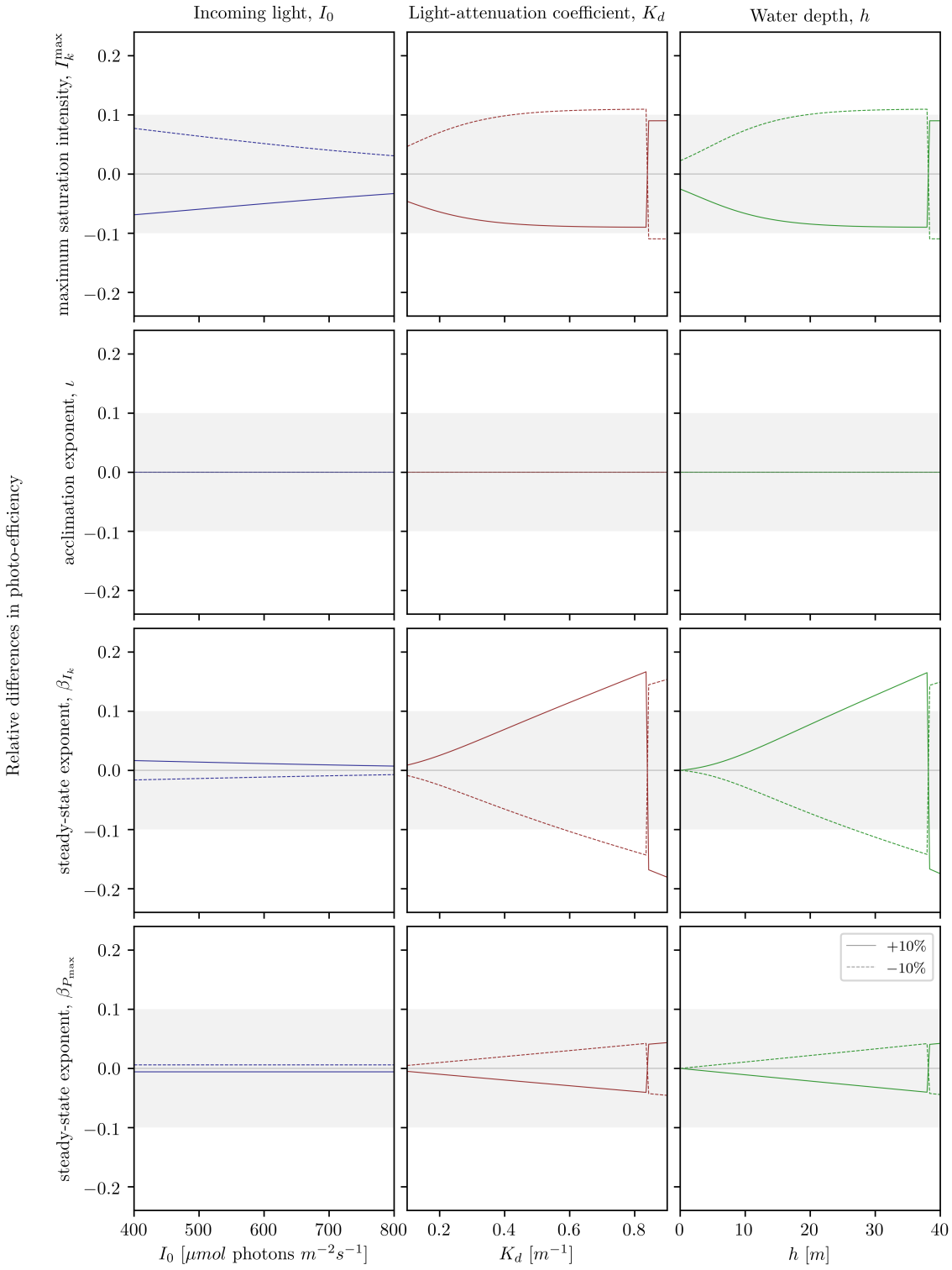

Figure D.5: Sensitivity analysis of the photosynthetic light dependency under steady-state conditions. The sensitivity of the parameters is expressed as relative difference in photosynthetic light dependency compared to the estimate (*see* Eq. D.1, and Tab. D.5). The gray-shaded area marks the threshold difference comparable to the imposed deviation; i.e. the 10% mark.

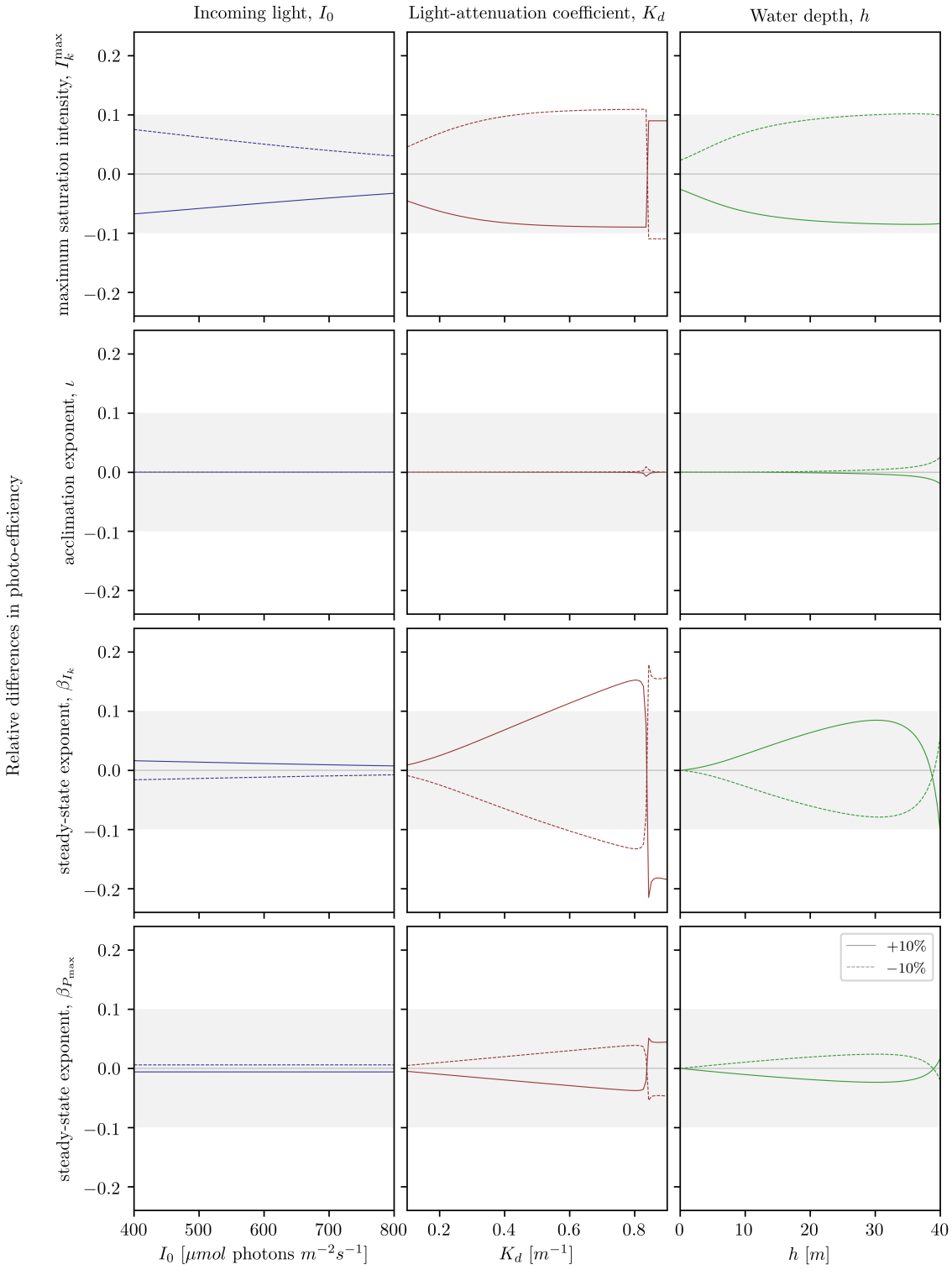

Figure D.6: Sensitivity analysis of the photosynthetic light dependency under time-varying conditions. The sensitivity of the parameters is expressed as relative difference in photosynthetic light dependency compared to the estimate (*see* Eq. D.1, and Tab. D.5). The gray-shaded area marks the threshold difference comparable to the imposed deviation; i.e. the 10% mark.

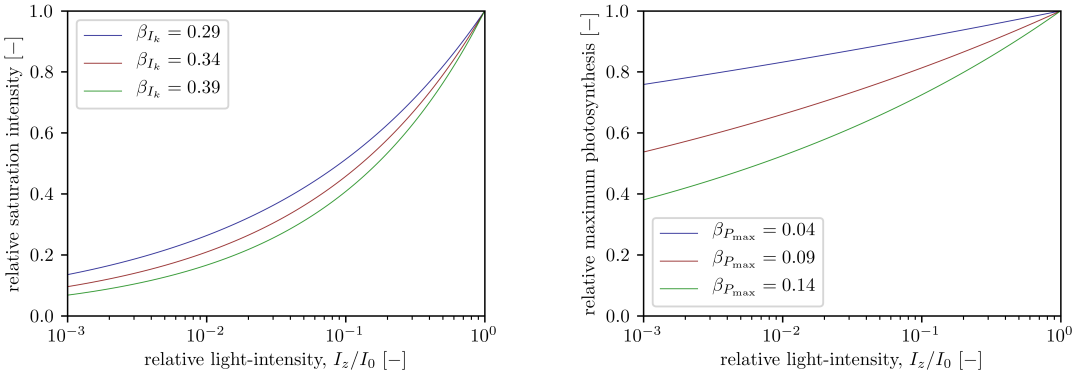

(a) Relative saturation intensity, $I_k/I_k^{\max}$.

(b) Relative maximum photosynthesis, $P_{\max}/P_{\max}^{\max}$.

Figure D.7: Effects of the steady-state exponents over the relative light-intensity. The deviations in the steady-state exponents are based on Anthony and Hoegh-Guldberg [2003a].

imposed deviations are sky-rocketing outside the euphotic zone, which takes away the attention from the area of interest.

The influence of the incoming light on the photosynthetic light dependency is negligible for most model parameter, where only the choice of the maximum saturation intensity might result in different outcomes (*see* Fig. D.5, first column).

Including the variation of the light-conditions over time results in two main effects compared to the steady-state solution: (1) the switching of the sign around the euphotic depth is smoothened; and (2) the photosynthetic light dependency is equally or less sensitive to deviations to the model parameters.

The sensitivity of the photosynthetic light dependency to the steady-state exponents taken over the LAC and the water depth is in two ways to be expected: (1) the relative light-intensity is exponentially related to the product of the LAC and the water depth (*see* Eq. 4.1); and (2) the differences grow—absolute and relative—for decreasing relative light-intensity (*see* Fig. D.7).

All in all, from Figures D.5 and D.6 becomes clear that the saturation intensity—defined by the maximum saturation intensity and its steady-state exponent—is the leading parameter in determining the photosynthetic light dependency. The sensitivity to this parameter increases towards the euphotic depth as the photosynthetic light dependency approaches zero.

D.3.2 Flow dependency

The photosynthetic flow dependency is determined based on only three parameters of which two are fitting parameters; i.e. model parameters. All three are presented in Table D.6. The range of the in-canopy flow presented in Table D.6 is capped at $u_{cm} = 1.00\ ms^{-1}$, as there are only differences for lower flow velocities; as presented in Figure D.8.

Figure D.8 shows that the sensitivity of the photosynthetic flow dependency to both model parameters approaches zero for $u_{cm} > 0.2\ ms^{-1}$ and the choice of the critical flow velocity has only limited influence. The minimum flow efficiency, however, has a more pronounced influence for low flow velocities, where for no flow the photosynthetic flow dependency is defined by this minimum. Thereby, the maximum error due to the choice of the minimum flow efficiency ($P_u^{\min}$) is the error due to this choice.

Fortunately, there is flow over a coral reef and so the sensitivity—and thereby the error—of the model to the minimum flow efficiency is lower than the error made in determining its value. However, the range of

Table D.6: Parameters determining the photosynthetic flow dependency. $P_u^{\min}$ is the minimum photosynthetic efficiency without flow; u_{cr} the critical flow velocity at which the photosynthesis is no longer limited by the flow conditions; and u_{cm} the in-canopy flow velocity.

	Parameter	Estimate	Deviation	Unit
model	$P_u^{\min}$	0.689	10%	–
	u_{cr}	0.172		ms^{-1}
input	u_{cm}	0.00–1.00	n/a	ms^{-1}

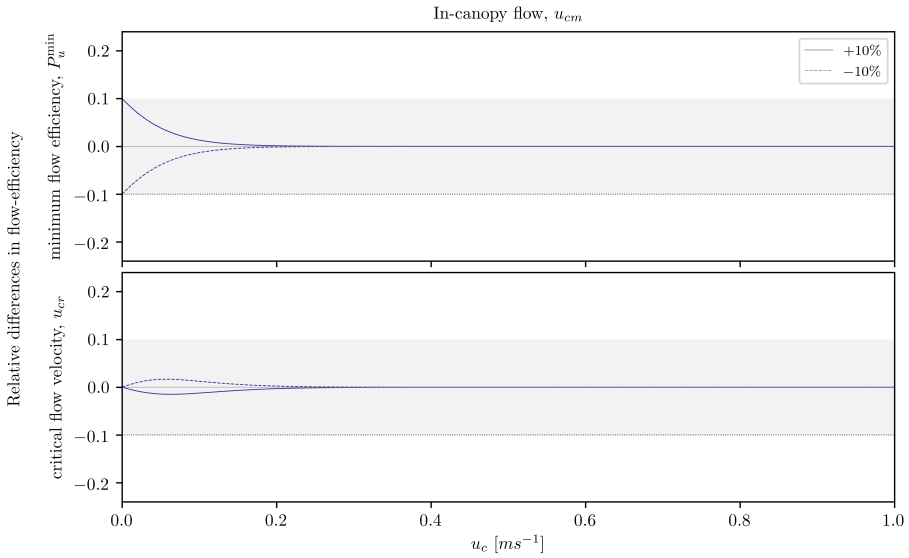

Figure D.8: Sensitivity analysis of the photosynthetic flow dependency. The sensitivity of the parameters is expressed as relative difference in photosynthetic flow dependency compared to the estimate (*see* Eq. D.1 and Tab. D.6). The gray-shaded area marks the threshold difference compared to the imposed deviation; i.e. the 10% mark.

in-canopy flow velocities found in nature are within the domain sensitive to the fitting parameters [e.g. Lowe et al., 2009; Monismith et al., 2015].

D.3.3 Thermal dependency

The sensitivity of the photosynthetic thermal dependency on its model and input parameters is determined by fluctuating the (coral) temperature within the thermal range, so no bleaching occurs. The photosynthetic thermal dependency consists of two mechanisms: (1) the adapted temperature response (*see* Eq. 4.50); and (2) the thermal envelope (*see* Eq. 4.54). Therefore, the analysis is broken down, showing the sensitivity of both mechanisms as well as their combined effect.

The analyses on the activation energy and the gas constant are assessed with respect to the optimal temperature instead of the (coral) temperature. This because (1) the insensitivity of the adapted temperature response to these two parameters (*see* Eq. 4.50); and (2) the insensitivity of the thermal envelope to the (coral) temperature and it being a function of the optimal temperature instead.

Tables D.7a and D.7b give an overview of the model and input parameters of the sensitivity analyses of the photosynthetic thermal dependency. Note that (1) the sensitivity analysis is split up; and (2) the thermal parameters deviate by 1.0°C instead of 10%. The results are presented in Figures D.9 and D.10.

Table D.7: Parameters determining the photosynthetic thermal dependency. ΔT is the thermal range; T_{opt} the optimal temperature; T_c the coral temperature; E_a the activation energy; and $\overline{R}$ the gas constant.

(a) Thermal characteristics.

	Parameter	Estimate	Deviation	Unit
model	ΔT T_{opt}	10.0 27.0	1.0	°C
input	T_c	T_{lo}–T_{hi}	n/a	°C

(b) Thermal constants.

	Parameter	Estimate	Deviation	Unit
model	$\frac{E_a}{\overline{R}}$	$6.0 \cdot 10^4$ 8.314	10%	$Jmol^{-1}$ $JK^{-1}mol^{-1}$
input	T_{opt}	20.0–30.0	n/a	°C

Figure D.9 clearly shows that the adapted temperature response is mainly determined based on the thermal range; while the thermal envelope is mainly determined by the optimal temperature. These sensitivities are straightforward, when reading the associated formulations (*see* Eqs. 4.50 and 4.54):

1. The shape of the adapted temperature response (f_1, Eq. 4.50) is mainly determined by the thermal range, where the optimal temperature—or one of the thermal limits—defines the location on the thermal spectrum. Furthermore, the insensitivity of the adapted temperature response to the activation energy and the gas constant is straightforward, as these parameters are not included in the formulation of the adapted temperature response (*see* Eq. 4.50).
2. In the formulation of the thermal envelope (f_2, Eq. 4.54), the thermal range is not included and so does not impose any changes on the outcomes of the thermal envelope. All other three assessed parameters are part of the formulation. Figure D.9 clearly shows the sensitivity of the thermal envelope—and thereby the thermal dependency—on the optimal temperature. Furthermore, deviations in the activation energy as well as the gas constant are magnified at optimal temperatures higher than the calibration value; i.e. $T_{opt} > 300\ K$. On the other hand, these same deviations are reduced for optimal temperatures lower than the calibration value; i.e. $T_{opt} < 300\ K$.

While the relative differences remain constant over the thermal range (*see* Fig. D.9), the absolute differences follow the cubic shape of the adapted temperature response (not shown). Thereby, the relative temperature within the thermal range plays a substantial role on the long-term, also on the sensitivity to the correctness of the thermal limits.

D.3.4 Aragonite dependency

The assessment of the sensitivity of the calcification rate due to the acidity—i.e. the aragonite saturation state—consists of two formulations of the aragonite dependency: (1) the Michaelis-Menten equation (*see* Eq. 4.62); and (2) the tangent-hyperbolic function (*see* Eg. 7.1). The latter is taken into account due to its slightly better fit to the data (*see* Sec. 7.2.4 and Fig. 7.6).

An overview of the calibration constants for both formulations is given in Table D.8. Note that the dilution saturation (Ω_0) in case of the tangent-hyperbolic function is not deviated by 10% but by an absolute value. This is because a relative deviation from zero always equals zero, and so the sensitivity of the aragonite dependency cannot be assessed.

The results of the sensitivity analyses are presented in Figure D.11 from which becomes clear that the sensitivity is most profound in the lower domain of the aragonite saturation state. Especially for the dilution

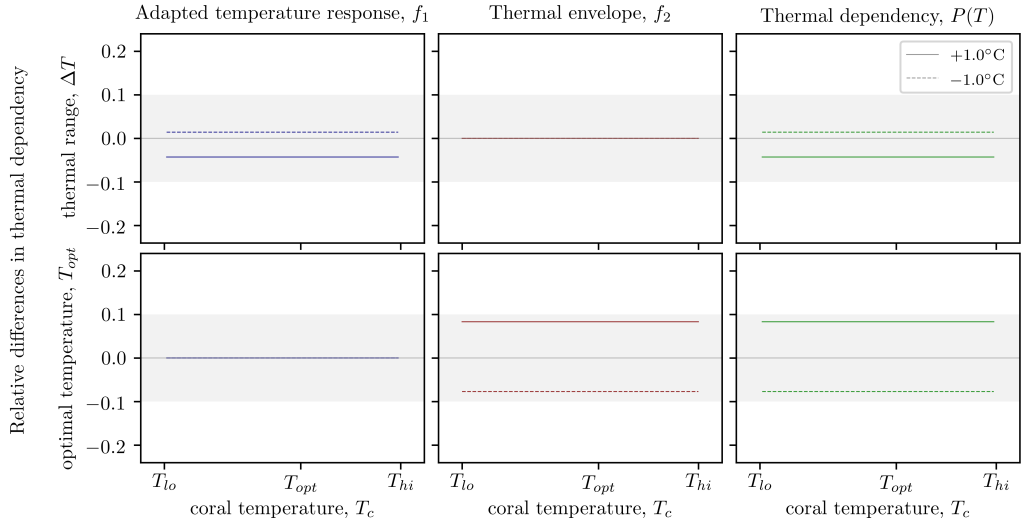

Figure D.9: Sensitivity analysis of the photosynthetic thermal dependency within the thermal range thermal characteristics. The absolute values of the lower and upper limits differ per combination of thermal range and optimal temperature. The sensitivity plots are transformed such that the effects are presented relative to the limits of the thermal range for comparison. The sensitivity of the parameters is expressed as relative difference in photosynthetic thermal dependency compared to the estimate (*see* Eq. D.1 and Tab. D.6). The gray-shaded area marks the threshold difference compared to the imposed deviation; i.e. the 10% mark.

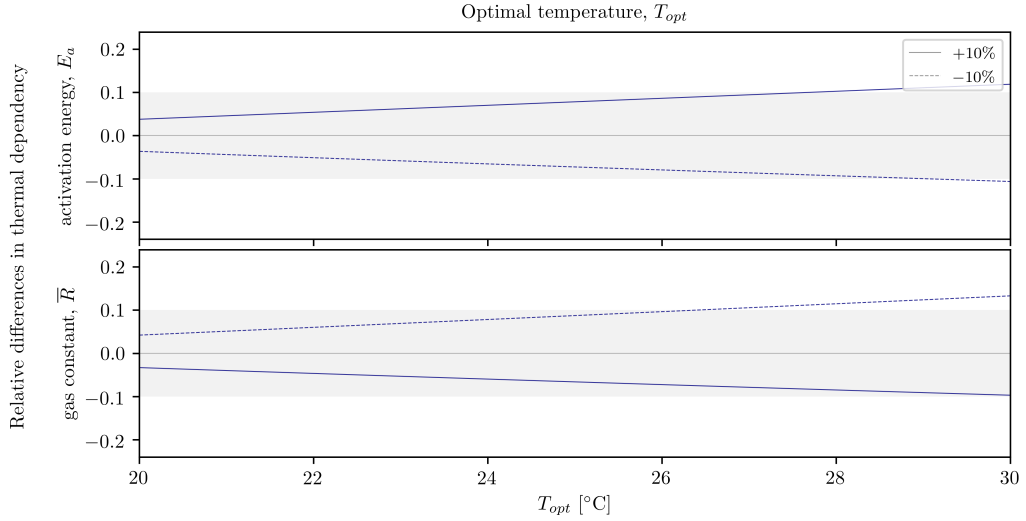

Figure D.10: Sensitivity analysis of the photosynthetic thermal dependency within the thermal range based on the thermal constants. The sensitivity of the parameters is expressed as relative difference in photosynthetic thermal dependency compared to the estimate (*see* Eq. D.1 and Tab. D.6). The gray-shaded area marks the threshold difference compared to the imposed deviation; i.e. the 10% mark.

Table D.8: Parameters determining the aragonite dependency. ω_0 is the dilution saturation; κ_a the half-rate coefficient; and Ω_a the aragonite saturation state.

	Formulation	Parameter	Estimate	Deviation	Unit
model	Michaelis-Menten (Eq. 4.62)	ω_0	0.1459	10%	–
		κ_a	0.6624		–
	tangent-hyperbolic (Eq. 7.1)	ω_0	0.0	0.01	–
		κ_a	2.1415	10%	–
input		ω_a	0.0–5.0	n/a	–

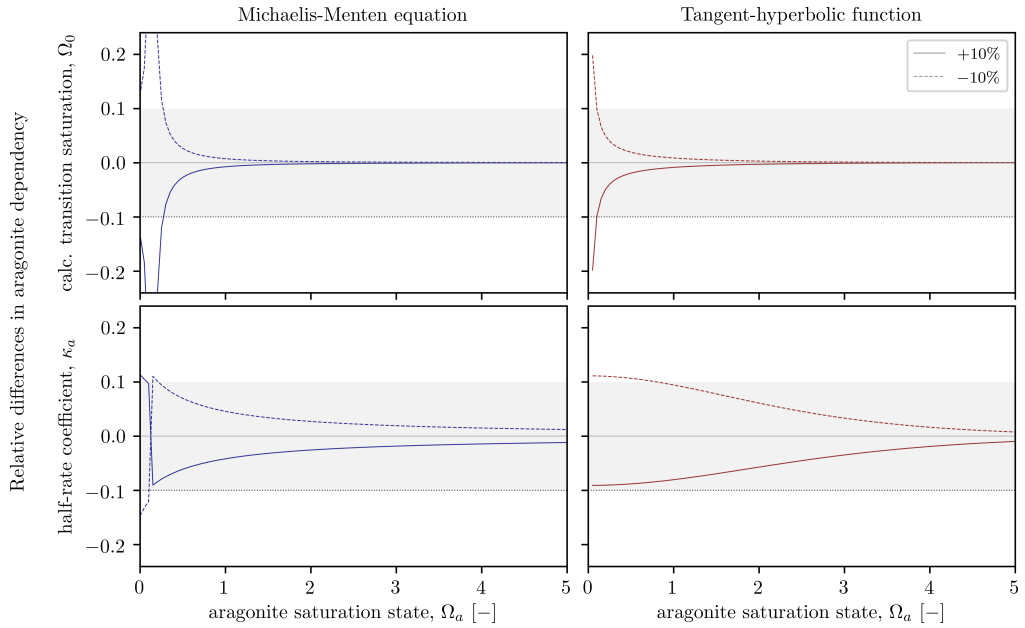

Figure D.11: Sensitivity analysis of the aragonite dependency. The sensitivity of the parameters is expressed as relative difference in aragonite dependency compared to the estimate (*see* Eq. D.1 and Tab. D.8). The gray-shaded area marks the threshold difference compared to the imposed deviation; i.e. the 10% mark.

saturation (Ω_0), which blows up near its estimate (*see* Fig. D.11, top row). Further away from its estimate, the sensitivity of the aragonite dependency reduces quickly and approaches zero for approximately $\Omega_a > 1.5$; for both formulations.

The half-rate coefficient (κ_a) has an elongated influence on the aragonite dependency (*see* Fig. D.11, bottom row). However, it does not blow up, nor amplify substantially; only for aragonite saturation states below the dilution saturation result in larger errors in the output than the deviation of the input, i.e. crosses the 10% mark.

As the aragonite saturation state is commonly well above the dilution saturation the process-based Michaelis-Menten equation is less sensitive to its calibration parameters. This is mainly supported by the sensitivity of the two formulations to the half-rate coefficient, which reduces quicker with increasing aragonite saturation state for the Michaelis-Menten equation than for the tangent-hyperbolic function (*see* Fig. D.11, bottom row).

Table D.9: Parameters determining the morphological ratios. χ_f is the overall form proportionality constant; $\chi_{p,u}$ the flow plate proportionality constant; $\chi_{s,I}$ the light spacing proportionality constant; $\chi_{s,u}$ the flow spacing proportionality constant; $\langle I_z \rangle / I_0$ the representative relative light-intensity; and u_{cm} the in-canopy flow.

	Parameter	Estimate	Deviation			Unit
model	χ_f	1.0				–
	$\chi_{p,u}$	1.0	10%	50%	90%	–
	$\chi_{s,I}$	1.0				–
	$\chi_{s,u}$	1.0				–
input	$\langle I_z \rangle / I_0$	0.01–1.00	n/a			–
	u_{cm}	0.01–1.00				ms^{-1}
constants	χ_p	1/2	n/a			–
	χ_s	$1/(2\sqrt{2})$				–
	u_{cr}	0.172				ms^{-1}

Even though the tangent-hyperbolic function is a better fit to the data (*see* Sec. 7.2.4 and Fig. 7.6), the Michaelis-Menten equation is the better approach because (1) the root-mean-squared errors (RMSEs) of the tangent-hyperbolic function and the Michaelis-Menten equation are comparable; (2) the Michaelis-Menten equation is less sensitive to its calibration constants in the aragonite saturation state range of interest; (3) the absolute error of the tangent-hyperbolic function due to the deviations (not shown) is larger in the range of interest; and (4) the Michaelis-Menten equation is a process-based formulation instead of a best fit.

D.4 Coral morphology

Due to the large uncertainty in the formulations on the coral morphology as function of the light and flow conditions, a wider range of deviations is assessed: ±10%; ±50%; and ±90%. Two of the proportionality constants are defined by predefined constraints (*see* Sec. 3.3): (1) the overall plate proportionality constant, $\chi_p = 1/2$; and (2) the overall spacing proportionality constant, $\chi_s = 1/(2\sqrt{2})$.

Furthermore, the critical flow velocity (u_{cr}) is predefined as it is mainly a measure to make the formulations non-dimensional. To be consistent throughout on the notion of a critical flow velocity—as is also used in the description of the photosynthetic flow dependency—the same critical flow velocity is used as found for the photosynthetic flow dependency (*see* Sec. 7.2.2): $u_{cr} = 0.172\ ms^{-1}$. All parameters are listed in Table D.9 in which also the definitions of all the constants are presented.

The results are presented in Figure D.12, which slightly differs from the previous presentations of the sensitivity analyses due to the multiple imposed deviations considered. The shaded areas in Figure D.12 are coloured in line with the colors used to indicate the imposed deviations. These extra shaded areas are added (1) to show the non-linearity of the formulations as function of the proportionality constants alone; and (2) to compare the imposed deviation's magnitude to the relative error it induces on the morphological ratio.

The form ratio follows the imposed deviation on the overall form proportionality constant for both the considered light and flow condition ranges (*see* Fig. D.12), which is to be expected from the formulation of this ratio; it is purely linear (*see* Eq. 4.68a). The other morphological ratios show some differences:

1. The flow plate proportionality constant ($\chi_{p,u}$) is only affected by the in-canopy flow (*see* Fig. D.12) as the definition of the plate ratio does not include the (relative) light-intensity. The sensitivity as presented in Figure D.12 (second row) comes from the chosen value of the in-canopy flow velocity for which the results over the range of light-intensities is presented; which is $u_{cm} = 0.10\ ms^{-1}$.

   The intersection of all lines in the right column of Figure D.12 is at the flow velocity equal to the critical flow velocity; i.e. $u_{cm} = u_{cr}$. Before this intersection—thus for low flow velocities—the imposed deviation is amplified and so the plate ratio is very sensitive for the definition of the flow

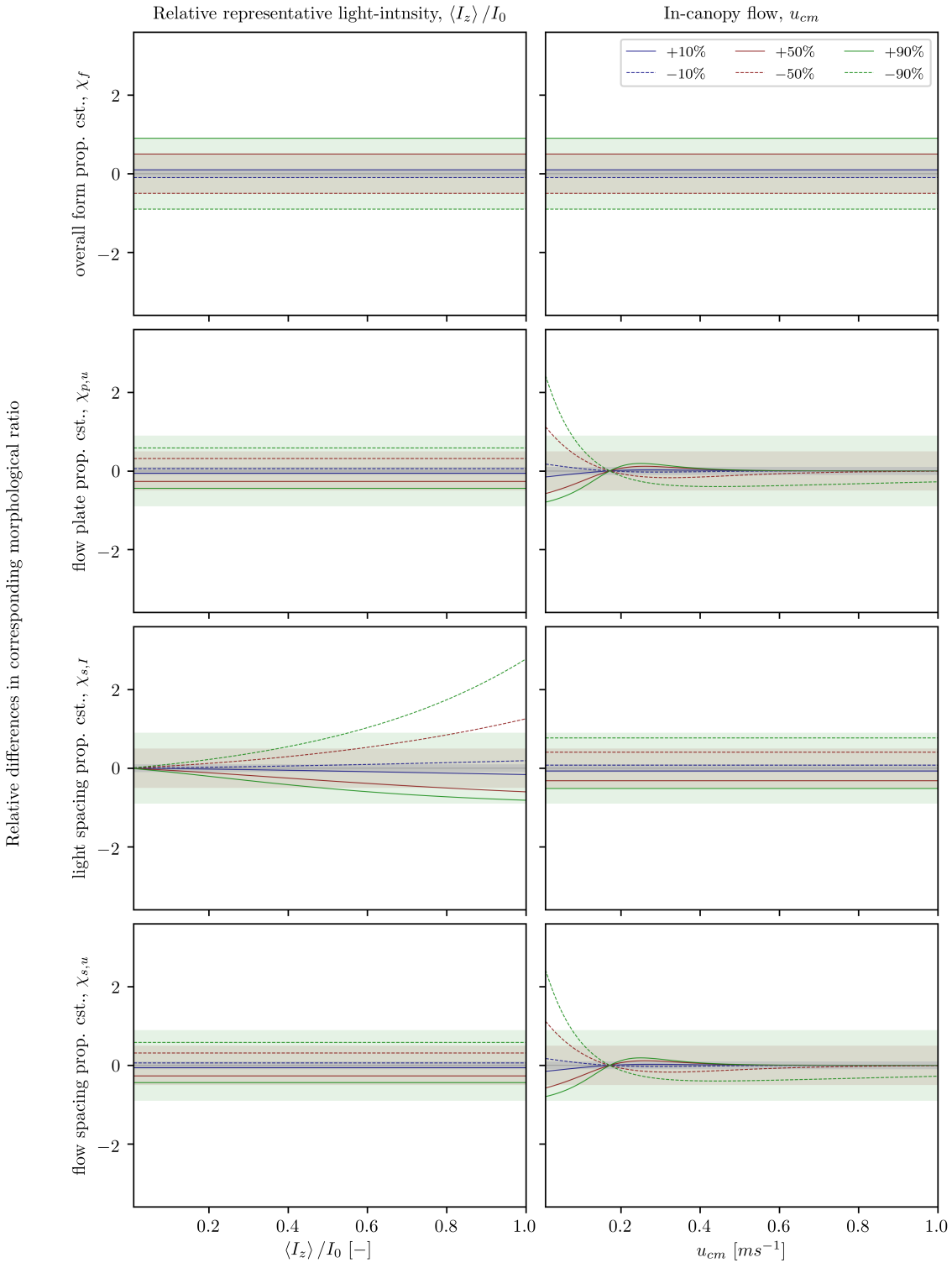

Figure D.12: Sensitivity analysis of the morphological ratios on the light and flow conditions. The sensitivity of the morphological ratios is expressed as relative difference compared to the estimate (*see* Eq. D.1 and Tab. D.9), where the morphological ratio under consideration is based on the proportionality constant: top row, r_f; second row, r_p; and third and fourth rows, r_s. The shaded areas mark the threshold relative differences compared to the imposed deviations; i.e. the blue-shaded area the 10% mark, the red-shaded area the 50% mark, and the green-shaded area the 90% mark.

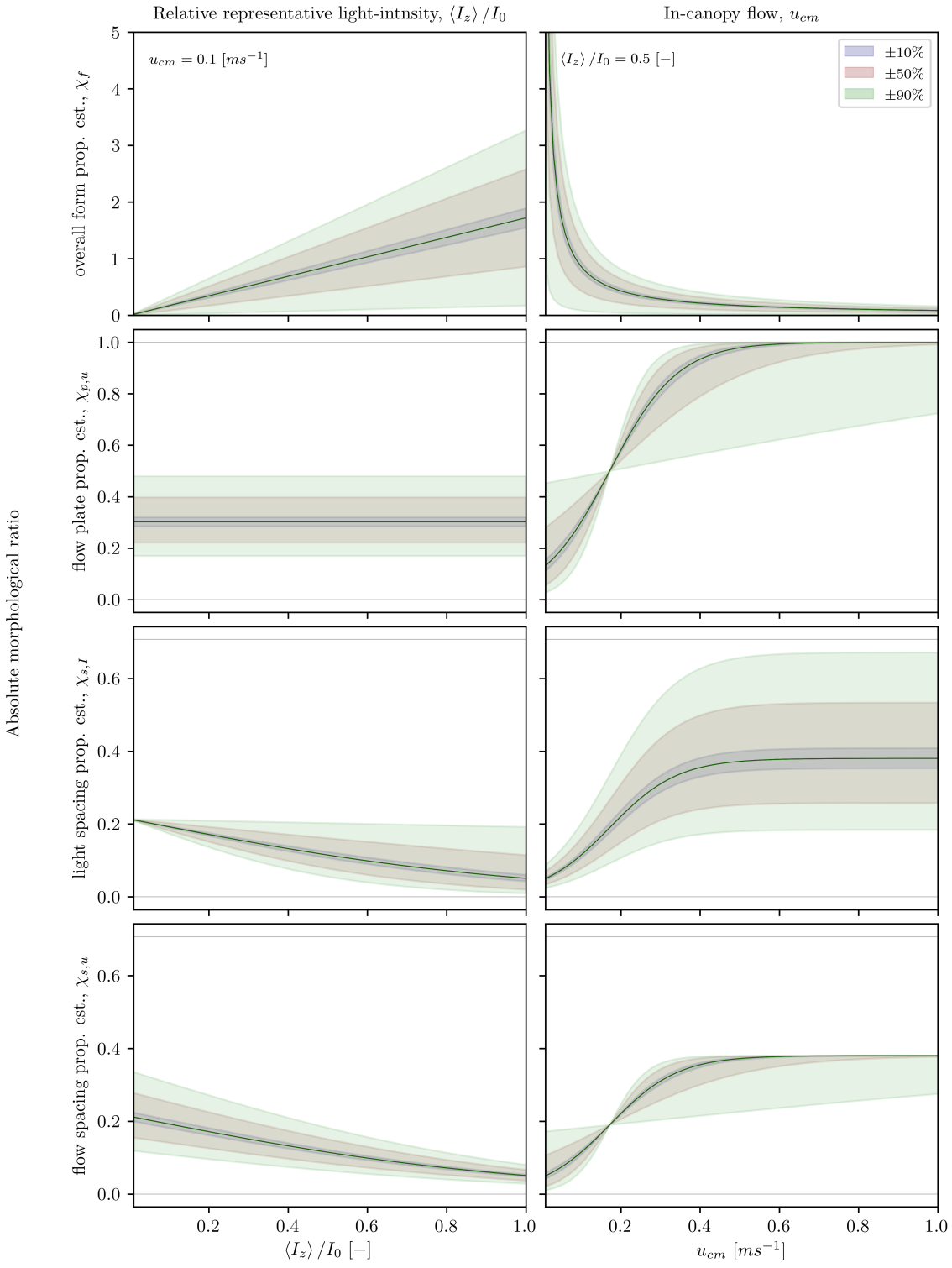

Figure D.13: Sensitivity of the morphological ratios to both the environmental conditions and the proportionality constants. The sensitivity of the morphological ratios are presented in their absolute values, where the shaded areas mark the extends due to the imposed deviations (*see* Tab. D.9).

plate proportionality constant, $\chi_{p,u}$. This sensitivity fades out for larger flow velocities. The difference is due to the description of the plate ratio for which a tangent-hyperbolic is used, which approaches one for larger values.

2. The light spacing proportionality constant ($\chi_{s,I}$) is only affected by the relative representative light-intensity (*see* Fig. D.12) as it is the proportionality constant associated with the light conditions. The sensitivity of the spacing ratio on this constant increases for increasing light-intensity, and the relative error in the spacing ratio is even tripled when a deviation of -90% is imposed at high light-intensities.
3. The flow spacing proportionality constant ($\chi_{s,u}$) accounts for the dependency of the spacing ratio on the in-canopy flow velocity and so the light conditions do not influence the sensitivity of the spacing ratio to this proportionality constant (*see* Fig. D.12, bottom row). The sensitivity of the spacing ratio to the flow spacing proportionality constant is equal to the sensitivity of the plate ratio to the overall plate proportionality constant (*see* Fig. D.12, second row), which is due to the comparable formulations (*see* Eqs. 4.68b and 4.68c).

In Figure D.13 the different morphological ratios are presented over the ranges of environmental conditions including the results due to the imposed deviations on the proportionality constants. As becomes clear from Figures D.12 and D.13 is that the morphological ratios are sensitive to their proportionality constants and that this sensitivity varies over the environmental gradients. Even though the sensitivity expressed as relative differences suggests that the sensitivity amplifies for higher light-intensities and lower flow velocities, in absolute sense this is not necessarily the case.

D.5 Coral bleaching

The sensitivity analysis on the bleaching of corals is twofold: (1) the susceptibility of bleaching (App. D.5.1); and (2) the associated population dynamics due to bleaching (App. D.5.2). The first shows great comparison with the sensitivity analysis on the photosynthetic thermal dependency (*see* App. D.3.3), but includes the effects of bleaching which is excluded from this analysis.

D.5.1 Bleaching susceptibility

The susceptibility of bleaching—and thereby the calcification rate and healthy coral cover—is analysed for a given coral temperature signal. This signal touches the limits of the thermal range to assess the sensitivity of a small deviation of the lower and upper limits on the average calcification rate in which the healthy coral cover is implicitly taken into account (the coral population dynamics is analysed in App. D.5.2).

In this assessment, either the lower or the upper limit is modified, which implicitly results in deviations of the thermal range and the optimal temperature. Furthermore, the assessment differs from the others due to its implications. The sensitivity of the limits on the long-term temperature signal—twenty years—deviates $\pm 1.0^{\circ}$C. This deviation is in line with the thermal flow dependency (*see* App. D.2.3).

A visualisation of the sensitivity analysis on the susceptibility of bleaching is given in Figure D.14, and the results are presented in Figure D.15. The thermal limits show an asymmetric response: a steep decline in the calcification rate occurs when bleaching takes place due to (1) an increased lower limit; and/or (2) a reduced upper limit.

When the limits of the thermal range are taken further away from the extremes of the thermal signal, the average calcification rate increases. This effect becomes most pronounced for the upper limit. The dissimilarity between the two limits is due to the cubic function that describes the adapted temperature response (*see* Eq. 4.50). The slope at the upper limit is larger than at the lower limit resulting in a more pronounced response of the model near the upper limit.

This asymmetric response is also clearly visible in Figure D.14 in which the thermal dependency for different thermal limits is presented by the gray-shaded area. Near the lower limit, this area is more confined compared to near the upper limit. Moreover, near the optimal temperature, the differences are limited. Note that the

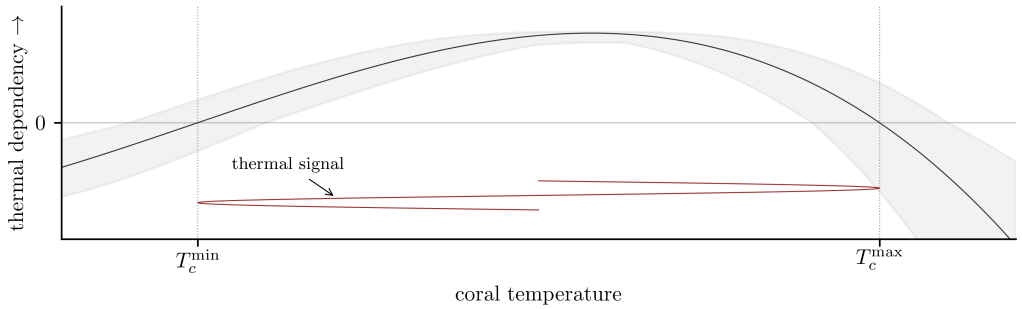

Figure D.14: Visualisation of the sensitivity analysis on the bleaching susceptibility. The imposed thermal signal is presented by the red line, which moves between two temperatures. The black line is the photosynthetic thermal dependency when the thermal range limits corresponds with the limits of the signal. The gray-shaded area covers the range of thermal responses for deviations of the thermal range limits with a maximum of 1.0°C; i.e. $T_{lo} = T_c^{\min} \pm 1.0°\text{C}$ and $T_{hi} = T_c^{\max} \pm 1.0°\text{C}$.

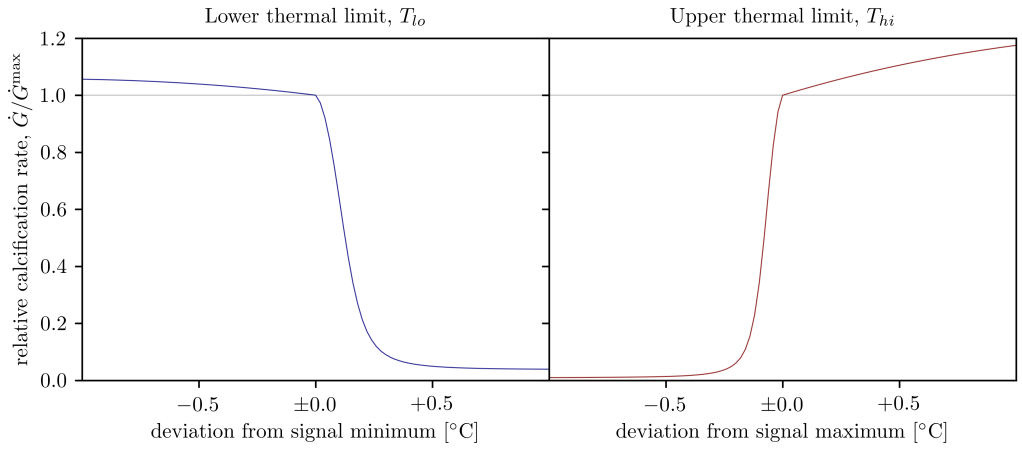

Figure D.15: Sensitivity analysis of the bleaching susceptibility. $T_c^{\min}$ and $T_c^{\max}$ are the respectively minimum and maximum of the thermal signal imposed (*see* Fig. D.14).

changes in the optimal temperature—as a side-effect of the changing thermal limits—are up to 10%, as the optimal temperature ranges between ±1.0°C (*see* Sec. D.3.3 and Fig. D.9).

Furthermore, exceeding the limits of the thermal range—i.e. bleaching—substantially alters the outcome. The calcification rate approaches zero quickly when the thermal limits are chosen such that bleaching occurs. This drop is due to the reduction in healthy coral cover, which is the only population state that contributes to the calcification (*see* Eq. 4.36). Again, this is more pronounced around the upper limit, where the reduction of healthy population is more severe.

D.5.2 Population dynamics

The sensitivity analysis concerning the population dynamics is based on the scenario in which a bleaching event occurs, while all corals are healthy. The length of this event is taken as variable as well, and after the bleaching event the conditions return to optimal conditions.

To eliminate the influences of any of the aforementioned dependencies and fully focus on the population dynamics, the photosynthetic rate is used as input parameter; without the use of temperatures whatsoever.

Table D.10: Parameters determining the population dynamics. r_G is the growth rate; r_R the recovery rate; r_M the mortality rate; r_B the bleaching rate; $|P_{opt}|$ the magnitude of the photosynthetic rate; C_{sp} the species constant; and t_B the duration of the bleaching event.

	Parameter	Estimate	Deviation	Unit
model	r_G	0.002	10%	–
	r_R	0.2		–
	r_M	0.04		–
	r_B	8.0		–
input	$\|P_{opt}\|$	0.01–1.00	n/a	–
	C_{sp}	0.1–1.0		–
	t_B	1–14		*days*

The value of the photosynthetic rate is assumed to represent the coral under ideal conditions; i.e. the coral's maximum photosynthetic rate. When the coral experiences stresses the photosynthetic rate switches sign. Thus, $P(I,T,u) = P_{opt}$ in case of no stresses; and $P(I,T,u) = -P_{opt}$ in case of stresses.

The effects of the population dynamics is twofold: (1) the health of the corals; and (2) the calcification—i.e. the growth—of the corals. Therefore, the output is presented as the influence on (1) the healthy coral cover and (2) the calcification. Both compared to the situation in which no bleaching would have occurred. Furthermore, the species constant is taken as an input parameter due to its non-linearity in the partial differential equations describing the population dynamics (*see* Eqs. 5.1a to 5.1d). An overview of all analysed parameters is given in Table D.10.

The results of the sensitivity analyses are presented in Figures D.16 and D.17. First of all, the stepwise increase and decrease due to the length of the bleaching event (*see* Figs. D.16 and D.17, last column) is due to the time-step used in the calculations of the population dynamics; namely a time-step of one day. Next, the duration of the bleaching event over which the gradients of the photosynthesis and the species constant are analysed is three days. For this duration, a maximum of around 80% of the corals has died. For longer bleaching durations, the analysis of the sensitivity of the constant rates becomes more troublesome as the full population is dead before recovery can start. This is clearly visible in the last columns of Figures D.16 and D.17 in which the sensitivity to the rates increases for increasing bleaching duration up to a certain tipping point after which the sensitivity declines again. This tipping point is marked by such a loss of living corals, that it is (almost) beyond recovery. Furthermore, the most pronounced sensitivities to the model parameters—for long bleaching events (*see* Figs. D.16 and D.17)—coincide with absolute errors of approximately zero (not shown). This is in line with the fact that there is no living coral cover left when the bleaching events are too long.[2]

The accuracy of the growth rate is of importance for both an increasing photosynthetic rate and an increasing species constant. Furthermore, one must bear in mind that this constant becomes especially important on the long-term dynamics at which the population needs to regrow as is shown by the green lines in Figures D.16 and D.17 (top rows). These lines represent the sensitivity after five years (1825 days equals five years). The growth rate's accuracy becomes more important for increasing bleaching duration as more has died and has to regrow, which is linearly dependent on the growth rate (*see* Eq. 5.1a).

The sensitivity of the population dynamics to the recovery rate is limited for longer time spans. On the other hand, close in time to the bleaching event its resulting error on both the healthy coral cover and the calcification is in the order of the imposed error; in most cases even less. As the recovery rate is only of importance when the coral bleaches but remains alive, its sensitivity approaches zero when the duration of the bleaching event increases and more of the corals die. Thus, the sensitivity of the population dynamics

[2] At what point a bleaching event is considered as 'too long' depends on the photosynthetic rate and the species constant, as those two parameters—in combination with the bleaching rate—define the rate at which the coral cover bleaches and eventually dies (*see* Eq. 5.1d).

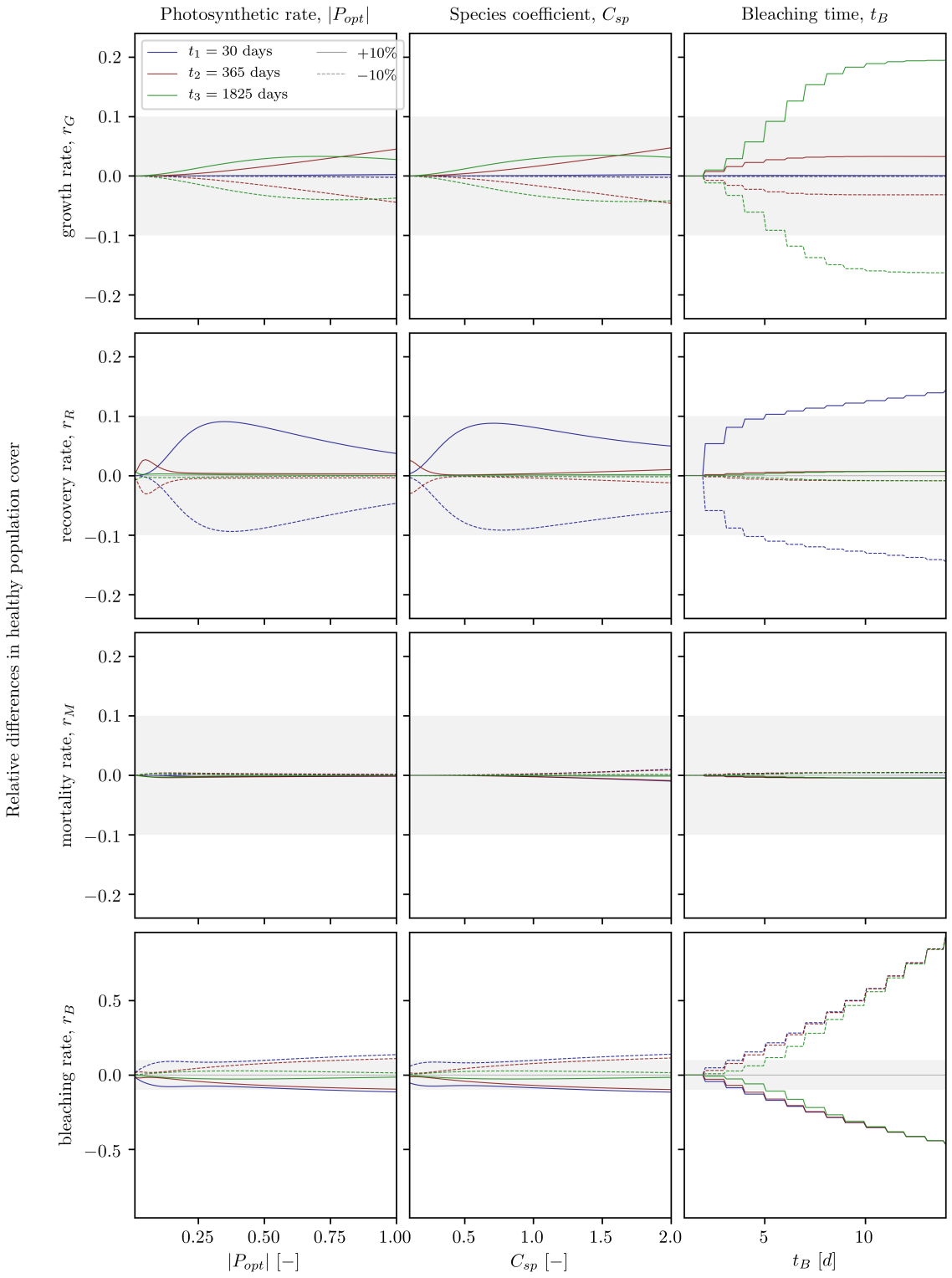

Figure D.16: Sensitivity analysis of the population dynamics on the health of the corals. Note the different scale used for the plots on the bottom row compared to all the other plots. The sensitivity of the parameters is expressed as relative difference in healthy population compared to the estimate (*see* Eq. D.1 and Tab. D.10). The gray-shaded area marks the threshold difference compared to the imposed deviation; i.e. the 10% mark.

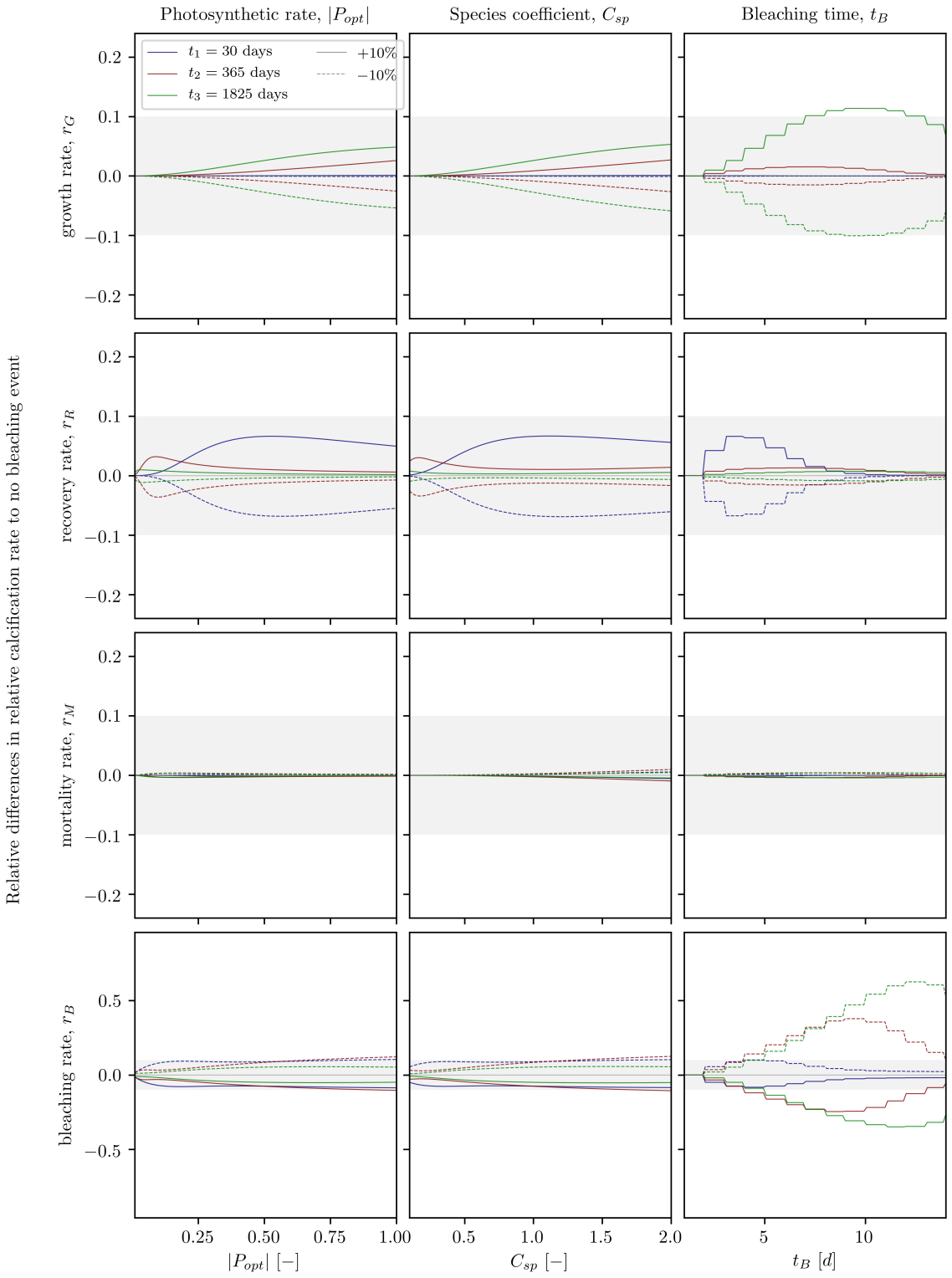

Figure D.17: Sensitivity analysis of the population dynamics on the calcification. Note the different scale used for the plots on the bottom row compared to all the other plots. The sensitivity of the parameters is expressed as relative difference in calcification compared to the estimate (*see* Eq. D.1 and Tab. D.10), where the calcification is taken with respect to the situation in which there would not have been a bleaching event. The gray-shaded area marks the threshold difference compared to the imposed deviation; i.e. the 10% mark.

on the recovery rate increases when the fraction of corals turning pale and bleached increases, but without much of this fraction dying. The increasing sensitivity of the healthy coral cover to the recovery rate for longer bleaching events (*see* Fig. D.16, second row, last column) is some misdirecting as the sensitivity seems the grow for longer bleaching events. This increasing sensitivity is due to the fact that the absolute error approaches zero (not shown).

The results are close to insensitive to the mortality rate in both cases (*see* Figs. D.16 and D.17, third row). Nevertheless, the importance of the mortality rate increases for increasing species constant as well as for decreasing photosynthetic rate. These dependencies are in line with the formulation of the continued mortality even though the stresses have gone (*see* Eq. 5.1c). The continued mortality of the bleached corals is the product of the mortality rate and the species constant. Thus, the contribution—and so the sensitivity—of the mortality rate increases when the species constant increases. Moreover, due to the absence of the photosynthetic rate in this formulation, this parameter does not contribute to the sensitivity to the mortality rate. It even reduces its relevance as it stimulates the recovery and thereby reduces the bleached fraction of corals (*see* Eq. 5.1b).

The healthy coral cover as well as the calcification are very sensitive to the bleaching rate at increasing duration of the bleaching event. This amplifies for longer time-scales and is mainly contributed to the (almost) complete disappearance of the coral cover due to the longer bleaching events. Thereby, the recovery is substantially reduced and so the healthy coral cover, which results in the reduction in calcification. However, one must take into account that in such situations close to all coral cover is dead and so analysing relative differences becomes more prone to rounding and computing errors. Nevertheless, the reduction in sensitivity is still computed (*see* Fig. D.17, bottom row, last column), which is due to the aforementioned complete removal of living coral.

All in all, the accuracy of the mortality rate is of limited importance and all other model parameters result in a deviation in the outcome comparable to the deviation imposed on the parameter, with the exception for longer bleaching events. In those cases, the relative error increases for increasing duration of bleaching. However, at the same time the absolute error is reducing and approaching zero. By approaching zero, the calculations behind the analyses are more prone for rounding and computing errors. Thereby, the outcomes could be misleading. From all model parameters, errors in the estimate of the bleaching rate result in the largest deviations in the outcomes concerning the population dynamics. Thereby, it results in the largest errors in the calcification; both in relative sense and in absolute sense.

D.6 Coral dislodgement

The sensitivity analysis on the dislodgement is rather ambitious as the coral colony is dislodged, or not; i.e. it is a binary process instead of a continuum. Nevertheless, a continuum is created to analyse the influence of various parameters. The dislodgement threshold is rewritten into a 'safety number' using its two components; the dislodgement mechanical threshold (DMT), and the colony shape factor (CSF) (*see* Eq. 6.1):

$$S_D = \frac{DMT}{CSF} \tag{D.3}$$

in which

$$DMT = \frac{\sigma_t}{\rho_w C_d u_b^2} \tag{D.4a}$$

$$CSF = \frac{16}{\pi b_c^3} \int_0^{h_c} \hat{z} w_c(\hat{z}) \, \mathrm{d}\hat{z} \tag{D.4b}$$

where the CSF is fully described by the colony morphology via the morphological ratios in combination with the coral volume; and $\hat{z}$ is the vertical axis that is positive upwards with $\hat{z} = 0$ at the bottom. The larger the safety number, the less prone the coral colony is to dislodgement.

Again, the influence of the morphology is analysed using the three representative morphologies as used previously: (1) branching; (2) massive; and (3) plate. However, the volume of the coral is taken as a continuum to represent the growth of the coral. Hereby, the coral can become more susceptible to dislodgement. An overview of all parameters included in the sensitivity analysis is presented in Table D.11.

Table D.11: Parameters determining the dislodgement susceptibility. r_f is the coral form ratio, or the height-to-diameter ratio; r_p the plate ratio, or the base-to-diameter ratio; C_d the drag coefficient; σ_t the tensile strength of the substratum; u_m the (depth-averaged) flow velocity; ρ the density of water; and V_c the coral volume.

	Parameter	Estimate	Deviation	Unit
model	r_f	*see* Tab. D.1	10%	–
	r_p			–
	C_d[a]	1.11		–
	σ_t	$2.0{\cdot}10^5$		Nm^{-2}
input	u_m	1.0–10.0	n/a	m^{-1}
	ρ	1,000–1,030		$kg\ m^{-3}$
	V_c	0.01–1.00		m^3

[a] The estimate is chosen such that the drag coefficient has a minimum of one, which is a constrain due to its definition (*see* Eq. 4.24).

The results of the sensitivity analyses are presented in Figures D.18 and D.19. These figures only contain the results for the massive morphology, as all other morphologies show comparable plots in which only the magnitude might differ. The shape of the plots, however, is the same. Including these plots does not contribute to the clarification of the sensitivity analysis of the dislodgement susceptibility.

From Figure D.18 becomes clear that the sensitivity of the model parameters is independent of the input parameters; i.e. there is a linear relation. Nevertheless, the safety number does change over the gradients of the flow velocity and the density of water, where the gradient in the latter is hard to distinguish from Figure D.18 due to the small range covered. However, the volume of the coral colony does not result in different outcomes of the sensitivity of the safety number in both the relative and the absolute sense (*see* Figs. D.18 and D.19); even for unrealistic ranges of coral volumes. This suggests that the dislodgement of corals is insensitive to its volume, as long as its morphological ratios remain the same.

At first, this seems counterintuitive but when assessing the associated math it makes sense. All morphological dimensions are determined based on the morphological ratios in combination with the volume of the coral colony. Thereby, all these dimensions are proportional to the cube-root of the coral volume; i.e. $d_c, h_c, b_c, t_c \propto \sqrt[3]{V_c}$. This dependency of the morphological dimensions cancels out in the determination of the CSF, which is a dimensionless number. Therefore, the CSF is solely based on the morphological ratios and is independent of the volume.

That the CSF is based on the form and plate ratios is clearly visible in Figure D.18, where the possible error of the ratio is amplified. The amplification of the error—i.e. the sensitivity—due to the plate ratio is most pronounced for the massive morphology, which results in approximately tripling of the imposed error. Nevertheless, the other morphologies result in at least a doubling of the error (not shown). The sensitivity to the form ratio is the same for all morphologies and also results in more than doubling of the error (*see* Fig. D.18, top row). This is, however, not the general case as clearly visible in Figure D.20. Note that the colorbar in Figure D.20 has a logarithmic scale.

The sensitivity analyses of the safety number to the drag coefficient and the tensile strength show a one-to-one relation (*see* Fig. D.18, third and fourth row). This does not pose any substantial problems in case of the drag coefficient. The drag coefficient equals one for larger flow velocities (*see* Fig. D.2), which can be stated with great certainty. The assumption of the drag coefficient to equal one does not result in noticeable errors, as the dislodgement of corals occurs only due to high flow velocities; when the drag coefficient approaches one [White, 2006]. Moreover, this assumption is commonly made [e.g. Madin and Connolly, 2006].

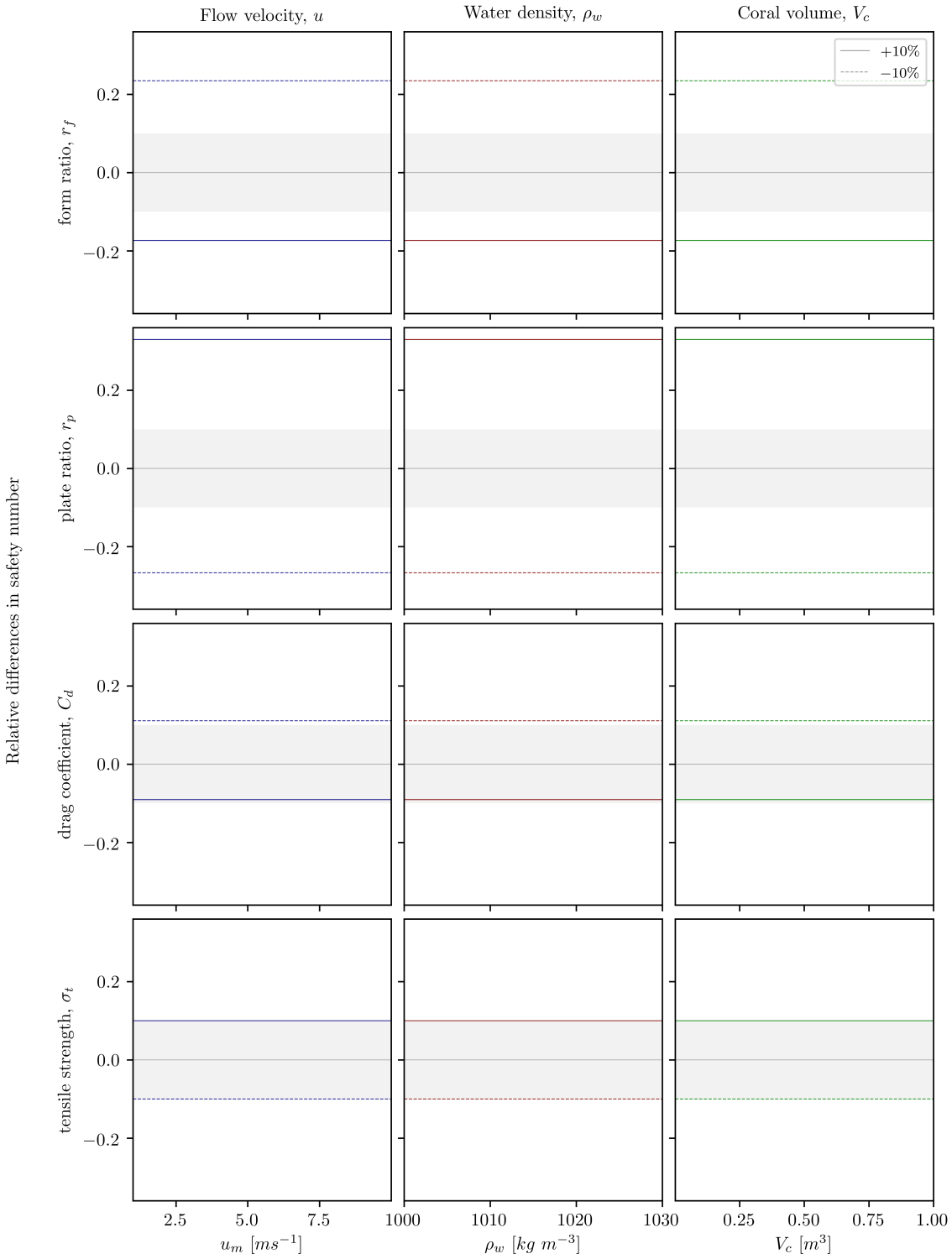

Figure D.18: Sensitivity analysis of the coral morphology on the dislodgement in relative differences. The sensitivity of the parameters is expressed as relative difference in safety number compared to the estimate (*see* Eqs. D.1 and D.3, and Tab. D.11). The morphology is based on the representative massive morphology (*see* Tab. D.11). The gray-shaded area marks the threshold difference compared to the imposed deviation; i.e. the 10% mark.

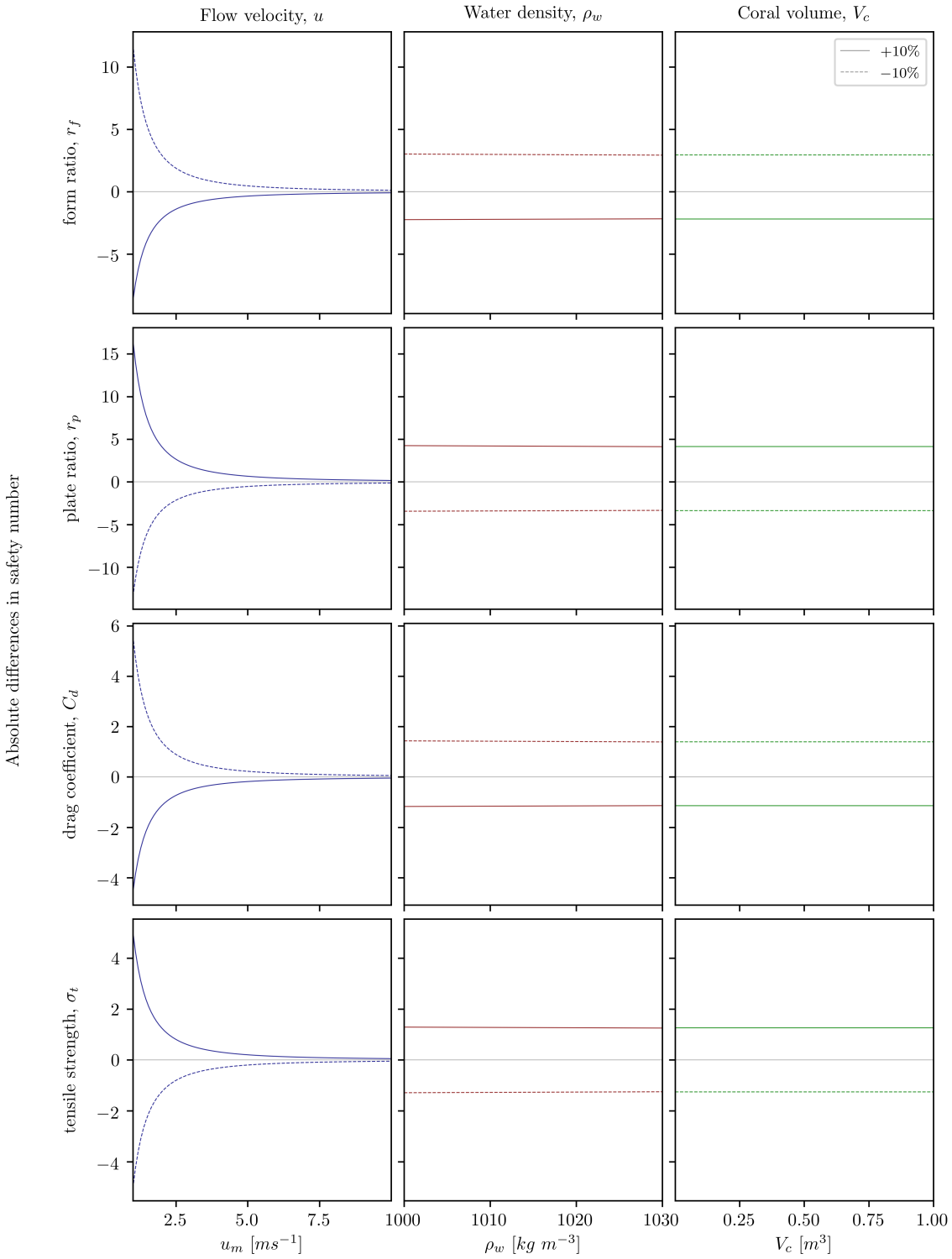

Figure D.19: Sensitivity analysis of the coral morphology on the dislodgement in absolute differences. The sensitivity of the parameters is expressed as absolute difference in safety number compared to the estimate (*see* Eq. D.3, and Tab. D.11). The morphology is based on the representative massive morphology (*see* Tab. D.11).

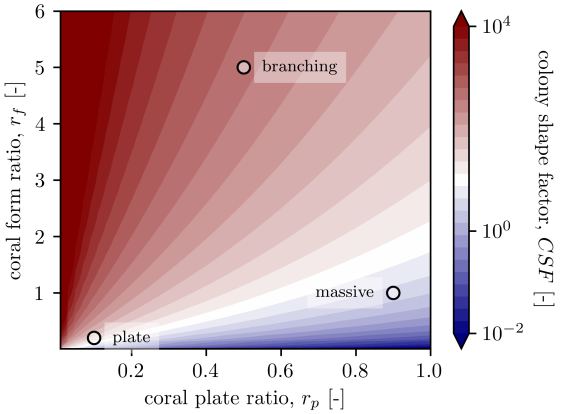

Figure D.20: The colony shape factor as function of the morphological ratios. Note the logarithmic scale of the colorbar. The representative morphologies as used in the sensitivity analyses are marked in this continuous plot. The CSF is fully described by the plotted morphological ratios and the coral volume does not affect the CSF (*see* text).

The sensitivity of the safety number to the tensile strength poses a more critical problem, as this parameter is hard to determine and shows a large range in literature [Madin, 2005]. Figure D.18 shows that an error of 10% in the determination of the tensile strength, would result in the same error of the safety number. This can have substantial effects on the computations associated with the dislodgement of corals. Especially because the tensile strength covers a range of multiple orders of magnitude [Madin, 2005].

All in all, the coral dislodgement is very sensitive to the coral morphology. Especially when taking the wide spreading of the morphological ratios into account (*see* App. D.4). The dislodgement is evenly sensitive to the drag coefficient as to the tensile strength. However, the drag coefficient equals one with great certainty, while the literature shows great spreading on the value of the tensile strength. This spreading covers multiple orders of magnitude, and so imposes a great sensitivity of the dislodgement susceptibility to the tensile strength.

D.7 Full model analysis

The set up of the sensitivity analyses of the full model is somewhat different from the modular analyses as the focus is on the sensitivity on the long-term; i.e. decades to centuries. Furthermore, a representative climate is considered for all four environmental factors in which some variation is included (*see* App. C). The selection of parameters is based on their effect on the long-term coral development. As the bleaching and storm events are the most pronounced contributors to substantial variations in the coral development, key parameters of these processes are included in the full analysis. Furthermore, the recovery after such an event is of importance for the long-term development as well, which is hard to analyse in the modular set up. Thus the parameters of interest are:

1. the thermal-acclimatisation coefficient, K_{var};
2. the strength of the substratum, σ_t; and
3. the probability of settlement, p_s.

Table D.12 gives an overview of the ranges over which the parameters are analysed.

The full model sensitivity analysis makes use of nine virtual stations that are placed at equal distance perpendicular to the shoreline (*see* Fig. B.1a, App. B.3). Virtual station 1 is at the deep end, and virtual

Table D.12: Overview of the selected parameters for the sensitivity analysis of the full biophysical model framework. The bleaching susceptibility is analysed via the sensitivity to the thermal-acclimatisation coefficient, K_{var}; the dislodgement susceptibility is analysed via the sensitivity to the tensile strength of the substratum, σ_t; and the recovery is analysed via the probability of settlement of coral larvae, p_s.

Parameter	Estimates			Unit	Reason
	min	mid	max		
K_{var}	2.00	2.45	3.00	–	Bleaching susceptibility
σ_t	0.1	0.2	1.0	$\times 10^6\ Nm^{-2}$	Dislodgement susceptibility
p_s	10^{-4}	10^{-2}	10^{-1}	–	Recovery

station 9 is closest to the beach. The reef flat already starts at virtual station 5 and the water depth slightly decreases towards virtual station 9.

The plots of the three sensitivity analyses are displayed on the following pages and briefly commented on in Appendices D.7.1 to D.7.3. All are presented by the differences on the healthy coral cover and the coral volume.

D.7.1 Bleaching

The sensitivity analysis on the bleaching susceptibility—i.e. on the thermal-acclimatisation coefficient—is presented in Figures D.21 and D.22 (pp. 174–175) for the coral cover and volume, respectively. First of all, the effects of the thermal-acclimatisation coefficient are substantial on the long-term development of corals; both on their cover and volume. The coral cover shows no clear dependency of the sensitivity on the depth gradient (*see* Figs D.21a to D.21i), while there is one on the coral volume (*see* Figs. D.22a to D.22i); the sensitivity increases towards shallower areas on the reef.

D.7.2 Dislodgement

The sensitivity analysis on the dislodgement susceptibility—i.e. on the tensile strength of the substratum—is presented in Figures D.23 and D.24 (pp. 176–177) for the coral cover and volume, respectively. As the dislodgement criterion is a binary output—dislodgement or not—only virtual station 2 (*see* Figs. D.23b and D.24b) show differences between the different values of the tensile strength of the substratum. This is because the tipping point of dislodgement is around this virtual station. The effects of meeting the dislodgement criterion or not are tremendous on both the coral cover and the volume.

D.7.3 Recovery

The sensitivity analysis on the recovery—i.e. on the probability of settlement of coral larvae—is presented in Figures D.25 and D.26 (pp. 178–179) for the coral cover and volume, respectively. All virtual stations show the dislodgement of corals due to a storm except for virtual station 1 (*see* Figs. D.25a and D.26a), which is out of the danger zone as the dislodgement criterion is not met. For the other virtual stations, a clear difference is present when the probability of settlement is one order of magnitude larger; i.e. from $p_s = 10^{-4}$ to $p_s = 10^{-3}$. Furthermore, there is a trend over the depth gradient, which is most pronounced for the coral cover (*see* Figs. D.25b to D.25i): the effects of the probability of settlement increase for decreasing depth. This holds for the coral volume as well (*see* Figs. D.26b to D.26i), but is less pronounced.

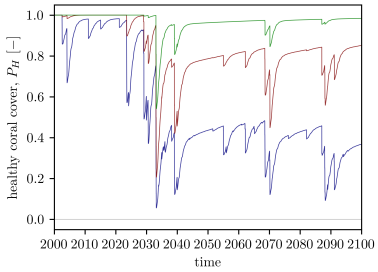

(a) Virtual station 1.

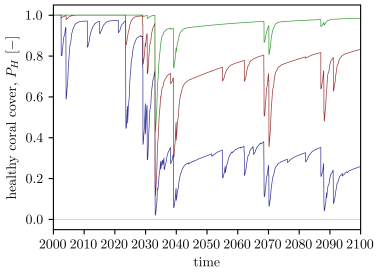

(b) Virtual station 2.

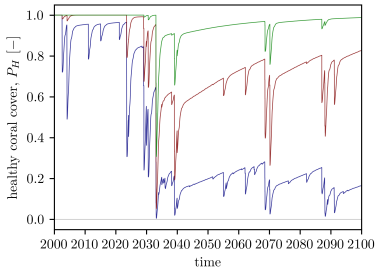

(c) Virtual station 3.

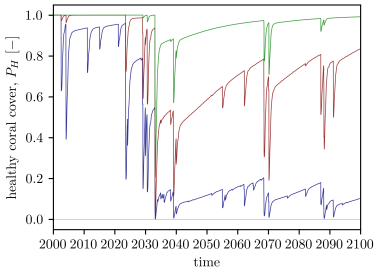

(d) Virtual station 4.

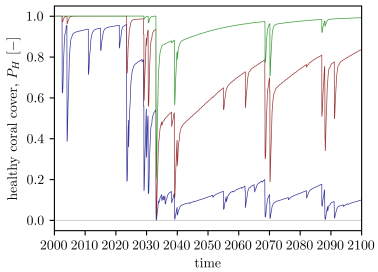

(e) Virtual station 5.

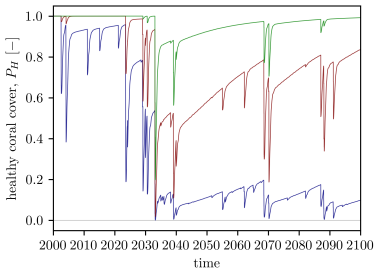

(f) Virtual station 6.

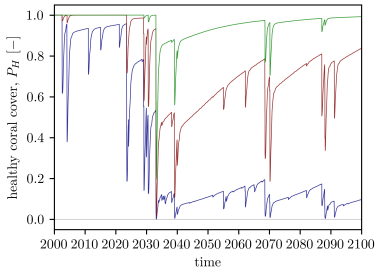

(g) Virtual station 7.

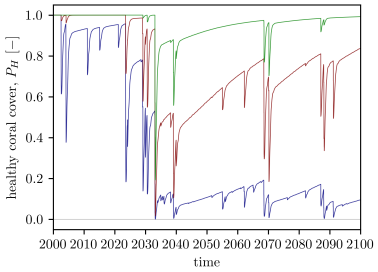

(h) Virtual station 8.

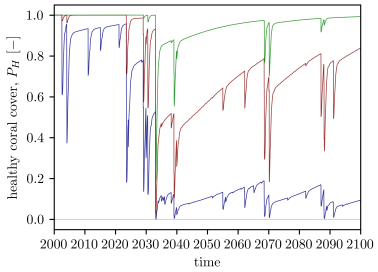

(i) Virtual station 9.

Figure D.21: Sensitivity of the healthy coral cover to the thermal-acclimation coefficient. Virtual station 1 is at the deep end of the fringing reef, and virtual station 9 at the shallow end (*see* Fig. B.1a, App. B.3).

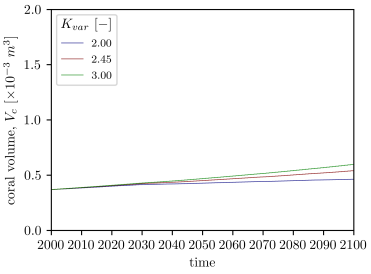

(a) Virtual station 1.

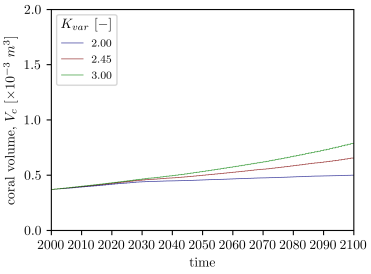

(b) Virtual station 2.

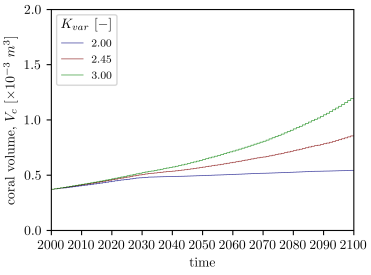

(c) Virtual station 3.

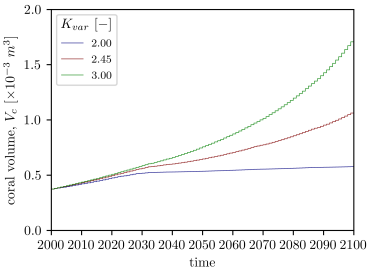

(d) Virtual station 4.

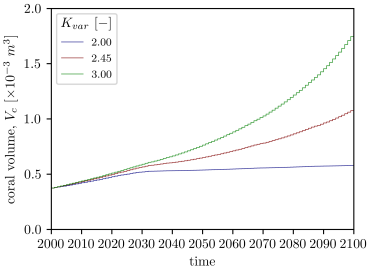

(e) Virtual station 5.

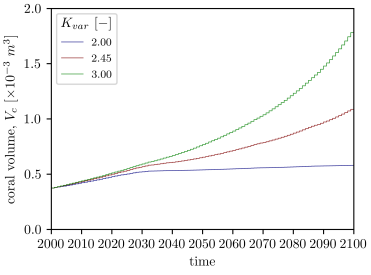

(f) Virtual station 6.

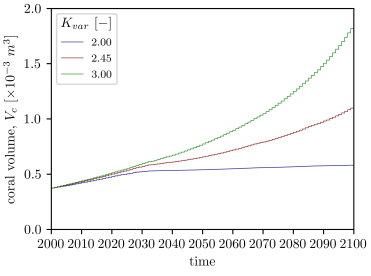

(g) Virtual station 7.

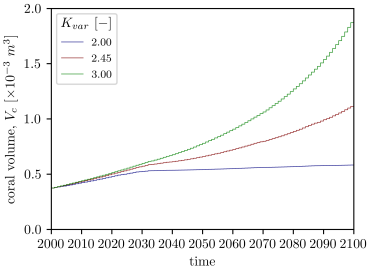

(h) Virtual station 8.

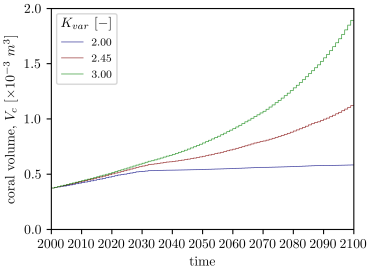

(i) Virtual station 9.

Figure D.22: Sensitivity of the coral volume to the thermal-acclimation coefficient. Virtual station 1 is at the deep end of the fringing reef, and virtual station 9 at the shallow end (*see* Fig. B.1a, App. B.3).

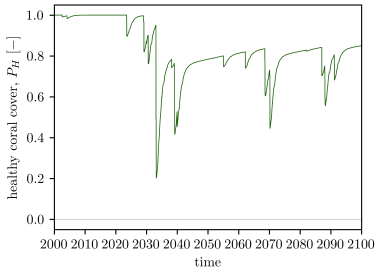

(a) Virtual station 1.

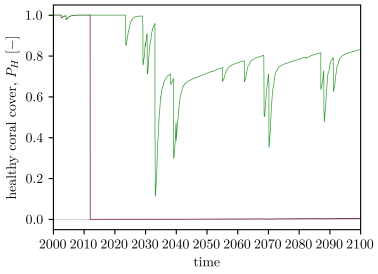

(b) Virtual station 2.

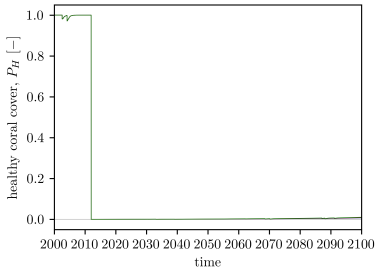

(c) Virtual station 3.

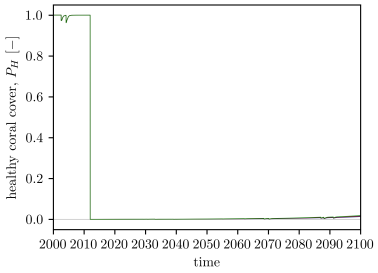

(d) Virtual station 4.

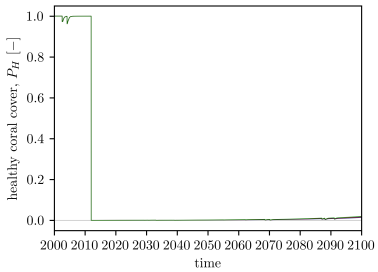

(e) Virtual station 5.

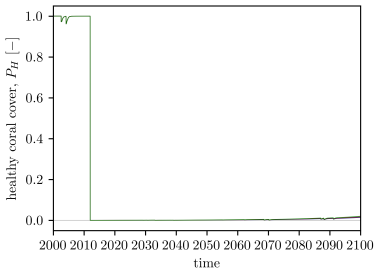

(f) Virtual station 6.

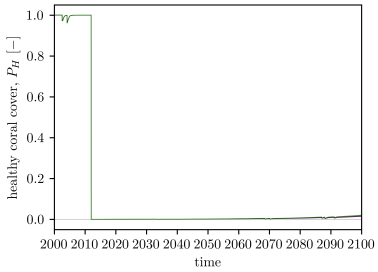

(g) Virtual station 7.

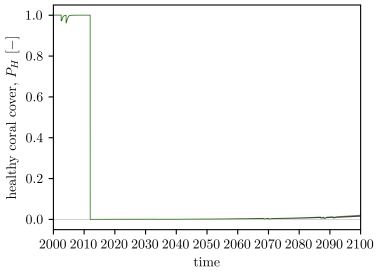

(h) Virtual station 8.

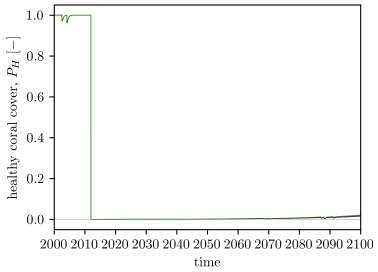

(i) Virtual station 9.

Figure D.23: Sensitivity of the healthy coral cover to the tensile strength of the substratum. Virtual station 1 is at the deep end of the fringing reef, and virtual station 9 at the shallow end (*see* Fig. B.1a, App. B.3).

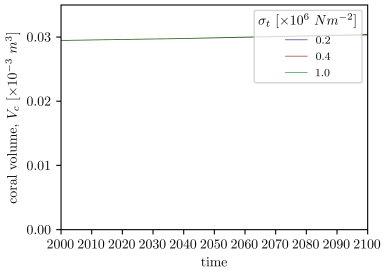

(a) Virtual station 1.

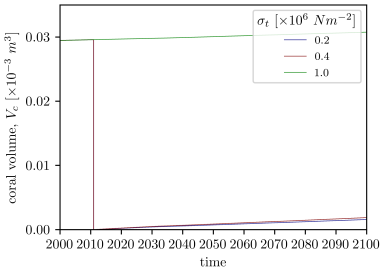

(b) Virtual station 2.

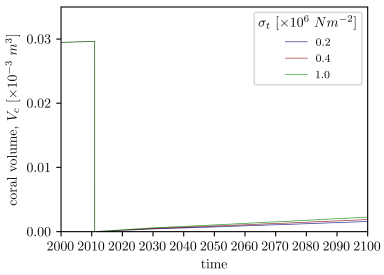

(c) Virtual station 3.

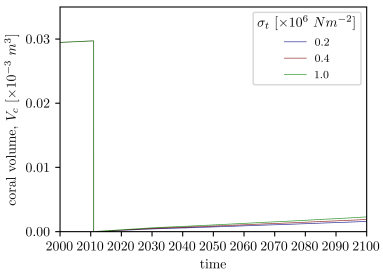

(d) Virtual station 4.

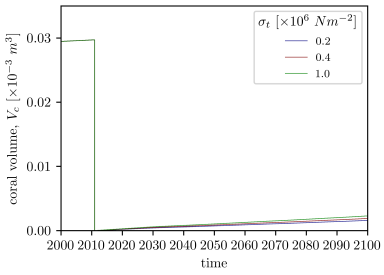

(e) Virtual station 5.

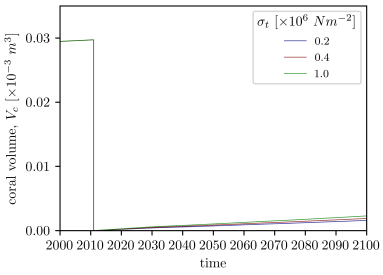

(f) Virtual station 6.

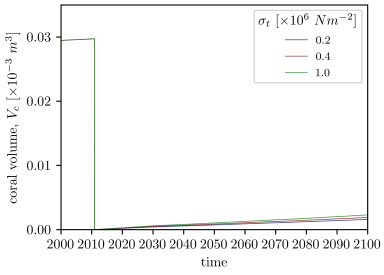

(g) Virtual station 7.

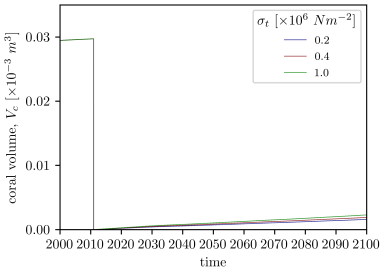

(h) Virtual station 8.

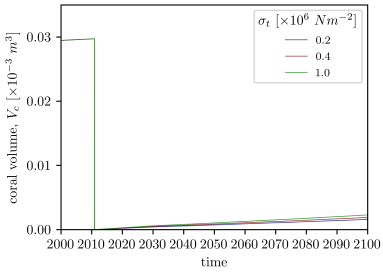

(i) Virtual station 9.

Figure D.24: Sensitivity of the coral volume to the tensile strength of the substratum. Virtual station 1 is at the deep end of the fringing reef, and virtual station 9 at the shallow end (*see* Fig. B.1a, App. B.3).

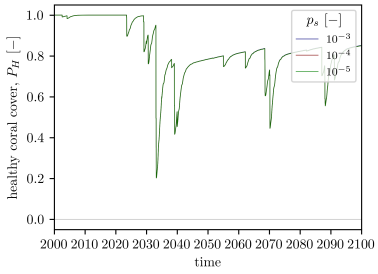

(a) Virtual station 1.

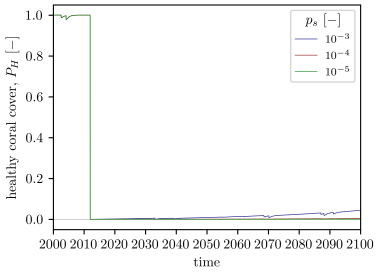

(b) Virtual station 2.

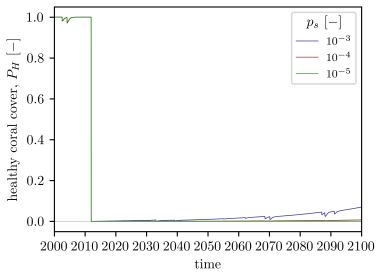

(c) Virtual station 3.

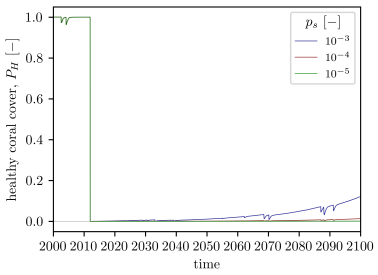

(d) Virtual station 4.

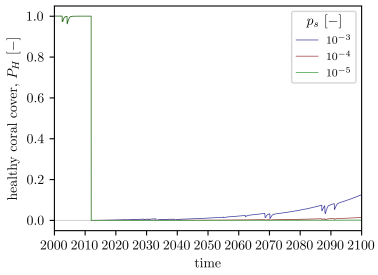

(e) Virtual station 5.

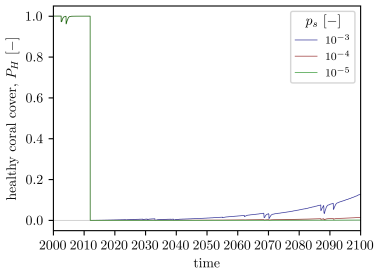

(f) Virtual station 6.

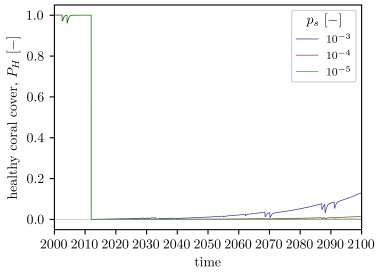

(g) Virtual station 7.

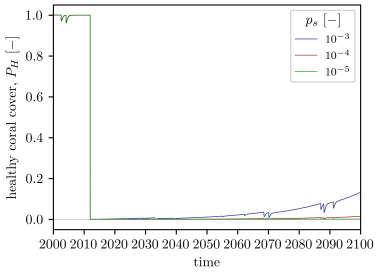

(h) Virtual station 8.

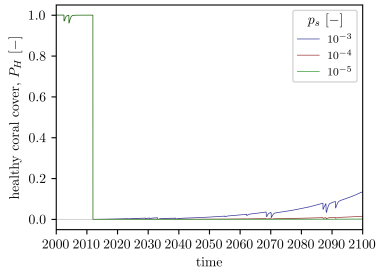

(i) Virtual station 9.

Figure D.25: Sensitivity of the healthy coral cover to the probability of settlement of coral larvae. Virtual station 1 is at the deep end of the fringing reef, and virtual station 9 at the shallow end (*see* Fig. B.1a, App. B.3).

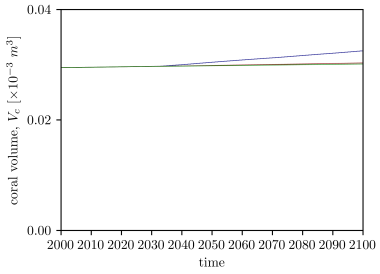

(a) Virtual station 1.

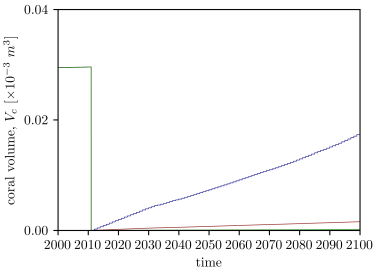

(b) Virtual station 2.

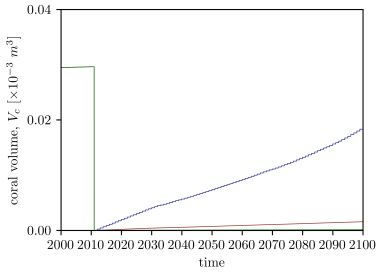

(c) Virtual station 3.

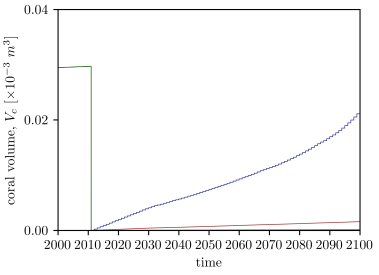

(d) Virtual station 4.

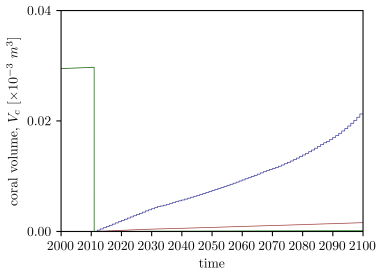

(e) Virtual station 5.

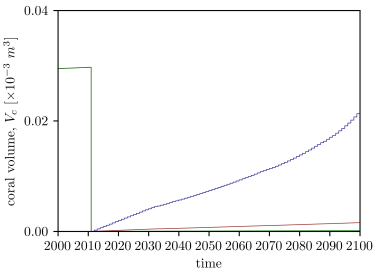

(f) Virtual station 6.

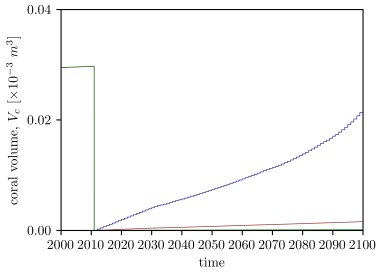

(g) Virtual station 7.

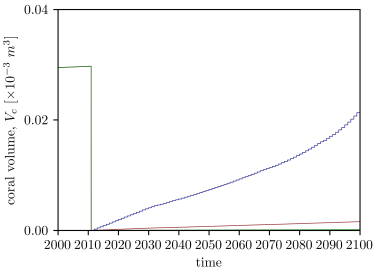

(h) Virtual station 8.

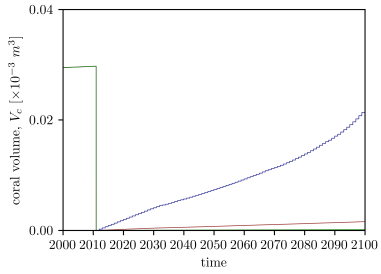

(i) Virtual station 9.

Figure D.26: Sensitivity of the coral volume to the probability of settlement of coral larvae. Virtual station 1 is at the deep end of the fringing reef, and virtual station 9 at the shallow end (*see* Fig. B.1a, App. B.3).

Appendix E

Canopy-Flow Theory: Derivations of formulae

This appendix shows the derivations of the various steps taken in the development of the formulae on the Canopy-Flow Theory (CFT). First, the two momentum balances are covered for (1) above the canopy (App. E.1); and (2) in the canopy (App. E.2). Second, the solution of the in-canopy flow is presented in Appendix E.3. Finally, approximations for the solutions of the CFT are discussed and presented in Appendix E.4.

A different frame of reference is used in the derivations used for the in-canopy flow formulations, compared to the main text. The differences are (1) the direction of the vertical axis, which is upward; and (2) the origin of the vertical axis, which is at the bottom. These modifications to the frame of reference clarify the derivations associated with the in-canopy flow. Because of the difference, the vertical axis is denoted differently to distinguish with the description used in the main text; this vertical axis is indicated by $\hat{z}$.

E.1 Above-canopy momentum balance

The momentum balance equation (*see* Eq. 4.12) forms the basis of the above-canopy. It is assumed that the above-canopy flow is not hindered by the canopy. Therefore, it is solely the balance between the flow acceleration and the pressure gradient:

$$\frac{\partial u}{\partial t} = -\frac{1}{\rho}\frac{\partial p}{\partial x} \tag{E.1}$$

Equation (E.1) is fully in line with linear wave theory. According to linear wave theory, the pressure is given by [Holthuijsen, 2007]:

$$p = \rho g a \frac{\cosh\left[k\left(z+d\right)\right]}{\cosh\left[kd\right]} \sin\left(\omega t - kx\right) \tag{E.2}$$

and the horizontal flow velocity is given by:

$$u = \omega a \frac{\cosh\left[k\left(z+d\right)\right]}{\sinh\left[kd\right]} \sin\left(\omega t - kx\right) \tag{E.3}$$

where ρ is the density; g the gravitational acceleration; a the wave-orbital motion; k the wave-number, $k = 2\pi/L$; ω the wave-frequency, $\omega = 2\pi/T$; z the vertical coordinate, which is vertical upward with $z = 0$ at mean sea level; d the water depth; x the horizontal coordinate positive in streamwise direction; and t the time coordinate.

From Equation (E.2) follows that the pressure gradient—i.e. $\partial p/\partial x$— is given by:

$$\frac{\partial p}{\partial x} = -\rho g k a \frac{\cosh\left[k\left(z+d\right)\right]}{\cosh\left[kd\right]} \cos\left(\omega t - kx\right) \tag{E.4}$$

From Equation (E.3) follows that the flow acceleration—i.e. $\partial u/\partial t$—is given by:

$$\frac{\partial u}{\partial t} = \omega^2 a \frac{\cosh\left[k\left(z+d\right)\right]}{\cosh\left[kd\right]} \cos\left(\omega t - kx\right) \tag{E.5}$$

Equations (E.4) and (E.5) are related via the dispersion relation:

$$\omega^2 = gk \tanh\left[kd\right] \tag{E.6}$$

When Equations (E.5) and (E.6) are combined, the result in given by:

$$\frac{\partial u}{\partial t} = gka \frac{\cosh\left[k\left(z+d\right)\right]}{\cosh\left[kd\right]} \cos\left(\omega t - kx\right) \tag{E.7}$$

From Equations (E.4) and (E.7), the relation becomes evident and is given by:

$$-\frac{1}{\rho}\frac{\partial p}{\partial x} = \frac{\partial u}{\partial t} \tag{E.8}$$

Thereby, the acceleration—or the unsteadiness [Zeller et al., 2015]—of the flow is related to the pressure gradient; according to linear wave theory.

E.2 In-canopy momentum balance

The momentum balance equation in streamwise direction (*see* Eq. 4.12) is repeated here for convenience:

$$\frac{\partial u}{\partial t} = -\frac{1}{\rho}\frac{\partial p}{\partial x} + \frac{1}{\rho}\frac{\partial \tau}{\partial z} - f_w \tag{E.9}$$

where u is the flow velocity; ρ is the density of the water; p the pressure; τ the shear stress; and f_w the resistance force, which is given by the well-known Morison equation:

$$f_w = f_d + f_i \tag{E.10}$$

where f_d is the drag force; and f_i the inertia force.

In Equation (E.9), the vertical advection is not taken into account as its relevance is shown to be negligible [Zeller et al., 2015].

The three forces in Equation (E.9) are treated separately in the following sections: (1) shear; (2) drag; and (3) inertia (Secs. E.2.1 to E.2.3, resp.).

E.2.1 Shear

The shear component is given by the turbulence-induced Reynolds stresses, which is given by:

$$\tau = -\rho \left\langle \overline{u'w'} \right\rangle \tag{E.11}$$

where τ is the shear stress; and the prime denotes the fluctuation over the ensemble average, i.e. the turbulent motion.

Lowe et al. [2005a] represents this shear stress using a friction coefficient, while Zeller et al. [2015] suggests to use Smagorinsky's model [Smagorinsky, 1963] for the representation of turbulence-induced shear. The two methods give in practice comparable results. However, the method as described by Zeller et al. [2015] is more process-based and therefore used in this study [Vreman et al., 1997]:

$$-\left\langle \overline{u'w'} \right\rangle = C_s^2 \Delta^2 \left| \frac{\partial u}{\partial z} \right| \frac{\partial u}{\partial z} \tag{E.12}$$

where C_s is the Smagorinsky constant; and Δ the filter length. When applying an implicit filter—i.e. $\Delta = \Delta z$—this reduces in the case of the canopy flow to:

$$-\left\langle \overline{u'w'} \right\rangle = C_s^2 \left| \Delta u \right| \Delta u \tag{E.13}$$

where Δu is the flow velocity above the interface subtracted by the flow velocity below the interface; e.g. in case of a single-layered canopy $\Delta u = u_f - u_p$, if the interface is at the top of the canopy.

This is in line with the turbulent kinetic energy budget [Zeller et al., 2015] in which the shear production at the interface gives similar results.

E.2.2 Drag

The drag component in Equation (E.9) is related to the production of wakes in the turbulent kinetic energy budget [Zeller et al., 2015]. King et al. [2012] suggests to add a factor incorporating the transfer of turbulent kinetic energy to heat due to the viscous stresses. However, this is negligible [Uijttewaal, 2019] and therefore not taken into account.

For the description of the drag component as function of the water depth, the λ-parameters [Britter and Hanna, 2003] are written as continuous functions over the vertical [Weitzman et al., 2015]:

$$\phi(z) = \frac{w_c(z)}{\frac{1}{2} a_c^2} \tag{E.14a}$$

$$\psi(z) = \frac{\frac{\pi}{4} w_c(z)^2}{\frac{1}{2} a_c^2} \tag{E.14b}$$

where $w_c(z)$ is the width—or diameter—of the obstruction as function of z.

Therefore, the drag component is given by the well-known formulation of the drag force per volume mass [e.g. van Rooijen et al., 2018] taken as integral over the canopy height:

$$f_d = \frac{F_d}{\rho} = \frac{1}{2} \int_{z=0}^{h} \frac{C_d \phi}{1 - \psi} u^2 \, \mathrm{d}z \tag{E.15}$$

where F_d is the drag force; and C_d the drag coefficient.

E.2.3 Inertia

The inertia component is unique for accelerating flows and is given by [Lowe et al., 2005a; Weitzman et al., 2015; Zeller et al., 2015]:

$$f_i = \frac{C_m \psi}{1 - \psi} \frac{\partial u}{\partial t} \tag{E.16}$$

where C_m is the inertia coefficient.

E.3 Solution in-canopy flow

First, the solution of the in-canopy flow is determined based on a two-layer system (Sec. E.3.1); i.e. in-canopy flow and above-canopy flow. Thereby, there is only one wave-attenuation coefficient (WAC). This solution can easily be extended to a multi-layer canopy, which is what this section concludes with (Sec. E.3.2).

E.3.1 Two-layer system

The formulation of the two-layer system (Eq. 4.15) is repeated here for convenience:

$$\frac{\partial\left(u_p-u_f\right)}{\partial t}=\frac{\left|u_f-u_p\right|\left(u_f-u_p\right)}{L_s}-\frac{\left|u_p\right|u_p}{L_d}-\frac{C_m\lambda_p}{1-\lambda_p}\frac{\partial u_p}{\partial t} \tag{E.17}$$

Luhar et al. [2010] suggests to solve this equation by writing the flow velocities as the real part of the complex wave notation:

$$u_p=\mathcal{R}e\{\beta\omega a_f\exp\left[i\omega t\right]\} \tag{E.18a}$$

$$u_f=\mathcal{R}e\{\omega a_f\exp\left[i\omega t\right]\} \tag{E.18b}$$

where ω and a_f are real and positive, while β may be complex; in which $\alpha_w=|\beta|$.

The solution of Equation (E.17) is then given as:

$$\begin{aligned}\frac{\partial}{\partial t}\Big(\mathcal{R}e\{\beta\omega a_f\exp\left[i\omega t\right]\}\Big)-\frac{\partial}{\partial t}\Big(\mathcal{R}e\{\omega a_f\exp\left[i\omega t\right]\}\Big)=\\ \frac{1}{L_s}\Big|\mathcal{R}e\{\omega a_f\exp\left[i\omega t\right]\}-\mathcal{R}e\{\beta\omega a_f\exp\left[i\omega t\right]\}\Big|\Big(\mathcal{R}e\{\omega a_f\exp\left[i\omega t\right]\}-\mathcal{R}e\{\beta\omega a_f\exp\left[i\omega t\right]\}\Big)\\ -\frac{1}{L_d}\Big|\mathcal{R}e\{\beta\omega a_f\exp\left[i\omega t\right]\}\Big|\mathcal{R}e\{\beta\omega a_f\exp\left[i\omega t\right]\}\\ -\frac{C_m\lambda_p}{1-\lambda_p}\frac{\partial}{\partial t}\Big(\mathcal{R}e\{\beta\omega a_f\exp\left[i\omega t\right]\}\Big)\end{aligned} \tag{E.19}$$

which results in:

$$\begin{aligned}i\left(\beta-1\right)\omega^2 a_f\mathcal{R}e\{\exp\left[i\omega t\right]\}=\\ \frac{\omega^2a_f^2}{L_s}\left|\left(1-\beta\right)\mathcal{R}e\{\exp\left[i\omega t\right]\}\right|\left(1-\beta\right)\mathcal{R}e\{\exp\left[i\omega t\right]\}\\ -\frac{\omega^2a_f^2}{L_d}\left|\mathcal{R}e\{\beta\exp\left[i\omega t\right]\}\right|\mathcal{R}e\{\beta\exp\left[i\omega t\right]\}\\ -i\frac{C_m\lambda_p}{1-\lambda_p}\beta\omega^2a_f\mathcal{R}e\{\exp\left[i\omega t\right]\}\end{aligned} \tag{E.20}$$

In Equations (E.19) and (E.20), the shear and drag length-scales are defined as:

$$L_s=\frac{h_c}{C_s^2} \tag{E.21a}$$

$$L_d=\frac{2h_c\left(1-\lambda_p\right)}{C_d\lambda_f} \tag{E.21b}$$

in which the frontal and planar λ-parameters are the depth-integrations of Equations (E.14a) and (E.14b) over the canopy height:

$$\lambda_f=\int_{\hat{z}=0}^{h_c}\phi\ \mathrm{d}\hat{z}=\frac{h_cd_c}{\frac{1}{2}a_c^2} \tag{E.22a}$$

$$\lambda_p=\int_{\hat{z}=0}^{h_c}\psi\ \mathrm{d}\hat{z}=\frac{\frac{\pi}{4}d_c^2}{\frac{1}{2}a_c^2} \tag{E.22b}$$

where λ_f and λ_p are the frontal and planar λ-parameters, respectively; and $\hat{z}$ is the vertical coordinate positive upward with $\hat{z}=0$ at the bottom.

Next, the complex wave notation is rewritten for which holds $\mathcal{R}e\{\exp\left[i\omega t\right]\}=\cos\left(\omega t\right)$, and the formulation is shortened:

$$\begin{aligned}i\left(\beta-1\right)\cos\left(\omega t\right)=\frac{a_f}{L_s}\left|1-\beta\right|\left(1-\beta\right)\cdot\left|\cos\left(\omega t\right)\right|\cos\left(\omega t\right)\\ -\frac{a_f}{L_d}\left|\beta\right|\beta\cdot\left|\cos\left(\omega t\right)\right|\cos\left(\omega t\right)-i\beta\frac{C_m\lambda_p}{1-\lambda_p}\cos\left(\omega t\right)\end{aligned} \tag{E.23}$$

Further simplification requires the linearisation of the quadratic terms using the first Fourier harmonic. This linearisation of the quadratic terms results in an constant that must be included. The linearised form of Equation (E.23) is given by:

$$i\left(\beta-1\right)\cos\left(\omega t\right)=\xi\frac{a_f}{L_s}\left|1-\beta\right|\left(1-\beta\right)\cos\left(\omega t\right)-\xi\frac{a_f}{L_d}\left|\beta\right|\beta\cos\left(\omega t\right)-i\beta\frac{C_m\lambda_p}{1-\lambda_p}\cos\left(\omega t\right) \tag{E.24}$$

in which this constant is given by:

$$\xi=\frac{\int_0^T\left|\cos\left(\omega t\right)\right|\cos\left(\omega t\right)\cos\left(\frac{2\pi t}{T}\right)\ \mathrm{d}t}{\int_0^T\cos\left(\omega t\right)\cos\left(\frac{2\pi t}{T}\right)\ \mathrm{d}t} \tag{E.25}$$

where

$$T=\frac{2\pi}{\omega} \tag{E.26}$$

Combining Equations (E.25) and (E.26) results in:

$$\xi=\frac{\int_0^T\left|\cos\left(\omega t\right)\right|\cos^2\left(\omega t\right)\ \mathrm{d}t}{\int_0^T cos^2\left(\omega t\right)\ \mathrm{d}t} \tag{E.27}$$

When integrating over the positive section of the cosine function—i.e. $0\leq t\leq T/4$—Equation (E.27) becomes:

$$\xi=\frac{\int_0^{T/4}\cos^3\left(\omega t\right)\ \mathrm{d}t}{\int_0^{T/4}\cos^2\left(\omega t\right)\ \mathrm{d}t} \tag{E.28}$$

Filling in the numbers results in:

$$\xi=\frac{8}{3\pi} \tag{E.29}$$

Thereby—by combining Equations (E.23) and (E.29)—the solution to Equation (E.17) results in the following, linearised formulation:

$$i\left(\beta-1\right)=\frac{8}{3\pi}\frac{a_f}{L_s}\left|1-\beta\right|\left(1-\beta\right)-\frac{8}{3\pi}\frac{a_f}{L_d}\left|\beta\right|\beta-i\frac{C_m\lambda_p}{1-\lambda_p}\beta \tag{E.30}$$

E.3.2 Multi-layer system

This principle can easily be extended to multiple layers within the canopy, which have different λ-parameters and so varying shear and drag length-scales. For convenience, a structured method is introduced in which multiple layers are systematically arranged (*see* Fig. E.1).

For the k-th layer, Equation (E.17) becomes:

$$\frac{\partial}{\partial t}\left(u_{p,k}-u_f\right)=\frac{\left|u_{p,k-1}-u_{p,k}\right|\left(u_{p,k-1}-u_{p,k}\right)}{L_{s,k}}-\frac{\left|u_{p,k}-u_{p,k+1}\right|\left(u_{p,k}-u_{p,k}+1\right)}{L_{s,k}}-\frac{\left|u_{p,k}\right|u_{p,k}}{L_{d,k}}-\frac{C_m\lambda_{p,k}}{1-\lambda_{p,k}}\frac{\partial u_{p,k}}{\partial t} \tag{E.31}$$

where $u_{p,k}=u_f$ if $k=0$, which implicitly states that the free flow is layer $k=0$ (*see* Fig. E.1). The top layer of the canopy is $k=1$ and k increases downwards until layer $k=K$, which is the bottom canopy layer. Furthermore, the shear component between the bottom canopy layer and the bottom—i.e. the substratum—is assumed to be zero, which can be represented by no velocity difference between the layers; i.e. $u_{p,K}-u_{p,K+1}=0$ in Equation (E.31).

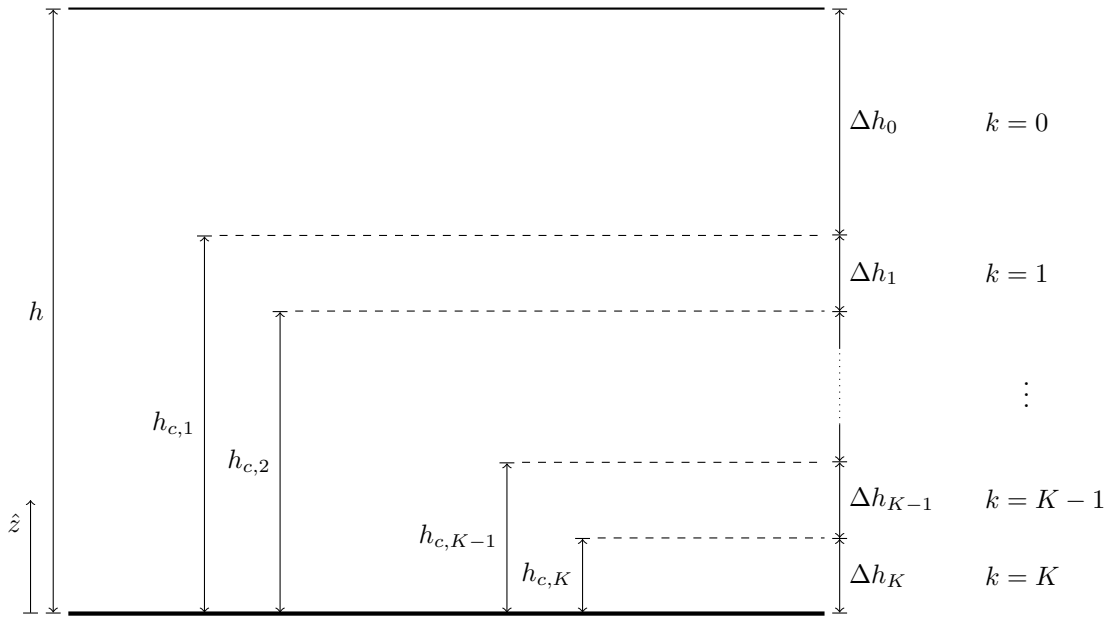

Figure E.1: Systematic notation for multi-layer canopy. h is the water depth; $h_{c,k}$ is the canopy height up to the k-th layer, i.e. the distance between the top of canopy layer k and the bottom; Δh_k the thickness of canopy layer k; and $\hat{z}$ the vertical axis, which positive upward and $\hat{z} = 0$ at the bottom.

The shear and drag length-scales are defined for a multi-layer canopy—in line with the single-layer canopy (*see* Eqs. E.21a, E.21b, E.22a and E.22b)—as follows:

$$L_{s,k} = \frac{\Delta h_k}{C_s^2} \qquad \text{(E.32a)} \qquad\qquad L_{d,k} = \frac{2\Delta h_k \left(1 - \lambda_{p,k}\right)}{C_{d,k}\lambda_{f,k}} \qquad \text{(E.32b)}$$

Following the same methodology as to get from Equation (E.17) to Equation (E.30), Equation (E.31) can be written as:

$$i\left(\beta_k - 1\right) = \frac{8}{3\pi}\frac{a_f}{L_{s,k}}\Big(\left|\beta_{k-1} - \beta_k\right|\left(\beta_{k-1} - \beta_k\right) - \left|\beta_k - \beta_{k+1}\right|\left(\beta_k - \beta_{k+1}\right)\Big) - \frac{8}{3\pi}\frac{a_f}{L_{d,k}}\left|\beta_k\right|\beta_k - i\frac{C_m\lambda_{p,k}}{1-\lambda_{p,k}}\beta_k \qquad \text{(E.33)}$$

in which the porous in-canopy flow is given by the real part of the complex wave notation:

$$u_{p,k} = \mathcal{R}e\left\{\beta_k \omega a_f \exp\left[i\omega t\right]\right\} \qquad \text{(E.34)}$$

where the WAC of the k-th layer is given by [Luhar et al., 2010]:

$$\alpha_{w,k} = \left|\beta_k\right| \qquad \text{(E.35)}$$

E.3.3 Numerical solving

To find the solution to either the single-layer canopy or the multi-layer canopy, the complex functions have to be solved iteratively. For this, a numerical solver is used, which solves for complex functions as well. This numerical solver is the built-in function `newton`, which is part of the package `scipy.optimize` in Python.[1]

[1] More information on the function: https://docs.scipy.org/doc/scipy/reference/generated/scipy.optimize.newton.html (retrieved January 23, 2020).

This numerical solver follows the Newton-Raphson method. For this solver to work properly for complex-valued functions—as is needed—the derivatives are needed. Therefore, the general derivative to the solution is derived in this section; i.e. the derivative of Equation (E.33).

First, Equation (E.33) is rewritten such that all terms are on one side:

$$f_k = i\left(\beta_k - 1\right) - \frac{8}{3\pi}\frac{a_f}{L_{s,k}}\left(\left|\beta_{k-1} - \beta_k\right|\left(\beta_{k-1} - \beta_k\right) - \left|\beta_k - \beta_{k+1}\right|\left(\beta_k - \beta_{k+1}\right)\right) + \frac{8}{3\pi}\frac{a_f}{L_{d,k}}\left|\beta_k\right|\beta_k + i\frac{C_m\lambda_{p,k}}{1-\lambda_{p,k}}\beta_k \tag{E.36}$$

A solution is found when Equation (E.36) is set equal to zero. The derivative of Equation (E.36) is given by:

$$\frac{\partial f_k}{\partial \beta_k} = i - \frac{8}{3\pi}\frac{a_f}{L_{s,k}}\left(\frac{\partial}{\partial\beta_k}\left(\left|\beta_{k-1} - \beta_k\right|\left(\beta_{k-1} - \beta_k\right)\right) - \frac{\partial}{\partial\beta_k}\left(\left|\beta_k - \beta_{k+1}\right|\left(\beta_k - \beta_{k+1}\right)\right)\right) + \frac{8}{3\pi}\frac{a_f}{L_{d,k}}\cdot\frac{\partial}{\partial\beta_k}\left(\left|\beta_k\right|\beta_k\right) + i\frac{C_m\lambda_{p,k}}{1-\lambda_{p,k}} \tag{E.37}$$

The derivatives due to the shear and drag terms are solved by following the product rule, which in general gives:

$$\frac{\partial}{\partial z_1}\left(\left|z_1 - z_2\right|\left(z_1 - z_2\right)\right) = \left|z_1 - z_2\right|\underbrace{\frac{\partial}{\partial z_1}\left(z_1 - z_2\right)}_{(1)} + \left(z_1 - z_2\right)\underbrace{\frac{\partial}{\partial z_1}\left(\left|z_1 - z_2\right|\right)}_{(2)} \tag{E.38}$$

where both z_1 and z_2 are complex valued parameters.

The first derivative in Equation (E.38)—marked with (1)—reduces to one. However, the second derivative in Equation (E.38)—marked with (2)—does not reduce to one due to the absolute value:

$$\begin{aligned}\frac{\partial}{\partial z_1}\left(\left|z_1 - z_2\right|\right) = &\frac{\mathcal{R}e\left\{z_1\right\}}{\sqrt{\left(\mathcal{R}e\left\{z_1\right\} - \mathcal{R}e\left\{z_2\right\}\right)^2 + \left(\mathcal{I}m\left\{z_1\right\} - \mathcal{I}m\left\{z_2\right\}\right)^2}} \\ &- \frac{\mathcal{R}e\left\{z_2\right\}}{\sqrt{\left(\mathcal{R}e\left\{z_1\right\} - \mathcal{R}e\left\{z_2\right\}\right)^2 + \left(\mathcal{I}m\left\{z_1\right\} - \mathcal{I}m\left\{z_2\right\}\right)^2}} \\ &+ i\frac{\mathcal{I}m\left\{z_1\right\}}{\sqrt{\left(\mathcal{R}e\left\{z_1\right\} - \mathcal{R}e\left\{z_2\right\}\right)^2 + \left(\mathcal{I}m\left\{z_1\right\} - \mathcal{I}m\left\{z_2\right\}\right)^2}} \\ &- i\frac{\mathcal{I}m\left\{z_2\right\}}{\sqrt{\left(\mathcal{R}e\left\{z_1\right\} - \mathcal{R}e\left\{z_2\right\}\right)^2 + \left(\mathcal{I}m\left\{z_1\right\} - \mathcal{I}m\left\{z_2\right\}\right)^2}}\end{aligned} \tag{E.39}$$

Note that the following definitions hold for complex numbers:

$$z = \mathcal{R}e\left\{z\right\} + i\,\mathcal{I}m\left\{z\right\} \tag{E.40a}$$

$$\left|z_1 - z_2\right| = \sqrt{\left(\mathcal{R}e\left\{z_1\right\} - \mathcal{R}e\left\{z_2\right\}\right)^2 + \left(\mathcal{I}m\left\{z_1\right\} - \mathcal{I}m\left\{z_2\right\}\right)^2} \tag{E.40b}$$

Rewriting Equation (E.39) using Equations (E.40a) and (E.40b) results in:

$$\frac{\partial}{\partial z_1}\left(\left|z_1 - z_2\right|\right) = \frac{z_1 - z_2}{\left|z_1 - z_2\right|} \tag{E.41}$$

Thereby, Equation (E.38) can be rewritten into:

$$\frac{\partial}{\partial z_1}\left(\left|z_1 - z_2\right|\left(z_1 - z_2\right)\right) = \frac{\left(z_1 - z_2\right)^2}{\left|z_1 - z_2\right|} + \left|z_1 - z_2\right| \tag{E.42}$$

Implementing these steps to the shear and drag terms results in the following, general derivative to Equation (E.36):

$$\frac{\partial f_k}{\partial \beta_k} = i - \frac{8}{3\pi}\frac{a_f}{L_{s,k}}\left(\frac{(\beta_{k-1}-\beta_k)^2}{|\beta_{k-1}-\beta_k|} - |\beta_{k-1}-\beta_k| - \frac{(\beta_k-\beta_{k+1})^2}{|\beta_k-\beta_{k+1}|} - |\beta_k-\beta_{k+1}|\right) + \frac{8}{3\pi}\frac{a_f}{L_{d,k}}\left(\frac{\beta_k^2}{|\beta_k|} + |\beta_k|\right) + i\frac{C_m\lambda_{p,k}}{1-\lambda_{p,k}} \quad \text{(E.43)}$$

Note the change of sign for the first shear term, which follows from the product rule (*see* Eq. E.38); the first derivative in Equation (E.38)—marked with (1)—does not reduce to one, but to negative one instead.

E.4 Approximations in-canopy flow

Lowe et al. [2005a] shows that the in-canopy flow is in one of three domains: (1) inertia-dominated domain; (2) general domain; or (3) unidirectional domain. For the first and latter domains, simplified expressions have been found. For the general domain, these simplifications do not hold. In this section, both the inertia-dominated approximation as the unidirectional approximation are derived (Secs. E.4.1 and E.4.2, resp.).

Both derivations start from the single-layered canopy after which the same methods are extended to the multi-layer canopy.

E.4.1 Inertia-dominated domain

Equation (E.30) is used as a starting point for the single-layer canopy from which the simplified form is derived. The inertia-dominated domain is defined as the cases in which the wave orbital motion is significantly smaller than the drag and shear length-scales, but the inertia component is not negligible; i.e. $a_f \ll L_d$ and $a_f \ll L_s$. This results in the following approximation of Equation (E.30):

$$i\left(\beta_i - 1\right) = -i\frac{C_m\lambda_p}{1-\lambda_p}\beta_i \quad \text{(E.44)}$$

where the subscript i denotes the approximation for the inertia dominated domain.

After some simple algebra, one gets to the limiting case in which the wave-attenuation coefficient (WAC) is solely based on the inertia forces:

$$\lim_{\omega\to\infty}\alpha_w = \alpha_i = |\beta_i| = \frac{1-\lambda_p}{1+\lambda_p\left(C_m-1\right)} \quad \text{(E.45)}$$

Equation (E.45) is easily extended to a multi-layer canopy, as there are no interactions with other layers in the canopy involved. These inter-layer interactions are fully incorporated in the shear components (*see* Eq. E.31). Therefore, the multi-layer approximation of the inertia-dominated domain is given by:

$$\lim_{\omega\to\infty}\alpha_{w,k} = \alpha_{i,k} = \frac{1-\lambda_{p,k}}{1-\lambda_{p,k}\left(C_m-1\right)} \quad \text{(E.46)}$$

E.4.2 Unidirecitonal domain

The approximation of the WAC in the unidirectional domain is considered for both a single-layer canopy and a multi-layer canopy—just as with the approximation in the inertia dominated domain—but also for two types of expressions for the shear stresses:

1. The 'simplified' form describes the shear stress assuming the difference between the two flow velocities is dominated by the faster flow, and so is given by this flow velocity only. As the flow is attenuated in the canopy, the flow higher in the water column is expected to be larger than the flow underneath. In the general notation (*see* Fig. E.1): $u_{p,k-1} \gg u_{p,k}$. This assumption gives the following description of the shear stress:
$$\tau_c(\hat{z} = h_{c,k}) = \rho C_s^2 \left|u_{p,k-1}\right| u_{p,k-1} \tag{E.47a}$$
2. The 'full' description includes the difference between the two flow velocities, which complicates matters. This results in the following description of the shear stress:
$$\tau_c(\hat{z} = h_{c,k}) = \rho C_s^2 \left|u_{p,k-1} - u_{p,k}\right| (u_{p,k-1} - u_{p,k}) \tag{E.47b}$$

Single-layer canopy

The approximation of the WAC in the unidirectional domain for the single-layer canopy starts from the beginning; i.e. with the streamwise momentum balance (Eq. E.9). The unidirectional domain is characterised by an infinitely long wave. In this special case, the time-derivatives approach zero and Equation (E.9) collapses into:
$$-\frac{1}{\rho}\frac{\partial p_c}{\partial x} + \frac{1}{\rho}\frac{\partial \tau_c}{\partial \hat{z}} - f_c = 0 \tag{E.48}$$
where the subscript c denotes the unidirectional case and in which the resistance force is solely based on the drag term, i.e.:
$$f_c = f_d \tag{E.49}$$
Because the resistance force above the canopy reduces to zero (i.e. $f_c(\hat{z} > h_c) = 0$), Equation (E.48) reduces to:
$$\frac{\partial p_c}{\partial x} = \frac{\partial \tau_c}{\partial \hat{z}} \tag{E.50}$$
where the gradient of the shear stress over the vertical is assumed to be linear. In combination with the assumption that the shear stress at the top of the water column is zero (i.e. $\tau_c(\hat{z} = h) = 0$)—e.g. no wind-induces shear stresses—the pressure gradient above the canopy can be written as:
$$\frac{\partial p_c}{\partial x}(\hat{z} > h_c) = \frac{\partial \tau_c}{\partial \hat{z}}(\hat{z} > h_c) = \frac{\tau_c(\hat{z} = h) - \tau_c(\hat{z} = h_c)}{h - h_c} = \frac{-\tau_c(\hat{z} = h_c)}{h - h_c} \tag{E.51}$$
Substituting Equations (E.49) to (E.51) into Equation (E.48) gives:
$$\frac{1}{\rho}\frac{\tau_c(\hat{z} = h_c)}{h - h_c} + \frac{1}{\rho}\frac{\partial \tau_c}{\partial z} - f_d = 0 \tag{E.52}$$
Averaged over the whole canopy and assuming the bottom stress to be negligible—i.e. $\tau_c(\hat{z} = 0) = 0$—Equation (E.52) results in:
$$\frac{1}{\rho}\frac{\tau_c(\hat{z} = h_c)}{h - h_c} + \frac{1}{\rho}\frac{\tau_c(\hat{z} = h_c)}{h_c} - f_{d,1} = 0 \tag{E.53}$$
in which (*see* Eq. E.15)
$$f_{d,1} = \frac{C_{d,1}\lambda_{f,1}}{2h_c\left(1 - \lambda_{p,1}\right)} \left|u_p\right| u_p \tag{E.54}$$
Substitution of the drag length-scale (*see* Eq. E.21b) in Equation (E.53) in combination with the drag formulation (*see* Eq. E.54), gives:
$$\frac{1}{\rho}\frac{\tau_c(\hat{z} = h_c)}{h - h_c} + \frac{1}{\rho}\frac{\tau_c(\hat{z} = h_c)}{h_c} - \frac{\left|u_p\right| u_p}{L_d} = 0 \tag{E.55}$$
The next step is to rewrite the shear stress terms. This is done for both formulations of the shear stress, as introduced in this section: (1) the simplified formulation; and (2) the full formulation (*see* Eqs. E.47a and E.47b, resp.).

1. Substituting Equation (E.47a)—i.e. the simplified formulation of the shear stress—into Equation (E.55) gives:
$$\frac{C_s^2 \left|u_f\right| u_f}{h-h_c} + \frac{C_s^2 \left|u_f\right| u_f}{h_c} - \frac{\left|u_p\right| u_p}{L_d} = 0 \tag{E.56}$$
Including the shear length-scale (*see* Eq. E.21a) this becomes:
$$\frac{\left|u_f\right| u_f}{L_s}\frac{h_c}{h-h_c} + \frac{\left|u_f\right| u_f}{L_s} - \frac{\left|u_p\right| u_p}{L_d} = 0 \tag{E.57}$$
After doing some straightforward algebra and using the definition of the WAC (*see* Eq. 4.19), the unidirectional limit of the WAC is given by:
$$\alpha_c = \frac{u_p}{u_f} = \sqrt{\frac{L_d}{L_s}\left(\frac{h_c}{h-h_c}+1\right)} \tag{E.58}$$
which is the positive result of the quadratic formulation, as only the positive result suits the definition of the WAC; $0 \leq \alpha_w \leq 1$.
2. Substituting Equation (E.47b)—i.e. the full formulation of the shear stress—into Equation (E.55) gives:
$$\frac{C_s^2 \left|u_f - u_p\right| (u_f - u_p)}{h-h_c} + \frac{C_s^2 \left|u_f - u_p\right| (u_f - u_p)}{h_c} - \frac{\left|u_p\right| u_p}{L_d} = 0 \tag{E.59}$$
Including the shear length-scale (*see* Eq. E.21a) this becomes:
$$\frac{\left|u_f - u_p\right| (u_f - u_p)}{L_s}\frac{h_c}{h-h_c} + \frac{\left|u_f - u_p\right| (u_f - u_p)}{L_s} - \frac{\left|u_p\right| u_p}{L_d} = 0 \tag{E.60}$$
Assuming that the above-canopy flow is larger than the in-canopy flow, which is again larger than zero—i.e. $u_f > u_p > 0$—Equation (E.60) becomes:
$$\frac{(u_f - u_p)^2}{L_s}\left(\frac{h_c}{h-h_c}+1\right) - \frac{u_p^2}{L_d} = 0 \tag{E.61}$$
When Equation (E.61) is divided by the square of the above-canopy flow and using the definition of the WAC (*see* Eq. 4.19), Equation (E.61) can be rewritten into a quadratic function:
$$\frac{1 - 2\alpha_c + \alpha_c^2}{L_s}\left(\frac{h_c}{h-h_c}+1\right) - \frac{\alpha_c^2}{L_d} = 0 \tag{E.62}$$
The solution of Equation (E.62)—using the *abc*-rule—for which $0 < \alpha_c < 1$ holds, is the unidirectional limit of the WAC:
$$\alpha_c = \frac{\frac{L_d}{L_s}\left(\frac{h_c}{h-h_c}+1\right) - \sqrt{\frac{L_d}{L_s}\left(\frac{h_c}{h-h_c}+1\right)}}{\frac{L_d}{L_s}\left(\frac{h_c}{h-h_c}+1\right) - 1} \tag{E.63}$$

The unidirectional limit of the WAC for which the full shear stress formulation is used, can be written in terms of the expression of the WAC as based on the simplified formulation of the shear stress:
$$\alpha_{c,f} = \frac{\alpha_{c,s}^2 - \alpha_{c,s}}{\alpha_{c,s}^2 - 1} \tag{E.64}$$
where the subscript f denotes the use of the full expression of the shear stress; and the subscript s the use of the simplified formulation.

Multi-layer canopy

Unfortunately, the formulations of the single-layer canopy cannot easily be translated to the multi-layer canopy as the canopy layers interact and so modify their outcomes. The starting point is again—as with the single-layer canopy—the streamwise momentum balance (Eq. E.9). As the first steps in the derivation of the unidirectional limit for the single-layer canopy are the same as for the multi-layer canopy (*see* Eqs. E.48 to E.52), the derivation for the multi-layer canopy starts from Equation (E.52) onwards; which is repeated here for convenience in which the notation for multiple layers as presented in Figure E.1 is used:

$$\frac{1}{\rho}\frac{\tau_c(\hat{z}=h_{c,1})}{\Delta h_0}+\frac{1}{\rho}\frac{\partial \tau_c}{\partial z}-f_d=0 \tag{E.65}$$

From here, the derivation for the multi-layer canopy differs as the canopy consists of multiple layers. Therefore, Equation (E.65) is averaged over the canopy layer, which gives for layer k the following expression:

$$\frac{1}{\rho}\frac{\tau_c(\hat{z}=h_{c,1})}{\Delta h_0}+\frac{1}{\rho}\frac{\tau_c(\hat{z}=h_{c,k})-\tau_c(\hat{z}=h_{c,k+1})}{\Delta h_k}-f_{d,k}=0 \tag{E.66}$$

in which (*see* Eq. E.15):

$$f_{d,k}=\frac{C_{d,k}\lambda_{f,k}}{2\Delta h_k\left(1-\lambda_{p,k}\right)}\left|u_{p,k}\right|u_{p,k} \tag{E.67}$$

Substitution of the drag length-scale (*see* Eq. E.32b) in combination with Equation (E.67) into Equation (E.66), gives:

$$\frac{1}{\rho}\frac{\tau_c(\hat{z}=h_{c,1})}{\Delta h_0}+\frac{1}{\rho}\frac{\tau_c(\hat{z}=h_{c,k})-\tau_c(\hat{z}=h_{c,k+1})}{\Delta h_k}-\frac{\left|u_{p,k}\right|u_{p,k}}{L_{d,k}}=0 \tag{E.68}$$

From here onwards, the derivations split—just as with the single-layer canopy—due to the implementation of the shear stresses. Both formulations are addressed: (1) the simplified formulation (*see* Eq. E.47a); and (2) the full formulation (*see* Eq. E.47b).

1. Substitution of the simplified formulation of the shear stress (*see* Eq. E.47a) into Equation (E.68) gives:
$$\frac{C_s^2\left|u_f\right|u_f}{\Delta h_0}+\frac{C_s^2\left|u_{p,k-1}\right|u_{p,k-1}}{\Delta h_k}-\frac{C_s^2\left|u_{p,k}\right|u_{p,k}}{\Delta h_k}-\frac{\left|u_{p,k}\right|u_{p,k}}{L_{d,k}}=0 \tag{E.69}$$
Including the definition of the shear length-scale (*see* Eq. E.32a), Equation (E.69) can be rewritten into:
$$\frac{\left|u_f\right|u_f}{L_{s,k}}\frac{\Delta h_k}{\Delta h_0}+\frac{\left|u_{p,k-1}\right|u_{p,k-1}}{L_{s,k}}-\frac{\left|u_{p,k}\right|u_{p,k}}{L_{s,k}}-\frac{\left|u_{p,k}\right|u_{p,k}}{L_{d,k}}=0 \tag{E.70}$$
Due to the multiple layers, the unidirectional limit of the WAC cannot be retrieved instantaneous from Equation (E.70) as the layer(s) above the layer under consideration—here layer k—determine the flow velocity. Therefore, one has to move down from the top canopy layer ($k=1$) to the bottom canopy layer ($k=K$). In the case of the top canopy layer, Equation (E.70) only consists of the above-canopy flow ($u_{p,0}=u_f$) and the in-canopy flow of this top canopy layer. Taking this direction of computations into account, a description of the unidirectional limit of the WAC for layer k can include the WAC of the layer above; i.e. $k-1$. Therefore, the three flow velocities in Equation (E.70) are clustered:
$$\left(\frac{L_{d,k}}{L_{s,k}}+1\right)\left|u_{p,k}\right|u_{p,k}=\frac{L_{d,k}}{L_{s,k}}\frac{\Delta h_k}{\Delta h_0}\left|u_f\right|u_f+\frac{L_{d,k}}{L_{s,k}}\left|u_{p,k-1}\right|u_{p,k-1} \tag{E.71}$$
Rearranging of Equation (E.71) such that the in-canopy flow of layer k and the above-canopy flow are on one side, and the rest is on the other side gives:
$$\frac{\left|u_{p,k}\right|u_{p,k}}{\left|u_f\right|u_f}=\frac{L_{d,k}}{L_{d,k}+L_{s,k}}\left(\frac{\Delta h_k}{\Delta h_0}+\frac{\left|u_{p,k-1}\right|u_{p,k-1}}{\left|u_f\right|u_f}\right) \tag{E.72}$$

Using the definition of the WAC (*see* Eq. 4.19) including its defined boundaries of zero and one, Equation (E.72) results in the unidirectional limit of the WAC of canopy layer k in which only the positive root is presented as the root that is physically sound:

$$\alpha_{c,k} = \sqrt{\frac{L_{d,k}}{L_{d,k} + L_{s,k}} \left(\frac{\Delta h_k}{\Delta h_0} + \alpha_{c,k-1}^2 \right)} \tag{E.73}$$

Note that Equation (E.73) is in line with the result for the single-layer canopy (*see* Eq. E.58), where by definition $\alpha_{c,0} = 1$. The difference between the two formulations is due to the assumption that the bottom shear stress is negligible and therefore not taken into account. This assumption also results in a modification of the unidirectional limit of the WAC for the bottom canopy layer. Following the same procedure, this results in the following expression—which is similar to Equation (E.58)—for $K = 1$:

$$\alpha_{c,K} = \sqrt{\frac{L_{d,K}}{L_{s,K}} \left(\frac{\Delta h_K}{\Delta h_0} + \alpha_{c,K-1}^2 \right)} \tag{E.74}$$

2. Substitution of the full formulation of the shear stress (*see* Eq. E.47b) into equation Equation (E.66) gives:

$$\frac{C_s^2 \left| u_f - u_{p,1} \right| (u_f - u_{p,1})}{\Delta h_0} + \frac{C_s^2 \left| u_{p,k-1} - u_{p,k} \right| (u_{p,k-1} - u_{p,k})}{\Delta h_k} - \frac{C_s^2 \left| u_{p,k} - u_{p,k+1} \right| (u_{p,k} - u_{p,k+1})}{\Delta h_k} - \frac{|u_{p,k}| \, u_{p,k}}{L_{d,k}} = 0 \tag{E.75}$$

Introducing the shear length-scale (*see* Eq. E.32a), Equation (E.75) can be rewritten into:

$$\frac{\left| u_f - u_{p,1} \right| (u_f - u_{p,1})}{L_{s,k}} \frac{\Delta h_k}{\Delta h_0} + \frac{\left| u_{p,k-1} - u_{p,k} \right| (u_{p,k-1} - u_{p,k})}{L_{s,k}} - \frac{\left| u_{p,k} - u_{p,k+1} \right| (u_{p,k} - u_{p,k+1})}{L_{s,k}} - \frac{|u_{p,k}| \, u_{p,k}}{L_{d,k}} = 0 \tag{E.76}$$

Next, the assumption is made that the flow velocity reduces further down the canopy in all cases, i.e.:

$$u_f > u_{p,1} > u_{p,2} > \ldots > u_{p,k-1} > u_{p,k} > u_{p,k+1} > \ldots > u_{p,K-1} > u_{p,K} \tag{E.77}$$

With this assumption, the difference between the two flow velocities as given in Equation (E.76) is always positive; $u_{p,k-1} - u_{p,k} > 0$ if $u_{p,k-1} > u_{p,k}$. Therefore, the absolute notation is not needed anymore, and Equation (E.76) simplifies to:

$$\frac{(u_f - u_{p,1})^2}{L_{s,k}} \frac{\Delta h_k}{\Delta h_0} + \frac{(u_{p,k-1} - u_{p,k})^2}{L_{s,k}} - \frac{(u_{p,k} - u_{p,k+1})^2}{L_{s,k}} - \frac{u_{p,k}^2}{L_{d,k}} = 0 \tag{E.78}$$

Equation (E.78) is divided by the square of the above-canopy flow, which in combination with the definition of the WAC results in the following quadratic formulation of the unidirectional limit of the WAC:

$$\alpha_{c,k}^2 = \frac{L_{d,k}}{L_{s,k}} \left(\frac{\Delta h_k}{\Delta h_0} (1 - \alpha_{c,1})^2 + (\alpha_{c,k-1} - \alpha_{c,k})^2 - (\alpha_{c,k} - \alpha_{c,k+1})^2 \right) \tag{E.79}$$

The unidirectional limit of the WAC following the full formulation of the shear stresses results in a set of non-linear equations that must be solved.

Appendix F

Coral recruitment: Recommendation

In Section 6.3, the contribution of the reproduction of corals is included in a basic way; adding a certain amount of coral cover and volume to the existing cover and volume, representative for the contribution of spawning. This appendix presents a suggestion to include this in a more process-based manner. It includes suggestions on the mechanisms and some first attempts on the formulations. Because this is a field of research on its own, it is not fully included in the main study. Furthermore, there is still lots of research required on the leading mechanisms governing the dynamics associated with the coral recruitment.

This appendix starts with an introduction into coral recruitment in Appendix F.1. Next, the suggestion is presented on how the coral recruitment can be better incorporated in the developed biophysical model framework (BMF). This includes the formulations of the dynamics of the coral recruitment (App. F.2). Thereafter, a sensitivity analysis is presented in Appendix F.3. Finally, some concluding remarks concerning the coral recruitment are provided in Appendix F.4.

F.1 Introduction into coral recruitment

In the recolonisation of a coral reef, coral larvae are needed to repopulate the site. Therefore, the connectivity to other coral reefs—or other reef sections—is essential in the recovery of coral reefs [Hata et al., 2017]. Within the large amount of coral species, there are two reproduction modes [Baird et al., 2009b; Harrison and Wallace, 1990; Hughes et al., 2019]: (1) spawning; and (2) brooding. The majority of the corals, however, are spawners [Baird et al., 2009b]; around 85%. The difference between the two modes is:

1. Spawning corals release gametes—i.e. eggs or sperm—and fertilisation occurs externally.
2. Brooding corals release planulae—i.e. fertilised eggs—and fertilisation occurs internally.

The larvae of spawning corals can often cover larger distances before they settle [Connolly and Baird, 2010] and so are important for (1) the connectivity with other reefs; (2) buffering from local extinction; and (3) the establishment of new—or less populated—locations [Gaylord et al., 2013; Woods et al., 2016].

Because coral larvae are poor swimmers—as there swimming velocities are orders of magnitude smaller than the (turbulent) flow velocities [Chia et al., 1984; Hata et al., 2017; Koehl and Hadfield, 2010]—they substantially depend on the diffusion due to the hydrodynamics [Baird et al., 2009b]. Moreover, the turbulence created on a reef is generally insufficient to enable settlement [Hata et al., 2017], and so additional complexity is needed due to micro-structures as well as large scale complexity [Graham et al., 2015]. Therefore,

the probability of settlement is determined mainly by two factors: (1) the complexity of the area [Graham et al., 2015]; and (2) the hydrodynamic conditions.

For a successful recolonisation of the area, both aforementioned criteria must be met. The complexity of the area and the hydrodynamics extend over multiple length-scales [Graham et al., 2015; Hata et al., 2017].

Furthermore, the connectivity is of importance and described by a diffusion relation [Cowen et al., 2006; Cowen and Sponaugle, 2009] in which the mortality rate of the larvae decreases exponentially over time [Connolly and Baird, 2010]. The combination of the diffusive spreading translates—in combination with the mortality rate of the larvae—into the supply of larvae as function of distance and time [Connolly and Baird, 2010].

F.2 Coral recruitment dynamics

The coral recruitment dynamics is split in five topics: (1) the competence of larvae to be ready to settle (Sec. F.2.1); (2) the dispersion of the larvae (Sec. F.2.2); (3) the spawning of corals (Sec. F.2.3); (4) the settlement rate of larvae (Sec. F.2.4); and (5) the mortality of larvae while drifting around in the water column (Sec. F.2.5). Thereafter, Appendix F.2.6 presents the connection from the coral recruitment dynamics to the biophysical model framework (BMF). This section concludes with a summary in which all the five components of the coral recruitment are listed (Sec. F.2.7).

F.2.1 Larval competence

Larvae are not always competent from their release to settle [Miller and Mundy, 2003; Nozawa and Harrison, 2008], which is especially true for spawning corals [Connolly and Baird, 2010]. As the acquisition of competence can take days [Harrison and Wallace, 1990; Miller and Mundy, 2003; Nozawa and Harrison, 2008], this can have a profound influence on the distribution of settling coral larvae [e.g. Wilson and Harrison, 1998].

Therefore, the competency dynamics of coral larvae are taken into account to describe the full picture. In these dynamics, three phases are defined: (1) pre-competence; (2) competence; and (3) post-competence [Connolly and Baird, 2010]. These phases interact according to a set of differential equations [Connolly and Baird, 2010]:

$$\frac{\partial L_1}{\partial t} = -\alpha(t)L_1(t) - \mu(t)L_1(t) \tag{F.1a}$$

$$\frac{\partial L_2}{\partial t} = +\alpha(t)L_1(t) - \beta(t)L_2(t) - \mu(t)L_2(t) \tag{F.1b}$$

$$\frac{\partial L_3}{\partial t} = +\beta(t)L_2(t) - \mu(t)L_3(t) \tag{F.1c}$$

where L_i are the coral larvae in phase i; α and β the per capita competence acquisition and loss rate, respectively; and μ is the mortality rate (*see* Sec. F.2.5).

Many aspects influence the competence acquisition and loss rates [Álvarez-Noriega et al., 2016; Harii et al., 2007; Woods et al., 2016] and the pelagic larvae are vulnerable against slight environmental changes [especially the copper concentration Hédouin and Gates, 2013; Woods et al., 2016]. Nevertheless, this study assumes these rates to be constant, which is in line with Connolly and Baird [2010]. However, a time delay is added to the rate of acquisition of competence. Thereby, the competence acquisition and loss rates are given by respectively:

$$\alpha(t) = \begin{cases} 0 & \text{for } t_s \leq t < t_s + t_c \\ a & \text{for } \quad t \geq t_s + t_c \end{cases} \tag{F.2}$$

$$\beta(t) = b \tag{F.3}$$

where a and b are the constant rates of competence acquisition and loss, respectively; t_s is the time of spawning; and t_c the time delay in acquiring competence. This time delay is in the order of a few days from spawning [Baird et al., 2009b; Connolly and Baird, 2010; Harrison and Wallace, 1990].

F.2.2 Larval dispersion

Central in the determination of the recruitment of coral larvae is the dispersion of them from the source; i.e. the reproducing coral. The dispersion follows the advection-diffusion relation in which the coral larvae are active tracers due to their swimming:

$$\frac{\partial c}{\partial t} + \nabla \cdot (\mathbf{u}c) - \nabla \cdot (D \nabla c) = S \tag{F.4}$$

where c is the concentration, in this case the coral larvae; $\mathbf{u}$ the flow velocity vector; D the diffusion coefficient; and S the cumulative of the sources and sinks. This last parameters includes: (1) the mortality rate; (2) the settlement; and (3) the release of larvae into the water by the corals. Thus, all biological components involved in the dispersion of the larvae are bundled in this source/sink-parameter, and the physical processes are further determined based on the advection-diffusion relation (i.e. Eq. F.4).

Combining Equations (F.1) and (F.4), results in a set of advection-diffusion equations, which can collectively be written as:

$$\frac{\partial L_i}{\partial t} + \nabla \cdot (\mathbf{u}L_i) - \nabla \cdot (D \nabla L_i) = S_i \tag{F.5}$$

in which the interactions between the larval phases, the settlement of larvae and their mortality are included in the source/sink term, S_i:

$$S_1 = \quad +r(t) \quad -\alpha(t)L_1(t) \qquad\qquad\qquad\qquad -\mu(t)L_1(t) \tag{F.6a}$$

$$S_2 = \qquad +\alpha(t)L_1(t) \quad -\beta(t)L_2(t) \quad -\sigma(x,y;t)L_2(t) \quad -\mu(t)L_2(t) \tag{F.6b}$$

$$S_3 = \qquad\qquad +\beta(t)L_2(t) \qquad\qquad -\mu(t)L_3(t) \tag{F.6c}$$

where r is the spawning rate of corals (*see* Sec. F.2.3); and σ the settling rate of larvae (*see* Sec. F.2.4). These source and sink, respectively, are added with respect to Equation (F.1).

F.2.3 Coral spawning

The moment of (mass) spawning of corals is seasonal [e.g. Guest et al., 2005; Mangubhai and Harrison, 2008] and driven by environmental cues such as temperature and light [e.g. Harrison and Wallace, 1990; Van Woesik et al., 2006; Willis et al., 1985]. This broadcast spawning event is well-predictable in time [Vize, 2006; Willis et al., 1985], where the accuracy for some species is in the order of one minute and gets up to 1-2 hours for less punctual species [Baird et al., 2009b]. The exact timing of multiple species are, however, not aligned as much and can span over 2-3 months [Guest et al., 2005; Mangubhai and Harrison, 2008]

The spawning of corals occurs at a regular interval—namely annually [e.g. Vize, 2006]—and so can be defined as (1) a pre-set time-sequence [Vize, 2006; Willis et al., 1985]; and (2) a function of the environmental cues [Harrison and Wallace, 1990; Van Woesik et al., 2006]. To limit computational effort, the first option is more suitable in this study. Moreover, the exact timing is not of importance when assessing multiple decades or even centuries. In these cases, the interval between spawning events is dominant. Therefore, the time of spawning is indicate by t_s, which are all the moments of broadcast spawning, which can be given by the day of the year due to the annual spawning cycle of corals [Vize, 2006].

Furthermore, only healthy corals contribute to the reproduction [Evenhuis et al., 2015; Rodrigues and Grottoli, 2006] and so only the healthy coral cover releases larvae. Combining these two aspects results in the following formulation for the spawning rate of corals:

$$r(t) = \begin{cases} P_H R & \text{for } t = t_s \\ 0 & \text{for } t \neq t_s \end{cases} \tag{F.7}$$

where R is the amount of released larvae and is a calibration factor.

F.2.4 Larval settlement

The settlement of coral larvae is not only based on the competence of the larvae to settle, but also (1) the flow conditions; (2) the bottom complexity; (3) the attachment strength; and (4) the location of the larvae in the water column. The first two are related, as a higher bottom complexity substantially influences the flow structure near the bottom. Furthermore, the attachment strength is also related to the flow conditions near the bottom surface, as it determines whether the larva is able to remain attached to the bottom so it can metamorphose into a coral. The last aspect seems straightforward—as coral larvae cannot settle when they are high in the water column—but plays a substantial role on the dispersion of corals [Bradbury and Snelgrove, 2001; Smith et al., 2001]. This vertical position of coral larvae is assigned to their lipid content [Harii et al., 2002; Harii and Kayanne, 2003; Tay et al., 2011].

Furthermore, the settlement rate is determined by the available space for settlement; i.e. the portion of unoccupied suitable substratum. This suggests the use of a logistic bottleneck as used for the growth component in the population dynamics (*see* Eq. 5.1a). In fact, this part of the partial differential equations of the population dynamics includes—among others—the recolonisation of dead corals and the reproduction [Evenhuis et al., 2015]. However, for regrowth of the area an healthy population of coral(s) is needed (*see* Eq. 5.1a). Therefore, this component does not include the dispersion of coral larvae and thereby the influence of neighbouring coral colonies; where the word "neighbouring" must be taken in broad sense. Instead, it represents the internal recolonisation and reproduction.

As there is no clear relation between certain characteristics of the bottom profile and the flow structure, all these components are combined in one parameter; the so-called unrestricted probability of settlement. In combination with the logistic bottleneck, this results in the probability of settlement:

$$\sigma(x, y; t) = p_s \left(1 - \frac{P_T}{K}\right) \tag{F.8}$$

where p_s is the unrestricted probability of settlement; P_T the total population cover; and K the carrying capacity of the area. Note that the logistic bottleneck is determined by the total population, which (1) does not include the dead coral cover; and (2) includes all living population states, which are assumed to prevent new larvae to settle on them. The spatial and temporal variabilities are both in the unrestricted probability of settlement and the logistic bottleneck.

F.2.5 Larval mortality

There are three methods to describe the mortality rate, which are in increasing complexity: (1) constant; (2) monotonically increasing or decreasing; and (3) decreasing followed by increasing, and vice versa [Connolly and Baird, 2010]. The latter results in a bathtub-shape or a hump-shape. It is common practice to idealise the mortality rate as constant in dispersal models [e.g. Cowen et al., 2006; Siegel et al., 2008] even though this assumption is likely to be incorrect in nature [e.g. Graham et al., 2008].

Although Graham et al. [2008] suggests a bathtub-shaped mortality rate—i.e. high initial mortality that at first decreases to increase at the end again—Connolly and Baird [2010] showed that the inclusion of an extra parameter does not result in substantially more accurate model results. Therefore, they suggest to use the Weibull distribution instead of the generalised Weibull distribution [Connolly and Baird, 2010], which results in the following mortality rate:

$$\mu(t) = \gamma \lambda^{\gamma} \left(t - t_s\right)^{\gamma - 1} \tag{F.9}$$

where γ is the shape factor of the Weibull distribution; and λ the instantaneous mortality rate. For $\gamma < 1$, the mortality rate is decreasing over time; for $\gamma = 1$, the mortality rate collapses and becomes constant; and for $\gamma > 1$, the mortality rate is increasing.

F.2.6 Coral cover and morphology

Once the coral larvae have settled—for which the dynamics are described by the previous sections—they contribute to the coral cover as well as to the friction via changes in the morphology. Therefore, the settled larvae have to be translated into resulting changes on the coral composition. As the coral larvae are very small—order of magnitude is millimetres [e.g. Harrison and Wallace, 1990]—their contribution is limited, but still can lead to the recolonisation of an area. The volume of the coral larva is used in combination with the number of settled larvae to describe the contributions to the coral cover and volume.

First, the settled larvae are considered to be healthy and so their settlement results in an increase in healthy coral cover. This increase is described by:

$$\frac{\partial P_H}{\partial t} = \sigma(x, y; t)\ L_2\ d_l^2 \tag{F.10}$$

where d_l is the diameter of the larva.

This contribution is assumed to only occur when the thermal conditions are within the thermal range; i.e. when corals are not bleaching, $T_{lo} \leq T_c \leq T_{hi}$ (*see* Ch. 5). Due to the thermal stresses when the temperature is outside the thermal range, it is not beneficial for larvae to settle.

Second, the settled larvae contribute to the coral volume and so add to the morphological change as described in Equation (4.67). The contribution of the larvae is considered to be to the optimal morphological ratios. Thereby, the contribution of the recruitment results in the following formulation (*see* Eq. 4.67):

$$\frac{\partial \left(V_c r_i\right)}{\partial t} = \sigma(x, y; t)\ L_2\ d_l^3\ r_{i,opt} \tag{F.11}$$

Note that for the addition of coral volume due to the larval settlement, the thermal conditions must be favourable; i.e. within the thermal range. Otherwise, the larvae are assumed not to settle.

F.2.7 Summary

Thus, the relations determining the sources and sinks in the advection-diffusion relations (Eqs. F.6a to F.6c) are fivefold and given by:

1. The spawning rate, i.e. the release of gametes and larvae in the water column by healthy corals:

$$r(t) = \begin{cases} P_H R & \text{for } t = t_s \\ 0 & \text{for } t \neq t_s \end{cases} \tag{F.12}$$

   where R is the amount of coral gametes or larvae released in the water column per healthy coral cover; and t_s the moment of spawning.

2. The per capita acquisition of competence rate by coral larvae:

$$\alpha(t) = \begin{cases} 0 & \text{for } t_s \leq t < t_s + t_c \\ a & \text{for } \quad t \geq t_s + t_c \end{cases} \tag{F.13}$$

   where a is a constant acquisition of competence rate, which is species-spcific; and t_c the delay in the acquisition of competence [Connolly and Baird, 2010].

3. The per capita loss of competence rate by coral larvae:

$$\beta(t) = b \tag{F.14}$$

   where b is a constant loss of competence rate, which is species-specific.

4. The settlement rate of coral larvae to the substrate:

$$\sigma(x, y; t) = p_s \left(1 - \frac{P_T}{K}\right) \tag{F.15}$$

Table F.1: Parameters determining the recruitment. a is the rate of competence acquisition; b the rate of competence loss; R .

	Parameter	Estimate	Deviation	Unit
model	a[a]	0.4		d^{-1}
	b[a]	0.08		d^{-1}
	R[b]	$1.0{\cdot}10^6$	10%	larvae $m^{-2}d^{-1}$
	λ[a]	0.04		d^{-1}
	γ[a]	0.5		–
	d_l[c]	1.0		mm
input	$P_H^{(0)}$	0.1–1.0		–
	D[d]	5.0–20.0	n/a	$m^2 s^{-1}$
	p_s	10^{-4}–10^{-1}		d^{-1}
	t_c[e]	0–4		d

[a] Connolly and Baird [2010].
[b] Estimate based on larva concentrations used in studies [e.g. Miller and Mundy, 2003; Nozawa and Harrison, 2008]
[c] Harrison and Wallace [1990]; Mangubhai and Harrison [2008]
[d] Cowen et al. [2006].
[e] Baird et al. [2009b]; Harrison and Wallace [1990]

where p_s is the unrestricted probability of settlement in which the larvae are not limited due to the presence of other corals; P_T the total population cover; and K the carrying capacity of the area.

5. The mortality rate of coral larvae:

$$\mu(t) = \gamma \lambda^\gamma \, (t - t_s)^{\gamma - 1} \tag{F.16}$$

where γ is the shape factor of the Weibull distribution; and λ the instantaneous mortality rate. Here, the mortality rate decreases over time [Connolly and Baird, 2010]; thus $\gamma < 1$.

The connection between the coral recruitment dynamics and the developed BMF is via the (healthy) coral cover and the coral volume. This is done by adding the contributions due to the larval settlement to the corresponding (partial) differential equations.

F.3 Sensitivity analysis

The sensitivity analysis on the recruitment uses a simplified form of the dispersion relation in which the dispersion of the larvae is represented by a one-dimensional diffusion equation as the advection only moves the resulting distribution but does not affect its shape [Largier, 2003]:

$$\frac{\partial L_i}{\partial t} - D \frac{\partial^2 L_i}{\partial x^2} = S_i \tag{F.17}$$

where only the pre-competent (L_1) and competent (L_2) larvae are taken into account as the post-competent larvae do not contribute to the recruitment.

Furthermore, all coral cover is assumed to be healthy, if present; i.e. the various population states associated with bleaching and its recovery afterwards are not taken into account. Therefore, the differential equation associated with the rate of healthy—and thus total—coral cover is given by (*see* Eq. F.10):

$$\frac{\partial P_H}{\partial t} = \sigma \; L_2 \; d_l^2 \tag{F.18}$$

where σ is the probability of settlement (*see* Eq. F.8).

The recruitment is solely based on the diffusion for which one spatial cell contains a coral population and it is surrounded by empty, but suitable substratum. For the analyses, a time span of 40 days is modelled after which most of the competent larvae are either dead or turned to their post-competent stage [Connolly and Baird, 2010]. An overview of all the parameters considered is given in Table F.1.

The sensitivity is described by the deviations (*see* App. D.1) in the increased average coral cover due to the spawning. The results are presented in Figure F.1. The sensitivity analyses are elaborated on per model parameter—i.e. per row of Figure F.1—starting at the top of the figure.

The sensitivity of the recruitment on the rate of competence acquisition is very small (*see* Fig. F.1, top row) and it does not show any relations with the input parameters. The accuracy of the rate of loss of competence, however, is of greater importance (*see* Fig. F.1, second row) and its sensitivity shows to be related to the probability of settlement. This connection is reasonable, as the loss of competence results in less larvae available to be able to settle. When the larvae have a higher probability of settlement—i.e. they settle quicker—less larvae remain that might loose their competence. This both explains the substantial dependency of the recruitment on the rate of competence loss; and the interaction between this rate and the probability of settlement.

Furthermore, there is a one-to-one relation between the increase in coral cover and the spawning rate (*see* Fig. F.1, third row). This is due to the small contribution of the coral larvae to the coral cover initially, because the larvae are very small. Due to the small contribution, deviations in the spawning rate do not impose substantial differences in the settlement due to e.g. the logistic bottleneck. Otherwise, a non-linearity must have been present between the sensitivity to the spawning rate as function of the probability of settlement.

The mortality rate—described by the instantaneous mortality rate (λ) and the Weibull shape factor (γ)—shows interactions with both the probability of settlement and the competence delay time (*see* Fig. F.1, fourth and fifth row). These interactions are reasonable as all affect the amount of competent larvae:

1. The mortality rate becomes of less importance for increasing probability of settlement as more larvae are settled before they die. Thereby, the deviations in the mortality rate are less affecting the final outcomes.
2. The delay of competence enlarges the period in which larvae can only die but are unable to settle. Thereby, the mortality rate becomes more substantial in the computations on the recruitment.

The diameter of the larvae shows to result in the most substantial effects on the outcomes (*see* Fig. F.1, bottom row). This substantial dependency is assigned to the squared dependency of the settlement rate to the larval diameter (*see* Eq. F.10). Therefore, the relative error in the estimation of the larval diameter is squared as well. As this parameter directly contributes to the increase in coral cover, there are no dependencies between it and any of the input parameters.

Finally, the role of the probability of settlement on the outcomes is substantial—as might be expected—but this is not clearly visible in Figure F.1. Therefore, Figure F.2 shows the effect of the probability of settlement on the multiplication of the average coral cover for (1) the hypothetical case used for the sensitivity analyses as shown in Figure F.1 in which there is one computational cell containing a healthy population surrounded by empty, but suitable substratum (*see* Fig. F.2a); and (2) all suitable substratum is covered with healthy corals (*see* Fig. F.2b).

The differences in magnitude of the multiplication between Figures F.2a and F.2b is due to the logistic bottleneck that arises when most of the domain is covered with corals. As Figure F.2b represents an equal coverage of corals over the domain—i.e. the reef—differences arises due to the initial coral cover, where for large average coverage the influence of the probability of settlement reduces. However, for decreasing average coral cover the importance of a correct estimate of the probability of settlement increases rapidly.

The reason of the implementation of the coral recruitment was at first because of the full dislodgement, which leads to the disappearance of coral cover for ever. Thereby, there is limited coral cover left after a storm

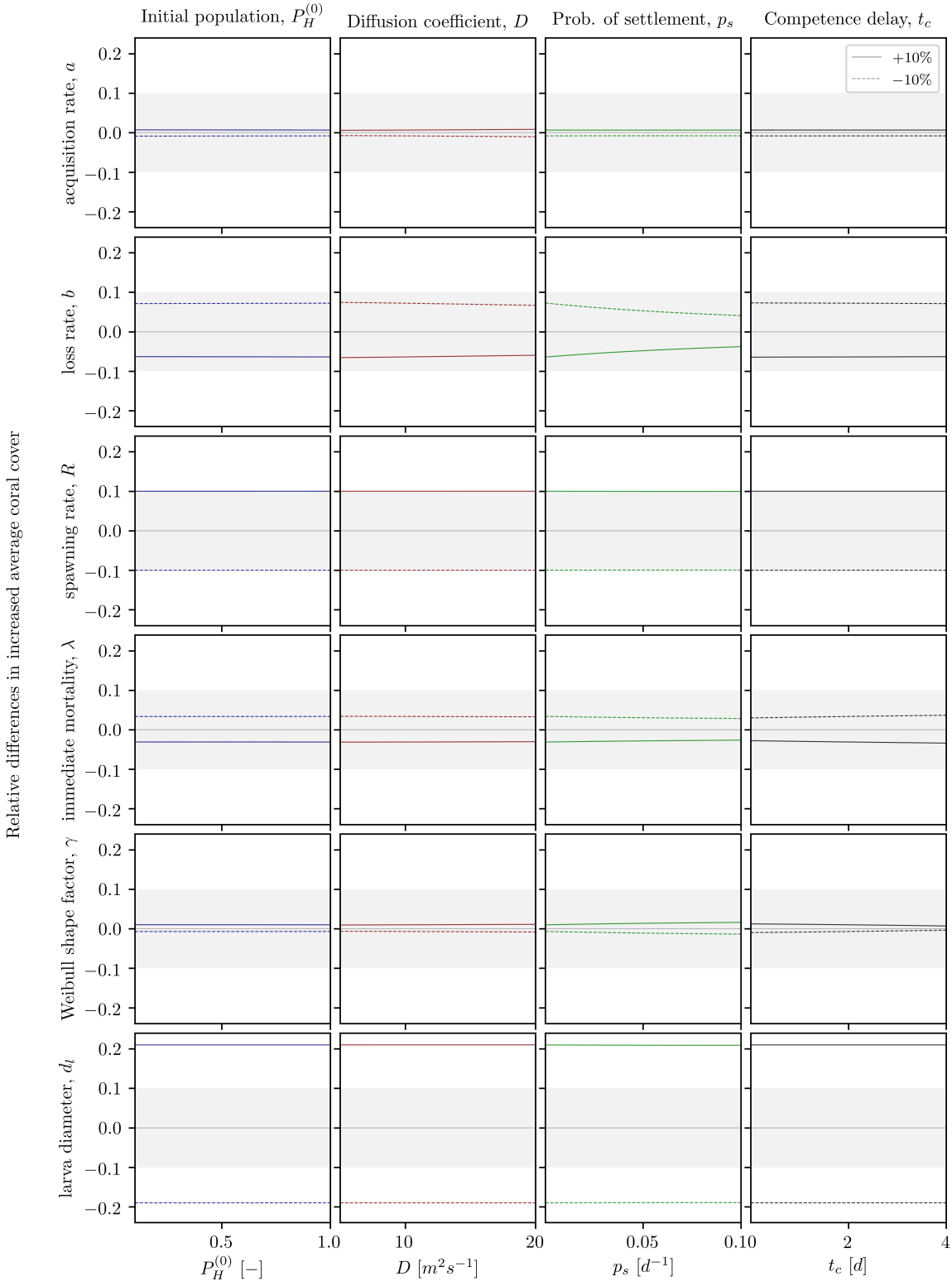

Figure F.1: Sensitivity analysis of the recruitment and increase in coral cover due to dispersal. The sensitivity to the parameters is described as relative difference in the increased average coral cover after a mass spawning event compared to the results based on the estimate (*see* Eq. D.1 and Tab. F.1). The gray-shaded area marks the threshold difference compared to the imposed deviation; i.e. the 10% mark.

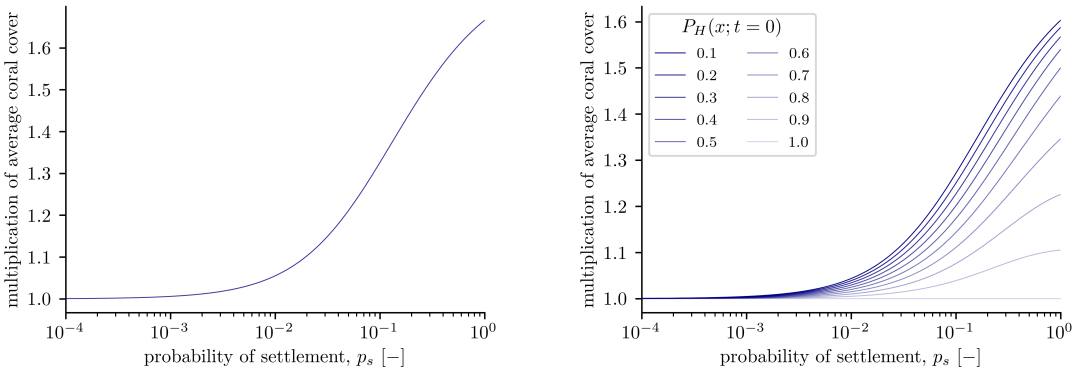

(a) $P_H(x = x_c; t = 0) = 1.0$.

(b) $P_H(x; t = 0) = 0.1..1.0$.

Figure F.2: The significance of the probability of settlement on the contribution of the coral recruitment on the coral cover. (a) One computational cell in the centre of the domain—at $x = x_c$—is fully covered with healthy corals and is surrounded by empty, but suitable substratum for settlement; and **(b)** the full domain has a coral cover of 90%. The significance of the probability of settlement is expressed as the multiplication of average coral cover over the whole domain due to the recruitment, 40 days since spawning.

event, even when partial dislodgement is considered. This means that the case in which there is limited existing coral cover is of most interest in the face of coral recruitment. As aforementioned and shown in Figure F.2b, the probability of settlement is one of the major processes of coral recruitment in this scenario.

F.4 Concluding remarks

The implementation of the recruitment dynamics enables the biophysical model framework (BMF) to better predict the recovery potential of coral reefs after a stress event. There are, however, some knowledge gaps that need to be filled before it can reliably used. The main topic of attention is the probability of settlement of coral larvae. There is not much known about the settlement process of the larvae, while it is one of the most important aspects of the coral recruitment dynamics.

The other aspects of the recruitment dynamics can be well represented with the current knowledge. For example, the larval dispersion is modelled by simulating the larvae by active tracers in a hydrodynamic model. These methods already exist and can be easily modified to suite the purpose of simulating coral larvae. All other aspects are a matter of data acquisition to gain more certainty but the sensitivity analysis suggests that their accuracy is of minor importance (*see* Fig. F.1).

Thus, the recruitment dynamics are simulated by releasing active tracers in a hydrodynamic model that represent coral larvae. These tracers are given the characteristics following the larval competence and mortality. Therefore, Equations (F.5) and (F.6a) to (F.6c) form the core of the recruitment dynamics. However, more research has to be done on the settlement process of larvae for this method to work properly.